

Department of Biotechnologies and Biosciences

PhD program in Chemical, Geological and Environmental sciences

PhD cycle XXXII

PhD curriculum: Chemical Sciences

# DESIGN, SYNTHESIS AND DEVELOPMENT OF GLYCOTOOLS FOR NEUROCHEMISTRY STUDIES

VACCHINI Mattia

Matriculation number: 708939

Scientific tutor: Laura Francesca Cipolla

Erasmus scientific mentor: Gordan Lauc

Erasmus scientific supervisor: Thomas Klarić

PhD program coordinator: Marialuce Frezzotti

PhD curriculum coordinator: Claudio Greco

**ACADEMIC YEAR 2018-2019**

© 2019 Mattia Vacchini. All rights reserved. No part of this book may be reproduced, stored in a retrieval system or transmitted in any form or by any means without permission of the author or the journals holding the copyrights of the published manuscripts.

The work presented in this thesis was performed at the Bioorganic Chemistry Laboratory of the Department of Biotechnology and Biosciences of the University of Milano-Bicocca, at the Mass Spectrometry laboratory of the University of Milano-Bicocca, and at Genos Glycoscience Research Laboratory Ltd., BICRO BIOCentar, Zagreb, Croatia.

The work carried out at Genos Ltd. was supported by the European Union Erasmus + Traineeship programme, with the agreements n° N. 2017-1-IT02-KA103-035644 and n° N. 2018-1-IT02-KA103-047473, CUP H44F1800006006.

ABSTRACT.	7
1. INTRODUCTION.	8
<b>1.1 N-GLYCOSYLATION RELEVANCE.</b>	<b>8</b>
1.1.1 <i>N</i> -glycosylation in life sciences.	8
1.1.2 <i>N</i> -glycosylation in biomedicine and industry.	8
<b>1.2 N-GLYCOSYLATION IN NEUROCHEMISTRY.</b>	<b>11</b>
1.2.1 <i>N</i> -glycosylation in vertebrates.	11
1.2.2 <i>N</i> -glycosylation in the nervous system.	14
1.2.3 <i>N</i> -glycosylation in neural development.	15
1.2.4 <i>N</i> -glycosylation in neural physiology.	18
1.2.5 <i>N</i> -glycosylation in neural pathology.	21
1.2.6 The <i>N</i> -glycosylation “brain-type” pattern.	22
1.2.7 <i>N</i> -glycosylation on a CNS protein target: the case of Neuroserpin.	24
<b>1.3 GLYCOANALYTICAL TOOLS FOR NEUROCHEMISTRY STUDIES.</b>	<b>27</b>
1.3.1 Glycan binding proteins: detection and targeting in the CNS.	27
1.3.2 Bioorthogonal chemical reporters for metabolic glycan labelling.	29
1.3.3 Chromatography and MS-based techniques.	30
1.3.4 LC-MS based <i>N</i> -glycomic approaches.	32
1.3.5 LC-MS based <i>N</i> -glycoproteomic approaches.	38
1.3.6 MS analysis of <i>N</i> -glycans and <i>N</i> -glycoproteins.	39
1.3.7 MS-based <i>N</i> -glyco(prote)omic applications for CNS studies.	42
<b>1.4 GLYCOTOOLS TOWARDS NEUROMEDICAL APPLICATIONS.</b>	<b>44</b>
1.4.1 Glycosides as potential neuroregenerative tools.	44
1.4.2 Glycodendrimers as potential neuromedical tools.	45
2. PREMISES AND OBJECTIVES.	50
3. RESULTS.	51
<b>3.1 A PRECISE AND VERSATILE PLATFORM FOR RAPID GLYCOSYLATION ANALYSIS OF BRAIN TISSUE.</b>	<b>51</b>
3.1.1 Framework of the study.	51

3.1.2 Sample preparation.	54
3.1.3 Sensitivity and precision: optimal amount of starting tissue.	55
3.1.4 Sensitivity and precision: effective range of starting tissue.	56
3.1.5 Selectivity.	57
3.1.6 Robustness and versatility.	58
3.1.7 Structural resolution of <i>N</i> -glycan samples derived using HSD and LSD.	65
3.1.8 Comparison of <i>N</i> -glycoprofiles obtained by LSD Vs HSD.	67
3.1.9 Conclusions and future perspectives.	71
<b>3.2 THE "REVERSE GLYCOPROTEOMICS" PROJECT.</b>	<b>74</b>
3.2.1 Framework of the study.	74
3.2.2 The RG strategy.	74
3.2.3 Brain proteome fractionation through SDS-PAGE.	75
3.2.4 In-gel deglycosylation (IGD).	76
3.2.5 In-gel trypsinisation after deglycosylation (IGaTD).	80
3.2.6 In-gel trypsinisation without deglycosylation (IGT).	83
3.2.7 Conclusions and future perspectives.	84
<b>3.3 CHEMOSELECTIVE MODIFICATION OF HUMAN NEUROSERPIN.</b>	<b>86</b>
3.3.1 Framework of the study.	86
3.3.2 Reductive amination for hNS labeling.	86
3.3.3 A quick glance at the dimethylation reaction outcome.	87
3.3.4 The dimethylation reaction is compatible with hNS folding.	88
3.3.5 Analytical evaluation of dimethylated mhNS and phNS peptides.	89
3.3.6 Conclusions and future perspectives.	99
<b>3.4 SYNTHESIS OF ALLYL AND DEC-9-ENYL <math>\alpha</math>-D-MANNOPYRANOSIDES.</b>	<b>101</b>
3.4.1 Framework of the study.	101
3.4.2 $\alpha$ -D-Mannopyranosides synthesis.	102
3.4.3 Conclusions and future perspectives.	102
<b>3.5 (GLYCO)DENDRIMERS CONVERGENT SYNTHESIS BY OLEFIN METATHESIS.</b>	<b>104</b>
3.5.1 Framework of the study.	104
3.5.2 (Glyco)dendrimers synthesis.	104
3.5.3 Conclusions and future perspectives.	105



4. EXPERIMENTAL SECTION.	107
<b>4.1 A PRECISE AND VERSATILE PLATFORM FOR RAPID GLYCOSYLATION</b>	
<b>ANALYSIS OF BRAIN TISSUE.</b>	<b>107</b>
4.1.1 Chemicals.	107
4.1.2 Sample preparation.	107
4.1.3 LSD workflow.	107
4.1.4 HSD workflow.	109
4.1.5 HILIC-UPLC-FLR profiling and data analysis.	109
4.1.6 <i>N</i> -glycan enrichment by Porous Graphitized Carbon-SPE.	110
4.1.7 HILIC-UPLC-ESI-QqTOF MS profiling and data analysis.	110
4.1.8 Statistics.	111
<b>4.2 THE "REVERSE GLYCOPROTEOMICS" PROJECT.</b>	<b>112</b>
4.2.1 Chemicals.	112
4.2.2 Sample preparation for SDS-PAGE fractionation.	112
4.2.3 SDS-PAGE recipes and run specifications.	112
4.2.4 SDS-PAGE bands excision and destaining.	113
4.2.5 In-gel deglycosylation (IGD).	113
4.2.6 <i>N</i> -glycans labelling, purification, concentration, and UPLC analysis.	113
4.2.7 In-gel trypsinisation after/without deglycosylation (IGTaD/IGT).	113
4.2.8 Deglycosylated peptides purification and enrichment with RP-SPE.	114
4.2.9 Deglycosylated peptides RP-nanoUPLC-ESI-QqTOF MS profiling.	115
4.2.10 Glycopeptides purification and enrichment with cotton-HILIC chromatography.	116
<b>4.3 CHEMOSELECTIVE MODIFICATION OF HUMAN NEUROSERPIN.</b>	<b>117</b>
4.3.1 Chemicals.	117
4.3.2 Dimethyl labelling of hNS.	117
4.3.3 nanoESI-QqTOF-MS, Far-UV CD, SEC and FLR analyses of intact mhNS.	117
4.3.4 In-solution enzymatic digestion of hNS.	117
4.3.5 Peptides purification and enrichment with RP-SPE.	117
4.3.6 Orbitrap Fusion HR-MS analysis of hNS peptides.	118
4.3.7 Statistics.	119
<b>4.4 SYNTHESIS OF ALLYL AND DEC-9-ENYL <math>\alpha</math>-D-MANNOPYRANOSIDES.</b>	<b>120</b>
4.4.1 General Methods.	120

4.4.2 Allyl $\alpha$ -D-mannopyranoside synthesis (1).	120
4.4.3 Dec-9-enyl $\alpha$ -D-mannopyranoside synthesis (2).	121
4.4.4 Allyl 2,3,4,6-tetra- <i>O</i> -acetyl- $\alpha$ -D-mannopyranoside synthesis (3).	121
4.4.5 Dec-9-enyl 2,3,4,6-tetra- <i>O</i> -acetyl- $\alpha$ -D-mannopyranoside synthesis (4).	122
<b>4.5 (GLYCO)DENDRIMERS CONVERGENT SYNTHESIS BY OLEFIN METATHESIS.</b>	<b>123</b>
4.5.1 General Methods.	123
4.5.2 Dendrimer precursors synthesis (1, 5, 9).	123
4.5.3 Boc-protected tetravalent dendrimer synthesis (2).	123
4.5.4 Deprotected tetravalent dendrimer synthesis (3).	124
4.5.5 Tetravalent glycosylated dendrimer synthesis (4).	124
4.5.6 Boc-protected octavalent dendrimer synthesis (6).	124
4.5.7 Deprotected octavalent dendrimer synthesis (7).	125
4.5.8 Octavalent glycosylated dendrimer synthesis (8).	125
4.5.9 Boc-protected hexadeca dendrimer synthesis (10).	126
 5. CONCLUDING REMARKS.	 127
 6. APPENDIX.	 129
6.1 MS analysis of samples prepared by LSD and HSD (Table A-1).	129
6.2 Calculation of derived traits.	147
6.3 Glycoproteins identified by downstream proteomics applications (Table A-2).	148
6.4 Chymotryptic peptides identified from mhNS MS analysis (Table A-3).	150
6.5 Chymotryptic peptides identified from phNS MS analysis (Table A-4).	155
6.6 Alkenyl- $\alpha$ -D-mannopyranosides NMR spectra.	161
 7. BIBLIOGRAPHY.	 169
 8. AKNOWLEDGMENTS.	 208
 9. PUBLICATIONS.	 209

## ABSTRACT.

*Background.* Glycans play crucial roles within the central nervous system (CNS) and their study is essential for a thorough comprehension of neurochemistry, but the scientific knowledge about CNS glycans remains scarce. The aim of this thesis is to provide the glycochemist and glycoanalyst with novel tools for neurochemistry studies, towards the exploration of glycan roles in the CNS. This thesis presents a novel analytical method for brain *N*-glycans investigation (LSD); the state of the art of an ongoing work for the investigation of *N*-glycans and *N*-glycoproteins differentially expressed in brain tissues of different species; an efficient chemical labelling method for (glyco)proteins, successfully applied on Neuroserpin (NS), a pathologically-polymerising CNS *N*-glycoprotein; and the syntheses of glycosides and glycodendrimers with potential room for neuromedical studies.

*Methods.* LSD comprised brain tissue (bt) chemical lysis, proteome precipitation (i.e., methanol/chloroform), enzymatic deglycosylation (i.e., PNGase F), *N*-glycans purification, chemical labelling (i.e., reductive amination on terminal *N*-acetylglucosamine), and LC-MS bioanalysis. The method has been optimised on bt and thoroughly validated (i.e., sensitivity, precision, linearity, range, selectivity, robustness). *N*-glycans analysis has also been carried out through protein electrophoresis in-gel deglycosylation, while in-gel trypsinisation was used for the LC-MS identification of *N*-glycoproteins and *N*-glycosylation sites. NS has been dimethylated (i.e., reductive amination on lysine) in its monomeric (mhNS) and polymeric (phNS) forms, and the reaction outcome has been evaluated using MS, towards the investigation of NS polymerisation-driving molecular features. Glycosides were synthesised with a Fischer-type glycosylation reaction on unprotected monosaccharides using either allyl alcohol or decenol as glycosyl acceptors, while glycodendrimers were obtained decorating olefin-metathesis-synthesised dendrimers with maltose moieties, exploiting oxime chemistry.

*Results.* LSD displayed the lowest detection limit (1 mg of bt) in comparison to many other works reported in the literature and is the most thoroughly validated neuro-*N*-glycomic method reported to date. In-gel deglycosylation for brain *N*-glycans analysis furnished informative chromatograms for every proteome fraction with high resolution (e.g., sensitivity up to 100 EU from a single gel band), permitting the analysis of deglycosylated peptides from the same sample (i.e., a total of 1200 peptides, 570 proteins, 57 *N*-glycoproteins, and novel *N*-glycosylation sites identified). NS chemical labelling displayed high efficiency (i.e., 80-90% yield), compatibility with the protein folding, and suitability towards the intended purpose, being able to highlight statistically significant differences in mhNS and phNS labelling patterns (i.e., 9 lysines). The syntheses of glycosides furnished products with good yield (i.e., 70%) and  $\alpha$ -stereoselectivity, while that of glycodendrimers afforded molecules exposing several maltose moieties, employable in the context of neurochemistry studies.

*Conclusions.* Methods and molecules delivered within this thesis will benefit the glycochemistry community, by enlarging the glycochemist and glycoanalyst toolkits to carry on the investigation of glycans-related effects in neurological and neuromedical context.

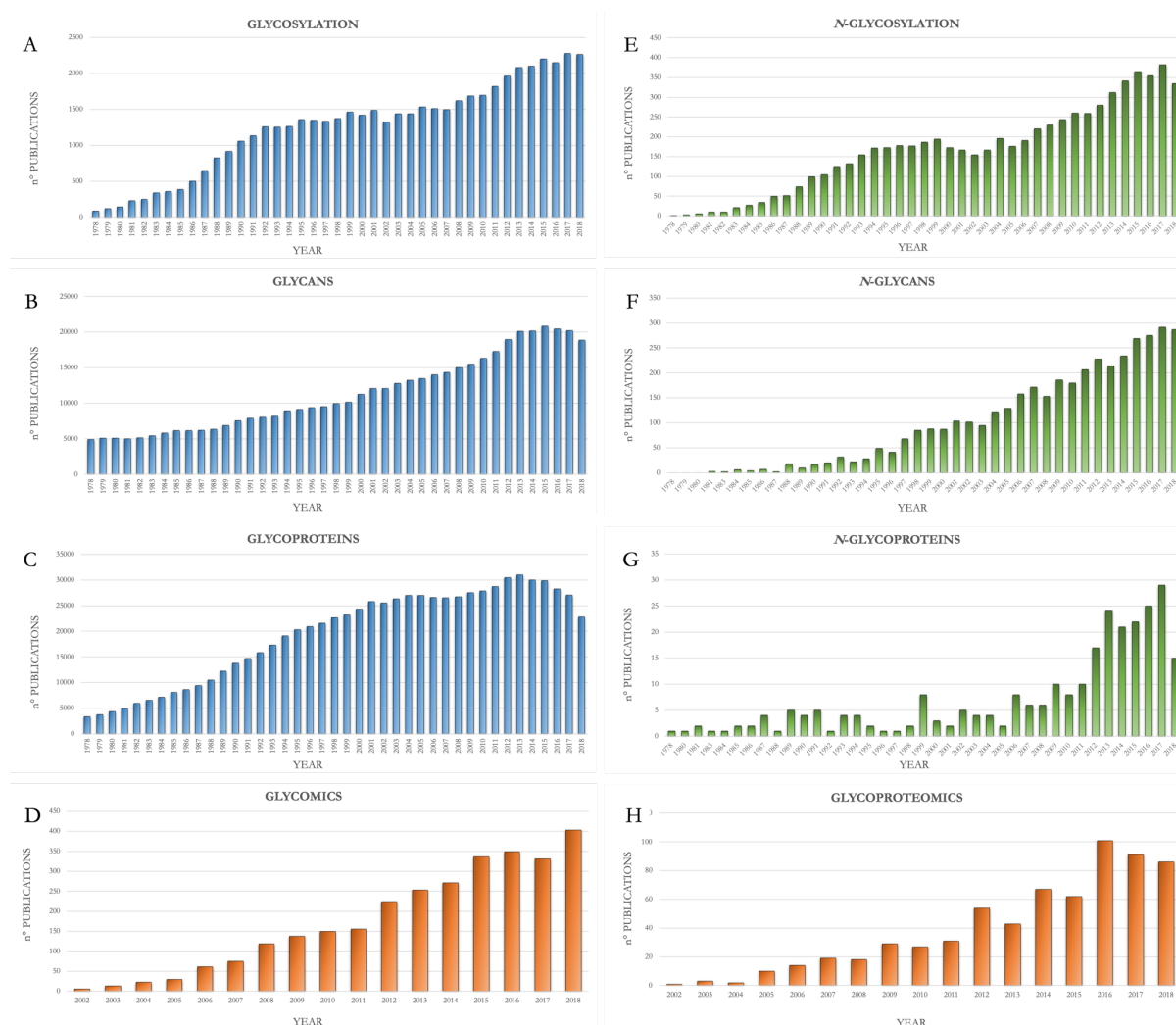
## 1. INTRODUCTION.

### 1.1 N-GLYCOSYLATION RELEVANCE.

**1.1.1 N-glycosylation in life sciences.** *N*-glycosylation is a widespread post-translational modification, in which oligosaccharides or polysaccharides (*N*-glycans) are covalently linked to proteins at asparagine residues (N) by an *N*-glycosidic bond. *N*-glycosylation modulates cellular biochemistry in all the domains of life, Eukarya, Bacteria, and Archaea.<sup>1,2</sup> Although the existence and biological relevance of glycans and glycoproteins were long known since the beginning of the 20<sup>th</sup> century (e.g., Fischer's works on hexoses; Landsteiner's study of ABO blood groups),<sup>3</sup> only about the end of the 90s the life sciences community initiated to substantially dedicate its attention to this class of macromolecules, and the interest in their features and biological effects has grown ever since. Simple researches within the PubMed database [National Center for Biotechnology Information (NCBI)], deliver a measure of the growing interest of the life sciences community in glycobiology. When general terms, such as "glycosylation", "glycans" and "glycoproteins" (i.e., not confined to *N*-glycosylation, but also including any other kind of mono/di/oligo/polysaccharide glycosidically linked to a biomolecule or chemical functionality; e.g., *O/C*-glycosylation on proteins, glycolipids, synthetic glycosides or other glycomolecules) are used as database queries, the amount of returned articles increased several folds during the last forty years (1978-2018; **Fig. 1.1, A-C**); and even when more specific terms, such as *N*-glycosylation, *N*-glycans and *N*-glycoproteins are fed to the database, the results of the research follow the same trend (**Fig. 1.1, E-G**). More recent concepts, such as "glycomics" and "glycoproteomics" (i.e., the study of the entire glycan ensemble of a glycosystem; e.g., a cell or tissue glycan or glycoproteomic repertoire) behave similarly under the same parameters (2002-2018; **Fig. 1.1, D, H**), therefore further demonstrating the consistency of the growing relevance of glycobiology in life sciences.

**1.1.2 N-glycosylation in biomedicine and industry.** Stemming from the interest of the life sciences community into glycobiology, a substantial number of glycotools and glycan-based applications have contributed to the evolution of biomedicine.<sup>3</sup> Glycan-based small molecule drugs proved to be biomedically valuable in the fields of antibacterial (e.g., aminoglycosides like neomycin),<sup>4</sup> antiviral (e.g., zanamivir),<sup>5</sup> and glycan-based diseases treatment (e.g., miglitol<sup>6</sup> for diabetes and miglustat<sup>7</sup> for Gaucher disorder), among others.<sup>3</sup> Another class of glycan-based biomedically effective molecules are carbohydrate-based vaccines, either derived from natural sources (e.g., *Salmonella typhi*, TYPHIM Vi; *Streptococcus pneumonia*, Prevnar; *Neisseria meningitides*,

Menactra; *Haemophilus influenzae* type b; Hib, Hiberix, Comvax),<sup>8</sup> or fully synthetic (e.g., *Haemophilus influenzae* type b; Quimi-Hib),<sup>9</sup> with many others showing promising results in animal models.<sup>3</sup>



**Fig. 1.1.** N-glycosylation in life sciences. Histograms show the amount of retrieved articles (n° PUBLICATIONS) per single query (histogram titles) per year (1978-2018 for A-C and E-G; 2002-2018 for D and H), resulting from searches in the PubMed database [National Center for Biotechnology Information (NCBI)].

Apart from these already on the market glycan-based biomedical systems, various other (macro)molecules, such as multivalent glycoconjugates (glycopolymers, glycodendrimers and glyconanoparticles), showed promising potential towards biomedical applications either at the *in vitro* or *in vivo* evaluation step.<sup>3</sup> A recently synthesised glycopeptide, containing the glycopeptide recognised by the human PG9 antibody (i.e., a broadly neutralising antibody, capable of neutralising different HIV genetic variants) furnished a specific example of N-glycan based biomedically relevant biomolecule in the context of carbohydrate-vaccines.<sup>10</sup> Two closely spaced N-glycans, harboured on N160 and N156, and belonging to gp120 (i.e., a hIV envelope

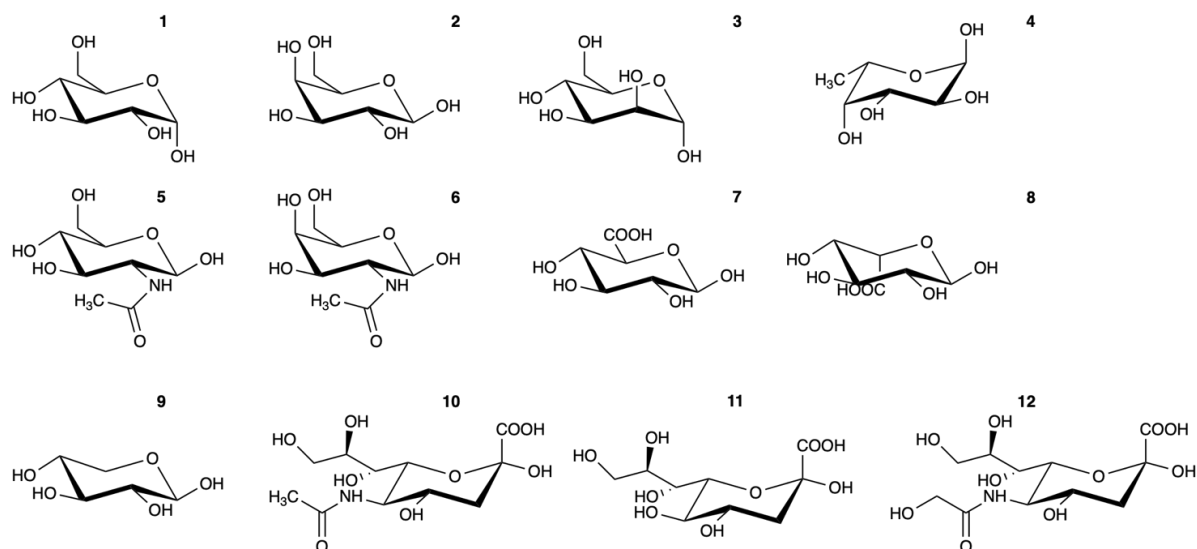
glycoprotein) are contained in the glycopeptide, making it capable of binding the PG9 antibody with high affinity. The glycopeptide immunogenicity and HIV protective potential is currently under evaluation in animal models. Another prominent field where *N*-glycosylation is studied and exploited towards more efficient biomedical applications is biotherapeutics development. Protein-based therapeutics are clinically highly successful. Hundreds of natural or modified therapeutic proteins have been approved for clinical use in Europe and the US, generating hundreds of billions of USD revenues every year.<sup>11</sup> To date, many glycoproteins such as erythropoietin, cytokines, antibodies, glycosyltransferases, and glycosidases are present on the market, generating tens of billions of USD revenues per year.<sup>12</sup> The most successful biotechnological case to date is that of Erythropoietin (EPO; i.e., a circulating cytokine that binds the erythropoietin receptor, which induces the proliferation and differentiation of the erythroid progenitors in the bone marrow), developed to treat anaemias deriving from lack of endogenous EPO or chemotherapy-related effects. EPO is a glycoprotein, carrying three sialylated complex *N*-glycans and one sialylated *O*-glycan, which activity *in vivo* is reduced by almost 90% for the underglycosylated versions, due to increased and quicker kidney clearance. Undersialylated EPO is also rapidly cleared by galactose receptors in hepatocytes and macrophages. These evidences demonstrate the importance of glycosylation profiles of glycotherapeutics for *in vivo* biomedical applications and highlight the necessity to develop highly controlled manufacturing procedures ensuring batch-to-batch consistency of the product glycosylation array. This is crucial, since more than half of human proteins are estimated to be glycosylated,<sup>13</sup> and the majority of therapeutic proteins are produced as a mixture of glycoforms (i.e., different forms of a glycoprotein showing diverse glycan components),<sup>14</sup> showing unequal properties and biological activity.<sup>15</sup> Therefore, producing and isolating homogeneously glycosylated products remain a necessary and delicate task to be carried out to achieve better biomedical efficacy and avoid antigenic reactions.<sup>16,17</sup> Recombinant monoclonal antibodies (mAbs) are the dominant class of *N*-glycoprotein therapeutics to date and the fastest growing class of biopharmaceuticals, with a global market valued around tens of USD billion and expected to reach hundreds of USD billion by 2024.<sup>18</sup> More than sixty mAbs and fusion molecules, against over thirty molecular targets linked to cancer, autoimmune and cardiovascular diseases, have received the USFDA approval since the 80s.<sup>19</sup> Notwithstanding their significant employment in many disease treatments and the evolving technologies permitting a finer regulation of the mAbs molecular features (i.e., post-translational modifications; e.g., *N*-glycosylation), even fully human mAbs, such as the current market best-seller adalimumab<sup>®</sup>, still show immunogenicity.<sup>20</sup> Recent studies,<sup>21,22</sup> analysing evidences of benefits on survival and quality of life gained in association with the use of USFDA-approved cancer treatments (including mAbs),

concluded that the extent of these benefits is in fact only marginal, and only a small proportion of these drugs showed unequivocal enhancement of the quality of life or overall survival. These studies significantly suggested, in addition to the possibility of reconsidering some parameters of the drug approval process towards more empirically-driven verifications, the necessity to further fine-tune mAbs production and analytical quality control, towards the development of more efficient and safer *N*-glycotherapeutics. Despite these limitations, reported examples of glycomolecules and therapeutic glycoproteins demonstrate that *N*-glycan-based therapeutics are already a viable and concrete option in biomedicine, in addition to their above introduced value as interesting targets for basic science investigations. Proposed examples thereby highlight *N*-glycans and *N*-glycoproteins as a substantially interesting, biomedically promising, and highly profitable classes of biomolecules.

## 1.2 *N*-GLYCOSYLATION IN NEUROCHEMISTRY.

**1.2.1 *N*-glycosylation in vertebrates.** In vertebrates, *N*-glycosylation is one of the most frequent, abundant and ubiquitous post-translational protein modifications<sup>23</sup> and, although not being a prerequisite for the viability of mammalian cultured cells,<sup>24</sup> defects in its wild-type (WT) pattern result in mice embryonic lethality.<sup>25,26</sup> Human embryos with complete defects in one step of glycosylation do not usually survive, and deficiencies in the assembly of the *N*-glycans precursor in the endoplasmic reticulum (ER) and abnormal *N*-glycan processing, concretising in mis-glycosylated proteins, are the basic mechanisms of type I and II congenital disorders of glycosylation, which imply a variety of severe developmental and motor deficits, along with serious organ and tissue problems.<sup>27</sup> Mammalian glycans are assembled from a limited subset of monosaccharides (**Fig. 1.2**): Fucose (Fuc), galactose (Gal), glucose (Glc), *N*-acetylgalactosamine (GalNAc), *N*-acetylglucosamine (GlcNAc), glucuronic acid (GlcA), iduronic acid (IdoA), mannose (Man), sialic acids (*N*-acetylneuraminic acid; NeuAc; *N*-glycolylneuraminic acid, NeuGc; and 2-keto-3-deoxy-D-glycero-D-galacto-nononic acid, KDN), and xylose (Xyl).

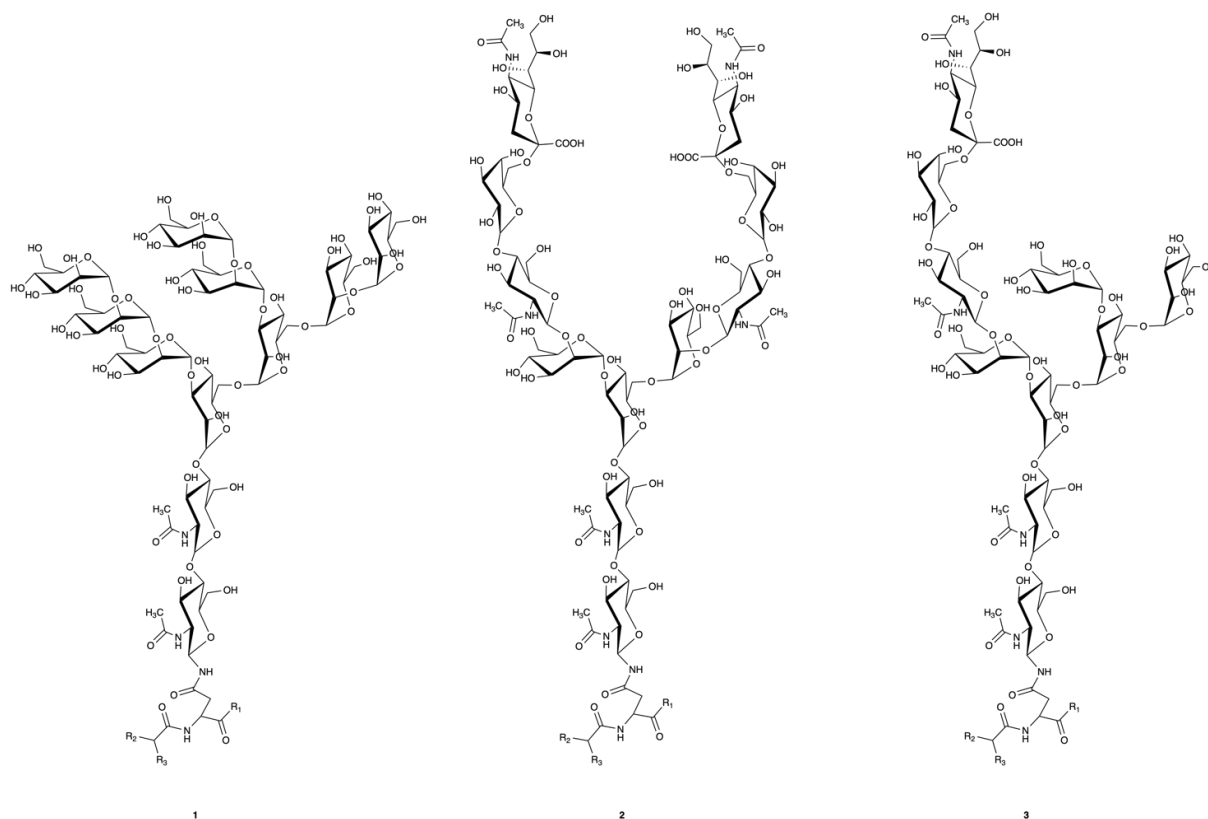




**Fig. 1.2.** Monosaccharides used to assemble mammalian glycans. Monosaccharide structures are reported with the anomeric configuration mainly present in mammalian biology (1-7, 10-12 are found in *N*-glycans; 8, 9 are found in glycosaminoglycans and *O*-glycans).<sup>28</sup> **1.**  $\alpha$ -D-glucose. **2.**  $\beta$ -D-galactose. **3.**  $\alpha$ -D-mannose. **4.**  $\alpha$ -L-fucose. **5.**  $\beta$ -D-*N*-acetylglucosamine. **6.**  $\beta$ -D-*N*-acetylgalactosamine. **7.**  $\beta$ -glucuronic acid. **8.**  $\beta$ -iduronic acid. **9.**  $\beta$ -xylose. **10.** *N*-acetylneuraminic acid. **11.** 2-keto-3-deoxy-D-glycero-D-galacto-nononic acid. **12.** *N*-glycolylneuraminic acid.

All *N*-glycans share a common core structure (Man $\alpha$ 1-3(Man $\alpha$ 1-6)Man $\beta$ 1-4GlcNAc $\beta$ 1-4GlcNAc $\beta$ 1-Asn), which precursor is synthesised in the ER on a polyisoprenoid lipid, and then transferred to nascent proteins (usually on a canonical, but not unique, glycosylation sequon: *N*-X<sub>+1</sub>-S/T<sub>+2</sub>, where X cannot be Pro), successively undergoing various modifications within the ER and the Golgi complex, to acquire the final chemical architecture. *N*-glycans can be divided into three main groups: oligomannose *N*-glycans, in which only Man residues extend the core; complex *N*-glycans, in which “antennae” initiated by GlcNAc extend the core; and hybrid *N*-glycans, in which Man extends the Man $\alpha$ 1-6 arm of the core, and one or two GlcNAc extend the Man $\alpha$ 1-3 arm (**Fig. 1.3**).





**Fig. 1.3.** Exemplifying chemical structures of the three main classes of *N*-glycans. **1.** Oligomannose. **2.** Complex. **3.** Hybrid.

The number of glycan determinants in the human glycome is estimated to be more than 7000 (700 proteins required to generate its full diversity), of which  $\sim 3000$  belong to *N/O*-linked glycans and glycolipids,<sup>29</sup> and over 2000 *N*-glycan structures were experimentally determined.<sup>30</sup> However, these numbers likely represent an underestimation, since the real *N*-glycan complexity of a cell repertoire, let alone an organism, is given by intricate biosynthetic pathways, in which multiple enzymes potentially compete for the same glycan substrate, giving rise to a vast ensemble of differentially branched glycan structures, alternatively present even at the same glycosylation site of otherwise identical proteins (glycoforms), a phenomenon known as “microheterogeneity” (site-specific glycan structure).<sup>31,32</sup> To further complicate one organism glycosylation profile there is another phenomenon, called “macroheterogeneity” (glycosylation site occupancy), which is the structural diversity arising due to the absence or presence of a glycan at one protein glycosylation site. This is because glycosylation pathways are inherently inefficient, especially the initial transfer of the oligosaccharidic core to the nascent protein (which could be *N*-glycosylated even if not presenting the canonical glycosylation sequon), and this inefficiency shapes an additional layer of structural diversity in mature glycoproteins.<sup>33</sup> In addition to differences in monosaccharide compositions, glycan diversity is further broadened by the monomer anomeric state ( $\alpha$  or  $\beta$ ), type of

linkage (e.g., 1-3, 1-4; 2-3, 2-6, 2-8), branching, and chemical modifications (e.g., phosphorylation, sulfation, acetylation),<sup>34</sup> suggesting a potentially huge number of possible combinations, creating a complex and dynamic system which reflects the actual metabolic state of the cell.<sup>35</sup> Despite this overwhelming scenario, the analysis of *N*-glycans is still a feasible task. In fact, the number of glycosyltransferases is limited, and this severely contains the ensemble of occurring structures. For example, the analysis of free oligosaccharides in human milk, carried out with liquid chromatography coupled with mass spectrometry (LC-MS) approaches, showed that rather than the potentially millions of structures thought to be present, a single mother's milk contained approximately between 23 and 130 structures, and five different mothers produced less than 500 different structures in total.<sup>36</sup> In another work, the creation and investigation of a neural network of potential oligosaccharides afforded the different compositions that could be produced, and the estimated size of the serum *N*-glycome: employing standard monosaccharides found in humans, less than 500 possible compositions were highlighted as plausible.<sup>37</sup> Furthermore, the resulting glycosylation pattern in one tissue appears to be phenotypically conserved: the serum glycomic profile of an individual is highly reproducible, in regards to *N*-glycan structures and their abundances.<sup>38</sup> Even the *N*-glycoprofile of more complex tissues (e.g., brain) of different species is not so diverse (e.g., including, but not limited to, rodents<sup>39</sup>), and main differences are observed in the *N*-glycan relative abundances rather than in *N*-glycan structural differences (e.g., rodents, dogs, primates, humans; Klarić T., Gudelj I., unpublished work). These works and evidences suggest that, amongst the almost infinite possible monosaccharide combinations within *N*-glycans, only some are really present in biological samples, due to biological constraints. This suggestion depicts a much more experimentally-friendly scenario, in which the glycome is in fact limited and characterizable in its entirety using annotated glycan libraries, some of which have been already started to be compiled.<sup>37,40,41</sup> The best known function of protein *N*-glycosylation in eukaryotes is protein folding and quality control within the cellular secretory pathway,<sup>31</sup> but *N*-glycans are implicated in a full plethora of other cellular events, ranging from the interactions with the extracellular microenvironment, providing cues mediating cell adhesion and signalling, through the alteration of the dynamics of glycoprotein endocytosis and cell surface half-life,<sup>42</sup> to the modulation of macromolecule interactions and pathogen infection.<sup>43,44</sup> The “glycode”<sup>45</sup> is thus a complex set of information manoeuvring many vital cellular aspects, recognised as being the third alphabet of life,<sup>46,47</sup> with *N*-glycans representing a substantial part of its biological words.

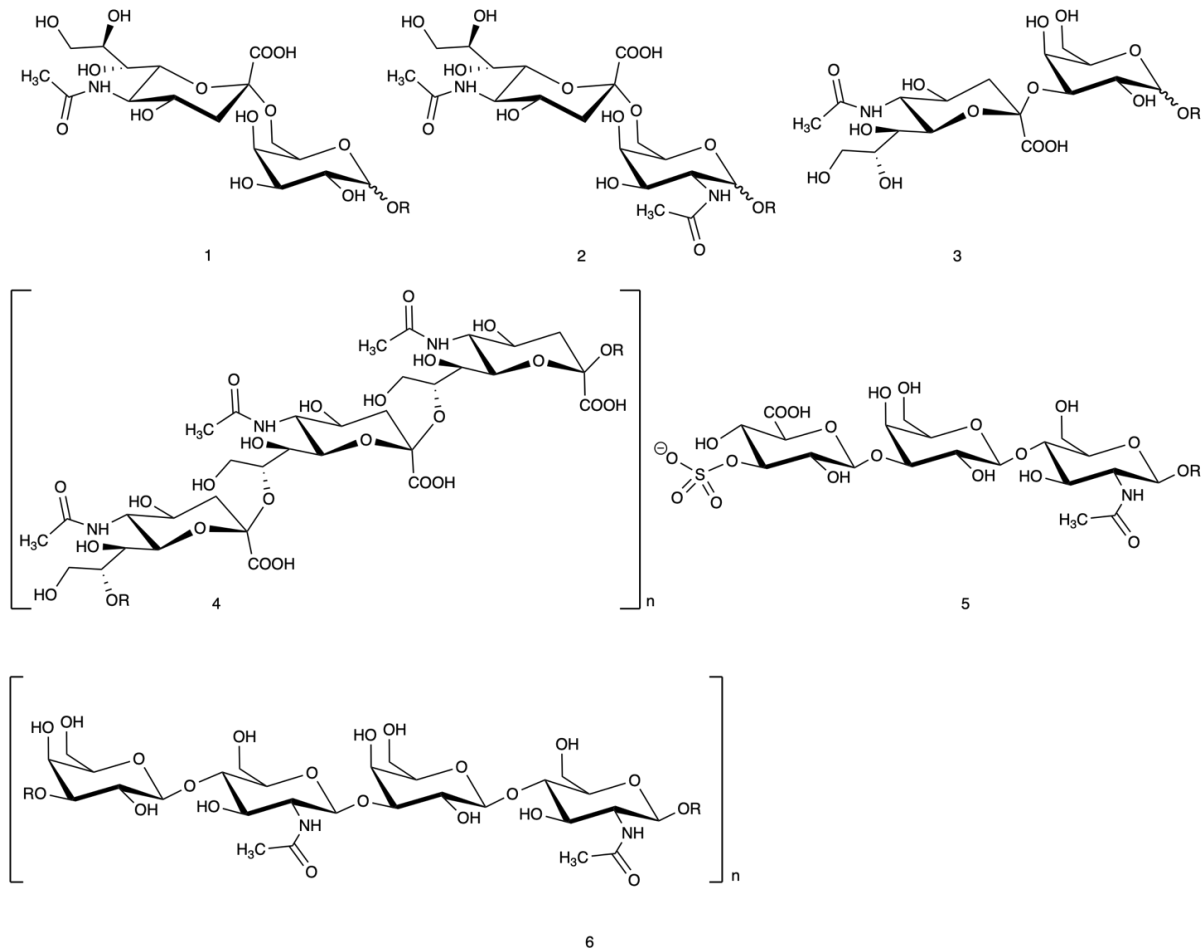
**1.2.2 *N*-glycosylation in the nervous system.** A growing body of evidences is highlighting *N*-glycosylation crucial involvement within the nervous system, where it influences a plethora of aspects of brain development and physiology, such as cell adhesion, axonal targeting, synaptic

transmission and excitability.<sup>48,49</sup> Furthermore, many glycosylation disorders impact the central nervous system (CNS)<sup>50</sup> and *N*-glycosylation alterations appear to play an important role in diverse neuropathies,<sup>51</sup> like Alzheimer's,<sup>52</sup> Parkinson's,<sup>53</sup> and Prion<sup>54</sup> diseases among others. In addition, defects in *N*-glycosylation result in remarkable neurological abnormalities at birth and during childhood, as demonstrated by the studies on human congenital disorders of glycosylation.<sup>55</sup> Although the roles of *N*-glycosylation in guiding protein folding are fairly known, *N*-glycans mechanisms outside the cell are still poorly understood. These *N*-glycosylation mechanisms, as stated above, are in fact complex, pleiotropic and dependent on the metabolic state of the cell, and therefore require, along with preliminary investigations carried out with *ex vivo* screenings, *in vivo* analyses to be fully addressed. In this context, the genetic inactivation of glycosyltransferase genes in cells and mice has been fundamental to unveil the importance of *N*-glycosylation in the pathophysiology of the nervous system.<sup>56</sup>

**1.2.3 *N*-glycosylation in neural development.** Although the brain-targeted inactivation of the enzyme  $\beta$ -1,6-*N*-acetylglucosaminyltransferase (GlcNAcT)-I (gene MGAT1), required for the biosynthesis of hybrid and complex *N*-glycans in the medial Golgi complex, resulted in severe neurological phenotypes and early postnatal death in mice,<sup>57</sup> the detailed analysis of *N*-glycosylation mutants with defects in the core structure is complicated by the above-mentioned complexity and pleiotropy of mammalian *N*-glycosylation. A more informative approach is the generation of *N*-glycosylation knockout mutants in which *N*-glycan terminal epitopes are altered, towards more nuanced, specialised, and thus easier to study cellular effects. In this context, a clear example is given by studies conducted to unveil the remarkable role of sialic acids (SA) in CNS development. SA are a vast family of organic acids, comprising nearly 50 members which are derivatives of the structures displayed in **Fig. 1.2** (10-12). Neuraminic acid, another member of SA carrying a free amine at C-5, can also exist in glycosidic linkages, being however rare in nature. NeuAc is the most common structure in vertebrates, along with NeuGc which, however, is not present in the CNS, and suggested to be toxic for vertebrate neural systems.<sup>58,59</sup> From a chemical point of view, the number and diversity of functional moieties carried by these molecules is remarkable: their basic structure comprises a carboxyl group (a strong acid, due to the anomeric position; pKa  $\sim$ 2.6), an exocyclic glycerol chain (C7, C8 and C9, each carrying a hydroxyl group) suitable for hydrogen bonding, an *N*-acetyl group (NeuAc) which can mediate hydrophobic interactions and be changed to a hydroxyl (KDN) or *N*-glycolyl group (NeuGc) to enhance the molecule hydrophilic properties. Each of these moieties can participate in the binding features of SA-containing glycans. Furthermore, SA as subjected to various additional substitutions on the hydroxyl groups at C-4, C-7, C-8, and C-9: *O*-acetylation, *O*-methylation, *O*-sulphation or *O*-

lactylation, extending the already wide gamut of their chemical potentialities. Further complexity arises from the fact that the carboxylate group at C-1 can condense with nearby sugars hydroxyl groups or with a free amino group at C-5, forming an uncharged lacton or lactam, respectively. Ultimately, different linkages at terminal positions of *N*-glycans ( $\alpha$ 2–3,  $\alpha$ 2–6,  $\alpha$ 2–8, **Fig. 1.4**, 1-4) in addition to the above-mentioned chemical modifications, make them very good candidates to shape the biochemical information for glycan-protein, cell-cell, and pathogen-cell interactions. SA are sharp and versatile molecular tools, among the most rapidly evolving classes of glycans in nature, which ensemble in a given biological system has deserved its own definition of “sialome”.<sup>60</sup> SA occur in the cell as monosialyl residues capping the branches of *N*-glycans (**Fig. 1.3**, 2-3), but often also as polymers, in the form of oligo and polysialic acids (PSA) on glycoproteins (**Fig. 1.4**, 4). In particular, PSA is one of the most biologically important glycoprotein epitope in vertebrates, it is conserved from the sea urchin to humans,<sup>61</sup> and represents a good example of *N*-glycan terminal epitope involved in neuronal development. PSA is a unique, linear homopolymer of  $\alpha$ 2–8 linked SA (Neu5Ac $\alpha$ 2-8)<sub>n</sub> (**Fig. 1.4**, 4), added mostly, but not only,<sup>61</sup> on the neural cell adhesion molecule (NCAM, a glycoprotein expressed on the surface of neurons, glia and skeletal muscles, critical for cell-cell interactions and cognitive functions) on the termini of two specific *N*-glycans, and it regulates brain development, neurite outgrowth and targeting, while also affecting synaptic plasticity, memory and learning.<sup>62–64</sup> PSA importance in neural development was demonstrated through the genetic deletions of ST8Sia II and IV polysialyltransferases in mice, which showed severe phenotypes in response, among which impaired movements and forebrain anatomical disorganisation associated with cellular apoptosis, leading to death within a few weeks.<sup>65,66</sup> PSA was found to be involved in the myelination process and the migration and differentiation of neural and glial precursor cells, and its deficit led to a decreased expression of Pax6, an important actor for cellular migration processes and for the differentiation of neural precursors during cortex development.<sup>67</sup> Another interesting example of *N*-glycan epitope involved in neural development is poly-*N*-acetylactosamine (poly-LacNAc, PLN), a polymer constituted by repeating units of the common disaccharide (Gal $\beta$ 1,4-GlcNAc $\beta$ 1,3)<sub>n</sub> (**Fig. 1.4**, 6), which synthesis, extension and branching are cooperatively regulated by the enzymes  $\beta$ 1,6-branching glycosyltransferase GCNT2 and glycosyltransferase  $\beta$ 3GnT2, which expression in the nervous system are restricted to the olfactory epithelium and other sensory ganglia.<sup>68</sup> Genetic deletion of the  $\beta$ 3GnT2 glycotransferase in mice led to multiple abnormalities in the development of both the main olfactory system (olfactory sensory neurons, OSN) and accessory olfactory system (chemosensory neurons of the vomeronasal organ, VNO), including axon guidance, functional connectivity defects and neuronal survival.<sup>69,70</sup> In the case of OSN in the main olfactory system, neural deficits are associated with

PLN hypoglycosylation of adenylyl cyclase 3, impairing the enzyme localisation and activity, leading to a decrement in the concentration of cAMP, which is a key signalling molecule in olfactory axon targeting.<sup>69</sup> The human natural killer-1 glycan antigen (HNK-1;  $\text{SO}_3\text{-3GlcA}\beta\text{1-3Gal}\beta\text{1-4GlcNAc}$ , **Fig. 1.4**, 5), was originally identified as a marker of human natural killer cells (CD57 in immunology)<sup>71</sup> and later found to be predominantly expressed in the nervous system on glycoproteins (*N*- and *O*-glycans) and glycolipids, being functionally involved in neural cell-adhesion, recognition and migration.<sup>72</sup> The HNK-1 antigen is widely expressed in CNS regions associated with neurogenesis and synaptic plasticity, such as the dentate gyrus of the hippocampus, perineuronal nets and in neural stem cells, where it has a direct impact on synaptic plasticity and higher brain functions such as spatial learning and memory formation.<sup>73-76</sup> The GlcAT-P glucuronyltransferase is a key enzyme in the HNK-1 glycan antigen biosynthesis: its deletion caused abnormal dendritic spine morphogenesis in early postnatal mice and in cultured hippocampal neurons. Although HNK-1 was suggested to regulate synaptogenesis and post-synaptic function through the ligand-gated channel AMPA-type ( $\alpha$ -amino-3-hydroxy-5-methyl-4-isoxazolepropionic acid type) glutamate receptor subunit GluR2, and post-synaptic protein PSD-95, this glycan epitope is widely expressed on a series of cell adhesion (e.g., NCAM, L1, MAG) and extracellular molecules (e.g., tenascin-R, phosphacan) in the nervous system, which are almost completely deleted of it in GlcAT-P-deficient mice. Therefore, the effects seen on GlcAT-P-deficient mice, could involve multiple HNK-1 bearing actors, making still not completely clear what are the precise molecular mechanisms of spine formation and synaptic plasticity regulated by the HNK-1 glycoepitope.<sup>77</sup> In this context, a recent work suggested that tenascin-C (TNC), an extracellular matrix protein that regulates neurite outgrowth by interacting with the GPI-anchored protein contactin-1 (CNTN), is one of the major HNK-1 carrier proteins in the embryonic brain, and that the HNK-1 epitope is a key modifier of TNC and CNTN in the regulation of embryonic brain development.<sup>78</sup> The authors showed that the presence of the HNK-1 antigen on the C domain of TNC promoted neurite outgrowth, that this signal was mediated by the HNK-1-expressing neuronal receptor CNTN, and that neurons lacking the glucuronyltransferases GlcAT-P and GlcAT-S, thus defective in neuronal HNK-1 expression, did not show neurite-promoting activity.



**Fig. 1.4.** *N*-glycan sialoepitopes involved in neural development. **1.** NeuAc $\alpha$ 2-6Gal (ST6GAL, 2 coding genes). **2.** NeuAc $\alpha$ 2-6GalNAc (ST6GALNAc, 6 coding genes). **3.** NeuAc $\alpha$ 2-3Gal (ST3GAL, 6 coding genes). **4.** (NeuAc $\alpha$ 2-8NeuAc) $_n$  (PSA, ST8SIA, 6 coding genes). **5.** -SO $_3$ -3GlcA $\beta$ 1-3Gal $\beta$ 1-4GlcNAc (HNK-1 antigen). **6.** (Gal $\beta$ 1,4-GlcNAc $\beta$ 1,3) $_n$  PLN.

**1.2.4 *N*-glycosylation in neural physiology.** *N*-glycosylation affects the functioning of various actors involved in synaptic-related processes, with multifaceted effects on synaptic physiology. The HNK-1 antigen (**Fig. 1.4, 5**), discussed in the previous section, is suggested to be important for synaptic functions: genetic inactivation of enzymes involved in its biosynthesis (GlcAT-P, sulfotransferase HNK-1 ST, and  $\beta$ 4-galactosyltransferase-2) caused neurological phenotypes in mice, comprising neural electrophysiological abnormalities, defects in neural plasticity, learning and memory, and reduced long-term potentiation of hippocampal synapses.<sup>75,79-81</sup> The HNK-1 glycan epitope was found to downregulate the endocytosis of the AMPA-type glutamate receptor subunit GluR2, to stabilise its expression on neuronal plasma membranes, and to possibly regulate the stability of GluR2 at synaptic connections by promoting its interactions with *N*-cadherin.<sup>77</sup> Other neurotransmitter receptors, that function as ligand-gated ion channels (LICs, commonly referred to as ionotropic receptors), mediating the communication between neurons and at neuromuscular junctions, are also commonly glycosylated on their extracellular



domain. Ionotropic glutamate receptors (iGluRs), a family encompassing large subfamilies of AMPA, kainate, and NMDA receptors, mediating fast synaptic transmission at the majority of mammalian excitatory synapses, and being involved in synaptic plasticity and extrasynaptic neuronal modulation,<sup>82</sup> are *N*-glycosylated. *N*-glycosylation does not seem to be generally required for iGluRs function, since the biosynthesis, the transport, and subunit assembly of functional receptors on the cell membrane are not significantly affected by the lack of glycosylation.<sup>83–85</sup> Furthermore, crystallisation studies on kainate receptors showed that *N*-glycosylation is not directly involved in ligand binding,<sup>86</sup> but *N*-glycans do affect desensitisation of these kind of receptors.<sup>87</sup> Nicotinic acetylcholine receptors (nAChRs) are another class of LICs bearing *N*-linked carbohydrates and belonging to the pentameric ligand-gated superfamily of ion channels, also including glycine, serotonin and  $\gamma$ -aminobutyric acid (GABA) receptors.<sup>88</sup> These receptors are involved in several neural functions, including the processing of sensory information, along with learning and memory, and regulate post-synaptic responses at neuromuscular junctions and brain synaptic connections.<sup>89</sup> The functional properties of these receptors are regulated by *N*-glycosylation: it promotes the local folding of some nAChRs functional domains,<sup>90,91</sup> it is implicated in receptor conductance and desensitisation,<sup>92</sup> and it influences their surface expression and cholinergic agonist-dependent gating.<sup>93,94</sup> Another *N*-glycosylated neural actor is synaptic vesicle protein 2 (SV2), which is ubiquitously present at vertebrate synapses, it is suggested to mediate a maturation step of primed synaptic vesicles, and is critical for synaptic physiology, since its targeted gene inactivation in mice caused postnatal lethality due to severe seizures in the brain, but without any sign of developmental defects.<sup>95</sup> There are three known SV2 isoforms, all harbouring *N*-glycans in their intravesicular loop, and the removal of all the *N*-glycosylation sites on SV2a (the most abundant isoform), inhibits its function and synaptic targeting, suggesting that SV2a *N*-glycans are important towards the protein proper folding and trafficking within the neuron.<sup>96</sup> Differently, the removal of individual *N*-glycosylation sites on SV2a, demonstrated that single *N*-glycans are partially dispensable and seemingly redundant for the proper sorting of this protein to synaptic vesicles.<sup>97</sup> In the same study, two other major glycoproteins of synaptic vesicles were taken into consideration, synaptogamin 1 and synaptophysin, and the results highlighted how *N*-glycans can play highly individualised regulatory roles, tailored for distinct glycoprotein targets dedicated to specific neural functions: *N*-glycosylation is completely dispensable for the sorting of synaptogamin 1, but essential for the synaptic localisation and function of synaptophysin. *N*-glycosylation can also alter ion channels biophysical properties influencing channel gating, as in the case of the agonist-mediated regulation of the transient receptor potential Vanilloid Type 1 (TRPV1, also known as capsaicin receptor), an unspecific cation channel functioning as a key

sensor of pain-sensing nerves,<sup>98</sup> and belonging to a large family of transient receptor potential (TRP) ion channels, playing essential roles in sensor physiology. Human embryonic kidney cells (HEK-293) expressing a non-glycosylated version of the receptor (TRPV1-N640T), correctly displayed it on the plasma membrane but were rapidly desensitised, after capsaicin-evoked increments in intracellular calcium, in comparison to WT TRPV1 HEK-293. This underlined TRPV1 *N*-glycosylation as a fundamental chemical determinant of TRPV1 capsaicin-evoked desensitization and ionic permeability, and suggested that pathophysiological alterations in TRPV1 glycosylation can affect the receptor function and, thus, pain transmission.<sup>99</sup> Another example in this context is given by the TRPM8 receptor, also known as the cold and menthol receptor 1 (CMR1), which is expressed in sensory neurons that respond to cold and cooling compounds (such as menthol). TRPM8 has been heterologously expressed in HEK-293 cells as both WT and unglycosylated mutant (TRPM8-N934Q), the latter showing a shift in the threshold of temperature activation and a reduced response to menthol and cold stimuli, due to a shift in the receptor voltage-dependent activation towards more positive potentials. This again showed the important roles that *N*-glycosylation can play in affecting the biophysical properties of receptors expressed in the nervous system.<sup>100</sup> *N*-glycosylation is also able to influence neural cell excitability by modulating the expression and physiological response of voltage-gated ion channels, which regulate the membrane permeability of certain cations like Na<sup>+</sup>, K<sup>+</sup> and Ca<sup>2+</sup> and contribute to directionally propagate the electric signals.<sup>101-105</sup> In this context, the importance of SA<sup>106</sup> (**Fig. 1.2-1.4**) in proper protein functioning is highlighted once again: Na<sup>+</sup> channels in vertebrates are heavily decorated with SA<sup>107</sup> and sialylated carbohydrate chains are negatively charged and can participate in electrostatic interactions with ions and other charged groups exposed on the cell surface, being also substantially present in the vicinity of the channel pore. Often this multiple SA are organised in the above-mentioned PSA molecule (**Fig. 1.4, 4**), and its involvement in the regulation of voltage-gated Na<sup>+</sup> channels was unveiled by studies conducted on mouse mutant cardiomyocytes, with the ST8Sia II polysialyltransferase genetically inactivated. This enzyme is involved in PSA biosynthesis and its inactivation caused defects in atrial myocytes excitability and channel gating, with abnormal action potentials characterised by altered waveforms with a delayed peak, considerable depolarising shifts of the gating curves, and compromised fast inactivation.<sup>103</sup> The role of channel sialylation in the nervous system was also investigated with murine models, by inhibiting the animal endogenous neuraminidase supply or treating the animals with exogenous neuraminidase, altering the SA physiological pattern in the brain: glycoprotein sialylation was found to profoundly affect the excitability of neural networks, also influencing the threshold for seizures in kindling epilepsy models.<sup>108,109</sup> Although further studies are still necessary to fully



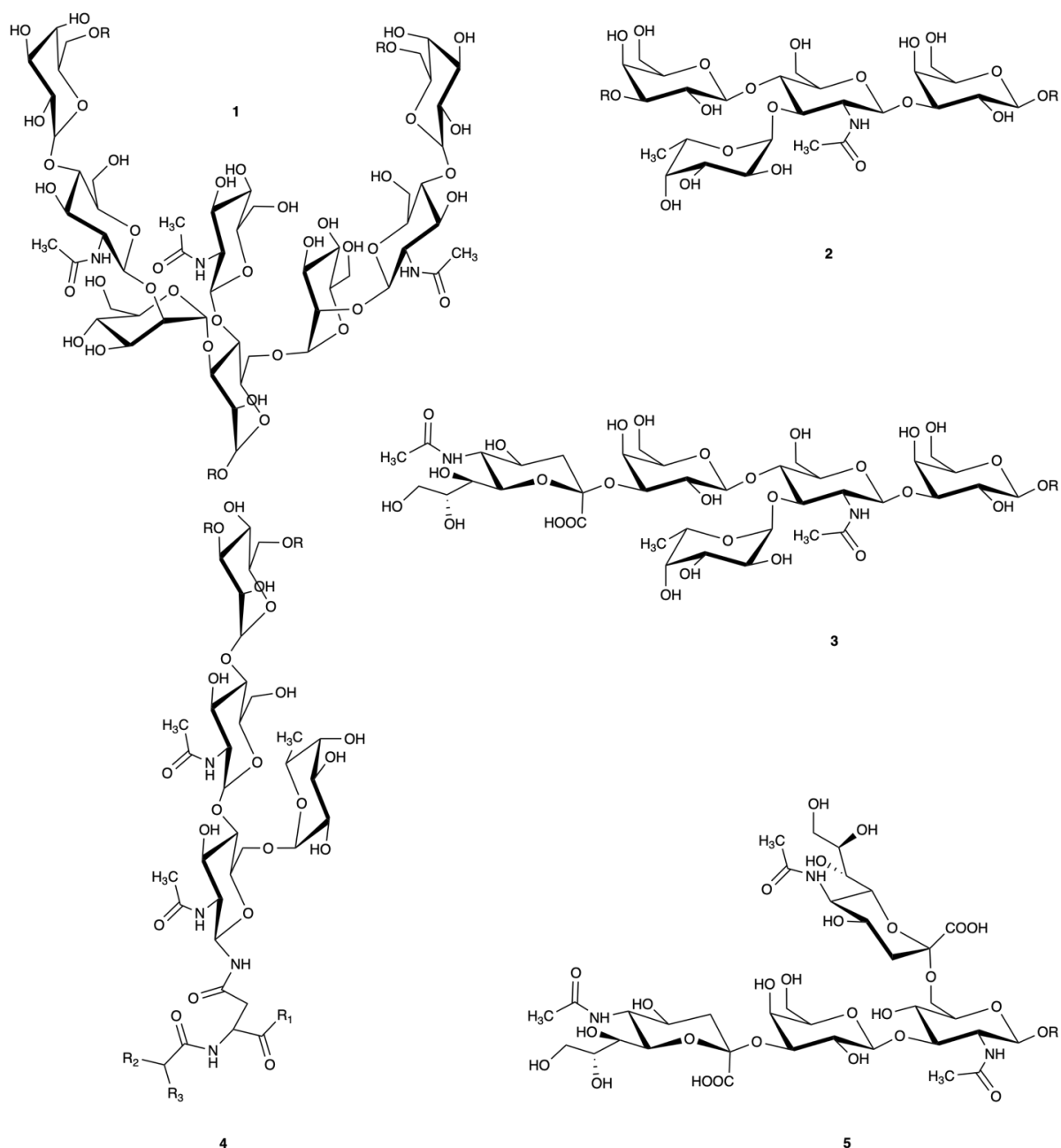
comprehend the extent and nuances of the *N*-glycosylation effects on neural glycoproteins, the examples presented within this section clearly demonstrate that *N*-glycans are important actors of vertebrate nervous system physiology and cannot be overlooked when dealing with neurobiochemical systems.

**1.2.5 *N*-glycosylation in neural pathology.** In the light of the aforementioned examples of *N*-glycans relevance in vertebrate nervous system physiology, it is not surprising that major *N*-glycosylation alterations have been observed in various CNS pathologies. For instance, considering Alzheimer's disease, lectin-based blotting and immunostaining experiments on human samples have highlighted a decrease in SA and PSA-NCAM molecules,<sup>110,111</sup> and anion-exchange column chromatography investigations led to the discovery of a non-physiological increment in high mannose and sialylated bi- and triantennary-type glycans on Tau proteins.<sup>112</sup> Considering Huntington disease, mass spectrometry (MS) analyses of mouse brain showed non-physiological increase of different *N*-glycans, among which core-fucosylated, bi-antennary sialylated, and bisecting GlcNAc (GlcNAc in a  $\beta$ 1-4-linkage to the mannose residue at the base of the trimannosyl core of the *N*-glycan, **Fig. 1.5**, 1) ones.<sup>113</sup> In amyotrophic lateral sclerosis, HPLC and MALDI-TOF-MS analyses on human sera showed an increase in sialylated glycan expression and a decrease of core-fucosylated glycans harboured on IgGs,<sup>114</sup> while immunostaining experiments highlighted an increase in PSA-NCAM in samples from patients with multiple sclerosis.<sup>115</sup> A fair number of studies have discovered altered *N*-glycosylation patterns in patients with schizophrenia. HPLC investigations showed that tetra-antennary, tetra-sialylated glycans with a PLN extension, from low abundance serum proteins, displayed a 2-fold increase in serum from male schizophrenia patients; tri-antennary tri-sialylated glycans containing the sialyl Lewis X glycoepitope (**Fig. 1.5**, 2) were significantly increased in male schizophrenia patients, on both high and low abundance serum proteins; and the levels of bisecting and sialylated glycans in the cerebrospinal fluid showed a general down-regulation in schizophrenia patients and a 95% positive predictive power for distinguishing patients from controls.<sup>116</sup> Immunostaining experiments showed reduced PSA-NCAM in the great majority of schizophrenic brain hippocampi, suggesting an altered plasticity of this structure in a large proportion of schizophrenic brains.<sup>117</sup> Western Blot (WB) analyses on post-mortem tissue from the dorsolateral prefrontal and anterior cingulate cortices of patients with schizophrenia showed a decrease in glycan expression on excitatory amino acid transporters, suggesting an altered functioning of the protein with a decreased capacity for glutamate reuptake.<sup>118</sup> Other WB and lectin affinity assays highlighted alterations of *N*-linked high mannose and/or hybrid glycans on ionotropic glutamate receptor subtypes.<sup>119,120</sup> Brain cancers also display aberrant *N*-glycosylation profiles seemingly promoting the disease pathological effects. In Glioblastoma

multiforme (GMB), label-free quantitative MS investigations, lectin microarray, and multi-lectin chromatography, showed an increase in fucosylated *N*-glycans expressed on human and mouse cell surfaces.<sup>121,122</sup> Furthermore, immunostaining studies revealed an increased content of PSA-NCAM in glioma cell lines, suggesting PSA-NCAM as a valuable biomarker for the prognosis of GBM patients.<sup>123</sup> In the context of paediatric brain cancers (astrocytoma and ependymoma), a study<sup>124</sup> conducted using lectin staining displayed an increase in bisecting *N*-glycans, coherently with what was seen in other experimental tumour models, in which bisecting GlcNAc was correlated with tumour progression, thus suggesting that bisecting GlcNAc in paediatric brain tumours may have a potential relevance as a tumour marker.

**1.2.6 The *N*-glycosylation “brain-type” pattern.** A fair number of glyco(proteo)mics studies have investigated *N*-glycosylation patterns and their roles on immunoglobulins,<sup>125,126</sup> plasma samples,<sup>127</sup> and even blood,<sup>128</sup> although comparatively scarce work has been carried out on solid tissues which, mainly due to their higher complexity, still remain a fairly underexplored territory. Early studies from the 90s comprising brain *N*-glycan purification and analysis, delivered the first evidence of a “brain-type” glycosylation pattern, highlighting the main types and distribution of *N*-glycans in rodent brains. *Wing et al.* generated a “library” of *N*-linked glycans from murine brain and they found that it was dominated by anionic *N*-glycans (~85%) that were heterogeneous in character: sialylated *N*-glycans were identified after neuraminidase treatment (~30%), along with sulphated (methanolysis, ~25%), phosphorylated (aq. hydrofluoric acid treatment, ~30%), and a small part of neuraminidase/methanolysis/HF-resistant but anionic species, suggested to belong to the uronic acid family (e.g., glucuronic acid).<sup>129</sup> *Chen et al.*, reported that the percentage of neutral *N*-glycans in the rat brain was approximately 25%, in agreement with the above-mentioned data, and demonstrated that the neutral *N*-glycan profiles deriving from adult mouse and rat brain tissue were basically identical.<sup>39</sup> They also showed, using MALDI-MS, exoglycosidase sequencing followed by one or two-dimensional HPLC analysis, that the neutral *N*-glycan fraction was composed, in respect to the total n° of glycans, by oligomannosidic *N*-glycans (~15%), di/tri-antennary complex *N*-glycans (~6 and 1% respectively), and hybrid structures (~3%), with the latter two classes being uniformly  $\alpha(1-3)$  fucosylated on the outer-arm (Lewis X determinant, **Fig. 1.5, 2**) and  $\alpha(1-6)$ -core fucosylated (**Fig. 1.5, 4**), but also carrying a bisecting GlcNAc residue (**Fig. 1.5, 1**), even if in a less uniform way. The relative abundance of oligomannosidic *N*-glycans (**Fig. 1.3, 1**), highlighting their substantial expression in the CNS, is significative, since this class of *N*-glycan is not usually associated with glycoproteins belonging to other tissues (e.g., kidney, liver).<sup>130</sup> A fair share of the analysed di-antennary complex neutral *N*-glycans were found to be truncated, lacking the Gal residue entirely or without having the Man $\alpha(1-3)$ -arm of the trimannosyl core

substituted, an observation coherent with previous studies, where a high proportion of *N*-glycans with non-substituted terminal GlcNAc residues (consistent with truncation) was found, along with bisecting GlcNAc residues.<sup>130</sup> Hybrid *N*-glycans (**Fig. 1.3**, 3) were also found, presenting an outer-arm Fuc in the absence of core fucosylation, another unusual feature in respect to other tissues. No terminal GalNAc residues or  $\alpha(1-2)$ -fucosylation of terminal Gal were found in this study, even if the former modification was found in sheep brain<sup>131</sup> and the latter is suggested to be involved in memory consolidation,<sup>132–134</sup> though they might be present in the brain *N*-glycan anionic fraction or be enriched in some other species apart from rodents. An extension of this work investigated the sialylated *N*-glycans from rat brain (~30% of the total *N*-glycan population), using a combination of endoglycosidase and exoglycosidase sequencing, anion-exchange chromatography, normal and reverse phase HPLC, MALDI-MS, and GC-MS. Mono/di/tri/tetra-sialylated *N*-glycans showed abundances of approximately 12, 10, 7 and 7% respectively (in respect to the total *N*-glycans population), and PLN-containing and hybrid *N*-glycans were detected too. The authors found that  $\alpha(1-3)$ -outer-arm and  $\alpha(1-6)$ -core fucosylation (**Fig. 1.5**, 2, 4), along with bisecting GlcNAcs (**Fig. 1.5**, 1) were frequently present, and structural groups such as sialyl Lewis X (**Fig. 1.5**, 3) and NeuAc $\alpha$ 2-3Gal $\beta$ 1-4GlcNAc antennae (**Fig. 1.4**, 3) were common. Furthermore, a widespread distribution of  $\beta$ 1-3-linked Gal was observed, allowing for a high degree of sialylation, as exemplified by the finding of the di-sialyl Lewis C epitope [NeuAc $\alpha$ 2-3Gal $\beta$ 1-3(NeuAc $\alpha$ 2-6)GlcNAc] (**Fig. 1.5**, 5).<sup>135</sup> These results highlighted how the *N*-glycans derived from adult rat brain are able to display rich and peculiar arrays of NeuAc residues, in the form of multi-antennary, PLN-containing and hybrid structures, along with exploiting the unusual sialylation of GlcNAc residues,  $\beta$ 1-3-linked to sialylated Gals within the di-sialyl Lewis C epitope, furnishing tailored patterns of information readable by neural lectins.



**Fig. 1.5.** *N*-glycan features typical of the “brain-type” *N*-glycome. **1.** Bisecting GlcNAc (GlcNAc $\beta$ 1–4Man). **2.** Lewis X antigen [Gal $\beta$ 1–4(Fuc $\alpha$ 1–3)GlcNAc $\beta$ 1–3Gal]. **3.** Sialyl Lewis X antigen [NeuAc $\alpha$ 2–3Gal $\beta$ 1–4(Fuc $\alpha$ 1–3)GlcNAc $\beta$ 1–3Gal]. **4.** Core Fucose (Fuc $\alpha$ 1–6GlcNAc $\beta$ 1–Asn). **5.** Di-sialyl Lewis C antigen [NeuAc $\alpha$ 2–3Gal $\beta$ 1–3(NeuAc $\alpha$ 2–6)GlcNAc].

**1.2.7 *N*-glycosylation on a CNS protein target: the case of Neuroserpin.** Neuroserpin (serpin I1, NS) is an axonally-secreted protein firstly identified from cultured chicken dorsal root ganglion neurons,<sup>136</sup> and later assigned to the serpin superfamily, a large family of serine protease inhibitors sharing a universal conformation called the “serpin fold” (three  $\beta$ -sheets core surrounded by 8-9  $\alpha$ -helices).<sup>137</sup> Serpins inhibit serine proteases with a particular mechanism: an exposed structural feature of the protein, called the reactive centre loop (RCL), acts as a pseudo-substrate for the

target protease, which cleaves it, causing a conformational transition in which the protease is translocated from the top to the bottom of the serpin, while its RCL inserts into its  $\beta$ -sheet A, leading to the protease irreversible inactivation by molecular rearrangement.<sup>138</sup> The serpin-protease stable complex reveals new epitopes, thanks to the conformational changes taking place during the process, which are recognised by membrane receptors mediating the complex cellular internalisation towards degradation.<sup>139</sup> Human NS (UniProtKB ID. Q99574) is a 46 KDa glycoprotein of 410 amino acids predominantly expressed in the nervous system. NS main target is the tissue plasminogen activator (tPA),<sup>140-142</sup> in both the single and double chain forms, while other proteases such as urokinase plasminogen activator (uPA), trypsin, NGF- $\gamma$ , plasmin, and thrombin are also inhibited, even if to a moderately to substantially lesser extent.<sup>143,144</sup> NS has been found involved in several physiological processes, such as the regulation of emotional behaviour, synaptic plasticity, neural functioning and neuroprotection; on the other hand, it has been linked to several neuropathologies, such as familial encephalopathy with neuroserpin inclusion bodies (FENIB), Alzheimer's, schizophrenia, and brain cancer.<sup>145</sup> Amongst these, FENIB is the most widely studied: this serpinopathy is caused by point mutations in key residues of the enzyme serpin fold ( $\beta$ -sheet A for RCL insertion), causing structural instability, and making NS prone to form loop-sheet polymers. NS mutations cause multiple damages: firstly, they lower the concentration of available NS through polymers and inclusion bodies formation, therefore impairing NS physiological effects; secondly, NS polymers overwhelm the cellular metabolic system, ultimately leading to cell death due to the activation of the ER overload response;<sup>146</sup> in addition, NS mutants display secretory problems, which prevent the enzyme to be in place to exert its function; and finally, NS mutants are poorer tPA inhibitors in comparison to WT NS.<sup>147-149</sup> These effects concretise in a severe neurodegeneration of FENIB patients, which worsen with the progression of the disease, along with epileptic events probably due to the protein loss-of-function.<sup>149,150</sup> NS presents three glycosylation sites on N157, 321 and 401, an important feature for its maturation quality control, since NS mutants are directed to protein degradation through the ER-associated protein degradation (ERAD) system, thanks to the interactions with the OS-9 lectin, depending on the *N*-glycans at positions N157 and N321.<sup>151</sup> While it is logical to imagine a role for NS *N*-glycans in its folding, stability and functioning, little work has been done so far to investigate these aspects, both in physiological and pathological context. Moreover, a structural characterisation of NS *N*-glycan chemical structures is still lacking. *Moriconi et al.*,<sup>152</sup> demonstrated that N157 and N321 are glycosylated in human WT NS and in its pathogenic versions (e.g., G239E, S49P, S52R, H338R), while N401 usually does not harbour *N*-glycans. However, when the G392E NS mutant was analysed, the authors found a variable portion of it presenting the N401 site glycosylated in a

cell-type independent fashion. Furthermore, they showed that this different glycosylation pattern is not common in other NS polymerogenic mutants and that the portion of NS molecules bearing it increased with the mutant time of residence within the ER. The authors set out to investigate NS glycosylation role in the serpin polymerisation mechanism, by creating and analysing the N157A, N321A, and N157A/N321A WT and G392E mutants. Through SDS-PAGE, WB and ELISA approaches, they observed a small to moderate increase of polymer formation for the single mutants, augmented in the case of the double ones, suggesting that NS *N*-glycosylation plays a role in preventing aberrant polymer formation within the ER. The presence of the *N*-glycan chain at N401 on the G392E NS mutant increased with its time of permanence in the ER, and is specific to this mutant, since WT NS experimentally locked in the ER by the use of brefeldin A (an inhibitor of the normal ER-Golgi recycling, inducing accumulation of secretory proteins) did not show the modification. N401 glycosylation on G392E NS was then found to facilitate the mutant degradation when the proteasome machinery was inhibited, suggesting a role in the NS mutant clearance efficiency. The authors thus reported different roles for NS *N*-glycans: those at positions N157 and N321 protect against polymerisation, but not by stabilising the protein folding. In fact, the one displaying the strongest effect (N321) was tested for its ability to trigger the unfolded protein response (UPR, an ER stress response activated by the accumulation of misfolded proteins), by co-transfecting COS-7 cell lines with NS mutants and UPR reporter: no significant UPR activation was observed, indicating that the *N*-glycan is not required for the maintenance of NS globally folded state. Therefore, to explain the increased polymerisation behaviour of N321A and N157 NS, the authors ascribed the mutant effects to steric hindrance of intermolecular interactions or to stabilisation of a region with a tendency to increased conformational lability, particularly during polymerisation, as previously reported in analogous cases.<sup>153</sup> The addition of the *N*-glycan at position N401, a site present in most species and normally unmodified, was suggested to promote the mutant degradation when point mutations near this site cause local destabilisation, potentially leading to polymerisation. In this scenario, the *N*-glycan at position N401 would act as a reporter of NS C-terminal lability, even if this uncommon NS glycosylation was not associated with polymerisation across any of the other NS variants studied. This suggested that such C-terminal behaviour might not be critical for polymer formation in FENIB, indicating that different mechanisms might contribute through different extent towards the pathological effects of serpinopathies. Notwithstanding the relatively moderate and not so far clearly generalised effects of NS *N*-glycans, these experiments pointed out the involvement of these macromolecules in NS polymerisation behaviour, thus calling for further studies to fully unveil the seemingly fine glycochemical features of the process.



### 1.3 GLYCOANALYTICAL TOOLS FOR NEUROCHEMISTRY STUDIES.

In the light of the above-mentioned evidences of *N*-glycans involvement in a plethora of nervous system related pathophysiological processes and considering the complexity of *N*-glycan samples due to macro-/microheterogeneity, the necessity to have precise and robust glycoanalytical tools and methods for *N*-glycans thorough investigation is clearly crucial. Glycans have been in fact largely neglected in the large proteomic effort started decades ago,<sup>154</sup> arguably due to their high complexity, and glycoproteomic analyses still remain far from routine when compared to proteomics. It is thus imperative to develop efficient platforms for glycoanalysis, and to enrich the molecular toolkit of a glycoanalyst, in order to unveil reliable glycobiomarkers towards functional studies. In this context it is fundamental to consider the complete glycomolecular system to be investigated, which is always composed by the *N*-glycan(s) and the carrier glycoprotein, one influencing the properties of the other (e.g., protein folding affecting the exposure of the *N*-glycan on the surface and/or the *N*-glycan affecting the folding, and the biological recognition properties of the protein; different ensembles of *N*-glycans on the same glycoprotein site, creating glycoforms with possibly different folding/biochemical effects), in the context of a “breathing” object, which actual *in vivo* state is a function of the tissue metabolism. This translates into the necessity to perform *N*-glycoprotein analyses, which are more complicated than glycomic ones, because they involve the investigation of the glycan(s), the glycan-carrier protein, and its glycosylation site(s). Despite the need for comprehensive information regarding the glycomolecular system, glycomics data alone are certainly not useless, because they can often identify aberrant glycosylation changes in diseases and facilitate the characterization of glycoproteins, solving a part of the *N*-glycosylation puzzle, possibly simplifying and confirming the *N*-glycoproteomic analyses. Consequently, glycotools and glycoanalytical methods that facilitate precise and robust analysis of both neural *N*-glycans and their carrier *N*-glycoproteins presence, distribution and structure, are critical for advancing the understanding of *N*-glycosylation role in the CNS, and are also necessary for the discovery of new biomarkers for disease diagnosis and prognosis.

**1.3.1 Glycan binding proteins: detection and targeting in the CNS.** Lectins are one of the most basic though precious tools for glycobiology. Most of them originate from plants, but some also come from animals (e.g., snails) or mushrooms. Different lectins have different specificities towards *N*-glycan epitopes and usually show binding affinities ( $K_d$ ) of about 1-10  $\mu$ M (i.e., complex *N*-glycans), lowered to the nanomolar range for complex glycoconjugates with multiple determinants or multivalency. One well-known example is Concanavalin A (ConA), an  $\alpha$ -

mannose/ $\alpha$ -glucose-binding lectin that recognizes *N*-glycans and is not known to bind common *O*-glycans on animal cell glycoproteins. Its affinity is higher for oligomannose-type *N*-glycans than complex-type biantennary one, and it does not recognise more highly branched structures, though it can be used to bind hybrid ones. Other widely used lectins are *Lens culinaris* agglutinin that can be used for mannose residues; *Ricinus communis* agglutinin-I (RCA-I) which recognises  $\beta$ -linked terminal Gal; *Erythrina cristigalli* lectin (ECL), specific towards  $\beta$ 1-4-linked terminal Gal, and *Griffonia simplicifolia* agglutinin-I-B4 (GS-I-B4), binding  $\alpha$ 1-3-linked terminal Gal. There are also lectins able to discern the presence of Fuc residues: *Ulec europaeus* agglutini-I (UEA-I) and *Anguilla anguilla* agglutinin (AAA) recognise  $\alpha$ 1-2-linked Fuc present on Gal  $\beta$ 1-3/4-linked to GlcNAc; *Tetragonolobus purpureas* agglutinin-I (TPA) and *Aleuria aurantia* lectin (AAL) bind to  $\alpha$ 1-3-linked Fuc when carried by a GlcNAc residue eventually elongated by a Gal residue, without the addition of SA; AAA and AAL agglutinin and lectin are also capable of binding  $\alpha$ 1-4-linked Fuc, and the latter recognises  $\alpha$ 1-6-linked Fuc too; *Lens culinaris* agglutinin (LCA) and *Pisum sativum* agglutinin (pea lectin) are capable of binding di/tri-antennary-core  $\alpha$ 6-fucosylated complex-type *N*-glycans, but not tetra-antennary or 2,4-branched tri-antennary *N*-glycans. Similar to the latter examples, there are lectins specifically binding *N*-glycans features, like *Phaseolus vulgaris* erythroagglutinin (E-PHA), recognising bisected di/tri-antennary complex-type *N*-glycans; *Phaseolus vulgaris* leucoagglutinin (L-PHA), binding to 2,6-branched tri/tetra-antennary complex-type *N*-glycans; and *Datura stramonium* agglutinin (DSA), specific towards 2,4-branched tri/tetra-antennary complex-type *N*-glycans. There also lectins able to bind SA, of which importance and presence on CNS *N*-glycans has been previously discussed: wheat germ agglutinin (*Triticum vulgare*; WGA) and *Limax flavus* agglutinin (LFA) recognise SA ( $\alpha$ 2-3,  $\alpha$ 2-6 or  $\alpha$ 2-8-linked); *Maackia amurensis* leucoagglutinin (MAL) binds  $\alpha$ 2-3-linked SA when exposed on Gal residues  $\beta$ 1-4-linked to GlcNAc, but also 3-*O*-sulphated LacNAc residues; while *Maackia amurensis* erythroagglutinin (MAH) recognises 2-3-sialylated core 1 (sialylated T antigen), and *Sambucus nigra* agglutinin (SNA) is specific towards 6-*O*-sulphated LacNAc. Other lectins are useful towards linear and branched poly-*N*-acetyl lactosamine moieties, or terminal GlcNAc or GalNAc, making the glycoanalyst lectin-based toolkit rich and versatile.<sup>155</sup> Lectins have been exploited in the CNS for neuronal tracing applications, in which anatomical labelling approaches are used to understand the organisation of the brain, and where *in vivo* visibility is crucial for reliable high-resolution tracing of neuronal tracts. WGA capacity of binding neural cell-surface glycan epitopes such as SA and GlcNAc has been extensively exploited to study neuronal synapses and the wiring patterns among specific types of neurons that control the processing of the information in the brain.<sup>156</sup> More recently, a WGA tracer conjugated with an Alexa fluorophore was used for the same purpose within the mouse cerebellum, to mark and map

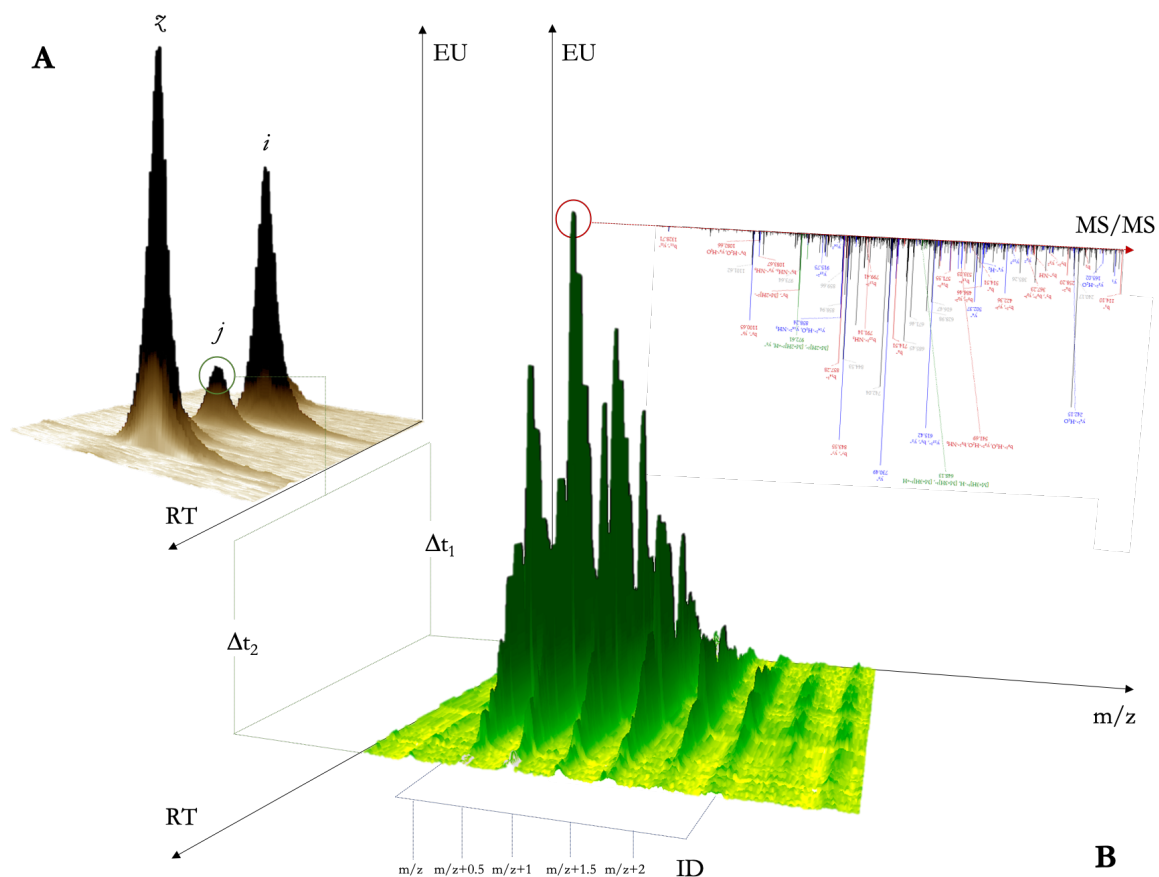


neural circuits controlling motor functions with high-resolution and specificity,<sup>157</sup> and for trans-neuronal tracing in other animal species, among which *Drosophila*<sup>158</sup> and rodent brains.<sup>159</sup> Lectins have been extensively used for neural glycoprofile and tracing, even if the generally exhibited low affinities, and the requirement of multivalency to achieve efficient binding, limit their suitability for glycomarker detection purposes. This limitation clearly highlights the necessity of finding/developing high-affinity glycan binding proteins, of which antibodies (Ab) represent one of the most promising candidates. Although Ab against protein antigens belonging to specific neural cell types have been developed and characterised,<sup>160</sup> efficient monoclonal anti-glycan Ab remain scarce, due to the challenging processes of development and selection.<sup>161</sup> IgM and IgG subtypes anti-glycan Ab obtained from mice are however fairly used in glycobiology, some of which are commercially available, while others only obtainable from individual laboratories or stock centres. Ab against mammalian antigens recognise mainly terminal glycan determinants, but a significant role in determining specificity and affinity is played by the context of the antigen expression (free glycan/glycoprotein/glycolipid), and the class of the glycan (N/O-linked), which means that also the non-terminal glycan architecture, and the global environment harbouring it, account for the recognition process. An example of anti-glycan Ab for CNS studies is given by the use of mAb735, which binds to the  $\alpha$ 2–8-linked SA chain of PSA (**Fig. 1.4**, 4). This Ab was used to demonstrate PSA involvement in the formation and maintenance of myelin. Immunofluorescence staining in transgenic mice models, using the above-mentioned Ab, showed that the down-regulation of PSA is a prerequisite for efficient myelination and myelination maintenance on mature oligodendrocytes.<sup>162</sup> More generally, glycan binding proteins can be used for glycan identification (e.g., using the right Ab to elucidate the presence of a specific glycan epitope in a biological system), purification (e.g., affinity chromatography, immunoprecipitation/lectin-induced precipitation, or WB approaches), characterisation of cell surface glycoconjugates (e.g., (immune)histochemistry techniques, flow cytometry with cell sorting, cell agglutination strategies), and to select cell lines expressing altered cell-surface glycans, among others.<sup>155</sup>

**1.3.2 Bioorthogonal chemical reporters for metabolic glycan labelling.** SA analogues (or biosynthetic precursors like *N*-acetylmannosamine) functionalised with chemically reactive and low cytotoxic groups (e.g., azide, thiol, alkene, alkyne, diazo, photo cross-linkers) are used to target and label sialoglycans in living animals, through a strategy called metabolic glycan labelling/engineering (MGL/MGE). In MGL, the SA promiscuous biosynthetic pathway, which enzymes tolerate subtle chemical differences of the substrates, is “hijacked” to make the animal expose sialoglycans modified with reactive functional groups, by feeding it with the biocompatible

but chemically modified sialo-analogue that is “naturally” incorporated in the final glycan. This biorthogonal chemistry approach grants the presence of reactive groups on the animal cell surface, that can be further *in vivo* bioconjugated with various functionalities (e.g., imaging probes or affinity tags), using a two-step chemical reporter strategy towards the desired investigation.<sup>163</sup> The methodology has been used for *in vivo* brain imaging,<sup>164–166</sup> even if the administration of sialo-analogues can be hampered by the presence of the blood-brain barrier (BBB). To overcome the problem, some strategies have been adopted, like further conjugating the sialo-analogues with neuroactive carriers such as choline, to exploit the carrier-mediated transport system at the BBB and reach the brain via simple tail intravenous injection in mice.<sup>166</sup> This approach is a powerful way to investigate one of the major components of the CNS *N*-glycome, exploitable to study the actual, *in vivo*, metabolic-state dependent sialoglycome composition.

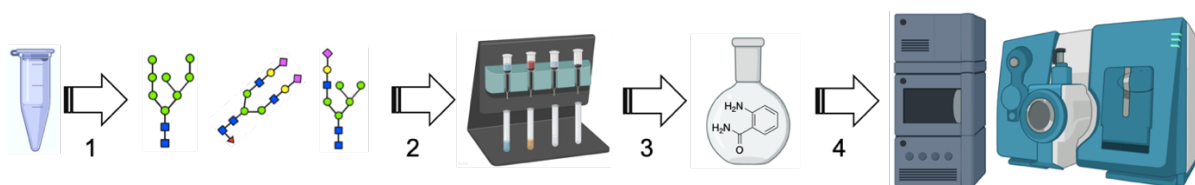
**1.3.3 Chromatography and MS-based techniques.** In addition to the investigation of the presence and distribution of *N*-glycans in neural tissues, a thorough chemical characterisation, by the point of view of monosaccharide composition, connectivity and stereochemistry, is necessary to fully unlock the chemical information within these structures. The chemical identification of the *N*-glycosylation pattern of a system (e.g., protein, cell or tissue) requires powerful analytical set-ups, able to separate and identify the *N*-glycan or *N*-glycoprotein components of the biological sample in the most possible accurate way. The most widely used technique to do so is probably liquid-chromatography coupled to (tandem) MS (LC-MS/MS), in which the chromatographic step, usually carried out employing (ultra)high-pressure liquid chromatography (HPLC/UPLC) analytical set-ups, furnishes the first two levels of information (intensity of the signal, e.g., fluorescence vs retention time of the analyte), while the detection step achieves two additional levels (identification of the mass of the analyte at a specific retention time, and fragmentation data deriving from the selected analyte, **Fig. 1.6**).



**Fig. 1.6.** Informational dimensions of a typical LC-MS/MS experiment. **A.** A 2D resolution is achieved in the chromatographic step, in which the analytes are separated according to their retention time (RT-axis) and the relative abundance of the chromatographic peaks ( $i$ ,  $j$ ,  $z$ ) containing the analyte(s) is measured using the chromatographic peak area, which is a function of the signal intensity (EU-axis = emission units; e.g., fluorescence) and the RT (i.e., peak elution window). **B.** An enlargement of peak  $j$  is shown (i.e., between  $\Delta t_1$  and  $\Delta t_2$ ): peak  $j$  is represented as an ideal peak in which only one analyte is contained. As the analytes are continuously eluted from the chromatographic step into the detection (MS), the instrument records the MS information ( $m/z$ , mass to charge ratio of the analyte), by acquiring an  $x$  number of spectra across the peak ( $x$  depends on the analytical set-up). MS scans of peak  $j$  are reported in green alongside the  $m/z$  axis; ID = isotopic distribution of the analyte contained in the  $j$  peak (i.e., in the example, a doubly charged ion). According to the experimental set-up of the spectrometer, a number of precursor ions (e.g., one, red circle) are chosen from the MS spectrum to undergo fragmentation, affording the MS/MS information necessary for the analyte structural determination.

These chromatographic analytical set-ups ensure a fair level of analyte separation within the analysed mixture, and the  $N$ -glycan labelling, achieved by using appropriate fluorophores (e.g., 2-Aminobenzamide, Procainamide), permits the analyte detection and boosts its ionisation, by augmenting its proton affinity, thus enhancing the structural identification via MS. As already introduced above,  $N$ -glycomics is the analysis of released  $N$ -glycans, without their protein carrier, while  $N$ -glycoproteomics is the analysis of the glycopeptides, retaining the information about both the protein and glycan component. The state of the art of both approaches will be briefly described in the following, focusing on the most recent methodological developments.

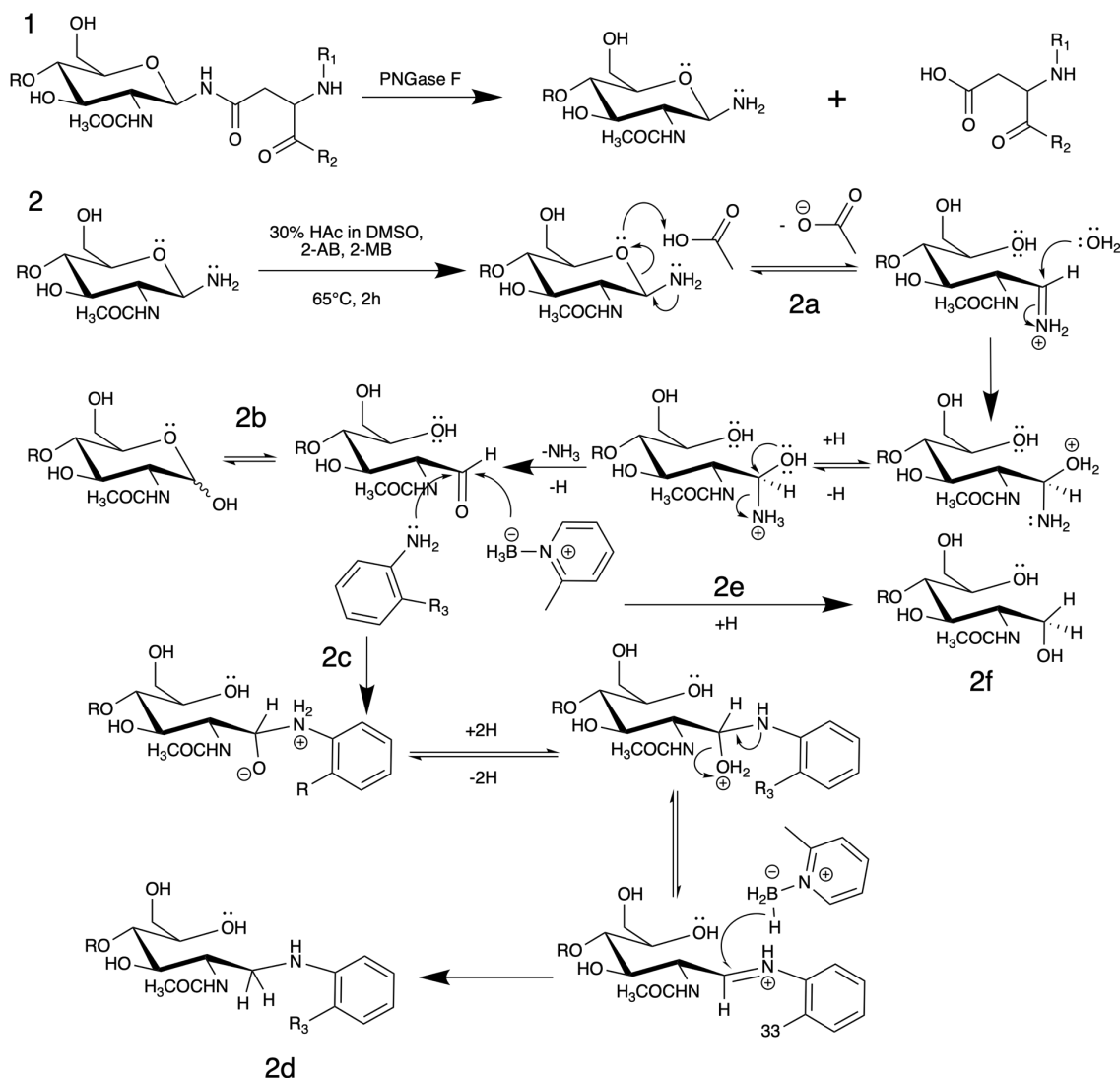
**1.3.4 LC-MS based *N*-glycomic approaches.** Considering LC-MS based *N*-glycomics, a basic qualitative workflow can be summarised as in the following (**Fig. 1.7**):



**Fig. 1.7.** Schematic representation of a general LC-MS based *N*-glycomics workflow. **1.** *N*-glycan release. **2.** *N*-glycan purification. **3.** *N*-glycan labelling. **4.** *N*-glycan separation and structural elucidation via LC-MS/MS.

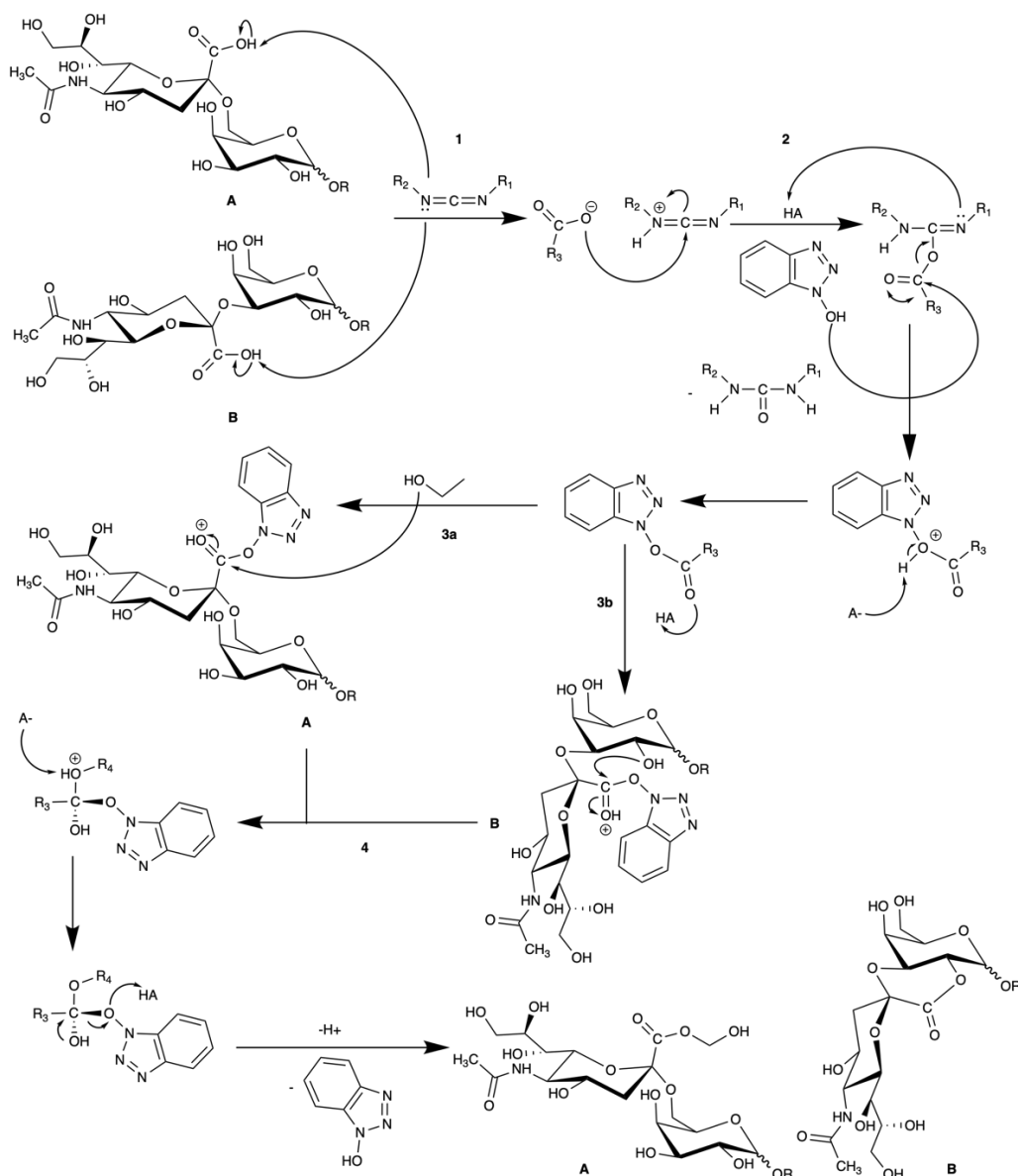
*N*-glycans are firstly released from the biological system under investigation, by using chemical treatment (e.g., hydrazinolysis,<sup>129</sup> NaClO – oxidative-release of natural glycans<sup>167</sup>) or enzymatic digestion (e.g., Peptide *N*-glycosidase F, peptide *N*-glycosidase A, endo- $\beta$ -*N*-acetylglucosaminidase H). Enzymatic digestion is generally preferable over chemical treatment for the release of *N*-glycans, because it can provide specific and efficient sugar removal under milder and cleaner conditions in respect to chemical treatments. The most common method for *N*-glycan release is enzymatic digestion using peptide-*N*-glycosidase F (PNGase F), in which the release of *N*-glycans from glycoproteins or glycopeptides contained in complex mixtures is usually achieved by overnight incubation at 37°C. There are also faster protocols involving microwaves (10 min)<sup>168</sup> or immobilised PNGase F under ultrasonication (2 min).<sup>169</sup> PNGase F is able to detach all kind of high-mannose, complex, and hybrid *N*-glycans except the ones with  $\alpha$ 1-3-linked core-Fuc.<sup>170</sup> There are also other enzymatic options such as PNGase A, which cleaves *N*-glycans with or without  $\alpha$ 1-3-linked core-Fuc residues, although being more efficient on glycopeptides than glycoproteins, meaning that an additional step of glycopeptides generation is required to fully exploit the enzyme performance. PNGase H<sup>+</sup>, is a novel bacterial enzyme showing the advantages of both PNGase F and A, although working at a pH optimum of 2.6,<sup>171</sup> in which the loss of SA is a probable drawback. A variety of endoglycosidases cleaving between the two GlcNAc residues in the core region (leaving one GlcNAc bound to the protein) also exist. These enzymes have narrower specificities for different types of *N*-glycans than PNGase F or A. Endoglycosidase H (Endo H) and Endo F1 cleave high-mannose and some hybrid-type oligosaccharides, but not complex-type oligosaccharides; Endo F2 cleaves high-mannose and biantennary complex-type oligosaccharides; Endo F3 works on bi-antennary and tri-antennary complex-type oligosaccharides, especially if core-fucosylated.<sup>172</sup> Free *N*-glycans obtained after enzymatic release are then purified/enriched with suitable methods (e.g., lectin-based,<sup>173</sup> solid-phase extraction-based<sup>174,175</sup>), and chemically labelled (e.g., reductive amination,<sup>176</sup> hydrazide chemistry,<sup>177</sup> carbamate

derivatisation<sup>178</sup>) to be analysed by the detection system (e.g., fluorescence/UV detection and/or mass analyser). The first kind of derivatisation usually performed on *N*-glycans is reducing end derivatisation, most commonly carried out through reductive amination (**Fig. 1.8**): the primary amine group from the fluorophore chosen for the labelling reacts with the aldehyde group of the glycan to form a secondary amine under reducing conditions.



**Fig. 1.8.** Proposed mechanism of reductive amination for *N*-glycan labelling. **1.** PNGase F cleaves the GlcNAc $\beta$ 1-Asn bond, releasing the *N*-glycan, terminating with a GlcNAc-glycosylamine (R = *N*-glycan; R<sub>1,2</sub> = protein). **2.** Reductive amination; 2a = the mildly acidic conditions promote glycosylamine hydrolysis, possibly through the formation of an iminium ion, as reported in the literature for less complex structures.<sup>179,180</sup> 2b = After glycosylamine hydrolysis, the GlcNAc-terminating *N*-glycan is present as an equilibrium between the hemiacetalic and aldehydic forms, with the latter promoted by the acidic conditions. 2c = The GlcNAc aldehydic group reacts with the fluorescent dye (e.g., aminobenzamide, 2-AB, R<sub>3</sub> = CONH<sub>2</sub>, used in excess), affording the iminium ion intermediate further reduced by the reducing agent (e.g., 2-methylpyridine borane complex, 2-MB) to yield the labelled *N*-glycan (2d). 2e = competing side reaction showing the direct reduction of the *N*-glycan aldehydic group by the reducing agent, yielding the unlabelled *N*-glycan (2f), invisible at the chromatographic level but detectable with MS.

A variety of reagents have been developed as chemical tags, adding a chromophore or fluorophore to the *N*-glycan structure, such as 2-aminobenzamide (2-AB), 2-aminobenzoic acid (2-AA), 2-aminopyridine (PA), 2-aminonaphthalene trisulfonic acid (ANTS), 1-aminopyrene-3,6,8-trisulfonic acid (APTS) and Procainamide (ProA).<sup>181–183</sup> As briefly mentioned above, apart for making it possible to identify the *N*-glycan structures and perform relative quantification using UV or fluorescence detectors, these chemical labels introduce functional groups (e.g., secondary amine) that can hugely improve the ionisation efficiency of glycans in positive ion mode when performing MS analyses. Reductive amination is not the only way to functionalise the reducing terminus of glycans, although the most widely employed: Michael addition reaction can be performed using 1-phenyl-3-methyl-5-pyrazolone (PMP) or its analogues,<sup>184,185</sup> and hydrazide labelling using (carboxymethyl)trimethylammonium chloride hydrazide was another tested strategy,<sup>186,187</sup> among the others.<sup>188</sup> A further step of the labelling strategy can also be adopted when the goal is also to elucidate some *N*-glycan isomers, and it concerns the *N*-glycan termini instead of the reducing end: SA  $\alpha$ 2,3 and  $\alpha$ 2,6 differential linkage can be discerned by performing an esterification reaction. Esterification (e.g., 1-ethyl-3-(3-(dimethylamino)propyl)carbodiimide, EDC; 1-hydroxybenzotriazole, HOBt; ethanolic solution) of SA results in linkage-specific mass shifts for the  $\alpha$ 2,3 and  $\alpha$ 2,6 linked forms: internal cyclic esters are generated in the former, while alkyl esterification reaction occurs in the latter, prompting defined mass differences easily recognisable in mass spectra (**Fig. 1.9**).



**Fig. 1.9.** Esterification reaction performed on  $\alpha$ 2-6-linked and  $\alpha$ 2-3-linked SA. **1.** The carboxyl group of  $\alpha$ 2-6-linked (A) or  $\alpha$ 2-3-linked (B) SA ( $R_3 = \text{glycan}$ ) reacts with EDC ( $R_1 = 1\text{-ethyl}$ ;  $R_2 = 3\text{-dimethylaminopropyl}$ ). **2.** The carboxyl group of SA is further activated with HOBT in acid catalysis (HA = acid,  $A^-$  = base) towards nucleophilic substitution with the desired alcohol (e.g., ethanol). **3a.** Nucleophilic substitution at  $\alpha$ 2-6-linked SA activated carbonyl group by ethanol. **3b.** In the case of  $\alpha$ 2-3-linked SA, intramolecular reaction involving the hydroxyl group at C-2 of the nearby monosaccharide (e.g., Gal) is favoured over nucleophilic substitution by the free alcohol. **4.** Subsequent acid-base reactions lead to the collapse of the tetrahedral intermediate and removal of HOBT as the best leaving group, affording the ethyl-esterified  $\alpha$ 2-6-linked sialoglycan (A) or the intramolecularly lactonized  $\alpha$ 2-3-linked one (B).

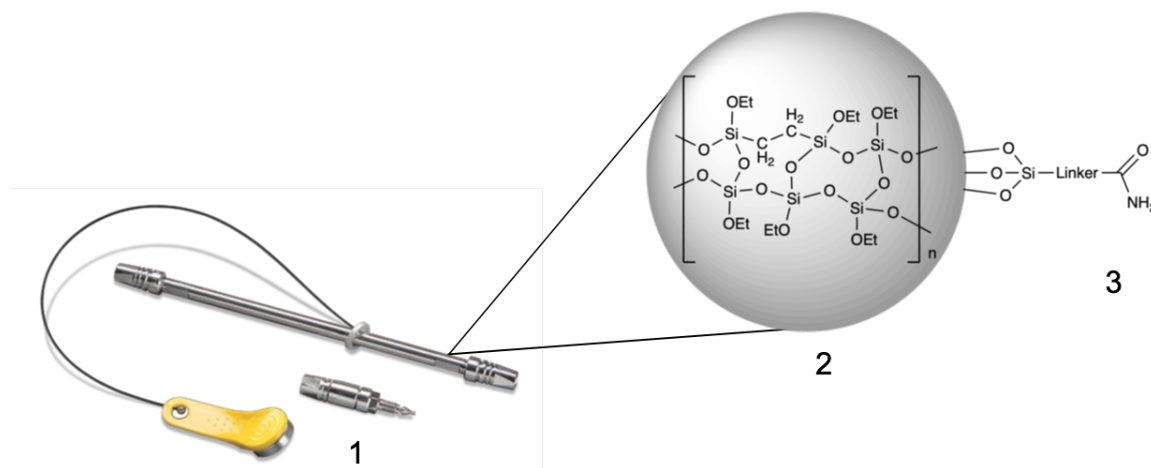
Furthermore, the procedure is efficient in stabilising acidic glycans, therefore enabling their simultaneous analysis along with the neutral ones.<sup>189</sup> Another chemical approach to enhance *N*-glycans stability prior to mass analysis is the use of permethylation (e.g., dimethyl sulfoxide, methyl iodide, solid hydroxide;<sup>190</sup> further improved more recently<sup>191–193</sup>), suitable for the aforementioned purpose with either matrix-assisted laser desorption ionization (MALDI) or electrospray ionization



(ESI),<sup>194</sup> and employable in combination with SA dimethylamidation to further boosts the experimental sensitivity.<sup>195</sup> After the labelling step, *N*-glycans are then separated with diverse methods, such as Hydrophilic Interaction Liquid Chromatography (HILIC),<sup>196</sup> or Porous Graphitised Chromatography (PGC),<sup>197</sup> (but non-chromatographic techniques can be used also, such as Capillary Electrophoresis<sup>198</sup> or Ion Mobility<sup>199</sup>), and their structural profile is detected using appropriate mass analysers within mass spectrometers able to deliver fragmentation data. If the goal of the analysis is the sample absolute quantification, the use of internal or external standards, as well as isobaric/isotopic labelling is necessary prior to detection.<sup>200</sup> The *N*-glycan separation step is of course crucial for further structural elucidation, and LC-based approaches are currently the most prevalent glycan separation technique for several reasons: (1) there is ample choice of methods for either native or derivatised glycans, based on the interaction between glycans and stationary phases; (2) the use of top-notch LC instrumentations, such as UPLC<sup>201</sup> (column packed with < 2  $\mu\text{m}$  sorbent particles, pressures up to 10.000-15.000 psi, flow rate of 0.5-1 mL/min) or nanoLC<sup>202</sup> (column packed with < 5  $\mu\text{m}$  sorbent particles, pressures up to 6000-7000 psi, flow rate of 50-500 nL/min) systems, further boost the separation efficiency and sensitivity, delivering on-line, continuous analyses when coupled with MS detection; (3) good isomeric separation can normally be achieved without the use of non-volatile salts, another parameter favouring the compatibility with MS detection. Despite the numerous techniques available to date, however, there still is an increasing demand for the identification and characterisation of glycan isomers which, notwithstanding the technological improvements, still represent a challenge. SA linkage isomers shape some Ab unique interactions,<sup>203</sup> and several types of carcinomas have been found to have aberrant expression of glycan isomers,<sup>204</sup> highlighting how the separation of these structures could be crucial in the context of biomedical applications. Considering the LC-based separation techniques, even though partial isomeric separation has been observed employing a C18 column<sup>205</sup> (i.e., hydrophobic stationary phase usually employed for peptides separation), PGC or HILIC columns definitely represent the most advanced LC stationary phases to date capable of facilitating the isomeric separation of glycans,<sup>206</sup> and the latter will be shortly introduced in the following since part of the analytical set-up used within this thesis experimental work. HILIC is a separation technique related to normal phase chromatography, differing from the latter from the point of view of the analyte interactions with the stationary phase. The chromatography of carbohydrates conducted on HILIC stationary phases (**Fig. 1.10**) has been shown to involve a partitioning mechanism in contrast to the traditional adsorption chromatography on normal phase materials.<sup>207</sup> In HILIC in fact, the analyte partitions between the mobile phase (organic solvent with a small percentage of buffers) and a water-enriched layer at the surface of the highly polar



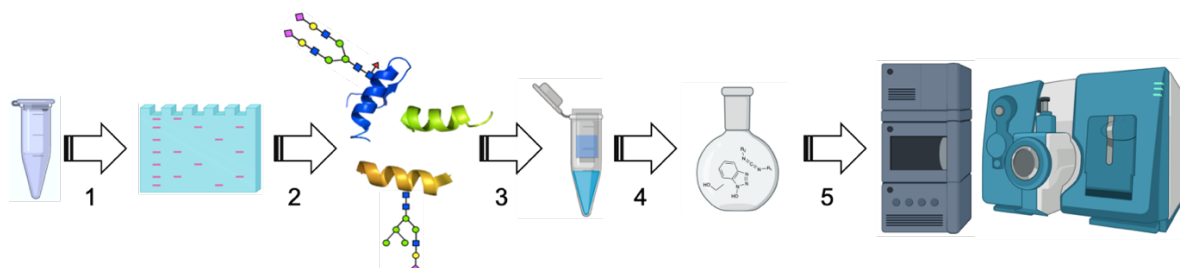
stationary phase, with a retention mechanism<sup>207,208</sup> involving hydrogen bonding, ion-dipole and dipole-dipole interactions, depending on the analyte in question and on the employed HILIC stationary phase (silica particles, amine-, hydroxy-, amide-bonded (**Fig. 1.10**), zwitterionic particles or monoliths).<sup>209,210</sup>



**Fig. 1.10.** HILIC stationary phase of the column (**1**, Waters, Milford, MA) used within this thesis experimental part. **2.** Bridged ethyl siloxane/silica hybrid particles (polyethoxysilane, 1.7  $\mu\text{m}$ ), synthesized from tetraethoxysilane and bis(tryethoxysilyl)ethane. **3.** Amide moiety linked to silica particles for analyte interaction.

Within HILIC, analytes interacting with highly polar stationary phases are eluted by usually applying a binary gradient consisting of an aqueous part and a less polar organic solvent (e.g., acetonitrile), with increasing aqueous portions promoting the elution of hydrophilic molecules. Generally used buffers for the polar part of the mobile phase are ammonium salts of acetate and formate (high volatility and excellent solubility in organic solvents), which are prepared at low concentrations (e.g., 100 mM or lower), within a 10-25% water in acetonitrile solution, representing the typical equilibration conditions for HILIC-(U)HPLC analysis of mono-/oligosaccharides and glycopeptides.<sup>211</sup> The aqueous fraction of the mobile phase is then usually gradually increased up to 50% for glycan elution. The retention of glycans or glycopeptides on HILIC material depends on the analyte hydrophilicity, influenced by structural features such as size, charge, composition, linkage and oligosaccharide branching<sup>212</sup> but, however, separation mainly occurs on the basis of the number of polar/charged groups, making the elution pattern rather intuitive and predictable.<sup>213</sup> HILIC is also quite a robust analytical tool, since it tolerates a vast variety of analyte modifications (e.g., different fluorescent tags, esterification, amidation), and permits a certain level of structural isomers resolution, along with providing retention of highly polar analytes that might be difficult to separate on reversed-phase material, making it a valuable tool for the separation and structural analysis of glycan and glycopeptide species.

**1.3.5 LC-MS based *N*-glycoproteomic approaches.** Different from the characterisation of *N*-glycans is those of *N*-glycoproteins, which however has the ability to provide both glycan and protein information, thereby linking glycomic and proteomic analyses. Glycoproteomics combines the tools, and the difficulties, of proteomic analysis and site-specific glycomics. As done in proteomics bottom-up approaches, the analyses of peptides and glycopeptides provide the simplest route for the development of glycoproteomic platforms. However, site-specific analysis of glycoproteins employing intact glycopeptides is challenging due to the presence of multiple glycosylation sites, which are subjected to glycan heterogeneity. MS analyses of glycopeptides are hindered by the fact that glycans tend to substantially diminish the respective peptides ionisation efficiencies, and that the vast number of glycoforms distribute further the peptide signals over several species. Furthermore, well-established proteomics tandem MS methods are not sufficient to obtain thorough and simultaneous information from both the glycan and the peptidic part. Considering LC-MS based *N*-glycoproteomics, a basic qualitative workflow can be summarised as in the following (**Fig. 1.11**): when the *N*-glycoproteome is obtained from the biological system under analysis, eventually fractionated to reduce the sample complexity,<sup>214–216</sup> and then usually enzymatically digested (e.g., Trypsin, Lys-C, Glu-C), a fundamental step to be performed prior to any other is glycopeptide enrichment.



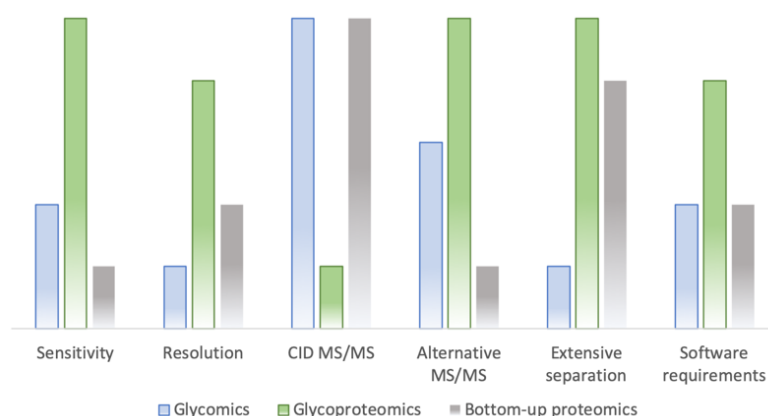
**Fig. 1.11.** Schematic representation of a general LC-MS based *N*-glycoproteomics workflow. **1.** Proteome fractionation. **2.** Glycopeptides generation (e.g., in-gel Trypsin digestion). **3.** Glycopeptides enrichment (e.g., HILIC). **4.** Chemical labelling of *N*-glycans (harboured on glycopeptides). **5.** *N*-glycopeptides separation and structural elucidation via LC-MS/MS.

The direct MS analysis of glycopeptides in complex samples is in fact analytically challenging, due to the low ionisation efficiency of glycopeptides and the low glycopeptide : peptide ratio, which causes glycopeptide signal suppression in favour of the most abundant non-glycosylated peptides, belonging either to glycoproteins or non-glycosylated ones. Therefore, isolating glycopeptides from complex samples by an appropriate enrichment method is the most efficient way to achieve in-depth glycoproteome analyses, and can be performed with several methods such as lectin affinity chromatography,<sup>217,218</sup> electrostatic repulsion hydrophilic interaction chromatography (ERLIC),<sup>219,220</sup> the already introduced HILIC,<sup>221,222</sup> hydrazide<sup>223</sup> or boronic acid<sup>224</sup>

chemical enrichments. Glycopeptides can be then chemically derivatised towards the desired purpose with basically the same set of reactions previously enlisted for *N*-glycomics (e.g., amidation, esterification, permethylation, isobaric/isotopic labelling),<sup>225</sup> and subsequently analysed via LC-MS/MS approaches in a qualitative or quantitative way. Although it has been facilitated thanks to recent progresses in chromatography techniques, labelling and derivatisation strategies, enrichment methods and bioinformatics,<sup>226–228</sup> quantitative *N*-glycoproteomics still remains an overwhelming analytical task, which is out of the scope of this thesis and thoroughly reviewed elsewhere.<sup>225,229</sup> The chromatographic separation of glycopeptides can be achieved with techniques similar to those already cited for glycan analysis (e.g., CE<sup>230</sup> or IM-MS<sup>231</sup>), though usually reversed-phase liquid chromatography (RPLC) employing a C18 column is the most widely used method for untargeted site-specific glycoproteome analysis, since the peptidic part of the glycopeptides significantly shift the macromolecule hydrophilicity towards more hydrophobic values. In fact, the RPLC separation of glycopeptides is mainly based on the binding interaction with the peptide backbone and the stationary phase, predictable by looking at the amino acid sequence.<sup>232</sup> Generally, the glycan moiety has less influence in the interaction of glycopeptides to RPLCs. However, it was observed that a reduction of retention time occurs with increasing number of neutral monosaccharide units on the glycan linked to the peptidic backbone, highlighting how the glycan composition and structure anyway influences the retention behaviour of glycopeptides even if to a lesser extent if compared to the amino acid sequence.<sup>233</sup> This evidences give the glycoanalyst a certain level of prediction power over the retention time of different glycoforms, even if the actual retention time is a function of various chromatographic conditions, and the number and kind of *N*-glycans harboured on the glycopeptide (e.g., SA).<sup>234</sup> RPLC has however some drawbacks when employed for glycopeptide analysis, like the poor retention of highly hydrophilic glycopeptides and the limited resolution power on different glycoforms; problems that can be overcome by employing orthogonal separation methods (e.g., combination of RPLC, PGC, HILIC), for more efficient site-specific analysis,<sup>235–237</sup> where complementary separation by PGC or HILIC can efficiently recapture the hydrophilic glycopeptides lost in the conventional RPLC step. After the chromatographic separation step, the detection of the analytes (for now on either *N*-glycans or *N*-glycopeptides, unless specified) occurs: usually, the labelled-analytes are detected thanks to an inherent (amino acids aromatics) or linked fluorophore (e.g., 2-AB) using fluorescence/UV detection (i.e., *N*-glycans), still within the chromatographic step, and then ionised in a mass spectrometer source, detected in a mass analyser, and finally fragmented for structural elucidation.

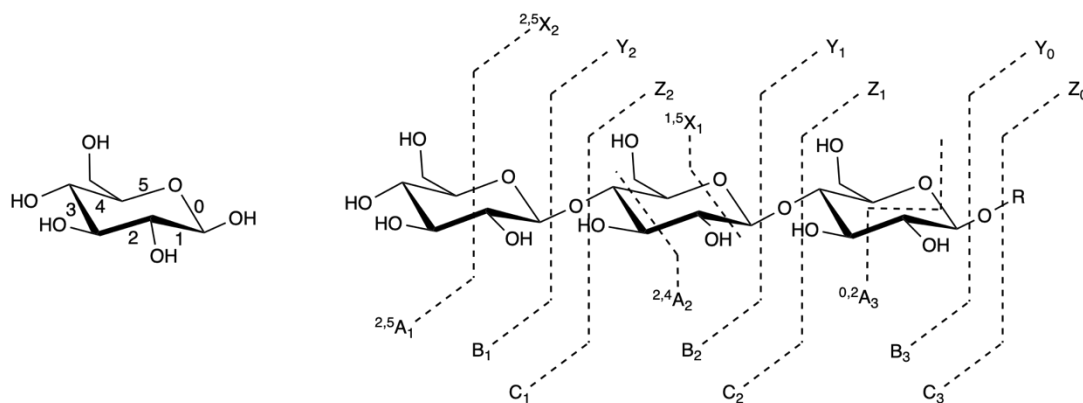
**1.3.6 MS analysis of *N*-glycans and *N*-glycoproteins.** MS is the ideal detection technique for *N*-glyco(prote)omics since it can provide structural information on small amounts of material,

reaching femtomolar to attomolar limit of detections for glycans, with a dynamic range (the ratio of the largest to smallest detectable signal) of typically 4/5 orders of magnitude.<sup>238,239</sup> Structural analysis of glycans can be performed on abundances typically in the femtomolar range, and there is no other method currently available able to reach such a low limit of detection while retaining the necessary structural information. The instrumental requirements for glycomics and glyco(prote)omics are summarized in **Fig. 1.12**,<sup>240</sup> and compared to bottom-up proteomics as well-established method.



**Fig. 1.12.** Qualitative depiction of the instrument and software requirements for glycomics and glycoproteomics. Requirement levels are given a score from 1 to 5, and percentages are reported. Bottom-up proteomics is reported as well-established method for quick comparison (adapted from *Rubaak et al., 2018*).

Glycomics and glycoproteomics experiments need a higher level of sensitivity in respect to bottom-up proteomics, because of the poorer ionisation efficiency of glycans and glycopeptides in comparison to peptides. Extensive separation of analytes (LC/CE) and glycan derivatisation boosting ionisation efficiency and therefore detection limit, are surely beneficial for glycomics experiments resolution and crucial in glycoproteomics. MS-derived structural data come from *N*-glycans or *N*-glycopeptides fragmentation patterns and, therefore, the MS/MS method is of crucial importance for structural glyco(prote)omics. Collision-induced dissociation (CID)<sup>241,242</sup> fragmentation is traditionally the low-energy method of choice for bottom-up strategies, providing a good level of information in glycomic experiments (**Fig. 1.13**),<sup>243</sup> but being generally not sufficient in glycoproteomics and intact glycoprotein analysis, where alternative dissociation techniques such as electron-transfer dissociation (ETD),<sup>244</sup> electron-transfer/higher-energy collision dissociation (EThcD),<sup>245</sup> ultraviolet photodissociation (UVPD),<sup>246</sup> or activated-ion ETD (AI-ETD),<sup>247</sup> are better suited to provide more comprehensive fragmentation patterns for both the peptide backbone and the glycan.



**Fig. 1.13.** Simplified model of glycans fragmentation using CID MS/MS. Fragmentation pattern presented according to the nomenclature introduced by Domon and Costello (1998),<sup>248</sup> based on peptide fragmentation (reducing end positioned in the same location of peptidic C-terminus), and exemplified on a glucose oligomer. Fragments containing the oligosaccharidic reducing end are indicated as X (cross-ring cleavage) and Y/Z (glycosidic bond cleavage). Fragments containing the non-reducing end are indicated as A (cross-ring cleavage) and B/C (glycosidic bond cleavage). Subscript numerals represent cleavage along the glycosidic bond, whereas superscript numerals denote the position of the cross-ring cleavage.

In fact, fragmentation of glycopeptides is complicated by the presence of two chemically dissimilar groups: glycan bonds are more labile than peptide bonds, and glycans also have significantly lower intrinsic basicity than peptides. This means that both the ionization and the fragmentation conditions of glycans differ significantly from that of glycopeptides, and that the latter requires tailored conditions, usually involving high-energy dissociation methods. CID fragmentation, in the case of native glycans, mainly affords cleavage along glycosidic bonds (**Fig. 1.13**); Fuc and SA are also readily lost, resulting in abundant fragment ions with Fuc/SA loss from the quasimolecular ion in immediate succession. SA are more labile than Fuc, and in the positive ion mode, they are the major fragment ions. An important issue with native glycans is the occurrence of migrating species during CID. When the MS analysis is performed in positive ion mode, Fuc tends to transfer from the termini to the reducing end in native glycans, which results in the loss of internal residues. This unwelcomed effect is however significantly diminished when the reducing end is reduced to alditol or derivatised, which is another reason why it is advantageous to analyse labelled glycans instead of underivatized ones.<sup>249</sup> It is also worth to note that, as introduced above, the main problem in glycan structural elucidation is isomers discernment, and the fragmentation method, along with the number of fragmentation events employed in the analysis (which depends on the mass spectrometer capabilities), plays a crucial role in that. Even if the main cleavage type in CID spectra of glycans is on the glycosidic bond, cross-ring cleavages may also occur and are enhanced through the use of multiple fragmentation events ( $MS^n$ , where  $n > 2$ ).<sup>250</sup> This permits the identification of the linkage position, even though without readily determining the stereochemistry nor the anomeric character of the linkage. Other fundamental

aspects of MS-based glyco(prote)omics are the instrument resolution, mass accuracy and scan rate. It is crucial to outline accurate masses, particularly in global profiling of released glycans, to ensure rapid differentiation of glycan peaks from non-glycan ones (e.g., peptides/lipid contaminants with masses that nominally corresponds to glycan compositions). Among the mass spectrometer currently available, Fourier transform ion cyclotron resonance MS (FTICR-MS) was the earliest technique used for high resolution analysis of glycans,<sup>251</sup> proven to be useful, for instance, in the global glycan profiling for cancer biomarker discovery.<sup>252</sup> However, these instruments are fairly expensive, not so widespread, and generally lacking the capability of fast LC-MS analysis required for glycoproteomics, even though they have been used also to this extent.<sup>253</sup> On the contrary, the still recent employment of Orbitrap technology for glycoproteomics investigations,<sup>254</sup> is on the rise,<sup>247</sup> thanks to its excellent performances and versatility. Time-of-flight analysers in QTOF and MALDI-TOF instruments represent the most common way to successfully deal with global glycan profiling. These instruments have high scan rates and are highly essential in high-throughput analyses to get reliable quantitative data, but can be also used in glycoproteomics to quantitate glycans and site-specific glycosylation.<sup>255,256</sup> Considering the mass spectrometer ion sources, MALDI<sup>257</sup> and ESI<sup>258</sup> are routinely used for oligosaccharide analysis, because glycans contain labile residues (e.g., Fuc, SA) easily fragmentable either in-source or post-source during ionisation, and therefore soft ionisation techniques delivering little excess energy and generating intact molecular ions are preferred for glyco(prote)omic analyses. Due to its greater sensitivity, its generally lower ionisation energy, and the capability to be coupled with liquid chromatography, granting on-line, continuous analyses of the sample exiting the chromatographic step, ESI is more commonly used for glycan analysis. Another advantage of the ESI set-up is that both neutral and anionic native glycans can be efficiently analysed in positive mode, whereas with MALDI neutral compounds are better resolved in positive mode while sialylated species in negative mode. The ESI-QqTOF MS set-up employed in the experimental section of this thesis will not be described here since it represent an MS basic configuration and has been thoroughly dissected elsewhere.<sup>259</sup>

**1.3.7 MS-based *N*-glyco(prote)omic applications for CNS studies.** Roughly ten years later the papers reported in section 1.2.6 of this introduction, new studies added pieces of knowledge about the brain *N*-glycome spatio-temporal composition and genetic regulation,<sup>260,261</sup> although providing little methodological improvements. In recent times, niftier bioanalytical methods strongly contributed to better resolve the brain *N*-glycosylation puzzle. These experimental workflows were able to produce reliable signals from milligram amounts of mouse and rat brain tissues, to strongly reduce the sample preparation time, and to often enhance the *N*-glycan recovery through PNGase F enzymatic release, employing more precise and sensitive analytical



set-ups.<sup>113,215,262–267</sup> However, these bioanalytical methods still present limitations. For instance, some proposed procedures employ hydrazinolysis for *N*-glycan release, complicating their purification after the chemical reaction with multiple chromatographic steps, yielding only few *N*-glycan structures,<sup>262,264</sup> and destroying the proteins.<sup>268</sup> In another case,<sup>263</sup> a smart approach almost eliminated the sample preparation steps but only achieved little improvement in resolution, affording 43 *N*-glycan monosaccharide compositions with very low precision (CV 35%). Other proposed methods follow a similar concept:<sup>266,113</sup> authors aimed to avoid laborious chromatographic steps for *N*-glycan purification employing a chemoselective procedure to trap *N*-glycans from unpurified proteolytic digest and quickly fish them out of the complex mixture. This approach led to the identification of 40 to ~80 *N*-glycan monosaccharide compositions from human and mouse brains respectively, but it employed trypsinisation before enzymatic deglycosylation, which prolongates the workflow in comparison to methods in which deglycosylation is carried out at the intact protein level. Other bioanalytical methods, focused on brain membrane-associated glycoproteins, resolved ~70 *N*-glycan monosaccharide compositions, even if with suboptimal mass accuracy (mostly > 20 ppm, up to 80 Da delta mass);<sup>215</sup> set the lowest starting amount of brain tissue producing reliable signals across the literature (1.5 mg) along with a resolution of up to 120 *N*-glycan monosaccharide compositions;<sup>265</sup> and efficiently distinguished the relative amounts of majorly expressed isomeric glycotopes with high sensitivity through MS<sup>2</sup>/MS<sup>3</sup> data acquisition, even if dedicating only little space to brain *N*-glycans, amongst *N*- and *O*-glycan analyses from adenocarcinoma cells.<sup>267</sup> Very recently, a new study of the mouse brain *N*-glycome was reported,<sup>269</sup> using LC-Orbitrap-MS set-up and HCD fragmentation, in both positive and negative ion modes, along with employing an in-house developed *N*-glycan database search engine named GlySeeker. In this work, both permethylated and native *N*-glycans belonging to mouse brain were analysed with C18-RPCL-ESI(+)-MS/MS (HCD) and PGC-LC-ESI(-)-MS/MS (HCD) set-ups respectively, identifying more than 200 *N*-glycans with putative topological structures (monosaccharide composition, sequence, and glycosidic linkages), and providing a basic reference for future glycosylation study of mouse brain. In the same year a similarly thorough work was carried out on glycopeptides from mouse brain tissue,<sup>247</sup> which analytical set-up, comprising the use of a quadrupole-Orbitrap-linear ion trap hybrid MS instrument equipped with AI-ETD fragmentation system, was able to capture the *N*-glycoproteome site-specific microheterogeneity. This large scale glycopeptide profiling method was ultimately capable of characterising 1.545 *N*-glycosites (> 5.600 unique *N*-glycopeptides) from mouse brain tissue, showing that the *N*-glycosylation profiles can differ between subcellular components (e.g., extracellular, cell surface, Golgi complex, lysosomes, vesicles, ER, secreted) and



between structural domains. Furthermore, the authors showed that *N*-glycosite heterogeneity manifests in several different forms, such as dramatic differences in glycoforms, and provided some visual maps summarising their large-scale glycoproteomic dataset that will serve as references for analysing intact glycopeptides in future studies.

## 1.4 GLYCOTOOLS TOWARDS NEUROMEDICAL APPLICATIONS.

**1.4.1 Glycosides as potential neuroregenerative tools.** Regenerative medicine aims to regenerate damaged tissues through tissue engineering, in which a structural and functional bioactive replacement of the injured tissue is created and implanted where the damage occurred, to promote and guide tissue restoration and healing.<sup>270</sup> Tissue engineering is usually pursued using a combination of cells and bioactive materials, carriers of physical and/or biochemical information able to influence cell microenvironments, guiding cell behaviours towards the desired effects. Bioactive materials or biomaterials, are chemically decorated scaffolds, exposing natural or synthetic (macro)molecules (e.g., peptides, growth factors, glycans), to orchestrate tissue formation and integration within the host environment. The covalent exposure of carbohydrates on biomaterial surfaces, through bioconjugation of previously synthesised glycosides, has been shown to be able to promote the interaction with cellular proteins, mimicking the biological and structural properties of the ECM, leading to a variety of biochemical responses and cellular behaviours of medical interest.<sup>271</sup> Although still representing a niche of biomaterials applications, glyco-functionalised scaffolds for neuroregeneration have displayed interesting features. Biomaterials choice and bioconjugation techniques to decorate the scaffolds for neuroregeneration are a research topic on their own and have already been discussed elsewhere.<sup>272</sup> Their detailed analysis is beyond the scope of this thesis, while some glycan epitopes that have shown interesting neuroactive properties will be briefly discussed in the following to give an overview of glycoside potentialities as bioactive cues for biomaterial decoration. *Russo et al.* demonstrated the ability of collagen scaffolds, covalently decorated with  $\alpha$ -glucoside residues (exposing  $\alpha$ -D-Glu, **Fig. 1.14**, 1), to drive F11 neuroblastoma cells differentiation into active neurons.<sup>273</sup> The authors showed, using confocal microscopy, that the cells displayed a significantly higher frequency of neuritic-like processes when grown on the glyco-functionalised biomaterial in comparison to the controls. Moreover, using immunofluorescent staining with Ab against the late neuronal marker  $\beta$ -tubulin III, the authors highlighted the presence of active neurons after seven days of cell growth on the glyco-functionalised biomaterial. More than 90% of these cells were able to generate a mature action potential and, due to the neuron electrophysiological properties, the authors inferred that the glyco-functionalised biomaterial favoured the expression of sodium and/or potassium

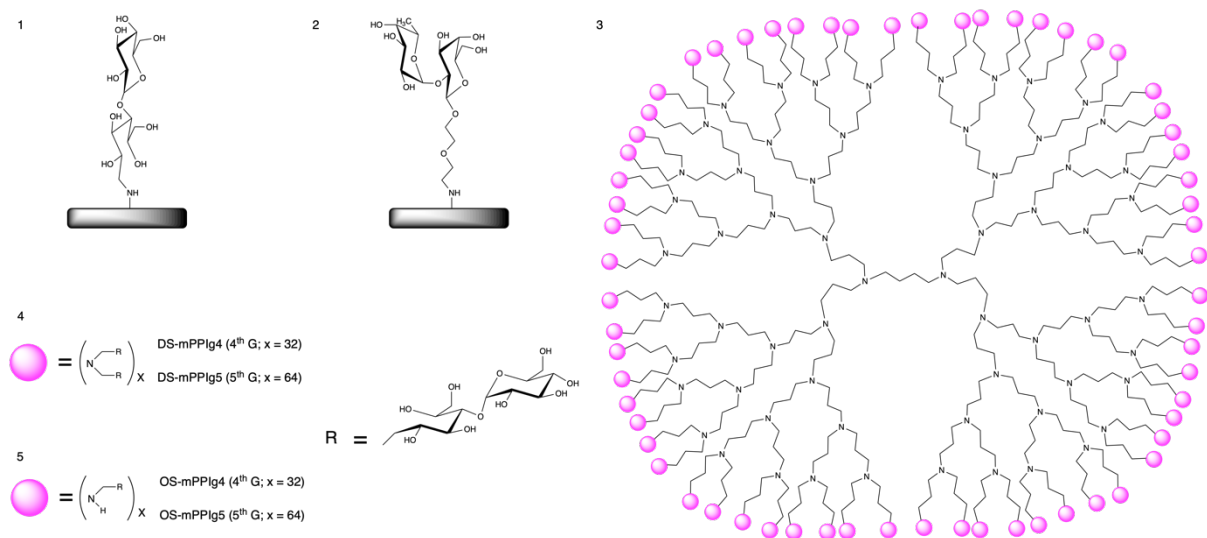
channels on cell membranes. In another work, *Masand et al.* investigated the effect of the HNK-1 carbohydrate and of PSA (**Fig. 1.4, 4**) on different neuronal cells when immobilised on collagen scaffolds.<sup>274</sup> Both HNK-1 and PSA are upregulated after neural injuries and this is required for effective regeneration, which stops when these molecules expression is experimentally inhibited. The authors demonstrated that motor neurons outgrowth was enhanced when neural cells were grown on a collagen scaffold functionalised with a hNK-1 glycomimetic peptide epitope, while grafted PSA glycomimetic peptide stimulated Schwann cells proliferation and process extension along with both sensory and motor neuron outgrowth. *Kalovidouris et al.*, demonstrated that Fuc  $\alpha(1-2)$ Gal disaccharides are able to dramatically change hippocampal neurons morphology and promote neurite outgrowth in a density-dependent way, when grafted onto polyacrylamide scaffolds (**Fig. 1.14, 2**); while the use of different glycans epitopes failed to reproduce the same results, highlighting a very specific structure-dependent response.<sup>275</sup> In a more recent work, *Zhang et al.* tested a polycaprolactone/PSA hybrid nanofiber scaffold, encapsulating glucocorticoid methylprednisolone (PLC/PSA/MP), in the treatment of spinal cord injury within rat models with spinal cord transection.<sup>276</sup> In addition to the demonstrated capacities of PSA in inducing peripheral nervous system cells proliferation and neuritogenesis,<sup>274</sup> the polysaccharide is itself biodegradable and widely studied for its ability to control the CNS development, by regulating cellular adhesive properties and promoting axonal growth. In fact, the transplantation of the PCL/PSA/MP nanofiber scaffold suppressed the tissue acute inflammation (decreased interleukin-6 and tumour necrosis factor- $\alpha$ ) and apoptosis (reduced Caspase-3 expression), enhanced axonal regeneration by inhibition of its demyelination process and the expression of the glial fibrillary acidic protein, along with increasing the expression of the neurofilament 200, greatly enhancing the neurological and functional recovery of injured rats, which actually showed improved locomotor behaviours in comparison to the control group.

**1.4.2 Glycodendrimers as potential neuromedical tools.** Dendrimers are highly branched, nano-sized molecules, comprising one or more dendrons originating from a single constitutional unit (central core). Dendrons are defined as a part of a molecule with only one free valence, comprising exclusively dendritic and terminal constitutional repeating units and in which each path from the free valence to any end-group comprises the same number of constitutional repeating units.<sup>277</sup> The number of monomers covalently linked to the core of dendrimers form consecutive layers called generations, exposing several functional groups on the surface, which are suitable for conjugation with different kinds of biomolecules. Dendrimers can be synthesized using mainly two distinct synthetic approaches, named convergent and divergent,<sup>278,279</sup> and using a variety of different cores and building blocks, giving rise to disparate structural features,<sup>280</sup> among which the

most important is monodispersity, granting ordered architectures more similar to uniform biological polymers.<sup>281</sup> Apart from the above-mentioned monodispersity, which favours reproducible pharmacokinetics, dendrimers display lack of immunogenicity, good stability, and high cellular uptake levels (due to efficient cell-membrane permeability), making them excellent tools for biomedical applications (e.g., drug and gene delivery, anti-cancer agents, magnetic resonance imaging contrast agents, photodynamic therapy).<sup>282–286</sup> Glycodendrimers appeared for the first time in the literature in 1993<sup>287</sup> and became quickly one of the most promising classes of dendrimers for biomedical applications, because the functionalization of dendrimer branches with sugar moieties significantly lowered the molecules cytotoxicity, improved biocompatibility and prolonged their blood half-life.<sup>288–290</sup> In addition, as saccharides are fundamental signalling molecules, glycodendrimers tend to display enhanced molecular recognition potential due to the sugar-dependent interactions with lectins, thus setting themselves as promising tools in the targeting of a variety of pathological states.<sup>291</sup> Among the broad spectrum of glycodendrimers therapeutic promises,<sup>292</sup> the treatment of neurodegenerative diseases is a growing field with encouraging studies, a selection of which is presented in the following to deliver an overview of these molecule potentialities towards neuromedical applications. Prion diseases, also called transmissible spongiform encephalopathies (TSEs), are triggered by the conversion of a normal cell-surface glycoprotein (PrPC) into a misfolded isoform (PrPSc), which is infectious in the absence of nucleic acids via transmission of its conformationally altered structure to other native PrPC units. This phenomenon causes the propagation of the pathological state and destruction of neuronal tissues through ordered proteins aggregation.<sup>293–295</sup> There is no effective therapy for prion diseases both in humans and animals, principally due to difficulties in identifying compounds affecting PrPSc, which are also capable of accessing the CNS by crossing the BBB. Specific glycodendrimers are promising molecules in this context, as they were shown to be able to cross the BBB and eliminate PrPSc in a dose and time dependent fashion. *McCarthy et al.*<sup>296</sup> described the efficacy of a low cytotoxic maltose poly(propyleneimine) generation five glycodendrimer (mPPIg5, **Fig. 1.14**, 3) in eliminating PrPSc from scrapie infected neuroblastoma cells, with therapeutic effects comparable to more established anti-prion compounds. Moreover, they investigated mPPIg5 intracellular therapeutic mechanism *in vitro* within cells and prion infected brain homogenates and noted that glycodendrimers can alter the PrPSc structure, most likely by rendering the glycoprotein susceptible to proteolysis and unable to induce PrPC misfolding. The most prevalent neurodegenerative disorder is Alzheimer's disease (AD), triggered by pathological protein misfolding and aggregation, which leads to toxic effects mediated by both soluble amyloid beta peptides (A $\beta$ ) oligomeric species and A $\beta$  fibrils (longer and highly structured  $\beta$ -sheet-like

aggregates of A $\beta$  oligomers).<sup>297</sup> No efficient nor definitive medication for AD is currently available, however, some treatments based on interference with the aggregation dynamics have been proposed. There are two seemingly contrasting strategies that involve glycodendrimers as new potential therapeutic candidates: i) the disruption of aggregated structures or avoidance of protein–protein interactions that could cause aggregate formation and ii) the promotion of protein aggregation in order to accelerate the formation of large inclusion architectures, locking A $\beta$  oligomers into A $\beta$  fibrils. The latter approach is based on evidence that classify soluble A $\beta$  oligomeric intermediates as the real neurotoxic species to be sealed into potentially less toxic A $\beta$  fibrils.<sup>298,299</sup> The fact that similar glycodendrimer structures can provoke quite opposite outcomes on A $\beta$  systems seems to be ascribable to dendrimer-peptide ratios (DPr) used in the experiments. A lower DPr seems to induce fibril clumping, while higher ratios favour non fibrillar structures, and both of these effects, as mentioned above, are expected to reduce the pathogenic properties of amyloids. Regarding the first strategy, *Janaszewska et al.*<sup>300</sup> tested the effect of a multivalent anionic 4th generation poly(propyleneimine) glycodendrimer, partially functionalized with sulphate groups in the outer shell (G4S), on the aggregation behaviour of A $\beta$  peptides and oligomers, in presence of Cu(II) as A $\beta$  aggregation promoter.<sup>301</sup> The study was conducted via a multidisciplinary approach comprising dynamic light scattering, circular dichroism, fluorescence, electron paramagnetic resonance and molecular modelling analyses. The general aim of the work was to clarify the role of Cu(II) ions in Alzheimer’s pathology and to prevent A $\beta$  fibrils formation through glycodendrimers interference. Different conditions were tested in the form of binary and ternary systems composed by a combination of Cu(II) ions, A $\beta$  and G4S. The toxicity of A $\beta$  oligomers and glycodendrimers as well as the mechanism of action of the latter against aggregates formation have been demonstrated in embryonic mouse hippocampal cells. Stable Cu(II)–peptide complexes were observed and Cu(II) effect was demonstrated to be responsible for A $\beta$   $\alpha$ -helix to  $\beta$ -sheet conformation transition, leading to aggregation into A $\beta$  fibrils. Lastly, glycodendrimer G4S was found to stabilize A $\beta$   $\alpha$ -helix structure, with or without Cu(II) ions, preventing their collapse into structured  $\beta$ -sheet-like fibrils. This work demonstrated that A $\beta$  fibrils formation resulted from specific interactions between A $\beta$  and Cu(II) ions, and that glycodendrimer G4S is able to perturbate these interactions, suggesting possible applications in neurodegenerative fibrillopathies treatments. Concerning the second strategy, *Klementieva et al.* investigated glycodendrimers therapeutic promises against neurotoxic A $\beta$  oligomers both *in vitro* and *in vivo*.<sup>302,303</sup> Maltose poly(propyleneimine) glycodendrimers (mPPI, **Fig. 1.14**, 3) were exploited to convert A $\beta$  oligomers into A $\beta$  fibrils, through a fibril clumping anti-amyloid toxicity strategy. The mechanism of action of mPPI against growing amyloid fibrils (A $\beta$ s) is not completely clear but cytotoxicity

reduction is suggested to be achieved by impeding A $\beta$ s to penetrate cells, blocking their putative intracellular detrimental effect. Glycodendrimers are suggested to bind to A $\beta$ s, changing their surface charge or simply clumping them into large size glyco-aggregates, thus reducing interactions with cell membranes. Different open-shell (OS) and dense-shell (DS) mPPIs (**Fig. 1.14**, 4-5) were tested *in vitro* on A $\beta$ s aggregation against A $\beta$  peptides stock solutions, and toxic AD brain tissue extracts were used on human neuroblastoma cell lines. In both cases, glycodendrimers effect resulted in enhanced fibrillar formation and lower cytotoxicity in a structure-dependent fashion. *In vivo* experiments were also conducted where OS/DS-mPPIs were FITC labeled and found to accumulate within APP/PS1 transgenic mice brain tissues after intranasal administration, indicating they had crossed the BBB in significantly different and structure-dependent amounts. Moreover, glycodendrimers have been found to be able to promote the aggregation of soluble A $\beta$ s into potentially less toxic fibrils in APP/PS1 mice. However, no memory improvement was detected via the two-object recognition test after chronic treatment in comparison with control animals. Unfortunately, significant detrimental effects were observed in WT APP/PS1 mice after chronic treatment with cationic OS-mPPIs, highlighting once more the known setbacks linked to positively charged structures when it comes to medical applications. In conclusion, glycodendrimers have demonstrated interesting features (see above, *Klementieva et al.*) ranging from their generally recognized biocompatibility,<sup>304</sup> ability to interfere with synthetic A $\beta$  fragments, human A $\beta$  fragments, and prion peptides/proteins assembly,<sup>305</sup> ability to cross the BBB, capacity to exclude prion proteins infection in pre-treated cells (see above, *McCarthy et al.*) as well as their destabilizing activity upon misfolded prion protein aggregates.<sup>306</sup> Apart from these potentialities, these studies also pointed out the necessity to refine glycodendrimers characteristics to reduce their conceivably harmful side effects before considering them for neuromedical applications.



**Fig. 1.14.** Exemplifying structures of glycosides and glycodendrimers for neurochemistry applications. Glyco-epitopes grafted on biomaterials:  $\alpha$ -D-Glu (**1**) and Fuc $\alpha$ 1-2Gal (**2**) functionalized collagen. **3.** Maltose poly(propyleneimine) glycodendrimer (mPPI) scaffold: idealized general structure exposing functional moieties in the outer shell. **4.** Representation of the functional moieties in dense-shell (DS) mPPI (n° of functional moieties reported for 4th and 5th generation mPPI). **5.** Representation of the functional moieties in open-shell (OS) mPPI (n° of functional moieties reported as before).

## 2. PREMISES AND OBJECTIVES.

Plenty of studies have been carried out to uncover how the biological information is translated into cellular effects from the Genome through the Proteome, unveiling how the letters of the first two alphabets of life, nucleotides and amino acids, assemble into genes and proteins, coding the message of cellular biochemistry. A fair body of biotherapeutics and biomedical applications has been generated throughout the years from both proteins and nucleic acids, starting from recombinant Insulin, through vaccines and mAbs, towards gene therapy. As amply referenced within this thesis introduction, the glycan component of any biochemical system plays a significant role in its development and behaviour. It is therefore imperative to distance the experimental lens from genes and proteins in order to broaden the scientific view, to include the letters of the third alphabet of life, the monosaccharides, which organize into glycans, towards the achievement of more complete and efficient biological models and biomedical applications. Glycans still represent a fairly overlooked biological component, which implications in cellular and tissues biochemistry, along with potentialities in biomedical applications, are suggested to be enormous by an already substantial and however fast-growing body of evidences. The core body of the studies investigating the glycosylation patterns and their roles regards immunoglobulins, plasma samples, and sometimes blood, but comparatively limited work has been conducted on more complex solid tissues which still remain an underexplored territory. Amongst these, the CNS is to date still almost an uncharted land when it comes to glycobiology, although suggested to be biomedically fertile by a growing body of interesting works. Considering the necessity to map this unfamiliar landscape, which calls for adequate instrumentations, equipment, and methods, the objective of the projects contained in this thesis is to provide the glycoanalyst with novel tools, glycoanalytical platforms, and glycomolecules for neurochemistry studies. This thesis experimental work travels from the big picture (brain *N*-glyco(proteo)mics approaches), through the analysis of single biological targets (a specific brain *N*-glycoprotein), towards the synthesis of small glycoepitopes for neural studies. More in detail, it comprises the design, development and thorough validation of a bioanalytical method for brain *N*-glycans investigation, eventually applicable to any other solid tissue; the state of the art of an ongoing work regarding the investigation of neurologically interesting *N*-glycans and *N*-glycoproteins found to be differentially expressed in brain tissues belonging to different animal species; the development of an efficient chemical labelling method for (glyco)proteins, successfully applied on Neuroserpin, an *N*-glycoprotein expressed in the CNS; and the syntheses of glycosides and glycodendrimers with potential room for neuromedical studies.



### 3. RESULTS.

#### 3.1 A PRECISE AND VERSATILE PLATFORM FOR RAPID GLYCOSYLATION ANALYSIS OF BRAIN TISSUE.

**3.1.1 Framework of the study.** As stated in section 1.3.7 of the introduction, the body of work carried out to investigate the CNS *N*-glycan repertoire is not vast and improved, reliable (e.g., precise, sensitive, robust) and versatile (e.g., compatible with diverse detection system and analytical set-ups) glycoanalytical workflows are required to broaden the glycoanalyst capabilities to investigate the pattern(s) of solid tissues glycosylation. Glycoanalytical workflows that optimize the sample preparation steps, minimize sample loss and reduce analytical variability are required to capture the spatio-temporal diversity of the brain *N*-glycome. Furthermore, methods able to provide glycomics and (glyco)proteomics analyses from the same sample have the potential to synergistically deliver a comprehensive investigation of glycan-related neurobiology. This is of paramount importance, since the nature of the brain *N*-glyco(proteo)me is so fluctuating<sup>265</sup> that any sample can be strikingly different from another one, even if derived from the same brain piece.<sup>263</sup> This means that combining the information deriving from both *N*-glycans and their respective *N*-glycoproteins from the same brain tissue sample is critical to build reliable knowledge towards functional studies and biomedical applications. Cell and tissue lysates are routinely prepared in many laboratories around the world and they are typically used for the extraction of various cellular components such as lipids, nucleic acids, and proteins for downstream analysis. However, to the best of the author's knowledge, currently no validated method has been described for the analysis of *N*-glycans from a crude lysate. Existing methods for the analysis of *N*-glycans from cells or tissues generally rely on the use of homogenates,<sup>39,113,265–267,129,135,196,215,260–262,264</sup> which differ from lysates in that they are typically obtained via physical disruption of the sample and are not stabilized by chemical means to prevent degradation of cellular components by autolysis. As a result, homogenates cannot be stored; they must be used immediately and therefore represent a transient, single-use medium from which typically only one component (i.e., kind of macromolecule) can be isolated in a single experiment. Lysates, on the other hand, represent a more versatile, multipurpose medium, since they have the advantage that they are stable, can be stored long-term, and hence can be re-used multiple times for different experiments of different modalities. In this project a method for the extraction and purification of *N*-glycans directly from a chemical lysate is described and, in doing so, a novel application of the common crude lysate is presented, thereby expanding the uses of this already multipurpose medium to the growing field of glycomics. In addition, a thorough validation of the method, called Lysate in-Solution

Deglycosylation (LSD), is presented. Furthermore, it is demonstrated that the LSD-isolated *N*-glycans can be labelled, modified, or derivatized as desired, and then investigated by common glycomics approaches, such as LC and MS. In addition, the crude lysate from which *N*-glycans are extracted, can be used for classical proteomics and glycoproteomics applications, such as gel electrophoresis and MS (i.e., sections 3.2.3 and 3.2.5). To evaluate and validate the LSD method, a lysate prepared from rat brain tissue was used, to ensure the applicability of the LSD method in analysing real biological samples. Furthermore, the same rat brain tissue lysate has been successfully employed to address real biological issues, by reporting *N*-glycoprotein and *N*-glycosylation site data (i.e., section 3.2.5). As amply referenced within this thesis introduction, a growing body of evidence is highlighting the crucial involvement of *N*-glycosylation within the nervous system, where it influences a plethora of aspects of brain development, physiology and pathology, such as cell adhesion, axonal targeting, synaptic transmission, excitability, Alzheimer's, Parkinson's and Prion diseases among the others.<sup>48–54</sup> Consequently, reliable and thoroughly validated bioanalytical methods that facilitate rapid, precise, sensitive, and robust analysis of both *N*-glycans and their respective *N*-glycoproteins from the same brain tissue sample are critical for advancing our understanding of *N*-glycosylation role in the CNS and are also necessary for the discovery of new biomarkers for disease diagnosis and prognosis. To place LSD in context, recent progresses and methodological advancements in the field of tissue *N*-glycomics have been reviewed and, with particular emphasis on brain *N*-glycomics, several of the pioneering methods (i.e., sections 1.2.6 and 1.3.7) that have preceded it have been examined (**Tab. 3.1.1**).<sup>39,113,264–267,269,129,135,196,215,260–263</sup> A recently published method (from now on called Homogenate in-Solution Deglycosylation, HSD) developed in the author Erasmus host institution,<sup>196</sup> was the first one to use HILIC-UPLC to separate the complex ensemble of *N*-glycans structures purified from brain tissue, with good sensitivity and resolution, but one limitation of the HSD method was that it was not possible to analyse both *N*-glycans and proteins from the same sample, thus losing valuable information about the *N*-glycoprotein component. One important shortcoming common to all of the above-introduced (i.e., sections 1.2.6 and 1.3.7) glycoanalytical workflows, when the analysis of *N*-glycans from brain tissue is considered, is the lack of adequate method validation. In this context, it is crucial for the analyst to deliver to the scientific community well-characterized and thoroughly validated bioanalytical methods, yielding reliable results, that can be easily interpreted to obtain grounded, biologically relevant conclusions. The publication of insufficiently validated analytical papers might fuel the reproducibility problems the scientific community is experiencing,<sup>307</sup> and contribute to the generation of results with questionable reliability, thereby lowering the quality of the published records, as recently highlighted in the context of quantitation

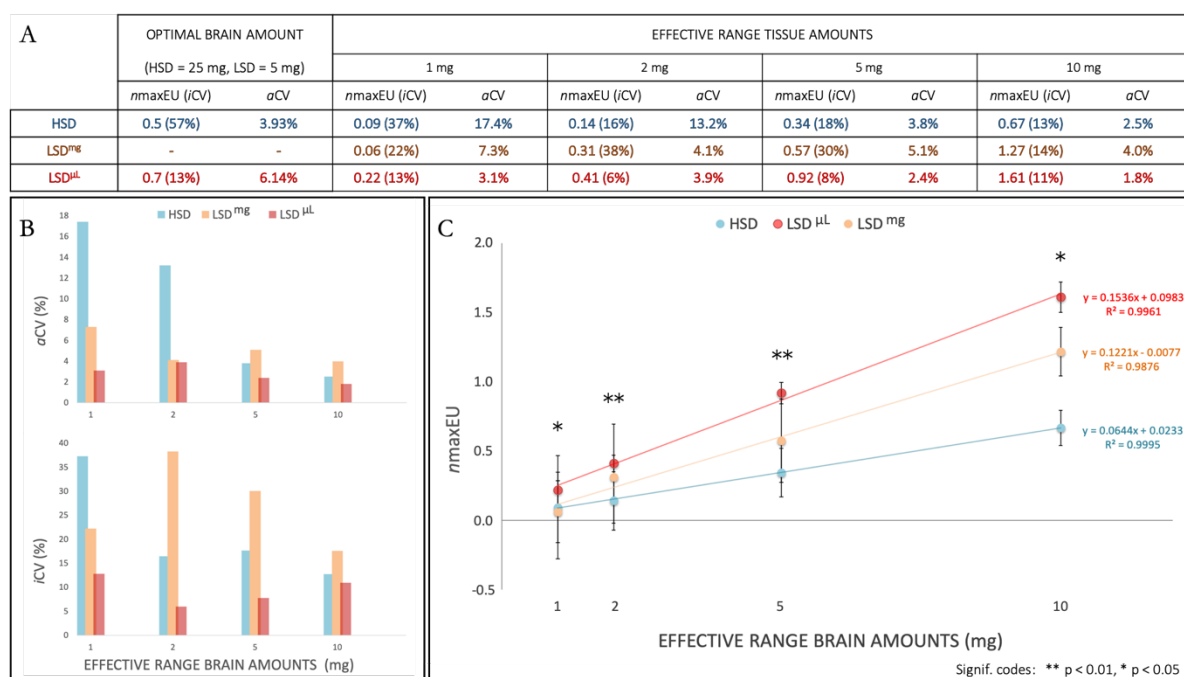
of antidiabetic agents in blood.<sup>308</sup> Of the fifteen works introduced above, only three<sup>196,263,265</sup> stated some validation parameters (e.g., sensitivity and precision), even if above the acceptance threshold for bioanalytical methods<sup>309,310</sup> (i.e., precision)<sup>263</sup>, or below it (i.e., precision)<sup>196</sup>, or lacking a proper mathematical definition (i.e., sensitivity)<sup>265</sup>. Twelve out of fifteen *N*-glycomic workflows applied to brain tissue samples completely lacked a proper method validation on brain tissue samples (**Tab. 3.1.1**). The aim of this project is, therefore, to introduce to the field a thoroughly validated method for the analysis of *N*-glycans from tissue samples that is simple, effective, and compatible with common proteomic workflows which typically begin with the generation of a sample lysate using chemical means. The newly developed method, LSD, is based on enzymatic deglycosylation of intact glycoproteins extracted directly from a tissue lysate and therefore allows researchers to perform both proteomics and *N*-glycomics analyses from the same sample. In light of the above stated importance of bioanalytical method validation, a thorough validation on LSD in terms of selectivity, precision, sensitivity, robustness, limit of detection (LOD), linearity, and range was carried out. Since the reporting of absolute values obtained from the application of only one method is not really informative without a proper control method analyzed under the same conditions, in this project the reliability and performance of LSD and HSD were directly compared side by side. LSD represents a significant improvement upon HSD and outperforms it in every tested aspect. Furthermore, in comparison with the aforementioned bioanalytical methods reported in the literature, LSD is the only one in which enzymatic deglycosylation is performed directly on intact proteins isolated from a chemically-produced tissue lysate, it boasts the smallest amount of starting brain tissue producing sensitive and precise results (1 mg), it displays quick sample preparation (3 days), consistent and very good precision over a range of brain tissue amounts (1 to 10 mg), optimal linearity, ample range, and specificity towards the detection of *N*-glycans only, in addition to being the most thoroughly validated *N*-glycomic method in the group (**Tab. 3.1.1**).

N-glycoanalytical workflow reference	Starting amount of brain tissue (mg)	Sample prep. (days)	Sensitivity	Precision (i.e., CV%, PCC)	Robustness	Linearity	Range (mg)	Selectivity
<i>Glycoconj. J.</i> , 1992, <b>9</b> , 293–301.	6000	> 3	X	X	X	X	X	X
<i>Eur. J. Biochem.</i> , 1998, <b>251</b> , 691–703.	6000	> 3	X	X	X	X	X	X
<i>Eur. J. Biochem.</i> , 1998, <b>258</b> , 243–270.	6000	> 3	X	X	X	X	X	X
<i>Glycobiology</i> , 2007, <b>17</b> , 261–276.	2	?	X	X	X	X	X	X
<i>J. Neurochem.</i> , 2007, <b>103</b> , 25–31.	> 3000	?	X	X	X	X	X	X
<i>Anal. Biochem.</i> , 2012, <b>423</b> , 253–260.	?	?	X	X	X	X	X	X
<i>Anal. Chem.</i> , 2013, <b>85</b> , 4074–4079.	< 0.001	< 3 (hours)	X	CV 35%	X	X	X	X
<i>J. Proteome Res.</i> , 2013, <b>12</b> , 5791–5800.	?	≥ 3	X	X	X	X	X	X
<i>Glycoconj. J.</i> , 2014, <b>31</b> , 671–683.	2	?	X	X	X	X	X	X
<i>Biochim. Biophys. Acta</i> , 2015, <b>1850</b> , 1704–1718.	?	≥ 3	X	X	X	X	X	X
<i>Anal. Chem.</i> , 2015, <b>87</b> , 2869–2877.	1.5	≥ 3	✓	PCC > 0.98	X	X	X	X
<i>Biochim. Biophys. Acta</i> , 2016, <b>1860</b> , 1716–27.	> 1000	≥ 3	X	X	X	X	X	X
<i>Mol. Cell. Proteomics</i> , 2017, <b>16</b> , 2268–2280.	?	≥ 3	X	X	X	X	X	X
<i>High-Throughput Glycomics and Glycoproteomics</i> , Humana Press, New York, NY, 2017, pp. 207–216.	25	≥ 3	X	CV 4%	X	X	X	X
<i>J. Am. Soc. Mass. Spectrom.</i> 2019, <b>30</b> (7), 1254–1261.	< 1	≤ 3	X	X	X	X	X	X
The LSD workflow presented in this work	1	3	✓	CV 6%	✓	R <sup>2</sup> = 0.9961	1-10	✓

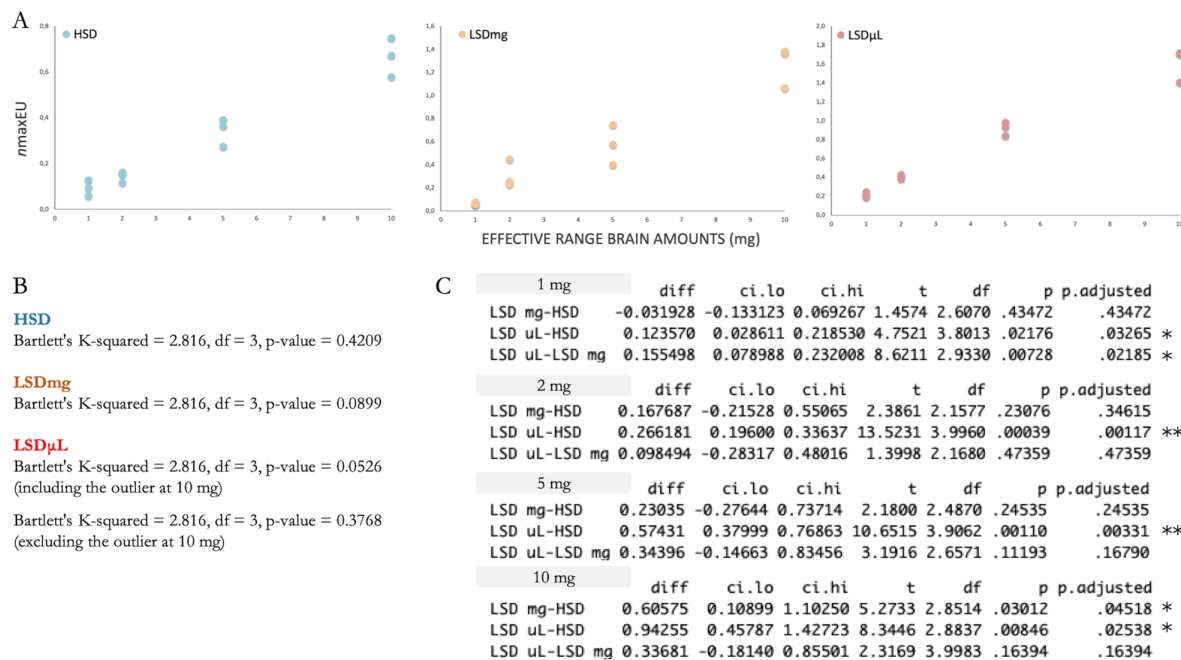
**Tab. 3.1.1.** Validation parameters of LSD in comparison to similar *N*-glycomic workflows in the literature. Parameters considered in this table are relative to the analysis of *N*-glycans from brain tissue samples. Method validation carried out on different samples (e.g., cell lysate, plasma, isolated *N*-glycoproteins) within papers also analyzing brain *N*-glycans is not considered: a validated method is not transferable between different kind of samples, unless evidence of its transferability is provided. Starting amount of brain tissue = mgs of fresh biological material entering the workflow; Sample prep. (days) = approximated value based on available information (e.g., available timings in the experimental section); Sensitivity = does the considered work contain any testing of the method sensitivity (e.g., slope of the calibration curve, normalized intensity of the signals at different sample concentrations)?; Precision = does the considered work contain any testing (e.g., CV%, PCC) of the method precision?; Robustness = was the capacity of the method to remain unaffected by small, but deliberate variations in its parameters tested?; Linearity = was the method tested on different amounts of starting material?; Was the linearity assessed by giving, at least, an R<sup>2</sup> value?; Range = does the considered work specify a range of sample amount on which the method's performance is reliable (e.g., precise, sensitive)?; Selectivity = was the method tested for its selectivity towards the desired analyte? Red-crossed cells = no data; Orange cells with question mark = not stated clearly / difficult to be inferred; CV = coefficient of variation; PCC = Pearson correlation coefficient.

**3.1.2 Sample preparation.** It is known that *N*-glycosylation patterns differ between different brain regions.<sup>311</sup> Therefore, to ensure that any differences in the obtained glycoprofiles are due to methodological aspects only (and not biological variation), it is imperative that the same sample is employed for both workflows. To overcome this problem, brain tissue samples employed within this study were all mildly blended prior to analysis to minimize potential differences arising from heterogeneous *N*-glycosylation patterns from different brain regions. The procedure (i.e., section 4.1.2) yielded a brain pseudo-homogenate (pHomo) and aliquots of this mixture were used as the starting material for both methods.

**3.1.3 Sensitivity and precision: optimal amount of starting tissue.** The optimal amount of brain tissue to be used for analysis represents the best trade-off between the quantity of sample employed in the analysis and the method performance in terms of precision and sensitivity. HSD and LSD precisions were evaluated by comparing chromatographic fraction areas and were tested as intermediate precision (same experiment performed four times, each time in tetraplicates, within the same laboratory, on different days, with freshly prepared solutions and using different UPLC machines and columns for the analysis). A measure of sensitivity on a single point (the optimal brain amount) is given by the ratio between the average nmaxEU displayed by the method and the starting amount of tissue employed. The optimal amount of brain tissue for use with HSD was determined to be 25 mg and this routinely gave interpretable chromatograms displaying an aCV of 4%<sup>196</sup> and a sensitivity of 0.02 nmaxEU/mg with an iCV of 57%. The optimal amount of starting tissue for the LSD method was found to be 5 mg (previously performed optimization experiments, data not shown) with an aCV of 6%, a sensitivity of 0.1 nmaxEU/mg, and an iCV of 13%. The analysis showed that on the optimal brain amount, the precisions (aCV) of HSD and LSD were comparable and well below the threshold for bioanalytical methods (CV < 15%),<sup>309,310</sup> with LSD being more sensitive and stable (nmaxEU values, iCV) than HSD (**Fig. 3.1.1**). A thorough validation of a bioanalytical method requires testing a broader range of conditions and cannot be reliable with data obtained on a single point. Furthermore, sensitivity can be more properly estimated as the slope of the calibration curve. Therefore, the authors decided to test both methods on a range of brain sample quantities to push their resolving power towards lower limits.



**Fig. 3.1.1.** Sensitivity and precision of HSD Vs LSD<sup>mg/μL</sup>. **A.** Calculated sensitivity (nmaxEU) and variability (iCV and aCV) of each method on every tested amount of tissue. **B.** Variability of fraction area (aCV) and maximum signal intensity (iCV) of each method for every amount of brain tissue within the effective range. **C.** Sensitivity and linearity of each method determined from a calibration curve. Descriptive error bars show data spread within replicates (n = 1, triplicates), and the value reported is ± iCV. Statistical significance of LSD<sup>μL</sup> Vs HSD comparison is reported as p-value above every point (LSD<sup>mg</sup> comparisons can be found in **Fig. 3.1.2**).

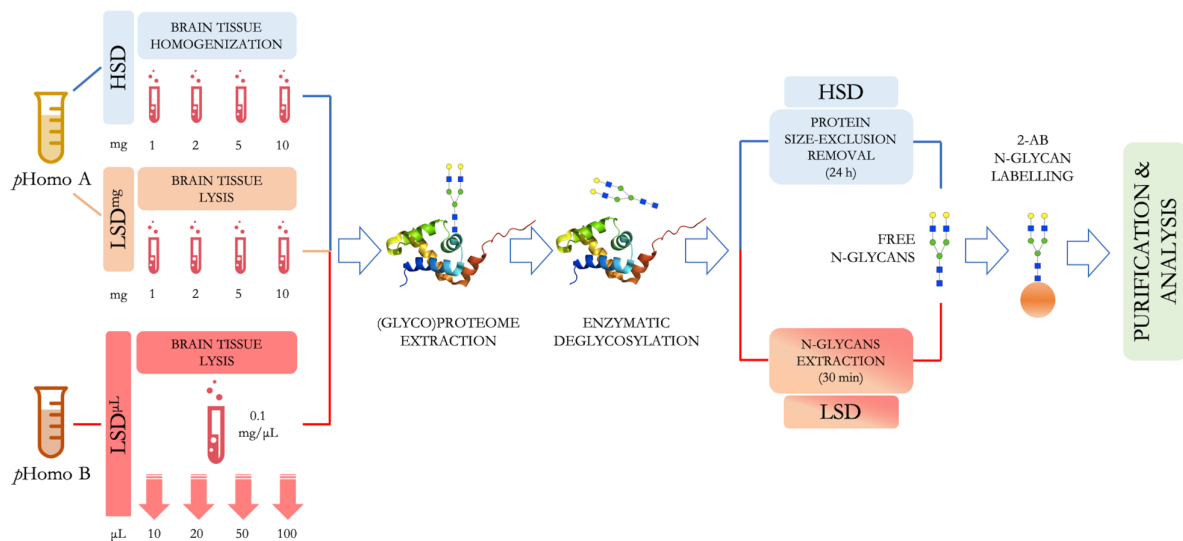


**Fig. 3.1.2.** HSD and LSD<sup>mg/μL</sup> linearity analysis. **A.** Scatter plots for a visual analysis of the variance of replicates for each starting amount of brain tissue in the effective range. **B.** Bartlett's test of homogeneity of variances: the test null-hypothesis is that all the replicates have the same variance. **C.** Statistical significance (Welch's ANOVA, Games-Howell post-hoc test) of the differences in nmaxEU between methods for each starting amount of brain tissue in the effective range (n=1, triplicates, \*p < 0.05, \*\*p < 0.01).

**3.1.4 Sensitivity and precision: effective range of starting tissue.** HSD and LSD performances were tested on 1, 2, 5 and 10 mg of starting brain tissue. HSD was performed as usual,<sup>196</sup> directly homogenizing the aforementioned brain quantities. LSD was further developed into two variants (i.e., section 4.1.3): LSD<sup>mg</sup> and LSD<sup>μL</sup>, respectively comprising the direct lysis of the aforementioned brain quantities (LSD<sup>mg</sup>) and volumes corresponding to the aforementioned brain quantities taken from a single lysate (LSD<sup>μL</sup>). As far as LSD<sup>μL</sup> is concerned, a single lysate with a concentration of 0.1 mg of tissue per μL was produced and 10, 20, 50, and 100 μL were taken and employed within the workflow. HSD and LSD<sup>mg</sup> were tested within the same experiment employing the same pHomo, whereas LSD<sup>μL</sup> was performed on a different pHomo (obtained exactly the same way), within a second experiment (**Fig. 3.1.3**). LSD<sup>μL</sup> was performed because the mechanical breaking of the tissue in the LSD<sup>mg</sup> lysis step caused a significant and variable loss of material in the upper part of the syringe due to the very small volumes employed, thus distorting



the real precision and sensitivity of the method. nmaxEUs for each brain quantity were used to create a calibration curve to test the methods' sensitivity, LOD, linearity and range. The comparison of chromatographic fraction areas in terms of aCV, was used to calculate precision over the entire range that, in this case, is repeatability (same experiment performed in triplicates, within the same laboratory, on the same day, with the same solutions and using the same UPLC machine and column for the analysis). All the results described below, are shown in detail in **Fig. 3.1.1**. HSD and LSD<sup>mg/μL</sup> showed a linear relationship between tissue amounts and signal intensities, with homoscedastic replicates (**Fig. 3.1.2**) and good R<sup>2</sup> values. Precision over the entire range was found to be substantially better for LSD<sup>μL</sup> (aCV and iCV) and, on average, better for LSD<sup>mg</sup> (aCV) than for HSD. LSD<sup>mg</sup> and LSD<sup>μL</sup> sensitivities, calculated as the slope of the calibration curve, were found to be 2 and 2.4-fold higher than HSD respectively. LSD<sup>mg</sup> and LSD<sup>μL</sup> produced interpretable chromatograms with acceptable precision even when performed on 2 and 1 mg of brain sample respectively, whereas HSD only performed reliably from 5 mg, therefore showing a smaller range and a higher LOD. While LSD<sup>mg</sup>, on average, performed better than HSD, LSD<sup>μL</sup> outperformed it, definitely being the most powerful version of the method.

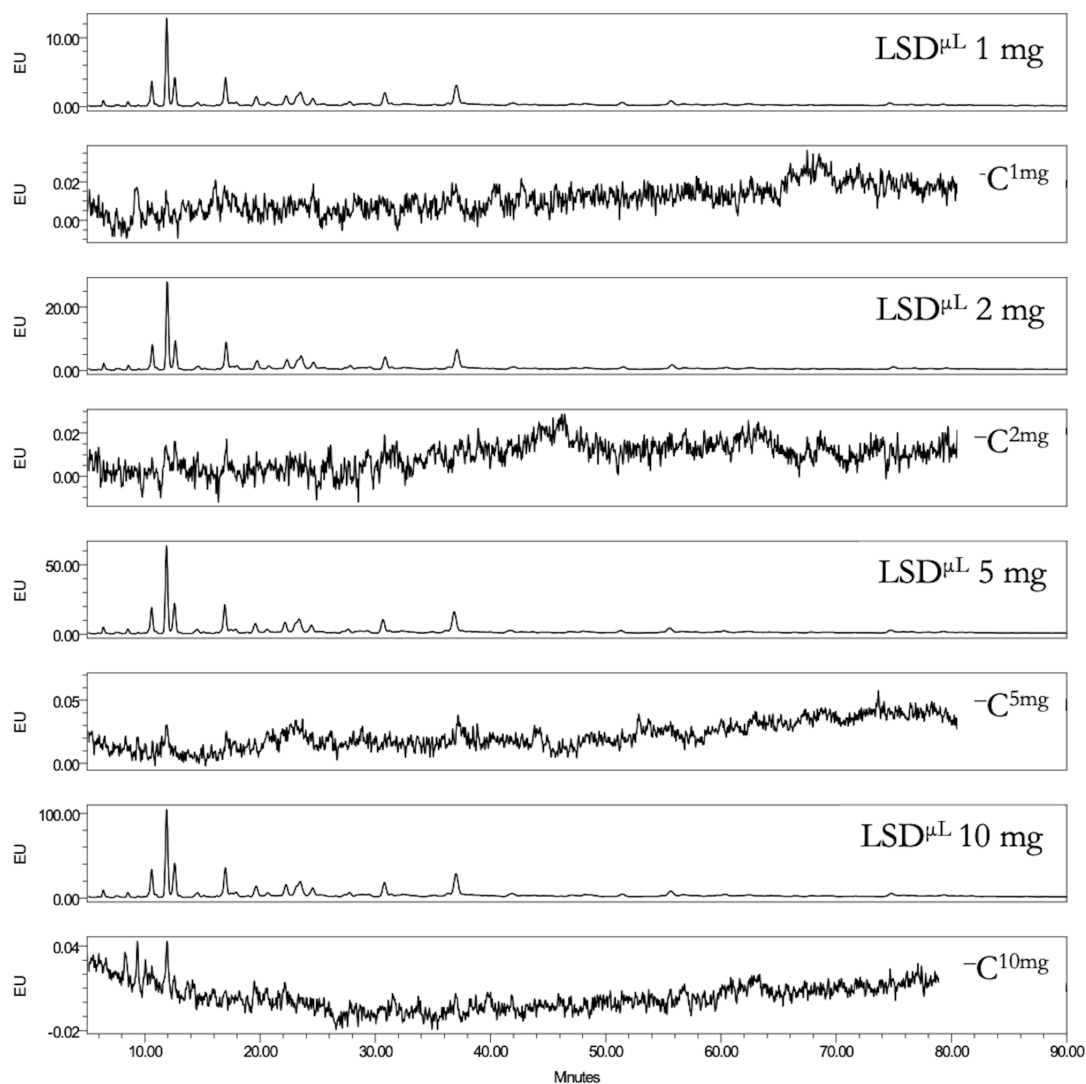


**Fig. 3.1.3.** HSD and LSD<sup>mg/μL</sup> *N*-glycan extraction and 2-AB *N*-glycan labelling. Purification & analysis include GHP for HILIC-UPLC-FLR and GHP followed by PGC-SPE for HILIC-UPLC-ESI-QqTOF-MS.

**3.1.5 Selectivity.** LSD<sup>μL</sup> selectivity was thoroughly tested using <sup>13</sup>C samples for each amount of starting tissue in the effective range, and the method was found to be specific for *N*-glycans, ruling out the possibility that eventual contaminants could absorb/emit at the same wavelength and

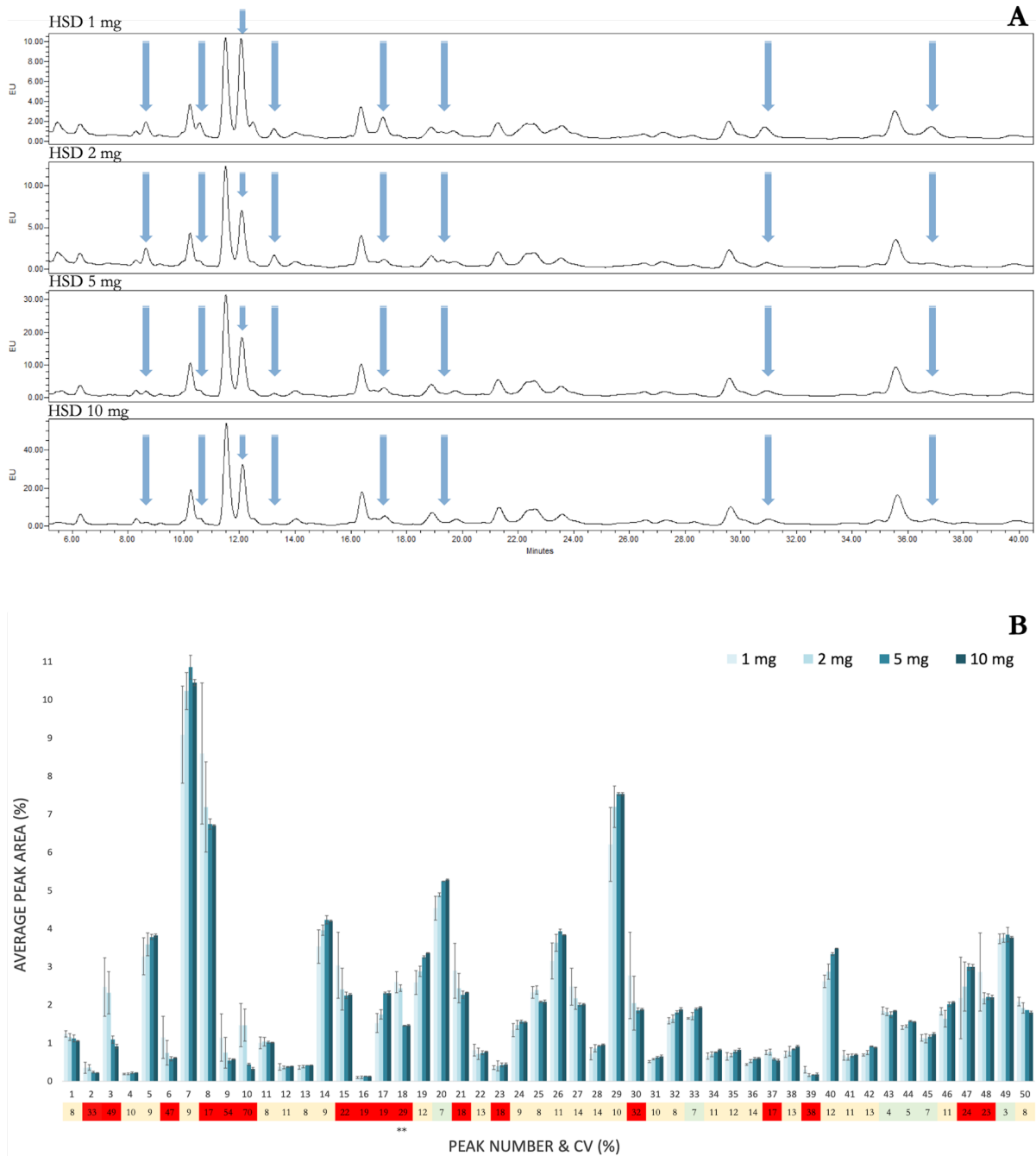


retention time window as the analytes. The same experiment gave the authors the possibility to assess another important aspect for bioanalytical method validation, namely carryover effect.<sup>309</sup> In fact, C samples were analysed by UPLC immediately after their corresponding samples, and water was analysed at the beginning and end of each chromatographic run, without seeing any contaminant nor analyte-related signals even at the highest tissue amount (**Fig. 3.1.4**).



**Fig. 3.1.4.** LSD $\mu$ L specificity and carryover effect. Chromatograms of labelled and unlabeled (-C) samples are shown for each starting amount of brain tissue in the effective range.

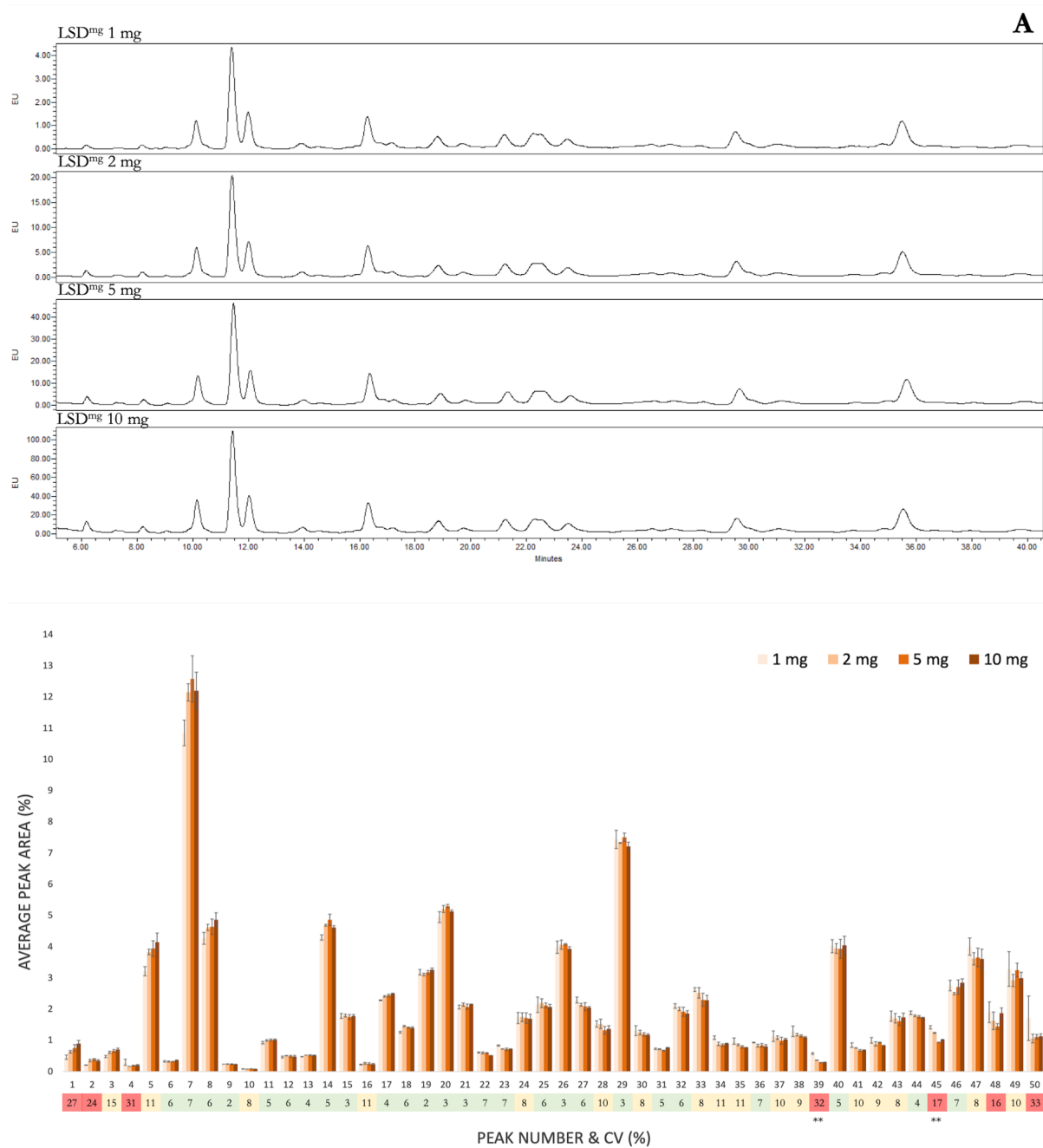
**3.1.6 Robustness and versatility.** Some important conclusions about robustness can also be drawn from these experiments. When performing HSD on different amounts of starting tissue within the effective range (but taken from the same pHomo), the derived chromatograms quantitatively varied depending on the amount of tissue employed, with higher levels of variability seen with smaller tissue amounts (**Fig. 3.1.5**).



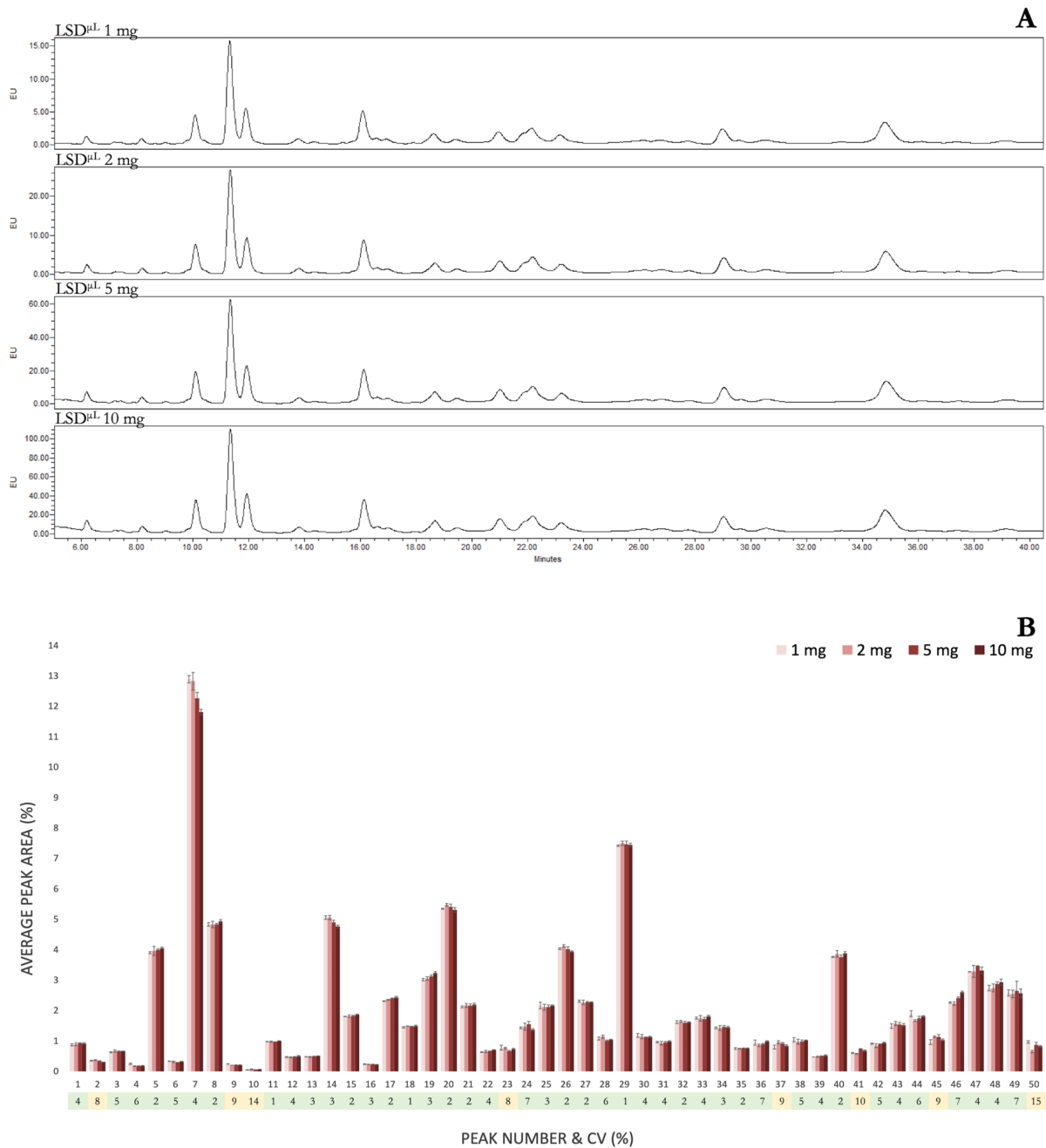
**Fig. 3.1.5.** Amount-dependent variation in the chromatographic profile of brain tissue samples analysed by HSD. **A.** Qualitative comparison of HSD chromatograms in the effective range of starting brain tissue amounts. Chromatograms are cut at 41 min to better highlight examples of varying fractions. Arrows indicate variable fractions. **B.** Quantitative comparison of HSD chromatograms in the effective range of starting brain tissue amounts. Descriptive error bars show data spread within replicates ( $n = 1$ , triplicates) as  $\pm$  SD. The CV for each fraction is reported as a measure of precision of the value of the fraction area between different brain amounts (green = CV  $\leq$  7%; yellow = 7% < CV  $\leq$  15%; red = CV > 15%). See Fig. 3.1.13 for integration boundaries. Statistical significance of the differences (1 mg and/or 2 mg Vs 10 mg, Welch's ANOVA, Games-Howell post-hoc test) regarding fractions with CVs > 15% is reported (\*\*  $p < 0.01$ ).

Specifically, a change in the relative abundance of certain fractions was observed when different amounts of the same pHomo were analysed using the HSD method. The quantitative profiles of

LSD chromatograms were much more consistent at all amounts of starting tissue within the effective range (Fig. 3.1.6, Fig. 3.1.7).



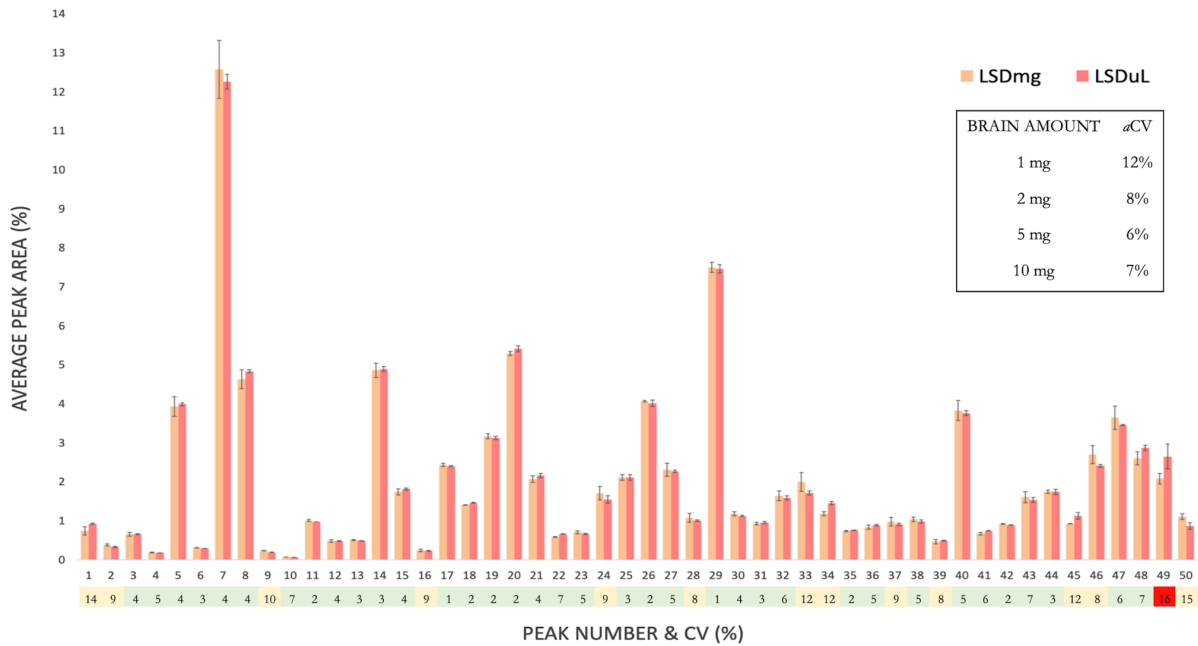
**Fig. 3.1.6.** Chromatograms of brain samples analysed by LSD<sup>mg</sup> are more consistent regardless of starting tissue amount. **A.** Qualitative comparison of LSD<sup>mg</sup> chromatograms in the effective range of starting brain tissue amounts. Chromatograms are cut at 41 min to highlight the same region considered in Fig. 3.1.5. **B.** Quantitative comparison of LSD<sup>mg</sup> chromatograms in the effective range of starting brain tissue amounts. Descriptive error bars show data spread within replicates (n = 1, triplicates) as  $\pm$  SD. CV for each fraction is reported as a measure of precision of the value of the same fraction area between different brain amounts (green = CV  $\leq$  7%; yellow = 7% < CV  $\leq$  15%; red = CV > 15%). See Fig. 3.1.13 for integration boundaries. Statistical significance of the differences (1 mg and/or 2 mg Vs 10 mg, Welch's ANOVA, Games-Howell post-hoc test) regarding fractions with CVs > 15% is reported (\*\* p < 0.01).



**Fig. 3.1.7.** Chromatograms of brain samples analysed by LSD<sup>μL</sup> are consistent regardless of starting tissue amount. **A.** Qualitative comparison of LSD<sup>μL</sup> chromatograms in the effective range of starting brain tissue amounts. Chromatograms are cut at 41 min to highlight the same region considered in Fig. 3.1.5 and 3.1.6. **B.** Quantitative comparison of LSD<sup>μL</sup> chromatograms in the effective range of starting brain tissue amounts. Descriptive error bars show data spread within replicates (n = 1, triplicates) as ± SD. CV for each fraction is reported as a measure of precision of the value of the same fraction area between different brain amounts (green = CV ≤ 7%; yellow = 7% < CV ≤ 15%; red = CV > 15%). See Fig. 3.1.13 for integration boundaries.

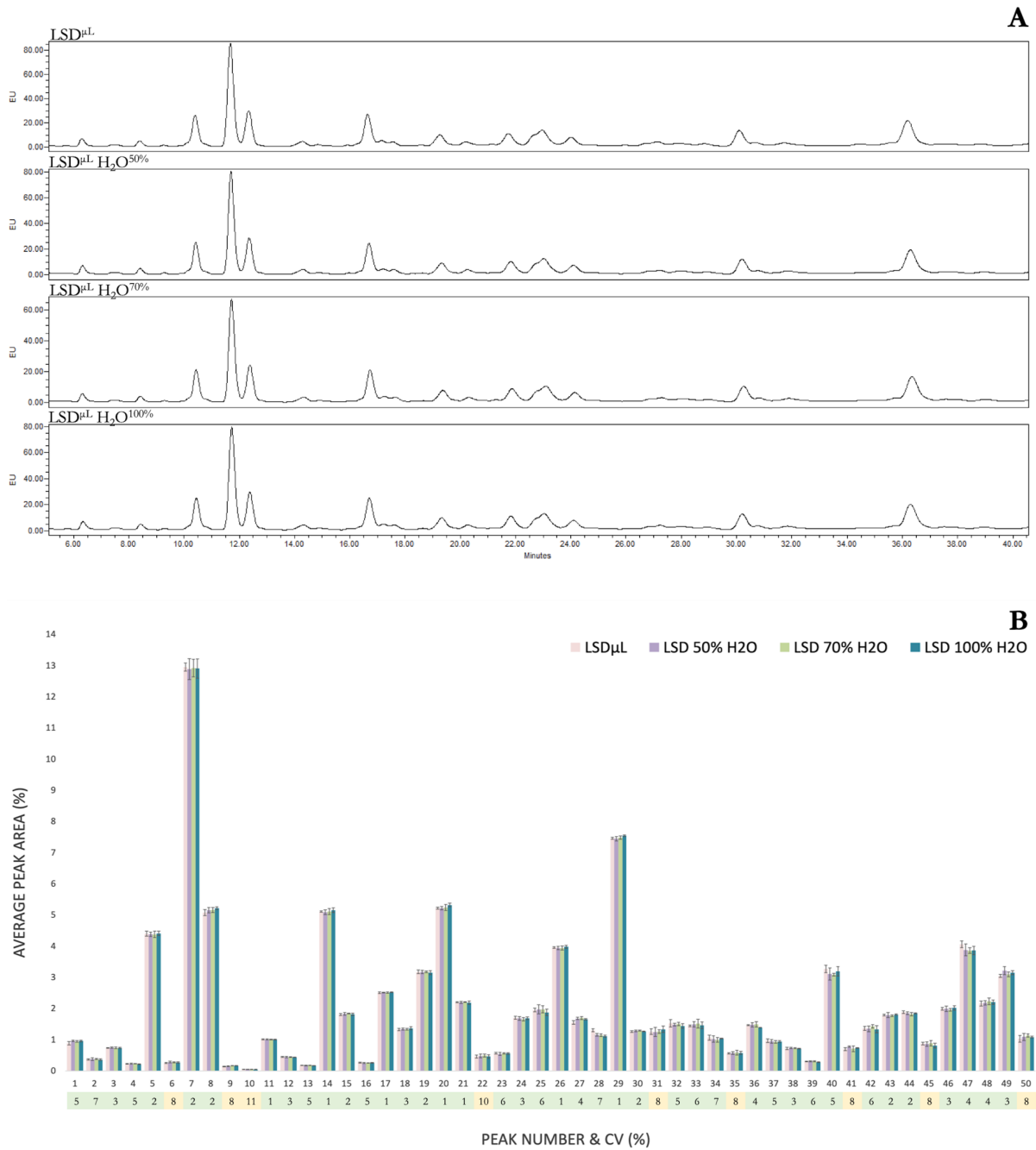
Furthermore, the chromatographic profiles of LSD<sup>μL</sup> and LSD<sup>mg</sup> were substantially consistent (49/50 fractions showed a CV < 15%; fraction 49 showed a CV of 16%), even if performed within

a different experiment, employing a different pH<sub>omo</sub> and different methodological procedures (Fig. 3.1.3), always showing aCV values < 15% (Fig. 3.1.8).



**Fig. 3.1.8.** Similarity of profiles obtained by LSD<sup>μL</sup> and LSD<sup>mg</sup>. Quantitative comparison of LSD<sup>μL</sup> and LSD<sup>mg</sup> chromatograms in the effective range of starting brain tissue amounts (5 mg profiles, representing the optimal brain amount, are displayed as an example). CV for each fraction is reported as a measure of precision of the same fraction area between the two versions of the LSD method (green = CV ≤ 7%; yellow = 7% < CV ≤ 15%; red = CV > 15%). No statistical significance (LSD<sup>μL</sup> 30.08 *V*s LSD<sup>μL</sup> 31.07, n=1, triplicates, Wilcoxon-Mann-Whitney) was found for the differences in fractions with CVs > 15%. aCVs for each starting amount of brain tissue within the effective range, calculated between the two LSD versions, are reported in the inset. See Fig. 3.1.13 for integration boundaries.

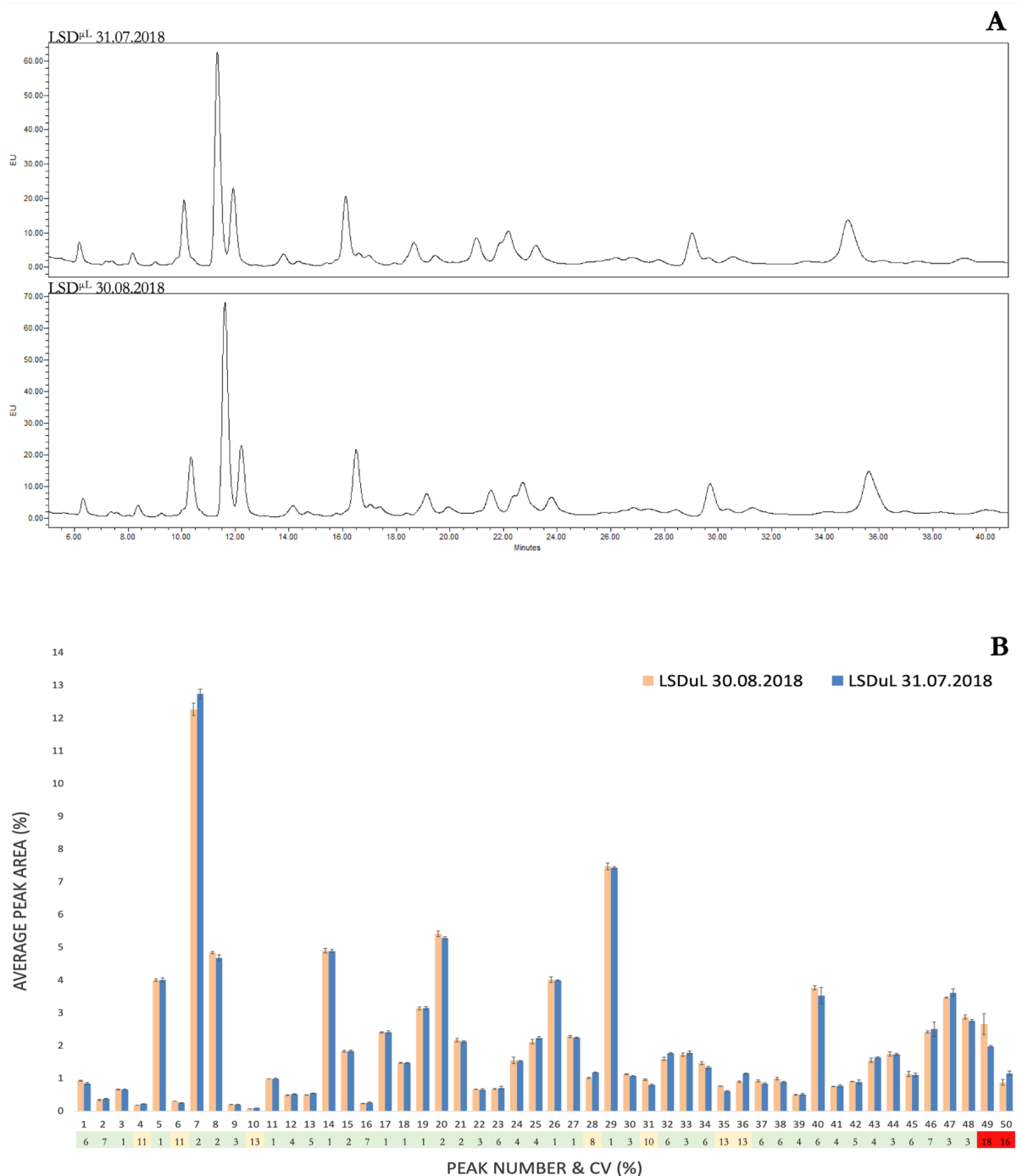
Additionally, in a previously performed LSD optimization experiment, the *N*-glycan extraction step was repeated twice, the second time with increasing polarity of the aqueous phase, but no differences were observed in the chromatograms, suggesting that the employed conditions are able to extract all the enzymatically released *N*-glycans within the sample. (Fig. 3.1.9).



**Fig. 3.1.9.** Adding a second round of *N*-glycan extraction has little effect on the chromatographic profile of brain samples analysed by LSD $\mu$ L even when the polarity of the aqueous phase is changed. **A.** Qualitative comparison of LSD $\mu$ L chromatograms obtained with a second round of *N*-glycan extraction, using aqueous phases of varying polarity. Chromatograms are cut at 41 min to better highlight the qualitative consistency of the profiles. **B.** Quantitative comparison of LSD $\mu$ L chromatograms obtained with the second round of *N*-glycan extraction with increasing polarity of the aqueous phase (% of H<sub>2</sub>O reported in the legend refers to the second *N*-glycan extraction round; LSD $\mu$ L was performed with a single extraction step). Descriptive error bars show data spread within replicates ( $n = 1$ , triplicates) as  $\pm$  SD. CV for each fraction is reported as a measure of precision of the value of the same fraction area amongst different aqueous phase polarities (green = CV  $\leq$  7%; yellow = 7% < CV  $\leq$  15%; red = CV > 15%). See Fig. 3.1.13 for integration boundaries.

Since robustness is defined as the method's capacity to remain unaffected by small, but deliberate variations in its parameters (different methodological procedures in the tissue lysis or

*N*-glycan extraction steps, different experiments carried out with slightly different equipment), and provides an indication of the method's reliability during normal usage,<sup>312</sup> the authors conclude that LSD<sup>μL</sup> is more robust and more reliable than HSD. In addition, some inferences can be drawn regarding the stability of LSD, another significant parameter of method validation,<sup>309</sup> since the brain tissue lysate representing LSD starting material was frozen and thawed multiple times and employed within different experiments in different months, always producing consistent chromatographic profiles (**Fig. 3.1.10**).

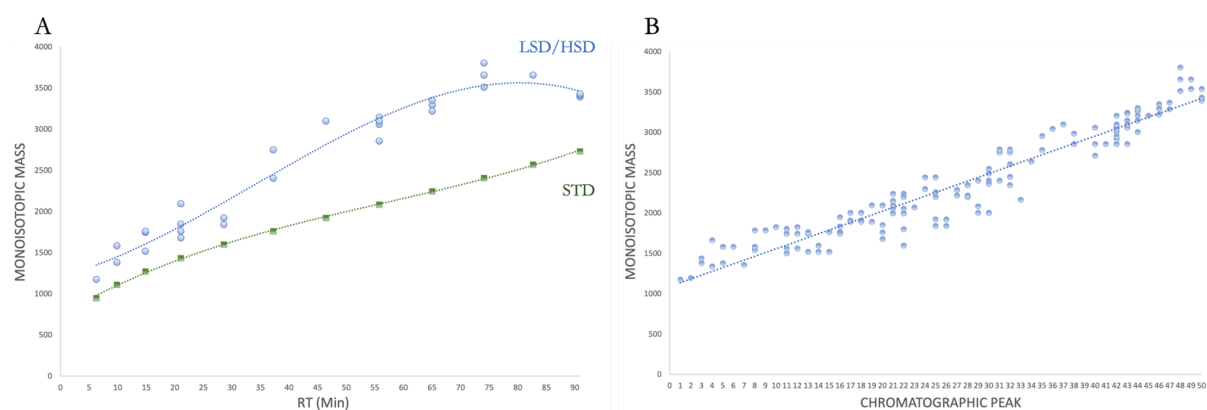




**Fig. 3.1.10.** Stability of samples stored in lysis buffer. *N*-glycome analysis by LSD<sup>μL</sup> was performed on the same brain tissue lysate, frozen-thawed multiple times over a period of one month. **A.** Qualitative comparison of LSD<sup>μL</sup> chromatograms in the aforementioned conditions. Chromatograms are cut at 41 min to be consistent with previously displayed sections. **B.** Quantitative comparison of LSD<sup>μL</sup> chromatograms in the aforementioned conditions. Descriptive error bars show data spread within replicates (n = 1, triplicates) as ± SD. CV for each fraction is reported as a measure of precision of the same fraction area between the two experiments (green = CV ≤ 7%; yellow = 7% < CV ≤ 15%; red = CV >15%). See Fig. 3.1.13 for integration boundaries. No statistical significance (LSD<sup>μL</sup> 30.08 *V*s LSD<sup>μL</sup> 31.07, n=1, triplicates, Wilcoxon signed-rank test) was found for the differences in fractions with CVs > 15%.

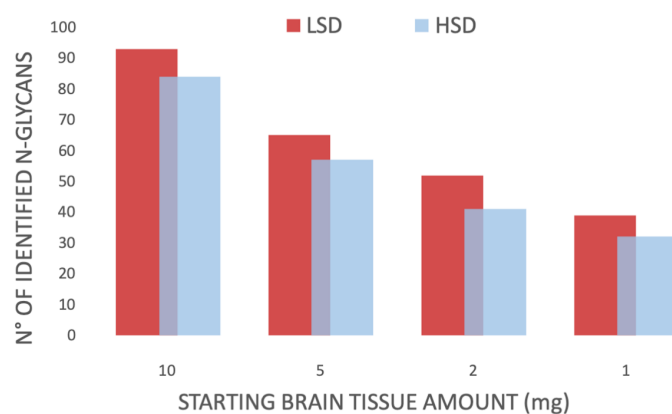
The lysate was also successfully used for analysis of (glyco)proteins by SDS-PAGE and MS (i.e., sections 3.2.3 and 3.2.5) thereby confirming its compatibility with downstream proteomics applications. The RIPA buffer used in the LSD method is a very commonly used lysis buffer and is routinely employed in many laboratories worldwide for the preparation of protein extracts from cultured cells and various tissue including kidney,<sup>313</sup> vascular vessels,<sup>314</sup> skeletal muscles,<sup>315</sup> lung,<sup>316</sup> and brain tissue<sup>317,318</sup> among others, suggesting that the LSD method is compatible with a large range of cell and tissue types. Indeed, laboratories using this buffer may have existing banks of sample lysates stored for future analysis, and LSD therefore provides an ideal platform for rapid glycosylation analysis of these archived samples, effectively enabling the extraction of an additional layer of information about these samples without the need to collect fresh biological material, thereby adding value to existing studies.

**3.1.7 Structural resolution of *N*-glycan samples derived using HSD and LSD.** LSD<sup>μL</sup> and HSD MS spectra related to each brain tissue amount in the effective range were analysed identically, as described in the experimental section. The brain *N*-glycan elution trend (masses over time/fractions) was found to be coherent in comparison to the pattern of the 2-AB-labelled hydrolysed glucose oligomers (external standard) analysed under the same conditions (**Fig. 3.1.11**).



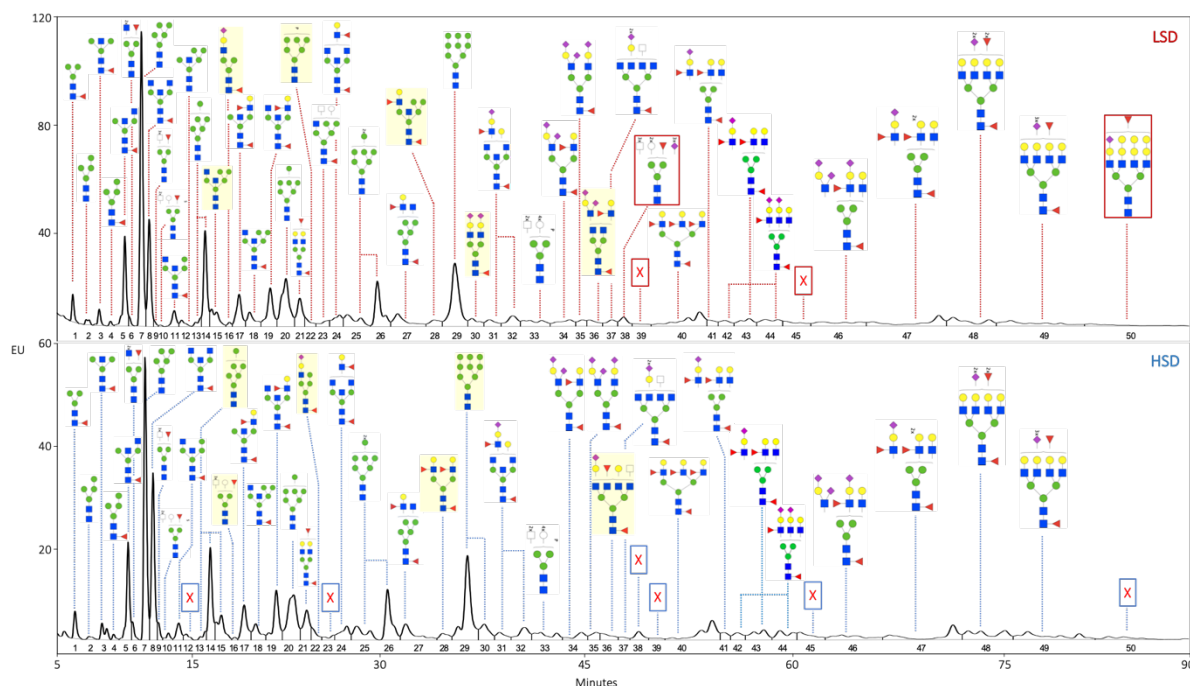
**Fig. 3.1.11.** Elution trend of the extracted brain *N*-glycans and external standard by monoisotopic mass. **A.** Comparison of the elution trend of the LSD/HSD *N*-glycan monoisotopic masses (blue) and the external standard of 2-AB labelled hydrolysed glucose oligomers masses (STD, green). **B.** LSD/HSD monoisotopic masses eluting in each chromatographic fraction.

For both methods, the number of identified *N*-glycans was proportional to the starting tissue amount (**Fig. 3.1.12**). However, LSD<sup>μL</sup> displayed on average 10% more *N*-glycan monosaccharide compositions than HSD for equivalent starting amounts, thereby confirming on a qualitative level that it is the more sensitive method of the two across the entire effective range.



**Fig. 3.1.12.** LSD and HSD structural resolution on each starting brain tissue amount.

LSD<sup>μL</sup> and HSD from 10 mg of tissue displayed the richest *N*-glycomic profiles (**Fig. 3.1.13**), comprising 81 and 77 *N*-glycan monosaccharide compositions respectively with excellent mass accuracy (79 compos. < 10 ppm; 2 compos. < 20 ppm). 34 *N*-glycan structures were assigned to these compositions with good confidence based on evidence from tandem MS (**Tab. A-1**). It has to be noted that, although LSD<sup>μL</sup> grants reliable chromatographic results even when performed on 1 mg of starting brain tissue with 2-AB as the fluorophore, at least 10 mg, and a concentration step prior to MS analysis (i.e., PGC-SPE), should be employed when performing annotation of 2-AB-labelled *N*-glycan structures.

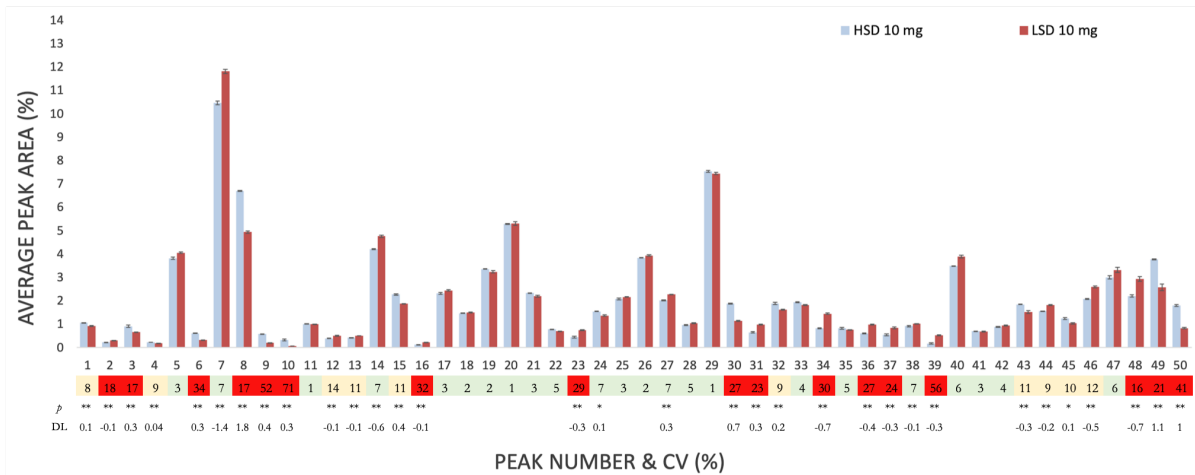


**Fig. 3.1.13.** Structurally annotated LSD and HSD *N*-glycomic profiles from 10 mg of starting brain tissue. Chromatograms from both methods are presented from 5 to 90 min (i.e. the *N*-glycan elution window; unbound 2-AB is eluted before 5 min) and were divided in the same manner into 50 fractions. The most abundant *N*-glycan within each fraction is displayed above the peak. Fractions for which no *N*-glycan signal was obtained at the chosen cut offs for the analysis are marked with X. Structures highlighted in orange are extracted by both methods with different relative abundances. Structures in red rectangles are uniquely extracted by LSD. For a comprehensive list of *N*-glycan structures identified by each method, please refer to **Tab. A-1**.

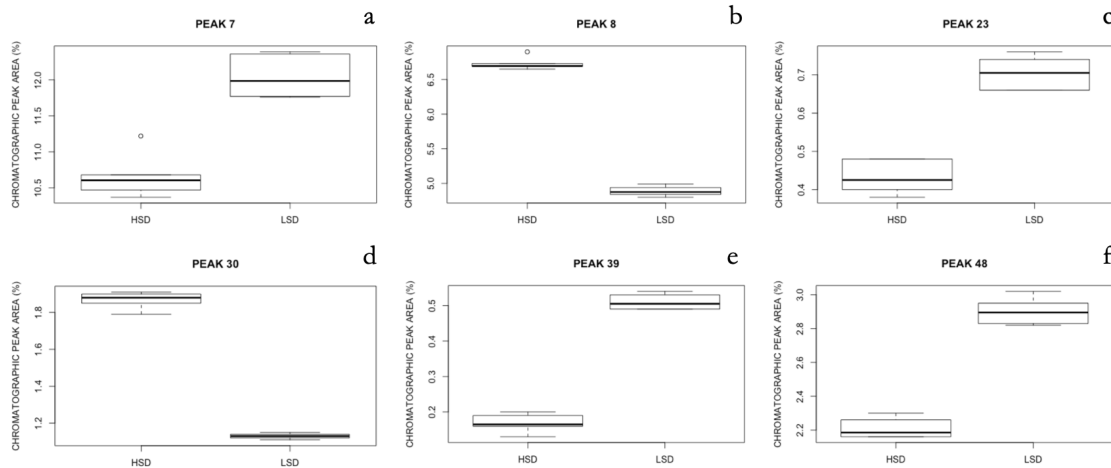
**3.1.8 Comparison of *N*-glycoprofiles obtained by LSD Vs HSD.** The two methods produced similar, but not identical, *N*-glycomic profiles from identical samples (**Fig. 3.1.13**, **Tab. A-1**). Quantitative analysis by UPLC showed that there were statistically significant differences in the relative abundance of many of the fractions (**Fig. 3.1.14**). Fractions that were relatively more abundant in LSD-derived *N*-glycoprofiles tended to have hybrid or sialylated complex *N*-glycans as the dominant species, while those that were relatively less abundant tended to have paucimannose or neutral complex *N*-glycans as the dominant species (**Fig. 3.1.15**). MS analysis also revealed that there were 4 *N*-glycan monosaccharide compositions uniquely identified by LSD<sup>μL</sup>, accounting for 0.7% of the total chromatographic area (exemplifying spectra are given in **Fig. 3.1.16**). Consistent with the quantitative analysis, three of the LSD-specific *N*-glycans are proposed to be of the sialylated, fucosylated, complex type (38, 44D and 50) while the fourth (22F) is a putative sulfated, hybrid *N*-glycan (**Tab. A-1**). Additionally, even when the same set of *N*-glycans was extracted within a given fraction by both methods, the relative abundances within the set sometimes varied, and the dominant structure of the fraction was not always the same across the methods (**Fig. 3.1.13**). To determine whether the two methods preferentially extract different

types of *N*-glycans, derived traits were used to group *N*-glycans from the 5 mg and 10 mg analyses according to structural features to estimate the relative abundance of each *N*-glycan type for each method. These two experiments were used as they show very similar aCVs (**Fig. 3.1.1**), chromatographic profiles, and the same *N*-glycan dominant structure for each peak (data not shown). *N*-glycans belonging to the hybrid, complex, sialylated, and bisecting GlcNAc groups were found to be more efficiently extracted by LSD, while the proportion of oligomannose, and paucimannose *N*-glycans was higher in HSD *N*-glycoprofiles (**Fig. 3.1.17**).

A



B

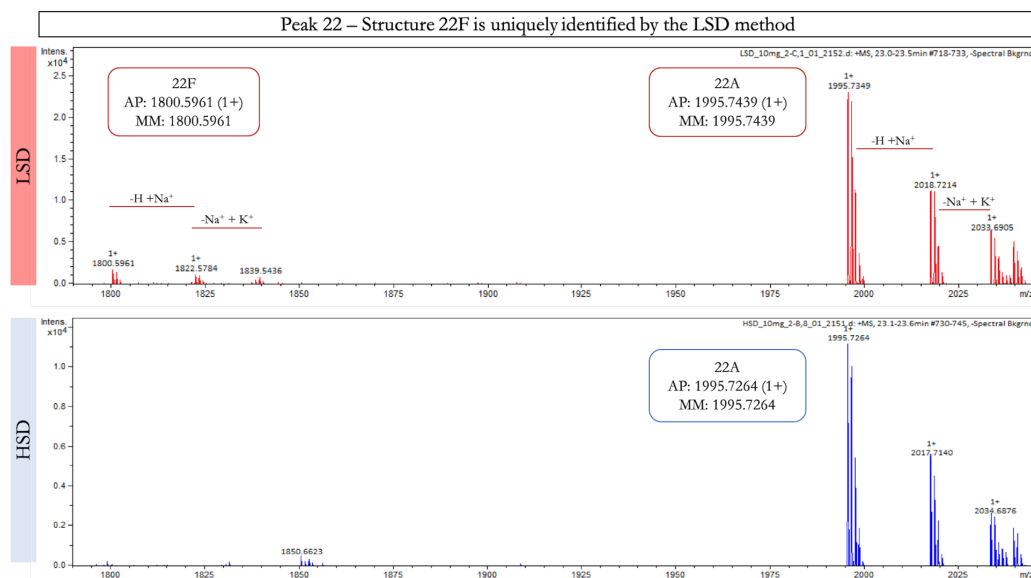


a: m[q] LSD = 11.98 [11.81, 12.28]; HSD = 10.61 [10.48, 10.68]; U = 0; p < 0.01; 0.95 CI [-1.83, -1.1]; DL = -1.40  
b: m[q] LSD = 4.87 [4.85, 4.92]; HSD = 6.69 [6.69, 6.72]; U = 36; p < 0.01; 0.95 CI [1.74, 1.93]; DL = 1.82  
c: m[q] LSD = 0.70 [0.67, 0.73]; HSD = 0.42 [0.40, 0.47]; U = 0; p < 0.01; 0.95 CI [-0.34, -0.21]; DL = -0.28  
d: m[q] LSD = 1.13 [1.12, 1.14]; HSD = 1.9 [1.85, 1.87]; U = 36; p < 0.01; 0.95 CI [0.68, 0.78]; DL = 0.75  
e: m[q] LSD = 0.5 [0.49, 0.52]; HSD = 0.16 [0.16, 0.17]; U = 0; p < 0.01; 0.95 CI [-0.37, -0.31]; DL = -0.34  
f: m[q] LSD = 2.89 [2.83, 2.95]; HSD = 2.18 [2.16, 2.24]; U = 0; p < 0.01; 0.95 CI [-0.79, -0.58]; DL = -0.67

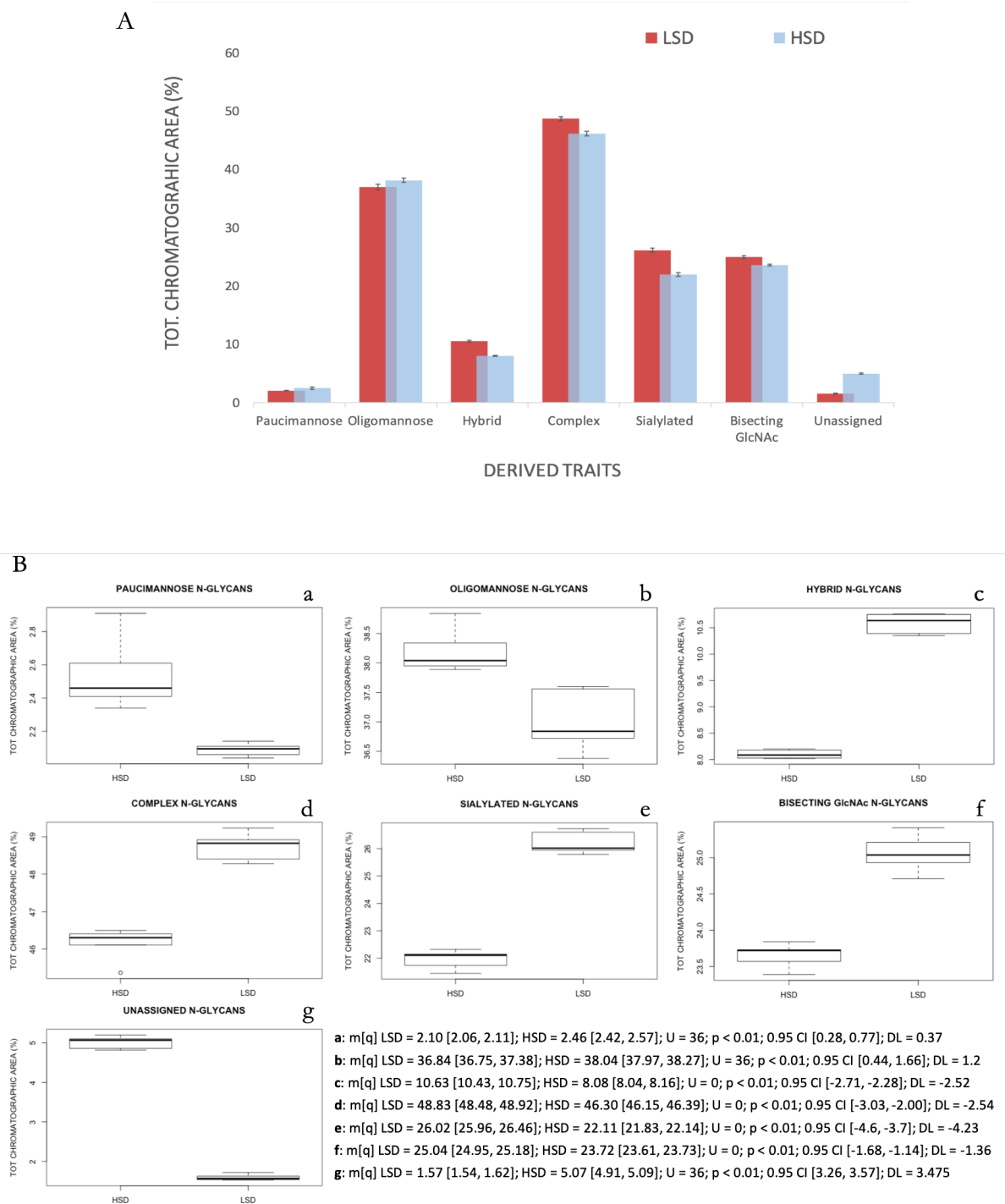
**Fig. 3.1.14.** Comparison of the profiles obtained by LSD<sup>μL</sup> and HSD. **A.** Quantitative comparison of LSD<sup>μL</sup> and HSD chromatograms (10 mg profiles, representing samples showing the richest *N*-glycomic profiles, are displayed as an example). Descriptive error bars show data spread within replicates ( $n = 1$ , triplicates) as  $\pm$  SD. CV for each peak is reported as a measure of precision of the value of the same peak area between the two methods (green = CV  $\leq 7\%$ ; yellow =  $7\% < CV \leq 15\%$ ; red = CV  $> 15\%$ ). The statistical analysis (Wilcoxon-Mann-Whitney,  $n = 2$ , triplicates, HSD  $V_s$  LSD<sup>μL</sup>, calculated using values of peak chromatographic areas deriving from both the 10 mg and 5 mg samples to improve the statistical outcome. The 10 and 5 mg samples from both methods show very similar *a*CVs (see Fig. 3.1.1) and the same dominant *N*-glycan structure for each peak (data not shown). *p*-values (\* $p < 0.05$ , \*\*  $p < 0.01$ ) and DL values for each peak comparison (CVs  $> 7\%$ ) are displayed. **B.** Box-plots indicate dispersion and skewness of the data for six peaks present in A, and the related statistical analysis is summarized in the lower part of the image through the presentation of relevant parameters.

Increased abundance in HSD		Increased abundance in LSD	
Fraction	Proposed N-glycan type	Fraction	Proposed N-glycan type
1	Paucimannose	2	Paucimannose
3	Paucimannose	7	Oligomannose
4	Paucimannose	12	Hybrid
6	Complex	13	Oligomannose
8	Complex	14	Oligomannose
9	Complex	16	Complex sialylated
10	Complex	23	Hybrid
15	Oligomannose	27	Hybrid
24	Complex	31	Complex sialylated
30	Oligomannose	34	Complex sialylated
32	Complex sialylated	36	Complex sialylated
43	Complex sialylated	37	Complex sialylated
45	Not determined	38	Complex sialylated
49	Complex sialylated	39	Not determined
50	Not determined	44	Complex sialylated
		46	Complex sialylated
		48	Complex sialylated

**Fig. 3.1.15.** Fractions whose abundance is significantly different between methods by *N*-glycan type and the proposed *N*-glycan type of the dominant *N*-glycan structure present in each fraction.



**Fig. 3.1.16.** MS spectra extracts exemplifying monosaccharide compositions uniquely identified by the LSD method. Numbers reported above each peak are isotopic masses. The charge state for each value is also reported; AP indicates the mass of the actual, non-deconvoluted, monoisotopic peak in the isotopic distribution (charge state is reported in brackets); MM indicates the monoisotopic mass of the deconvoluted signal. X-axis represents mass to charge ratio and Y-axis represents the absolute signal intensity. Inside each spectrum frame the following information is reported: name of the sample; MS acquisition mode (positive); start and end points of the averaged fraction (min); background removal type (spectral).



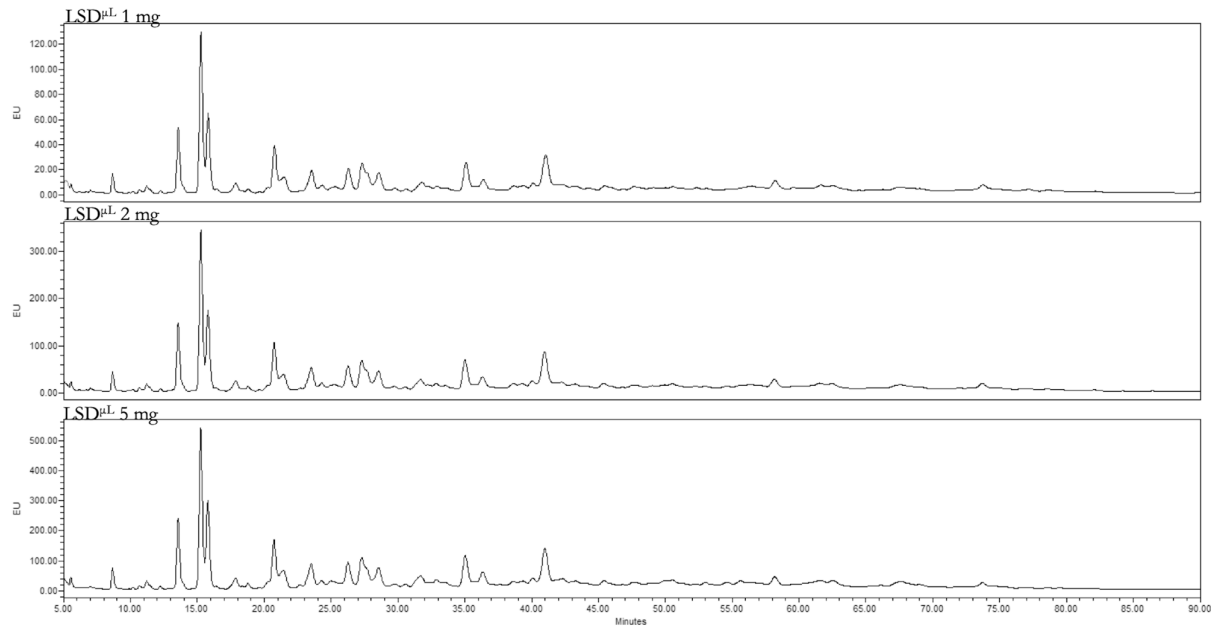
**Fig. 3.1.17.** Derived traits: grouping of *N*-glycans according to structural features for each method. The calculations for determining the derived traits are given section 6.2. Only *N*-glycan compositions that could unambiguously be assigned to certain structural groups were included. Note that it was not possible to assign all *N*-glycans to structural groups due to lack of MS data to resolve potentially ambiguous compositions. **A.** The percentage of the total chromatographic area for each derived trait and method is reported in the histogram. Descriptive error bars show data spread within replicates ( $n = 2$ , triplicates, as done for the analysis showed in 3.1.14) as  $\pm$  SD. **B.** Box-plots indicate dispersion and skewness of the data for every derived trait comparison reported in A. The statistical analysis (Wilcoxon-Mann-Whitney,  $n = 2$ , triplicates) is summarized in the lower part of the image through the presentation of relevant parameters.

This result was interpreted as an indication of the increased sensitivity of LSD rather than a chemically-based extraction bias. It was hypothesized that the lower LOD of LSD allows it to more efficiently extract low abundance *N*-glycans (i.e. fractions accounting for <2% of the total chromatographic area) which, in brain tissue, tend to be of the complex and sialylated type, resulting in an enrichment of these rarer *N*-glycans in LSD. However, given that an increase in one group must be offset by a decrease in other groups when relative quantification is implemented, as a consequence the relative contribution of more common *N*-glycans (i.e. oligomannose *N*-glycans in brain tissue) is diminished. Overall, the author concluded that while both methods yield a generally similar *N*-glycoprofile, the increased sensitivity of LSD results in more efficient extraction of low abundance *N*-glycan species and a resulting relative enrichment of hybrid and complex *N*-glycans compared to HSD.

**3.1.9 Conclusions and future perspectives.** Selective purification of analytes, methodological precision, robustness, good sensitivity and LOD, linearity and range, among others, are crucial parameters that must be evaluated when a new method is developed,<sup>309</sup> to ensure that the method is solid and will give consistent results. In a word, that it is reproducible, and can be used by, ideally, any researcher. Glycoanalytics is no exception, and since glycobiology is becoming a prominent language in many scientific fields,<sup>319</sup> thoroughly validated methods will be vital to properly answer interesting biological questions. In this project a robust, sensitive and precise method named LSD is presented and validated on brain samples, though feasibly applicable to other solid tissues and cell samples too. As a stand-alone method for *N*-glycan analysis of tissue samples, LSD is indisputably one of the most thoroughly validated methods in the field-related literature (**Tab. 3.1.1**), it employs the lowest amount of starting tissue able to produce precise results, and it compares favourably to analogous published methods across all parameters. However, the major advantage of the LSD workflow is that it can be seamlessly integrated into existing proteomic workflows as an “add-on” that allows researchers to extract another layer of information (i.e. *N*-glycosylation profile) from their lysate samples. The value and versatility added by LSD to classical proteomics workflows has been demonstrated by using the same lysate to perform *N*-glycomics analysis via LSD and also proteomics analysis using traditional methods, resulting in two complementary omics datasets generated from a single sample (i.e., sections 3.2.3, 3.2.4, 3.2.5). Furthermore, although LSD is a method conceived for the purification and analysis of *N*-glycans, its workflow is, in principle, compatible with the investigation of *O*-glycans too, since multiple analyses are possible from the same lysate. Indeed, even within the same experiment (the same lysate aliquot), after *N*-glycan release, the *O*-glycan-bearing proteome is available and could be re-purified for the release and analysis of *O*-glycans. LSD outperformed the previous method



developed in the author's Erasmus host institution, showing higher sensitivity and precision, a broader range, a lower LOD, substantially better robustness, and improved structural resolution when coupled with MS detection. Furthermore, LSD is quicker (3 days Vs 4 days for HSD) and simpler to perform, as well as being more cost effective (requiring less reagents and purification steps), thus paving the way towards high-throughput glycomics applications employing solid tissues. As a further bonus it is also safer and more environmentally friendly (it avoids dangerous chemicals employed through HSD, e.g., sodium azide), and it only uses a fraction of the initial lysate, leaving material available for other analyses, such as (glyco)proteomics. During the optimization of the LSD method, different lengths of the deglycosylation step were actually investigated and it was observed that, although using a reaction of shorter duration (i.e. only one overnight incubation) did not lead to a reduction in the overall signal intensity, it resulted in specific reductions in certain chromatographic peaks, mainly those containing a bisecting GlcNAc, within the chromatographic profile (data not shown). It was hypothesized that these peaks contain *N*-glycan structures that are more difficult to remove by PNGase F and therefore require an extended incubation time. It has been reported that not all *N*-glycans are cleaved with equal efficiency by PNGase F and that the kinetics of release are significantly lower for *N*-glycans containing a bisecting GlcNAc.<sup>320</sup> Therefore, although it is possible to perform a shorter version of the LSD protocol with a single overnight deglycosylation incubation (i.e., a two days workflow), the resulting profile will be incomplete and therefore employing the longer version of the protocol is recommended to allow the reaction to proceed to completion, which will provide a more accurate picture of the sample *N*-glycome. Although this work was carried out using 2-AB as the labelling agent in order to be consistent with previously published HSD data, the method was also tested using procainamide (ProA) as the fluorescent tag, which is known to be more sensitive for both fluorescence and MS detection,<sup>183</sup> and obtained a 10-fold increase in sensitivity (**Fig. 3.1.18**).



**Fig. 3.1.18.** LSD<sup>μL</sup> sensitivity increases 10-fold when *N*-glycans are labelled with Procainamide instead of 2-AB. 1, 2 and 5 mg profiles are reported as examples. Note the signal intensity on the y-axis.

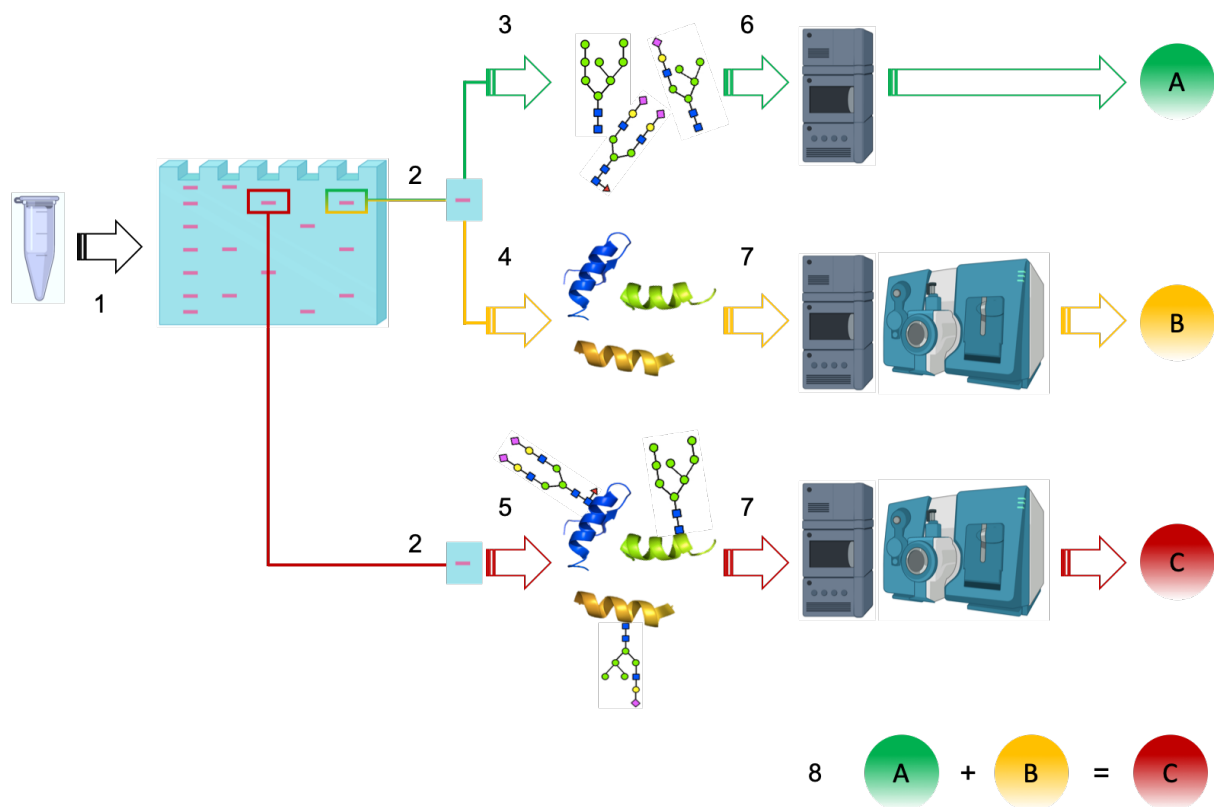
Therefore, the use of ProA instead of 2-AB for *N*-glycan labelling, using the same reaction conditions, boosts LSD performance and should be used in future LSD applications. The power of LSD is nonetheless bound by the current limitations of the *N*-glycomics field: relative quantification of *N*-glycans is feasible within the chromatograms, but it is not trivial to perform absolute quantification. Absolute quantification of *N*-glycans is a challenging task, but a fundamental one indeed for a complete method validation (e.g., investigating accuracy, limit of quantification, and recovery),<sup>309</sup> which is required for clinical use. Due to this, future developments in the field will undoubtedly furnish the tools to equip the LSD workflow with absolute quantification capabilities. In conclusion, although LSD is still far from being the perfect method for brain tissue *N*-glycan investigation, to the best of the author's knowledge, it is currently the most thoroughly validated Neuro-*N*-Glycomics method in terms of robustness, precision, sensitivity, selectivity, linearity and range,<sup>113,196,215,262–264,266,267,269</sup> while still performing reliably (e.g., precise and sensitive) on the smallest amount of starting brain tissue when compared to other methods in the literature,<sup>265</sup> and it therefore represents a significant step forward towards the achievement of biomedically employable glycomics workflows.

### 3.2 THE "REVERSE GLYCOPROTEOMICS" PROJECT.

**3.2.1 Framework of the study.** Since the brain *N*-glycan chemical information is only a part of the glycomolecular puzzle eliciting the biochemical response in a tissue, it is important to unveil the protein component of the system that carries the *N*-glycan, to individuate the glycoprotein as the complete putative glycobiomarker towards functional studies. In this context, previous works regarding the investigation of brain *N*-glycans in different species (Thomas Klarić and Ivan Gudelj, Genos Ltd; unpublished work), highlighted some *N*-glycan structures that were differentially expressed in brains belonging to different species (e.g., human, chimpanzee, macaque, dog, rat), different brain regions (e.g., cerebellum, hippocampus, striatum, frontal cortex), and brain developmental stages (e.g., fetus and adult). These specific *N*-glycans, which chemical structures will not be presented since part of a non-disclosure agreement with the author's Erasmus host institution (Genos Ltd), are of particular interest for the study of brain evolution, being candidate glycobiomarkers for brain functional studies. Stemming from these *N*-glycan data, the ongoing project presented in the following was developed and named "reverse glycoproteomics" (RG), since it aims to pinpoint the proteins carrying the above introduced neurologically interesting *N*-glycans, by starting from the already generated *N*-glycans data (i.e., reversing the more usual flow from proteomics to glycomics). This will permit the identification of the complete glycomolecular system eliciting the biological response in the context of brain evolution and functioning, opening the possibility to investigate its effects *in vitro* and *in vivo*. Methodological developments regarding the RG project, carried out on a test-sample (i.e., rat brain tissue lysate), are reported in the following in the context of an ongoing collaboration heading towards the identification of target glycoproteins from more precious brain tissues (e.g., human, chimpanzee, macaque, dog).

**3.2.2 The RG strategy.** The experimental strategy to highlight the proteins carrying the neurologically interesting *N*-glycans (**Fig. 3.2.1**) combines *N*-glycomics, proteomics and *N*-glycoproteomics approaches, and was adapted from a recently published glycoproteomics approach.<sup>215</sup> The starting sample of the analysis was the same brain tissue lysate employed in the LSD *N*-glycomomic workflow (i.e., section 3.1). Briefly, in-solution reduction, denaturation and alkylation were performed directly on the rat brain lysate, prior to brain proteome fractionation on SDS-PAGE. The protein bands were then excised from the gel, decoloured and prepared for subsequent analyses. Each band underwent in-gel deglycosylation using PNGase-F (IGD), to obtain the brain *N*-glycoprofile via UPLC (*N*-glycan masses within LC chromatographic peaks were already determined in previous study), yielding the *N*-glycomomic information (*N*-glycan masses, **Fig. 3.2.1**, A). Deglycosylated proteins still trapped in the gel underwent in-gel

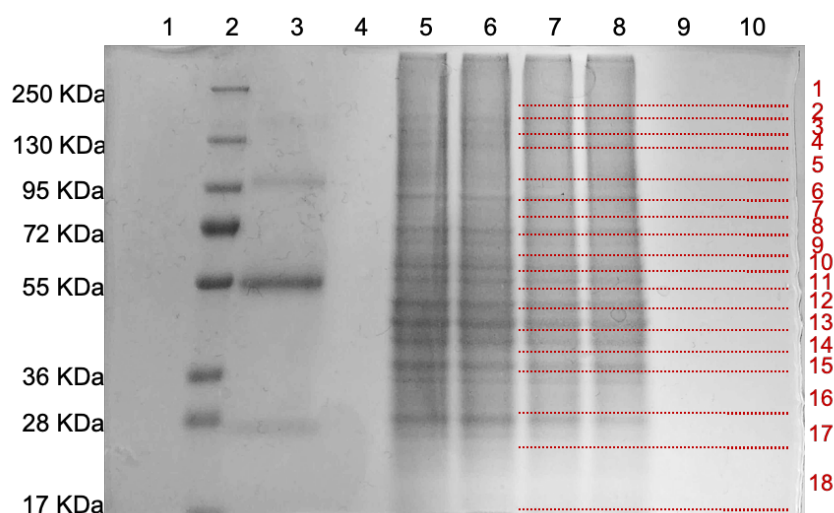
trypsinization after deglycosylation (IGTaD): deglycosylated peptides were analysed with UPLC-MS to obtain the proteomic information (peptide masses and *N*-glycosylation sites, **Fig. 3.2.1, B**). Finally, a proteome replicate run on SDS-PAGE using the same conditions (technical replicate), underwent in-gel trypsinization without deglycosylation (IGT), yielding the *N*-glycoproteomic information (*N*-glycopeptide masses, **Fig. 3.2.1, C**). The combination of these three pieces of information (the sum of the *N*-glycan and deglycosylated peptide masses will equal the *N*-glycopeptide mass) will make the identification of the *N*-glycoproteins carrying the neurologically interesting *N*-glycans feasible, thus highlighting putative glyco biomarkers for functional studies.



**Fig. 3.2.1.** RG experimental strategy. **1.** Proteins within the brain tissue lysate are directly denatured, reduced and alkylated prior to SDS-PAGE separation in technical replicates. **2.** Protein bands within the gel are excised and destined towards subsequent analyses. **3.** IG. **4.** IGTaD. **5.** IGT. **6.** Brain *N*-glycans analysis via UPLC (*N*-glycan masses already determined in previous study). **7.** Brain (de)glycosylated peptides analysis via UPLC-MS. **A.** *N*-glycan masses information. **B.** Deglycosylated peptide information. **C.** *N*-glycopeptide information. **8.** Linking the information A, B and C permits the identification of the *N*-glycoprotein of interest.

**3.2.3 Brain proteome fractionation through SDS-PAGE.** The first step for the RG project comprises the analysis of the brain proteome through SDS-PAGE. This step ensures a preliminary sample purification through a polyacrylamide gel, the proteome fractionation according to the apparent molecular weight of its protein constituents, and the simplification of the starting sample (in proteome fractions) towards easier (glyco)protein identification (experimental details in

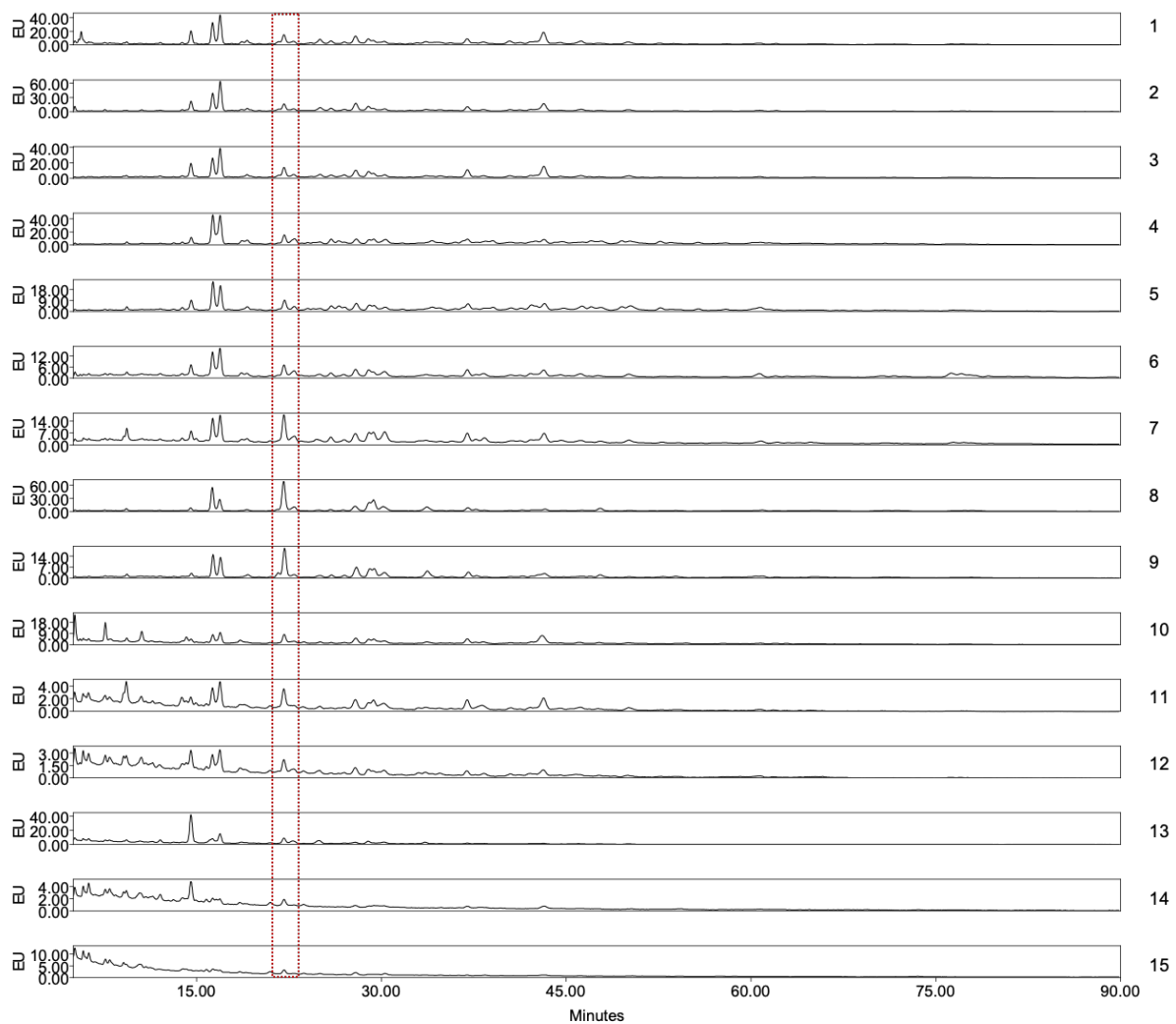
sections 4.2.2 to 4.2.4). Briefly, the brain lysate was denatured, reduced, alkylated with iodoacetamide for MS investigation, and directly loaded on a polyacrylamide gel for SDS-PAGE analysis. The gel was then fractionated according to the displayed protein bands: 18 fractions (**Fig. 3.2.2**, red) were chosen, and relative bands were excised from the gel for subsequent destaining using multiple cycles of acetonitrile/sodium bicarbonate. Gel bands were then dried under vacuum prior to IGD.



**Fig. 3.2.2.** Brain proteome fractionated on SDS-PAGE. SDS-PAGE of the reduced, denatured and alkylated lysate. 1,4,9,10 = blanks; 2 = molecular weight marker; 3 = human IgG as +C; 5,6,7,8 = brain tissue lysate; left legend = molecular weights of the marker bands; right legend (red) = fractionation pattern (18 fractions).

**3.2.4 In-gel deglycosylation (IGD).** The deglycosylation reaction was performed directly on the gel pieces using PNGase F in sodium bicarbonate buffer, at 37°C, overnight. After deglycosylation, the *N*-glycans were extracted from the gel pieces by the use of sonication, with several washes with water and acetonitrile, to make the polyacrylamide matrix efficiently release the oligosaccharides by shrinking and swelling cycles. *N*-glycans extracted from the gel were then dried and resuspended in formic acid, to hydrolyse the glycosylamine intermediate resulting from PNGase F cleavage and shift the reducing GlcNAc hemiacetalic/aldehydic equilibrium towards the latter, more reactive form. *N*-glycans were then labelled with ProA and purified prior to HILIC-UPLC analysis (experimental details in sections 4.2.5 and 4.2.6). Increasing the IGD step sensitivity was of paramount importance, since the *N*-glycans in each sample belong to the *N*-glycoproteins contained in a single gel fraction, an amount of protein material in itself unable to produce readable signals when fluorescence is used as detection (i.e., UPLC) and ProA is used as the labelling dye. In this context, different strategies have been tested to enhance the IGD step sensitivity. Formerly, the brain proteome was run in eight technical replicates and band pooling (adding to one sample

8 technical replicates of the same band) was performed to enhance the signals of ProA labelled *N*-glycans. This strategy permitted to obtain readable signals from 10 out of 15 gel fractions and showed that the enrichment of specific *N*-glycan peaks was possible, since several peaks within the brain *N*-glycoprofile displayed different relative abundances in different fractions (**Fig. 3.2.3**). However, band pooling is laborious and time consuming; furthermore, since SDS-PAGE runs of complex samples (e.g., brain proteome) are not always exactly identical, even considering technical replicates on the same gel (band smiling and distortions), pooling is also a not perfectly clean approach, though commonly used in proteomics. In addition, signals displayed in **Fig. 3.2.3** are only sufficiently above the threshold of readability, as underlined by those fractions that failed to yield satisfactory *N*-glycoprofiles (e.g., 10-12, 14,15). In the light of these limitations, the IGD workflow was refined to increase the sensitivity and obtain satisfactory *N*-glycoprofiles for each proteome fraction. Firstly, a two-step labelling reaction was employed instead of the previously one-pot version, used in preliminary RG project experiments and LSD method development (i.e., sections 1.3.3, 4.1.1, and 4.1.3). In fact, previous experiments have successfully optimised the *N*-glycan labelling reaction towards enhanced yields (data not shown), by decoupling the iminium ion formation step, from the iminium ion reduction step that yields the final secondary amine (**Fig. 1.8**). By avoiding the formerly employed one-pot version of the reaction, the amount of *N*-glycans reducing ends directly reacting with the reducing agent (2-methylpyridine borane complex), in place of the dye (ProA or 2-AB), was significantly lowered, as highlighted by a substantial decrease of the *N*-glycan + 2 Da (2H, aldehyde reduction) signals observed in MS experiments (data not shown, **Fig. 1.8**, 2e-f). Secondly, as done in sections 3.1.7 and 4.1.6, a concentration step using PGC-SPE substantially contributed to boost the IGD sensitivity, yielding optimal *N*-glycoprofiles, for a total of 18 fractions (therefore increasing IGD resolution), starting from a single gel band for each fraction and totally avoiding band pooling (**3.2.4**).

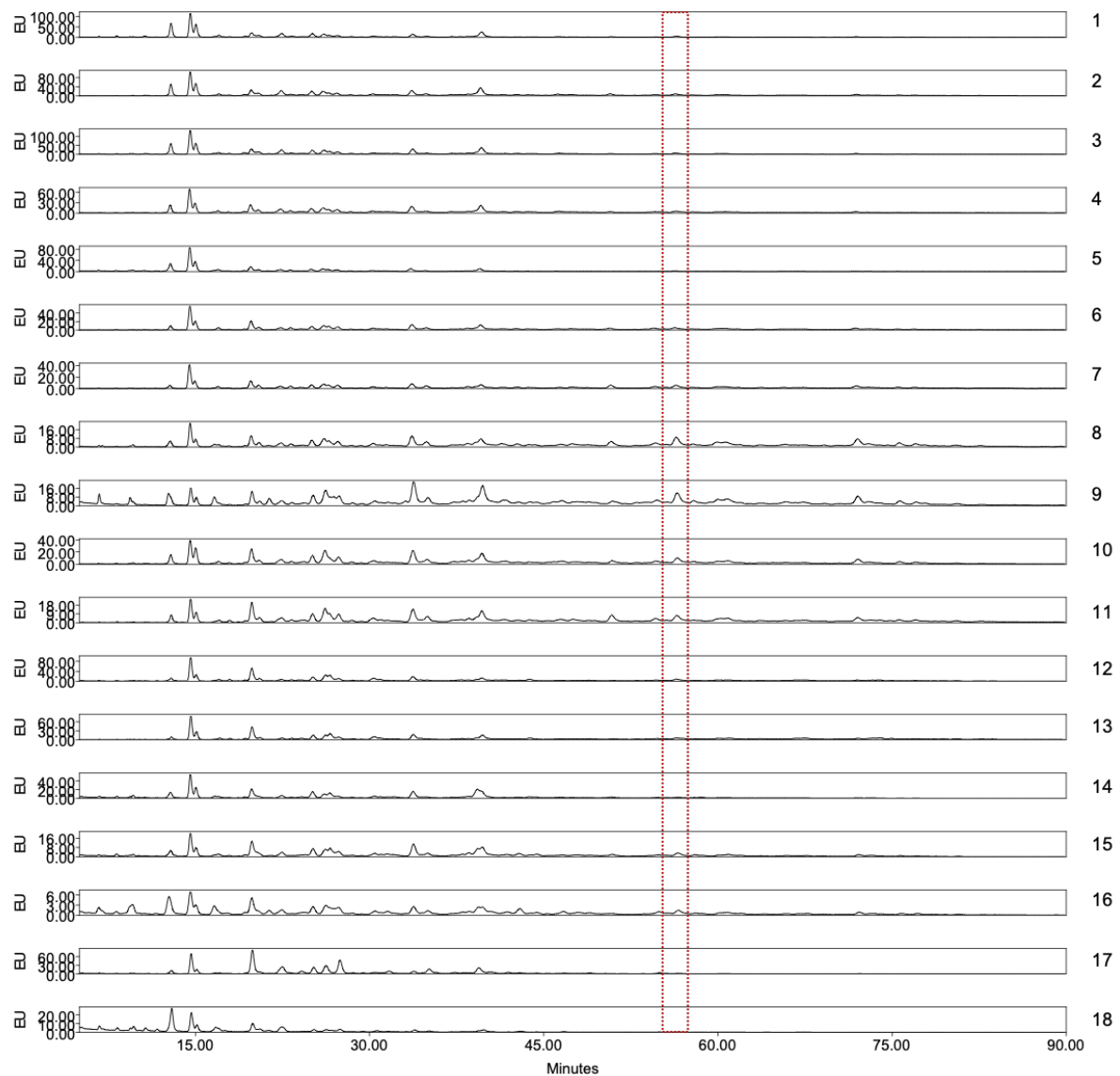


**Fig. 3.2.3.** HILIC-UPLC analysis of ProA labelled *N*-glycans obtained by pooling 8 technical replicates for each one of the 15 fractions excised from the SDS-PAGE gel. Chromatograms are presented from 5 to 90 min (e.g., the *N*-glycan elution window; unbound 2-AB is eluted before 5 min). EU = Emission Units (fluorescence). SDS-PAGE fraction numbers are reported on the right. Red dashed rectangle = an example of specific *N*-glycan peak enriched in some fractions (7-9).

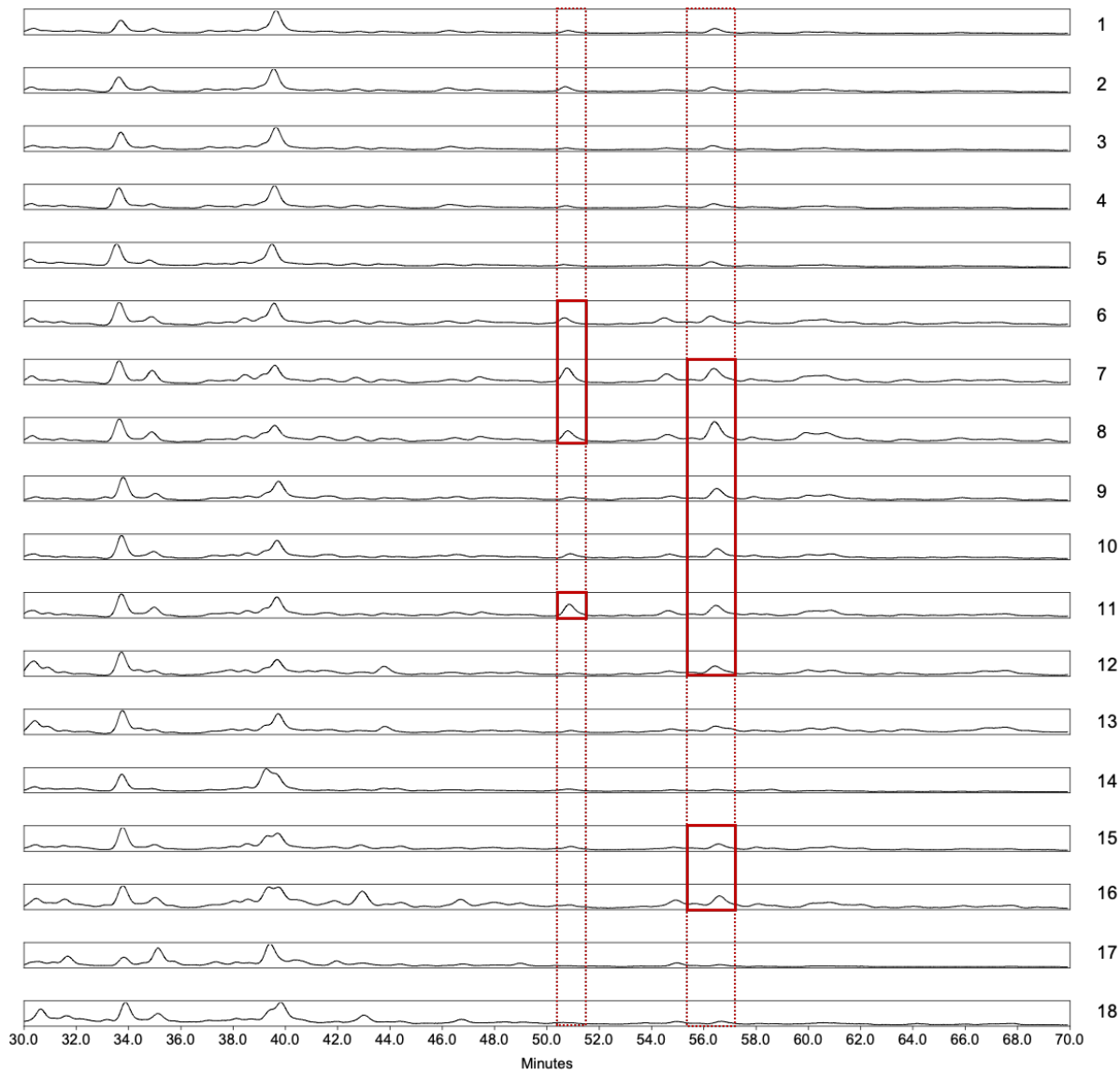
The ProA-labelled (Tomas Klarić, Matija Salopek, unpublished work) and 2-AB labelled (Tomas Klarić, Ivan Gudelj, unpublished work) brain *N*-glycomes have been previously annotated for different species (e.g., human, chimpanzee, macaque, dog, rat), by using MS data. Therefore, knowing which *N*-glycan structure lies under which peak, and considering the reproducibility of brain *N*-glycoprofiles (e.g., section 1.2.1), finding which fraction is enriched in a neurologically interesting *N*-glycan is feasible. For instance, the neurologically interesting structure A is eluted in a peak between 50.5 and 51 min (**Fig. 3.2.5**), which retention time window showed an enriched peak in fractions 6-8 and 11 (**Fig. 3.2.5**). Therefore, these fractions (i.e., 6-8,11) are the primary candidates to be investigated in the search for *N*-glycoproteins carrying the neurologically



interesting *N*-glycan A. Another example is the neurologically interesting structure B, eluted in a peak between 55.5 and 57 min (**Fig. 3.2.5**), which is enriched in fractions 7-12 and 15-16.



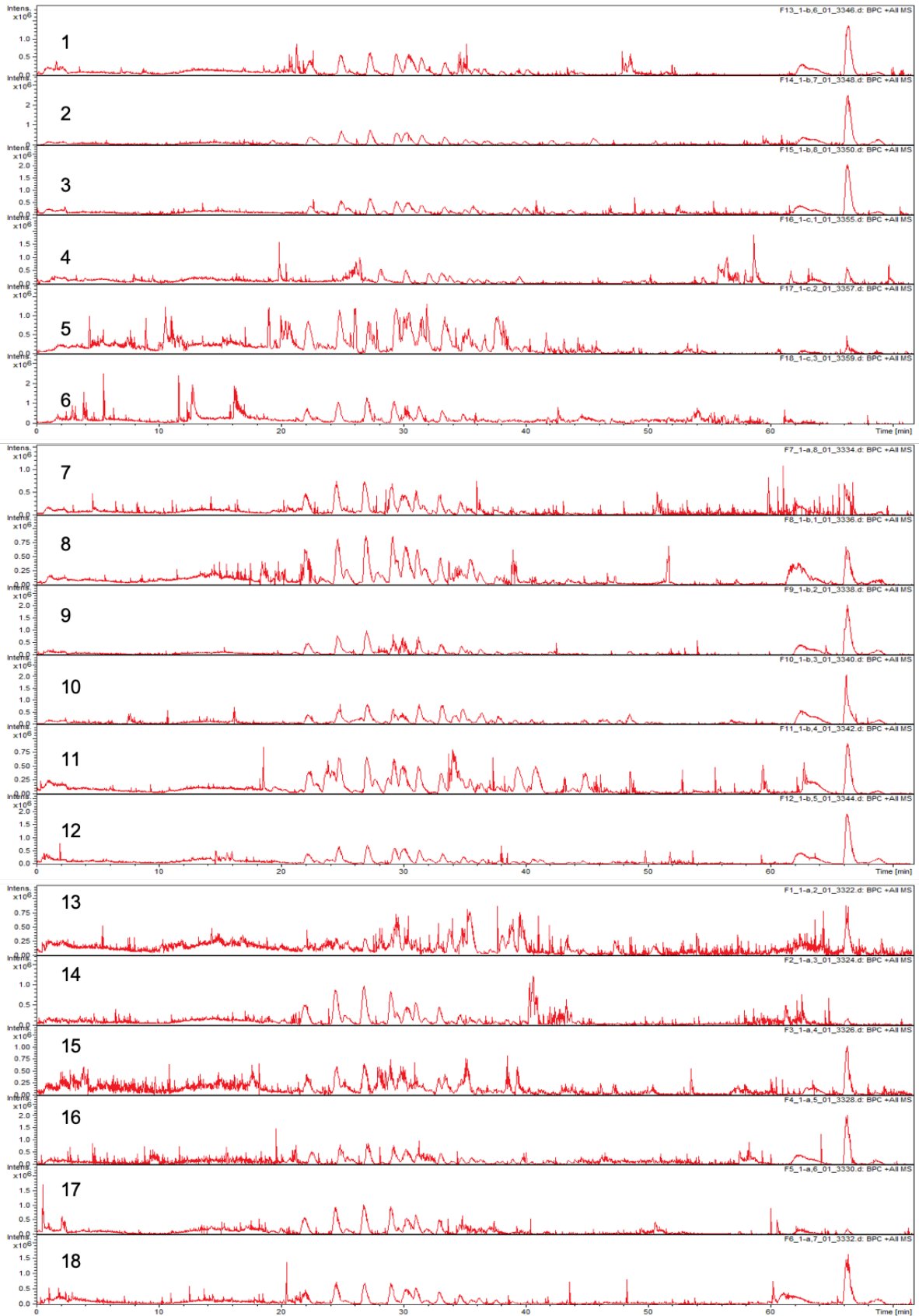
**3.2.4.** HILIC-UPLC analysis of ProA labelled *N*-glycans obtained by employing the optimised labelled reaction and PGC-SPE concentration prior to analysis. Chromatograms are presented from 5 to 90 min (e.g., the *N*-glycan elution window; unbound 2-AB is eluted before 5 min). EU = Emission Units (fluorescence). SDS-PAGE fraction numbers are reported on the right. Red dashed rectangle = an example of specific *N*-glycan peak enriched in some fractions (8-11).



**Fig. 3.2.5.** Examples of chromatographic peaks harbouring neurologically interesting *N*-glycans enriched in specific proteome fractions. Chromatograms are presented from 30 to 70 min to highlight the region of interest. No EU value is displayed because chromatographic intensities are normalised. SDS-PAGE fraction numbers are reported on the right. Red dashed rectangles = elution window of the neurologically interesting *N*-glycan A (50.5-51 min) and B (55.5-57 min); Red rectangles = chromatographic peaks enriched in the neurologically interesting *N*-glycan A (fractions 6-8, and 11) and B (fractions 7-12, and 15-16).

**3.2.5 In-gel trypsinisation after deglycosylation (IGaTD).** Protein digestion was performed directly on gel pieces using Trypsin in sodium bicarbonate buffer, at 37°C, overnight. After trypsinisation, deglycosylated peptides were extracted from the gel pieces with several washes using sodium bicarbonate buffer and acetonitrile, again exploiting the shrinking and swelling action of the aqueous/solvent addition cycles on polyacrylamide gel pieces, as done for IGD. Extracted deglycosylated peptides were then dried and resuspended in trifluoroacetic acid, to enhance their hydrophobicity and boost the binding on the solid phase within the subsequent reverse-phase

purification and concentration step, prior to RP-nanoUPLC-ESI-QqTOF MS profiling (experimental details in sections 4.2.7, 4.2.8, and 4.2.9). MS analyses of deglycosylated peptides (**Fig. 3.2.6**) highlighted more than 1000 peptides, 500 proteins, and 50 Asn→Asp modifications (**Fig. 3.2.7**), leading to the identification of glycopeptides, glycosylation sites, and glycoproteins (**Tab. A-2**), thereby confirming the LSD brain lysate (section 3.1) compatibility with downstream proteomics applications and the suitability of the IGTaD procedure to investigate deglycosylated peptides, towards glycopeptides and glycoproteins identification. The analysis of deglycosylated peptides identified some experimentally reviewed glycoproteins, such as Contactin-1, Myelin-associated glycoprotein, Excitatory amino acid transporter 2, Sodium/potassium-transporting ATPase (subunit beta-2), and Thy-1 membrane glycoprotein (**Tab. A-2**). In addition, the enzymatic deglycosylation step performed prior to trypsinisation made *N*-glycosylation sites analysis possible, identifying the *N*-glycan-bearing asparagine, and highlighting three novel putative glycosylation sites: N444 on a Neural cell adhesion molecule 1 (NCAM1) isoform, N356 on the Dihydropyrimidinase-related protein 2 (Dpysl2), and N201 on the BTB domain-containing 18 protein (Btbd18), which were not reported in the Uniprot KB database before. NCAM1 (Uniprot KB ID P13596) is a cell adhesion molecule involved in neural functioning, and reported *N*-glycosylation sites lie at N222, 316, 348, 434, 460, and 489. The IGTaD analysis showed that an NCAM1 isoform (Uniprot KB ID F1LNY3), presented a +0.984 Da shift at position N444 within the suitable *N*-glycosylation sequon *N*-Y-S (**Tab. A-2**), indicative of the presence of an *N*-glycan. Dpysl2 (Uniprot KB ID P47942) plays a role in neuronal developing and functioning and is reported to be phosphorylated but not glycosylated. The IGTaD analysis showed that a +0.984 Da shift is present at position N356 within the *N*-glycosylation sequon *N*-G-T (**Tab. A-2**), thereby highlighting Dpysl2 as a novel glycoprotein. Btbd18 (Uniprot KB ID D3Z9A5) is involved in male meiosis I and is required during spermatogenesis to promote the expression of piRNA precursors. The protein is not known to be glycosylated, but the IGTaD analysis highlighted the presence of an *N*-glycan on N201, within the suitable *N*-glycosylation sequon *N*-L-S (**Tab. A-2**), therefore suggesting Btbd18 to be a glycoprotein.



**Fig. 3.2.6.** LC-MS spectra of deglycosylated peptides obtained from the 18 fractions excised from the SDS-PAGE.

It should also be noted that, some of these identified proteins (Tab. A-2) are comprised within proteome fractions in which neurologically interesting *N*-glycans are actually enriched (Section 3.2.4, Fig. 3.2.5). For example, the Excitatory amino acid transporter 2 (P31596) is found in fraction 6, in which the neurologically interesting *N*-glycan A is IGD-enriched. Dpysl2 (P47942) is found in fraction 7 which, according to IGD data, harboured both the neurologically interesting *N*-glycans A and B. The Sodium/potassium-transporting ATPase subunit beta-2 (P13638) and Btbd18 (D329A5) followed the same trend being present in fractions 11 and 9, respectively. This piece of information is clearly insufficient to link the neurologically interesting *N*-glycans to their carrier *N*-glycoproteins (for which data on *N*-glycopeptides are essential) but represents indeed a partial confirmation of the methodology suitability towards the intended purpose, along with already providing some putative candidates for the *N*-glycoprotein targets at the level of methodological development.

F	nIPe	nIP	nIgP
1	64	23	3
2	54	35	6
3	107	49	2
4	103	38	2
5	22	20	1
6	47	28	2
7	75	49	4
8	45	14	2
9	81	25	5
10	99	41	7
11	52	19	2
12	61	22	5
13	26	12	4
14	86	28	4
15	68	44	2
16	62	52	1
17	99	35	3
18	54	40	2
Tot.	1205	574	57

**Fig. 3.2.7.** Number of identified peptides and proteins obtained from the 18 fractions excised from the SDS-PAGE gel. F = fraction; nIPe = n° of identified peptides in each fraction; nIP = n° of identified proteins in each fraction; nIgP = n° of putative glycoproteins identified in each fraction (at least one Asn→Asp, +0.984 Da; detailed examples of identified glycoproteins are given in **Tab. A-2**).

**3.2.6 In-gel trypsinisation without deglycosylation (IGT).** To link the information obtained within the IGD and IGTaD steps and highlight which *N*-glycoprotein carries the *N*-glycans of interest, the third piece of the RG puzzle is necessary. Therefore, *N*-glycopeptides, from the same sample from which *N*-glycans and deglycosylated peptides were generated, were prepared (e.g., using another lane of the SDS-PAGE, containing a brain tissue lysate replicate, see **Fig.**

**3.2.2).** The employed protocol was exactly the same of the IGTaD step, without performing IGD prior to trypsinisation. Generated *N*-glycopeptides were then purified and enriched using cotton HILIC<sup>174</sup> (experimental details in section 4.2.10), and are ready to be analysed in the frame of an ongoing collaboration with the author's Erasmus host institution (Genos Ltd).

**3.2.7 Conclusions and future perspectives.** The IGD step of the RG workflow has been optimised and is currently able to produce optimal *N*-glycan signals from the amount of proteins contained in a single SDS-PAGE gel band, highlighting the proteome fractions in which the chromatographic peak harbouring the neurologically interesting *N*-glycans are enriched, thereby providing indications about the SDS-PAGE gel bands containing the *N*-glycoproteins carrying the *N*-glycans of interest. Regarding the IGDaT step, preliminary experiments in the context of methodological optimisation gave promising results. At the current level of development this step is able to perform deglycosylated peptides analysis, to highlight glycoproteins and *N*-glycosylation sites, therefore confirming the methodological suitability for the intended purpose. Further developments are however still necessary to enhance peptides and deglycosylated peptides identification through LC-MS applications, since the number of identified glycoproteins is still not satisfactory, and a higher resolution power will be necessary to increase the possibility of identifying deglycosylated peptides carrying the neurologically interesting *N*-glycans. This will be achieved by further optimising the IGTaD step, and in this context several options will be pursued. Regarding the IGTaD sample preparation, the efficiency of the reverse-phase step of peptides purification could be theoretically improved, by increasing, for example, the volume of the C18 stationary phase, in order to bound more peptides, since the preliminary experiments presented in this thesis were carried out using a basic version of the protocol, usually employed for simpler system than tissues (e.g., isolated proteins), thereby probably containing less complex peptide ensembles. At the analytical level, the IGTaD LC gradient could be further improved by testing different lengths or final concentrations of ACN, to better separate the eluted peptides, thus increasing MS identifications. Also, the use of a step gradient instead of a linear one, might enhance peptide signals resolution. Despite the adjustments that can be tried at these levels, significant improvements in peptide signals resolution, and thus identification, would be achieved by employing a more efficient ion source, at the level of mass spectrometric analysis. In fact, a Bruker Compact mass spectrometer equipped with a standard ESI ion source was used for these preliminary experiments (i.e., section 4.2.9), but a more powerful ion source, called CaptiveSpray nanoBooster<sup>®</sup> (Bruker, Germany) is available in-house at the host institution on the same instrument, and it is capable of significantly enhancing peptide IDs. The CaptiveSpray nanoBooster<sup>®</sup> boosts the mass spectrometer proteomic performances by providing a vortex gas

sweeping around the ion source emitter spray tip, efficiently desolvating and focusing the ESI Taylor cone into the mass spectrometer inlet capillary, therefore reducing the sample loss deriving from unfocused Taylor cones, and augmenting the efficiency of the sample transfer from the spray tip into the instrument. In addition, to further increase the peptide and glycopeptide identification, the MS/MS conditions could be further optimised, to ensure the best possible trade-off between data acquisition and fragmentation efficiency (e.g., number of scans, number of precursor ions chosen in each scan, CID collision energy). Therefore, in the context of IGTaD, little adjustments still have to be made on the sample preparation steps, and a significant enhancement of peptide identifications could be achieved by further tailoring the MS analysis parameters. As far as the *N*-glycopeptide analysis is concerned, that is the third piece of the RG project, purified glycopeptides were prepared from all the eighteen fractions, furnishing ready-to-use biological material employable for LC-MS methodological development. Lastly, since the RG workflow is still at the level of methodological optimisation and in the light of what has been discussed in section 3.1.1, once its experimental workflow parameters will be tailored, at least a basic methodological validation should be provided (i.e., precision and sensitivity of the method), before moving onto its applications on precious brain samples (e.g., human, chimpanzee, macaque, dog) for the search of the *N*-glycoproteins carrying the neurologically interesting brain *N*-glycans.

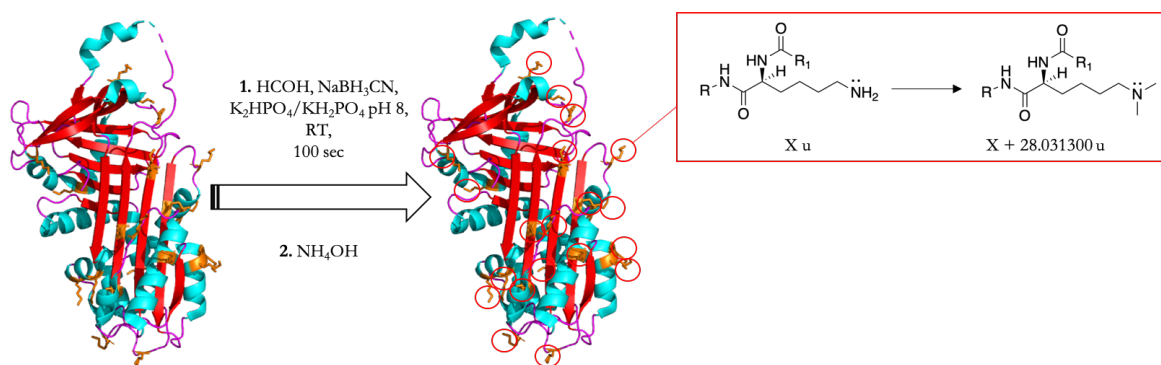


### 3.3 CHEMOSELECTIVE MODIFICATION OF HUMAN NEUROSERPIN.

**3.3.1 Framework of the study.** Human neuroserpin (hNS) is a metastable protein that pathologically polymerises with neurodegenerative consequences (section 1.2.7). Since the molecular mechanism of hNS polymerisation is still a matter of debate,<sup>149,321–325</sup> the aim of this study was to develop a chemical method suitable to unveil more pieces of information about the molecular determinants of hNS polymerisation. hNS is involved in many neurodegenerative pathologies (e.g., FENIB, Alzheimer's, brain cancer),<sup>326</sup> therefore elucidating hNS polymerisation mechanism is serviceable in casting light upon across-the-board neurodegeneration mechanisms, furnishing biomedically relevant information. The aim of this project was to develop an efficient and suitable chemical labelling procedure, able to maintain hNS folding and furnish a molecular marker for analytical evaluation. The strategy of this study was to covalently label hNS in its monomeric (mhNS) and polymeric (phNS) forms, and then to compare the labelling pattern of the two in an attempt to perform a topographical characterisation of the molecular regions involved in hNS polymerisation. These regions will be indicative of molecular candidates putatively involved in the protein polymerisation behaviour, to be further investigated and validated with biochemical studies. This project was carried out in collaboration with the protein aggregation laboratory of the University of Milano (Stefano Ricagno's group; hNS production and structural analyses) and the mass spectrometry laboratory of the University of Milano-Bicocca (Rita Grandori's group; MS analyses). This section will present a part of the whole work, comprising the description of the chemical procedure employed to label hNS and the analytical evaluation of the reaction outcome. Further biological conclusions drawn from the mhNS and phNS chemical labelling results (i.e., the identity and suggested biological functions of the highlighted putative molecular determinants of hNS polymerisation; e.g., by using bioinformatics and further biochemical analyses) will be the part of collaborators' theses and, in the frame of an ongoing collaboration, will coalesce into a joint scientific publication.

**3.3.2 Reductive amination for hNS labelling.** Developing an efficient chemical labelling able to cover enough protein sequence in order to give interpretable results imposes several boundaries. Firstly, a naturally displayed and suitable (i.e., reactivity) functional group on the protein surface is needed. Secondly, an adequate chemical label has to be chosen: it has to be soluble in the same buffer in which the protein is maintained in its native form, it has to react promptly with its partner and be able to give a reliable analytical signal. Finally, a proper set of reaction conditions have to be tailored to ensure a good reaction yield (i.e., sufficiently high to yield usable results). In this project, a water-soluble chemical label and a water-friendly reaction had to be selected, without

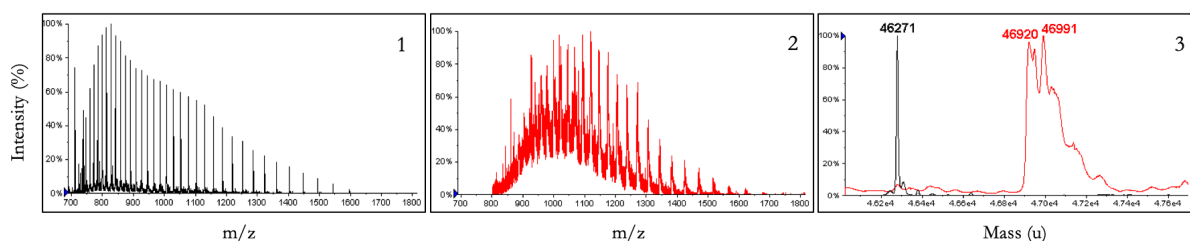
the possibility to raise the temperature in order to boost the chemical outcome or having the chance to employ denaturing reagents or solvents. Reductive amination is a well-known biocompatible reaction often employed to label bio(macro)molecules of interest (i.e., sections 1.3.3, 4.1.3, and 4.2.6), invented by nature to perform  $\alpha$ -amino acid biosynthesis from  $\alpha$ -ketoacids (i.e., carried out by transaminases). Since reductive amination exploits amino groups, protein primary amines (i.e., lysine and *N*-T) are a suitable candidate for protein conjugation with this reaction. Furthermore, the efficiency of the bioconjugation reaction depends on the functional group local environment, the protein structural flexibility and solvent accessibility of the conjugation site and, in this context, protein primary amines are usually high abundant, chemically reactive, and surface-accessible, therefore being optimal candidates for protein bioconjugation strategies.<sup>327</sup> mhNS and phNS have been dimethyl labelled via reductive amination adapting a published procedure exploited to label IgGs,<sup>327</sup> by using formaldehyde and sodium cyanoborohydride in potassium phosphate buffer (**Fig. 3.3.1**), furnishing a dimethyl chemical tag on the protein amino groups (i.e., 22 lysines and the *N*-T), accounting for a mass shift of +28.031300 u for every completely reacted amino group. Dimethyl labelling has been performed on mhNS and phNS, under the same conditions, and the reaction outcome was investigated through biochemical and proteomics approaches, using the same mass spectrometer and analytical workflow for both systems (experimental details in section 4.3).



**Fig. 3.3.1.** Reductive amination of hNS. hNS crystal structure is reported (PDB ID: 3FGQ, 2.09 Å, (x-ray); light blue =  $\alpha$ -helices; red =  $\beta$ -sheets; violet = loops; orange = lysines, 22 in total). **1.** Reductive amination conditions (HCOH = formaldehyde; NaBH<sub>3</sub>CN = sodium cyanoborohydride; K<sub>2</sub>HPO<sub>4</sub>/KH<sub>2</sub>PO<sub>4</sub> = 20 mM potassium phosphate buffer pH 8; RT = room temperature; 100 sec = reaction time). **2.** Reductive amination quenching step (NH<sub>4</sub>OH = ammonium hydroxide). Red inset = lysine dimethylation enlargement (R, R<sub>1</sub> = protein backbone), dimethylation mass shift is reported under chemical structures.

**3.3.3 A quick glance at the dimethylation reaction outcome.** Preliminary experiments performed in collaboration with the mass spectrometry laboratory of the University of Milano-

Bicocca (Rita Grandori's group), and carried out by direct injection of intact mhNS, furnished some basic evidences of the reaction capabilities (**Fig. 3.3.2**). mhNS profile before (**Fig. 3.3.2, 1**) and after (**Fig. 3.3.2, 2**) dimethylation showed a significant  $m/z$  shift, while deconvolution provided an experimental mhNS mass value coherent with a complete protein dimethylation (i.e., + 644.7199 u is the theoretical monoisotopic mass shift accounting for 23 dimethyl groups, while + 649 u is the experimentally derived mass shift between unmethylated and dimethylated mhNS; **Fig. 3.3.2, 3**). The appearance of other peaks visible after deconvolution (i.e., the main one showing a + 720 u mass shift, 46991 u, **Fig. 3.3.2, 3**), can be ascribed to subpopulations of mhNS carrying unspecific or different modifications (i.e., oxidations, adducts). These preliminary data suggested that the chemical reaction developed for the amino group dimethyl labelling efficiently worked on mhNS. Further demonstration of the labelling reaction suitability towards the intended purpose is given in the following paragraphs.

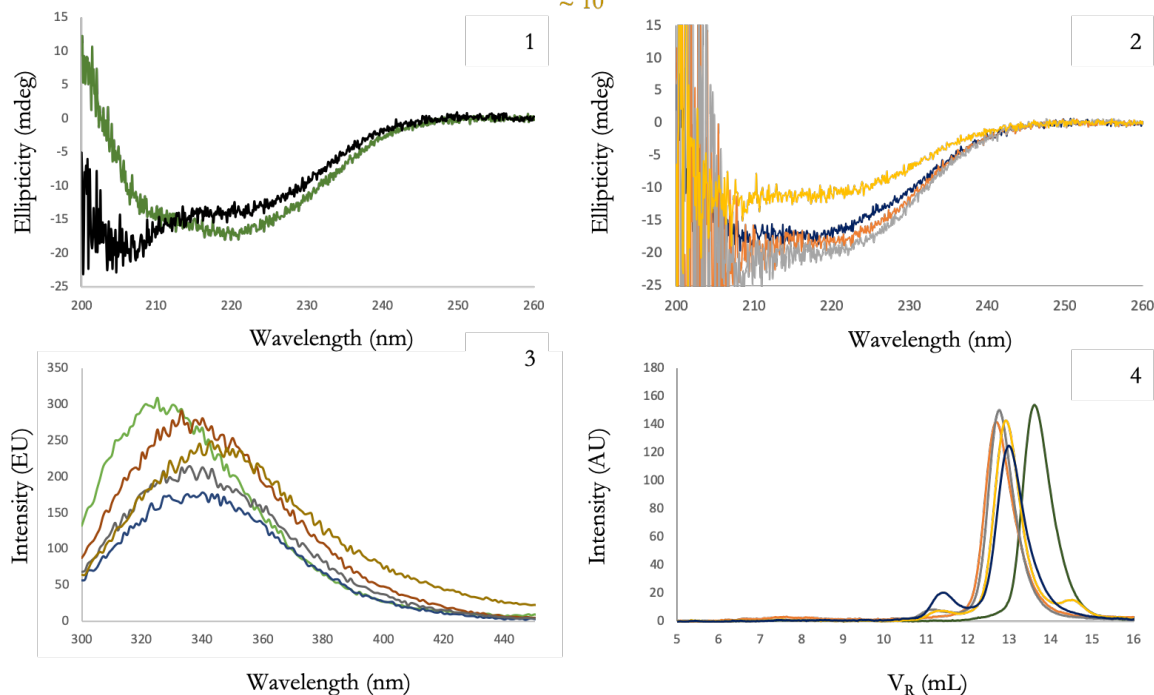


**Fig. 3.3.2.** MS analyses on intact unmethylated and dimethylated mhNS. **1.** MS spectrum of unmethylated mhNS. **2.** MS spectrum of dimethylated mhNS after 20 sec of reaction. **3.** Deconvoluted spectra of unmethylated (black) and dimethylated (red) mhNS after 20 sec of reaction (the 46271 u peak corresponds to unmethylated mhNS monoisotopic peak; the 46920 u peak represents the completely methylated mhNS peak, + 649 u in respect to unmethylated mhNS; the 46991 u peak highlights the presence of unspecific modifications, e.g., oxidations, adducts formation).

**3.3.4 The dimethylation reaction is compatible with hNS folding.** In order to perform a meaningful investigation of the putative hNS molecular features involved in the polymerisation process, mhNS must maintain its native structure after the dimethylation reaction and must not polymerise as a result of the chemical labelling. In order to evaluate this, biochemical analyses were performed in collaboration with the Stefano Ricagno's group (University of Milano) employing different lengths of the dimethylation reaction (i.e., 20 sec, 10 min, 1 hour), and samples were analysed through circular dichroism (Far-UV CD), fluorescence (FLR) and size-exclusion chromatography-fast protein liquid chromatography (SEC-FPLC; **Fig. 3.3.3**).<sup>328-330</sup> CD analyses showed that the final pH of the reaction (i.e., after quenching reductive amination with  $\text{NH}_4\text{OH}$ ; e.g., pH 10) only caused little perturbations on unmethylated mhNS folding, without altering it to a significant extent, after long incubation at high pH (**Fig. 3.3.3, 1**), while the dimethylated protein showed a substantial loss of secondary structure only after one hour of labelling reaction (**Fig.**

3.3.3, 2), thereby elucidating a 10 min safe reaction zone. FLR (Fig. 3.3.3, 3) and SEC-FPLC (Fig. 3.3.3, 4) analyses further demonstrated that lysine dimethylation did not substantially cause mhNS folding alterations nor trigger mhNS polymerisation, therefore confirming that the developed dimethylation reaction is a suitable option for hNS polymerisation studies.

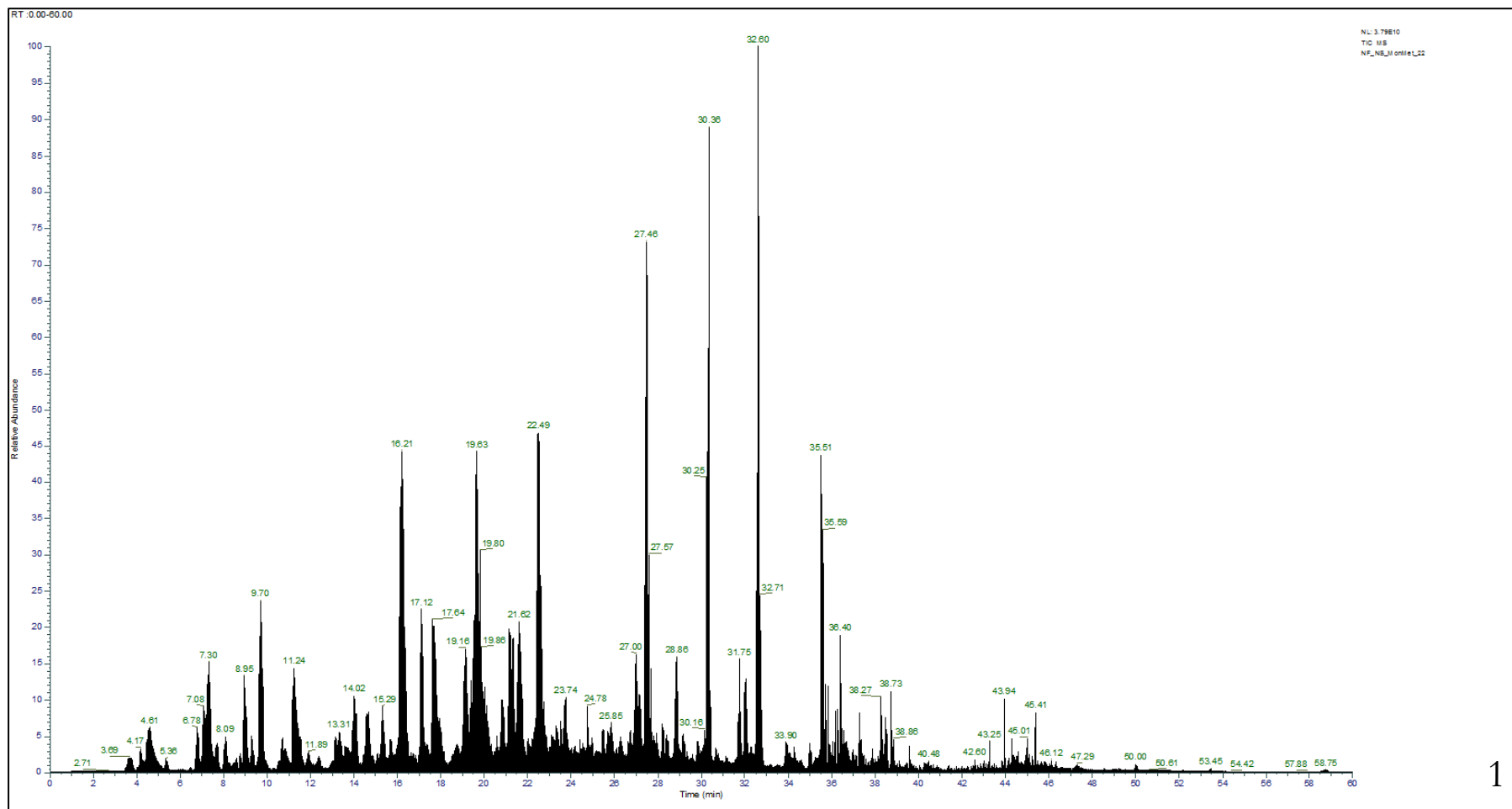
Legend: mhNS pH  $\approx$  7; mhNS pH  $\approx$  10; mhNS control pH  $\approx$  10; 20'' mhNS pH  $\approx$  10; 10' mhNS pH  $\approx$  10; 1h mhNS pH  $\approx$  10

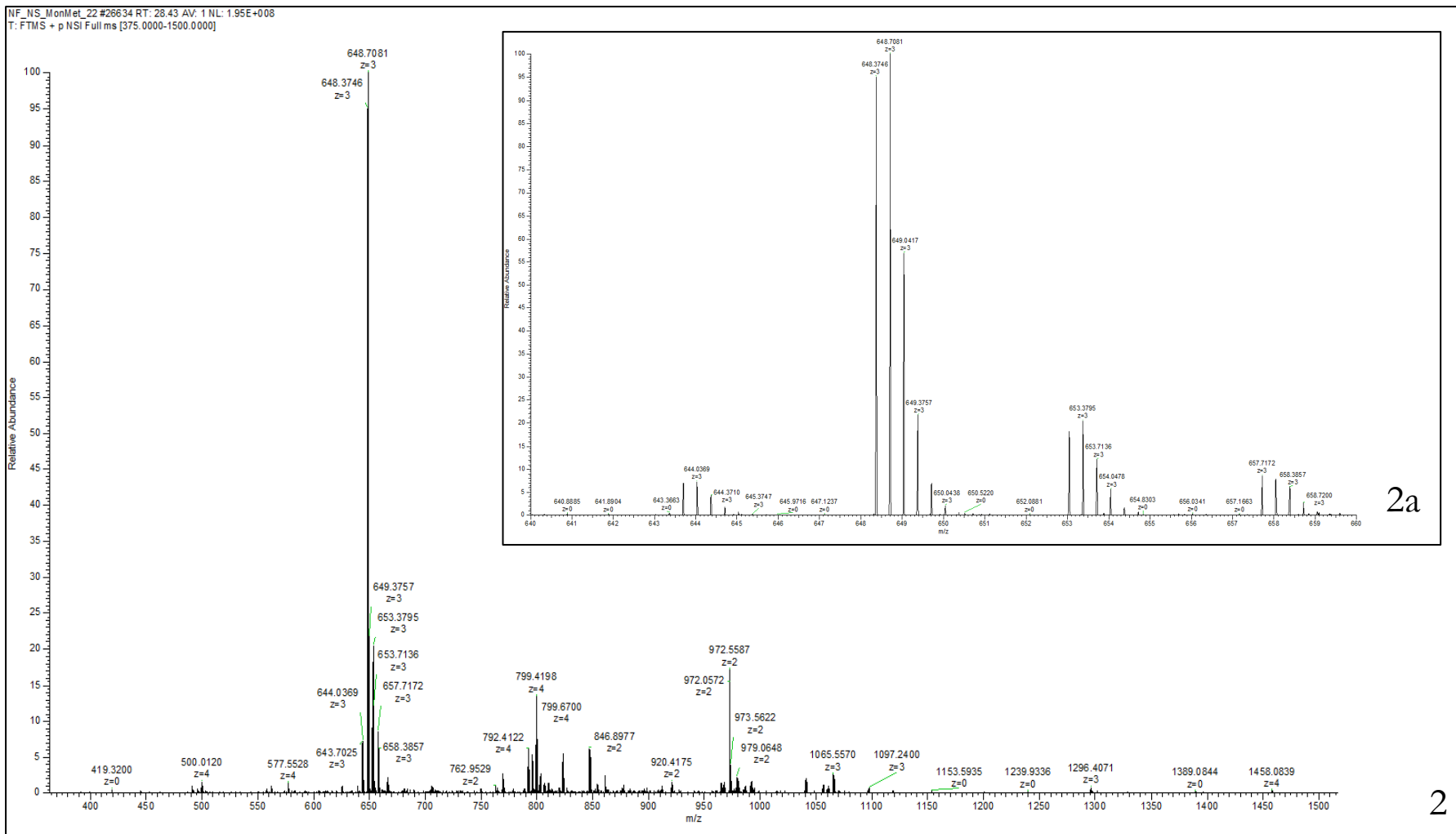


**Fig. 3.3.3.** Biochemical characterisation of mhNS (green = mhNS at pH 7, one hour incubation; black = mhNS at pH 10, one hour incubation; blue = mhNS, one hour of incubation with  $\text{NaBH}_3\text{CN}$ , followed by quenching with  $\text{NH}_4\text{OH}$  (reaction control); orange = dimethylated mhNS, 20 sec of reaction; grey = dimethylated mhNS, 10 min of reaction; yellow = dimethylated mhNS, 1 hour of reaction). **1.** Far-UV CD spectra of mhNS at different pH. **2.** Far-UV CD spectra of mhNS at different reaction times. **3.** Tyr/Trp Fluorescence analysis of mhNS (295 nm excitation; 300-350 emission) at different reaction times. **4.** SEC-FPLC analysis of mhNS (mhNS expected  $V_R = 14.5$  mL, phNS expected  $V_R = 7.1$  mL)<sup>328,330</sup> at different reaction times.

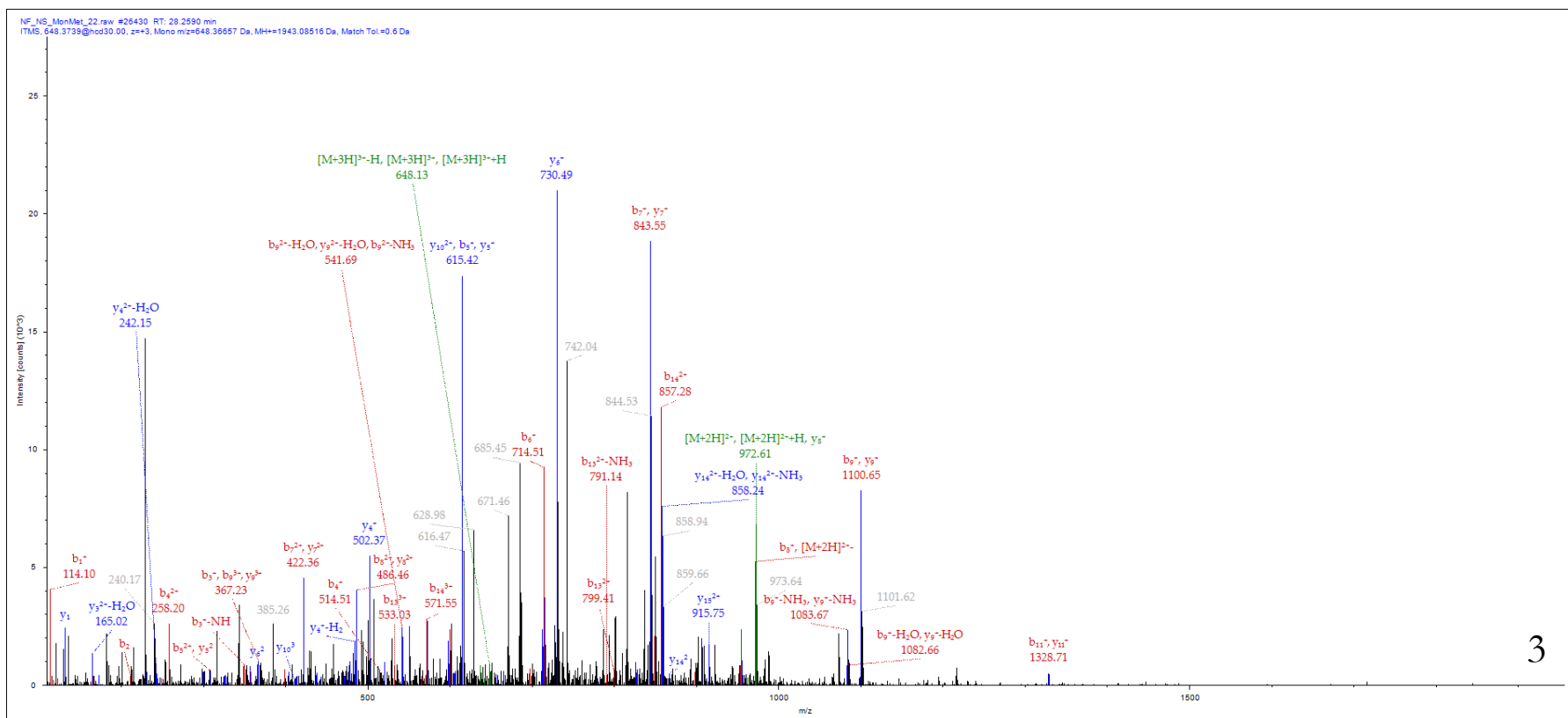
**3.3.5 Analytical evaluation of dimethylated mhNS and phNS peptides.** Dimethylated mhNS and phNS peptides were analysed in three biological replicates, accounting for a total of six technical replicates. Briefly, after quenching the dimethyl labelling reaction, proteins were in-solution digested with chymotrypsin, and peptides were cleaned up with a reverse phase step before Orbitrap MS bottom-up analysis. mhNS and phNS total ion chromatograms (TIC) of chymotryptic peptides are reported (Fig. 3.3.4, 1 and Fig. 3.3.5, 1), along with a selected peptide MS (Fig. 3.3.4, 2 and Fig. 3.3.5, 2), and  $\text{MS}^2$  (Fig. 3.3.4, 3 and Fig. 3.3.5, 3) exemplifying spectra for both hNS forms (i.e., LPRF<sup>T</sup>VEQEIDLKDV<sup>L</sup>,  $m/z = 648.366$ , 3+, theoretical  $[\text{M}+\text{H}]^+ = 1943.0848$  u, dimethyl K13). mhNS and phNS showed an average (i.e., six technical replicates)

sequence coverage value of 100% and 97.7% respectively, with more than one hundred unique peptides identified for each form (**Tab. A-3, Tab. A-4**), and each lysine amino group in mhNS and phNS sequences was found to be dimethylated at least once. Every mhNS and phNS lysine-containing peptide has been sorted and grouped according to the specific carried lysine (e.g., every peptide containing K70 in one group), by analysing the protein sequence. The Peptide Spectrum Match value (i.e., the number of times a single peptide is fragmented, PSM) for every lysine-containing peptide (i.e., peptides containing only one lysine) was used as a quantitative measure of the level of dimethylation (i.e., how many times the fragmented peptides containing a specific lysine showed dimethylation on that lysine) and unmethylation (i.e., how many times the fragmented peptides containing a specific lysine did not show dimethylation on that lysine). These data were used to calculate the dimethylation level (i.e., in percentage) for each lysine in mhNS and phNS. When peptides containing two (or more) lysines were encountered, these were labelled as uncertain (i.e., not possible to discern which lysine in the peptide harboured the dimethyl modification), and a dimethylation probability was assigned to each lysine contained in the peptide. The dimethylation probability was calculated by looking at the lysine dimethylation level (i.e., PSMs showing lysine dimethylation) in peptides containing the same lysines as unique lysines, and then by normalising the PSMs of the uncertain peptides by this value. This procedure was adopted to give an experimentally-based approximation (recalibrated dimethylation level) of which lysine had the highest probability of being dimethylated in peptides containing multiple lysines. Subsequently, dimethylated and unmethylated lysines in uncertain peptides were reassigned accordingly. The recalibrated dimethylation level was used to measure the extent of dimethylation on every hNS lysine (**Fig. 3.3.6**). Concerning mhNS, 54.5% of the lysines were found to be dimethylated with a dimethylation level higher than 90%; 22.7% with a dimethylation level comprised between 90 and 70%; 18.2% with a dimethylation level comprised between 70 and 50%; and 4.5% with a value lower than 50% (**Fig. 3.3.6**). Regarding phNS, 68.2% of the lysines were found to be dimethylated with a dimethylation level higher than 90%; 27.3% with a dimethylation level comprised between 90 and 70%; and 4.5% with a dimethylation level comprised between 70 and 50%. The average dimethylation levels for mhNS and phNS were between 80 and 90% respectively, underlining an excellent efficiency of the reductive amination dimethyl labelling.

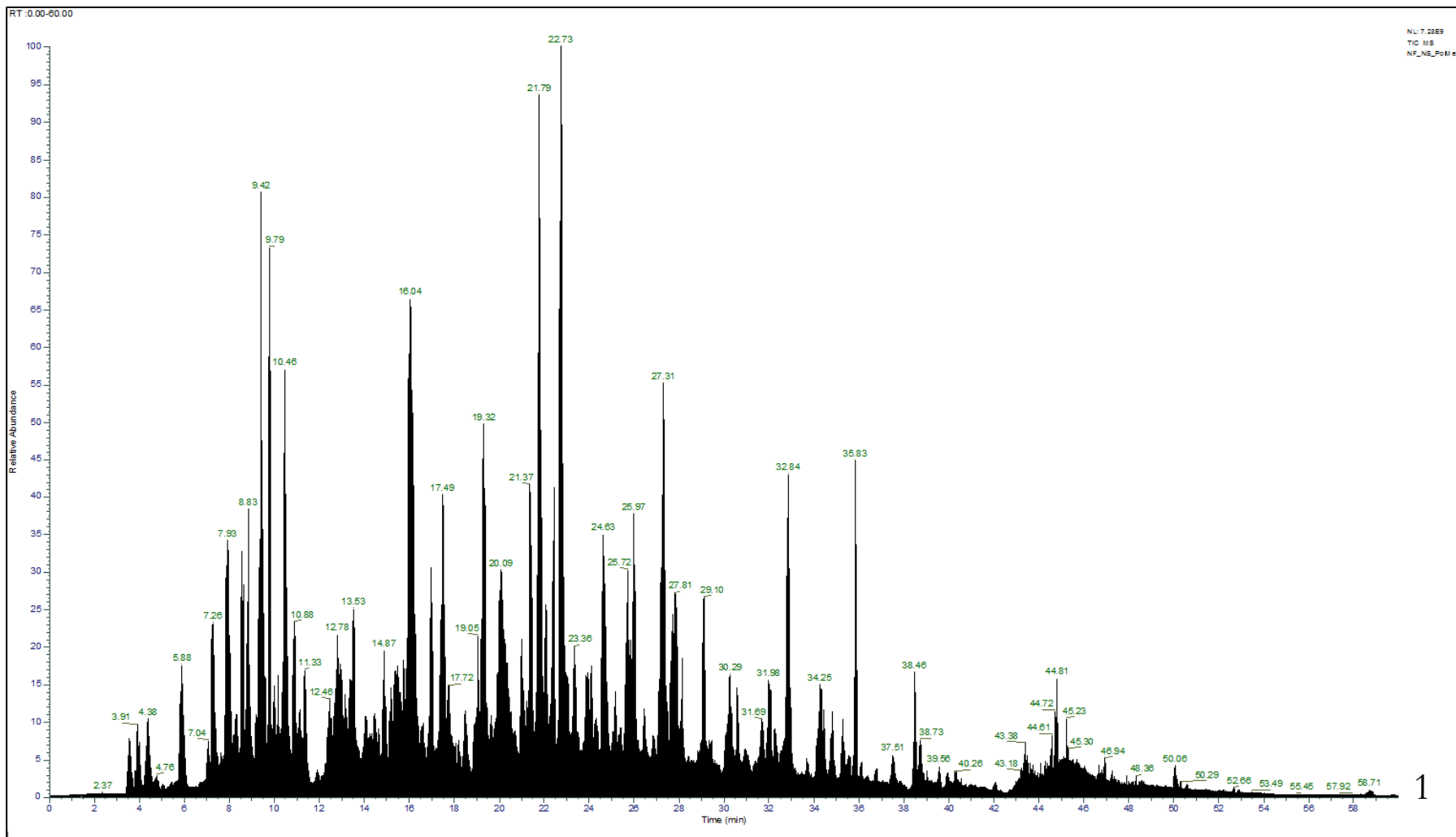


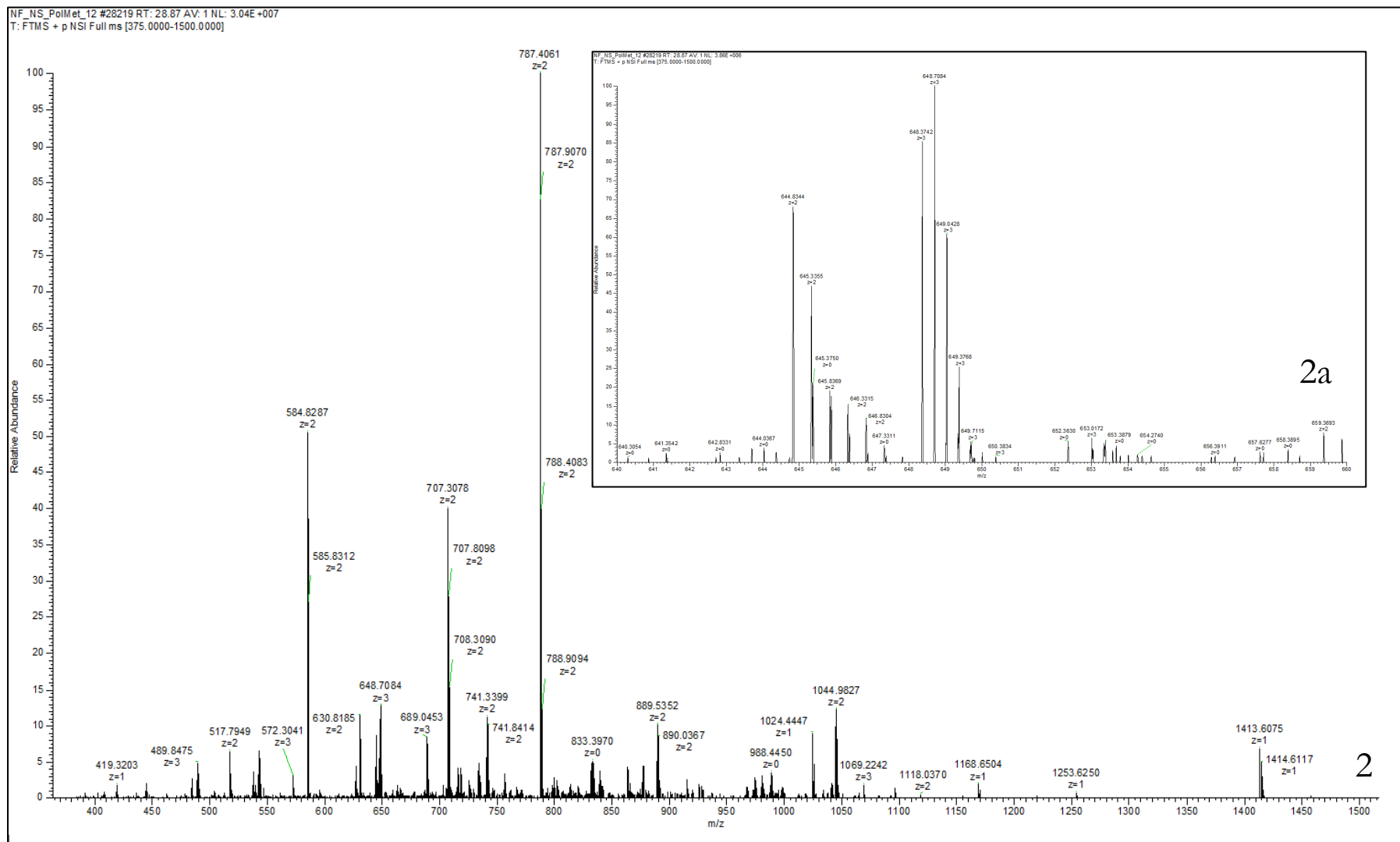


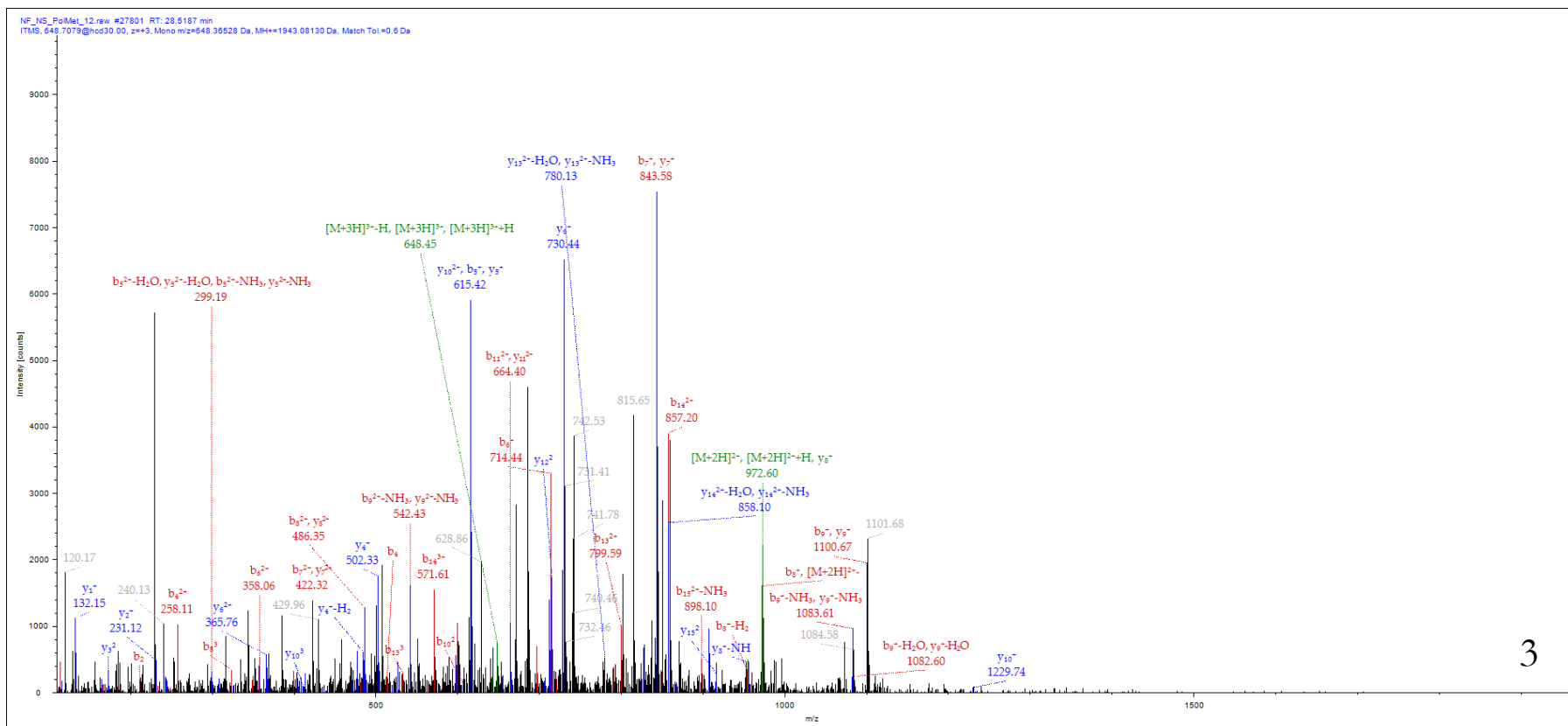




**Fig. 3.3.4.** Orbitrap MS analysis of dimethylated mhNS. **1.** TIC of the chymotryptic peptides generated from mhNS. **2.** MS spectra of a selected mhNS dimethylated peptide ( $m/z = 648.3746$ ,  $3+$ ,  $RT = 28.43$  min,  $PSMs = 166$ ,  $\Delta$  [ppm] = 0.66); 2a = enlargement on 648.3746 isotopic distribution. **3.** MS<sup>2</sup> annotated spectrum of the same mhNS dimethylated peptide presented in 2. ( $m/z = 648.3739$ ,  $RT = 28.2590$  min).



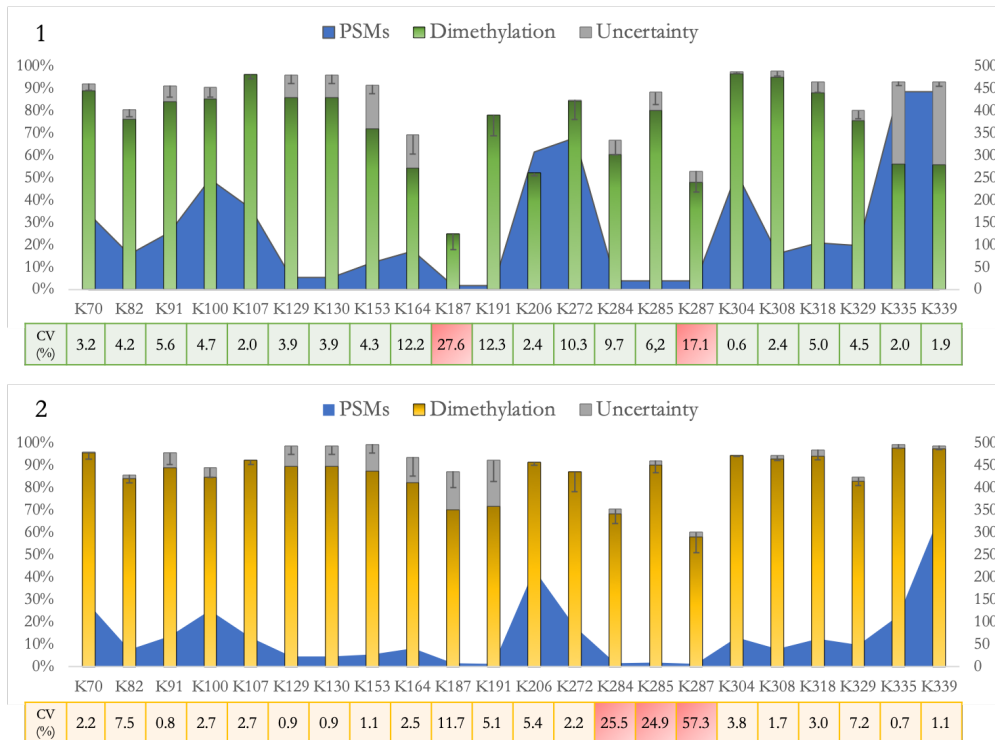




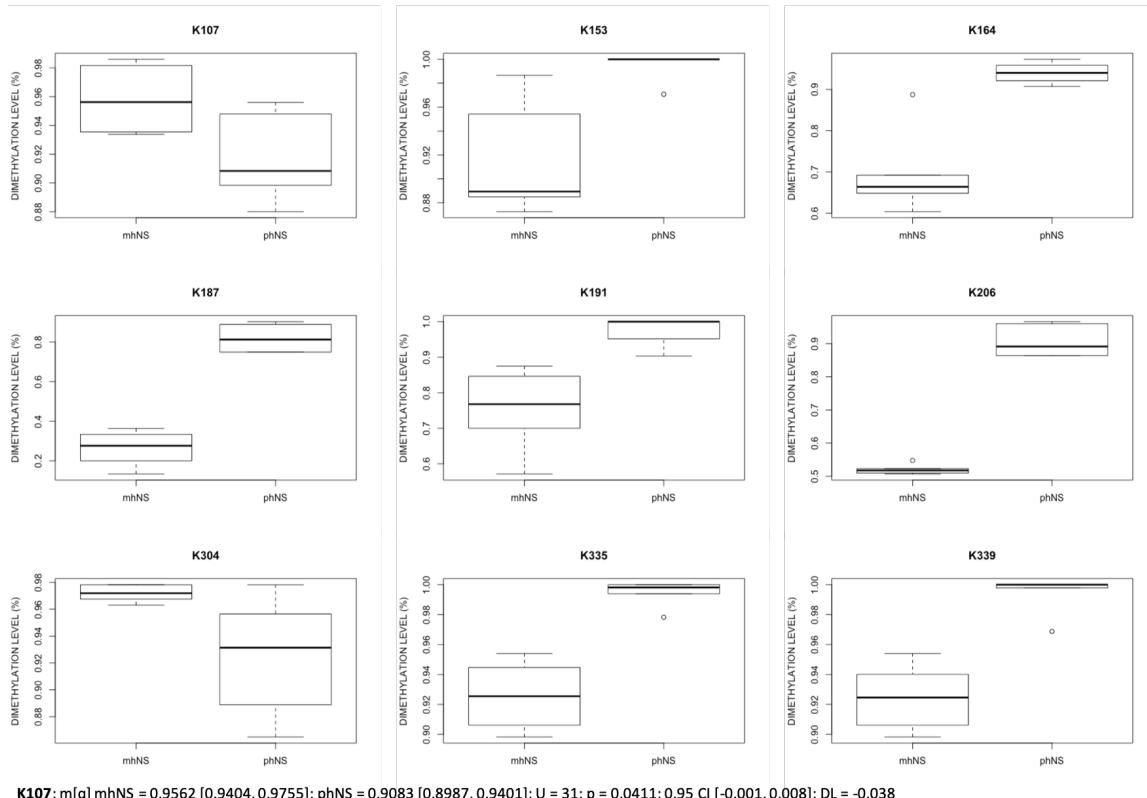
3

**Fig. 3.3.5.** Orbitrap MS analysis of dimethylated phNS. **1.** TIC of the chymotryptic peptides generated from phNS. **2.** MS spectra of a selected phNS dimethylated peptide (m/z = 648.3742, 3+, RT = 28.87 min, PSMs = 55, Δ [ppm] = 0.08); 2a = enlargement on 648.3742 isotopic distribution. **3.** MS<sup>2</sup> annotated spectrum of the same phNS dimethylated peptide presented in 2. (m/z = 648.3653, RT = 28.5187 min).

In addition, the dimethylation levels for every mhNS and phNS lysine were compared: nine lysines showed statistically significant differences, highlighting that NS monomeric and polymeric forms have different susceptibility to dimethyl labelling (**Fig. 3.3.7**), probably due to conformational alterations emerged after polymerisation. Thirteen lysines did not show relevant differences in the dimethylation level (**Fig. 3.3.8**), which suggests that these molecular elements are flagging hNS regions not directly involved in the polymerisation process.

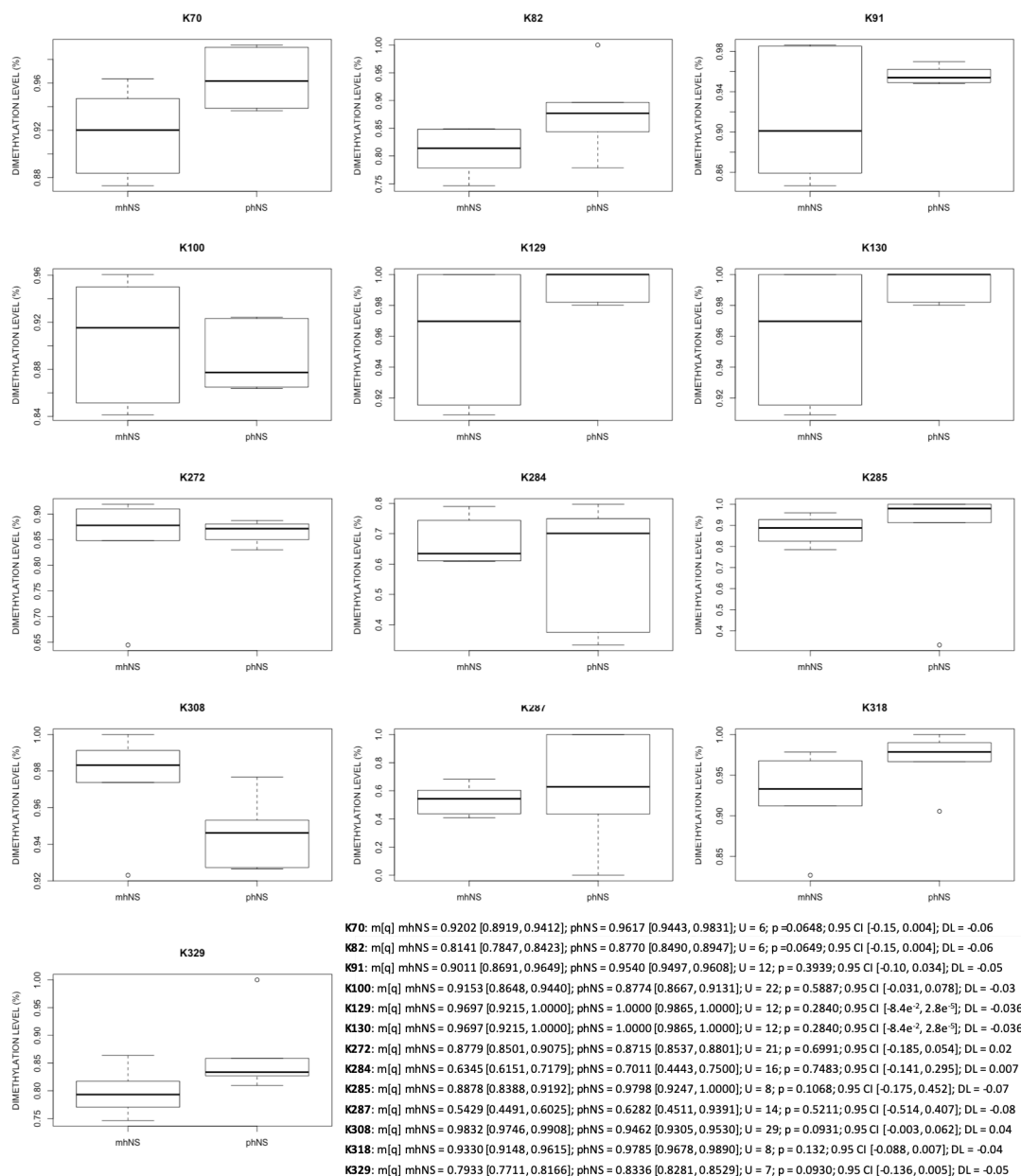


**Fig. 3.3.6.** mhNS and phNS lysines modification after dimethyl labelling. **1.** mhNS. **2.** phNS. The coloured part of the histograms represents the level of dimethylation (%) observed on peptides carrying a single lysine. The grey part represents the level of uncertainty (%) regarding which lysine is dimethylated within peptides bearing multiple lysines. The total histogram area (coloured + grey) represent the total level of dimethylation (%) for each lysine, since uncertain peptides have been recalibrated. The blue graph behind the histograms represents the value of PSMs for each hNS lysine. Descriptive error bars show data spread within replicates ( $n = 3$ , duplicates) as SD. Below each graph, CV values (%) for each hNS lysine are reported (i.e., calculated on the recalibrated dimethylation level between six replicates; red = > 15%).



**K107:** m[q] mhNS = 0.9562 [0.9404, 0.9755]; phNS = 0.9083 [0.8987, 0.9401]; U = 31; p = 0.0411; 0.95 CI [-0.001, 0.008]; DL = -0.038  
**K153:** m[q] mhNS = 0.8893 [0.8859, 0.9381]; phNS = 1.0000 [1.0000, 1.0000]; U = 1; p < 0.01; 0.95 CI [-0.115, -0.016]; DL = -0.11  
**K164:** m[q] mhNS = 0.6639 [0.6495, 0.6878]; phNS = 0.9400 [0.9251, 0.9543]; U = 0; p < 0.01; 0.95 CI [-0.319, -0.085]; DL = -0.27  
**K187:** m[q] mhNS = 0.2762 [0.2167, 0.3214]; phNS = 0.8125 [0.7500, 0.8821]; U = 0; p = 0.01; 0.95 CI [-0.703, -0.416]; DL = -0.55  
**K191:** m[q] mhNS = 0.7679 [0.7125, 0.8310]; phNS = 1.0000 [0.9758, 1.0000]; U = 0; p < 0.01; 0.95 CI [-0.428, -0.117]; DL = -0.21  
**K206:** m[q] mhNS = 0.5176 [0.5113, 0.5220]; phNS = 0.8913 [0.8699, 0.9439]; U = 0; p < 0.01; 0.95 CI [-0.447, -0.345]; DL = -0.37  
**K304:** m[q] mhNS = 0.9719 [0.9677, 0.9776]; phNS = 0.9314 [0.8971, 0.9527]; U = 31; p = 0.0303; 0.95 CI [8.6e<sup>-5</sup>, 9.8e<sup>-2</sup>]; DL = -0.04  
**K335:** m[q] mhNS = 0.9255 [0.9094, 0.9414]; phNS = 0.9981 [0.9944, 1.0000]; U = 0; p < 0.01; 0.95 CI [-0.094, -0.046]; DL = -0.07  
**K339:** m[q] mhNS = 0.9246 [0.9089, 0.9381]; phNS = 1.0000 [0.9983, 1.0000]; U = 0; p < 0.01; 0.95 CI [-0.094, -0.046]; DL = -0.07

**Fig. 3.3.7.** hNS lysines showing statistically significant differences in the dimethylation level between mhNS and phNS. Box-plots indicate dispersion and skewness of the data for mhNS and phNS lysines. The statistical analysis (Wilcoxon-Mann-Whitney, n = 3, duplicates) is shown through the presentation of relevant parameters.



**Fig. 3.3.8.** hNS lysines not showing statistically significant differences in the dimethylation level between mhNS and phNS. Box-plots indicate dispersion and skewness of the data for mhNS and phNS lysines. The statistical analysis (Wilcoxon-Mann-Whitney,  $n = 3$ , duplicates) is shown through the presentation of relevant parameters.

**3.3.6 Conclusions and future perspectives.** The labelling reaction developed for hNS polymerisation studies has shown excellent efficiency, compatibility with the protein folding, and suitability for the intended purpose. In fact, mhNS and phNS showed different labelling pattern after dimethylation, indicative of a different lysines exposure between the two forms, imputable to conformational changes occurring during the polymerisation process. Studies on hNS polymerisation support the model of an ordered process, in which the metastable hNS inserts a peripheral and flexible region (i.e., RCL), into the a central  $\beta$ -sheet region of another monomer,



thus locking the two into thermodynamically more stable polymers (section 1.2.7). These conformational rearrangements caused changes in the solvent accessibility of many amino acid residues (e.g., lysines) within the protein, therefore altering the labelling reaction efficiency. Lysines showing different dimethylation levels between mhNS and phNS can be therefore considered as flags of molecular regions putatively involved in hNS polymerisation mechanisms, to be further investigated with bioinformatic and biochemical analyses. One limitation of this project is that hNS has been produced by collaborators using heterologous expression in *E. coli*,<sup>328,331</sup> therefore providing a non-glycosylated protein. hNS is in fact an *N*-glycoprotein, and *N*-glycosylation has been suggested to play a role in the protein polymerisation mechanism.<sup>152</sup> Although the data collected in this study are still informative towards the elucidation of hNS biochemical behaviours, the experimental confirmation on the fully glycosylated version of the protein remains essential in order to achieved grounded biological conclusions. In this context, preliminary studies towards the *N*-glycosylation mapping and *N*-glycans structural analysis of hNS have already started, since hNS production in mammalian cells has just been achieved by collaborators. The author will take part in these studies, which will comprise an analytical evaluation of hNS *N*-glycans chemical structures and the validation of the chemical labelling procedure on *N*-glycosylated mhNS and phNS. The direct comparison of the chemical labelling pattern of non-glycosylated and *N*-glycosylated hNS, in both monomeric and polymeric forms, might also provide knowledge on the *N*-glycans influence on hNS folding features and further data on *N*-glycans involvement in the protein polymerisation behaviour.

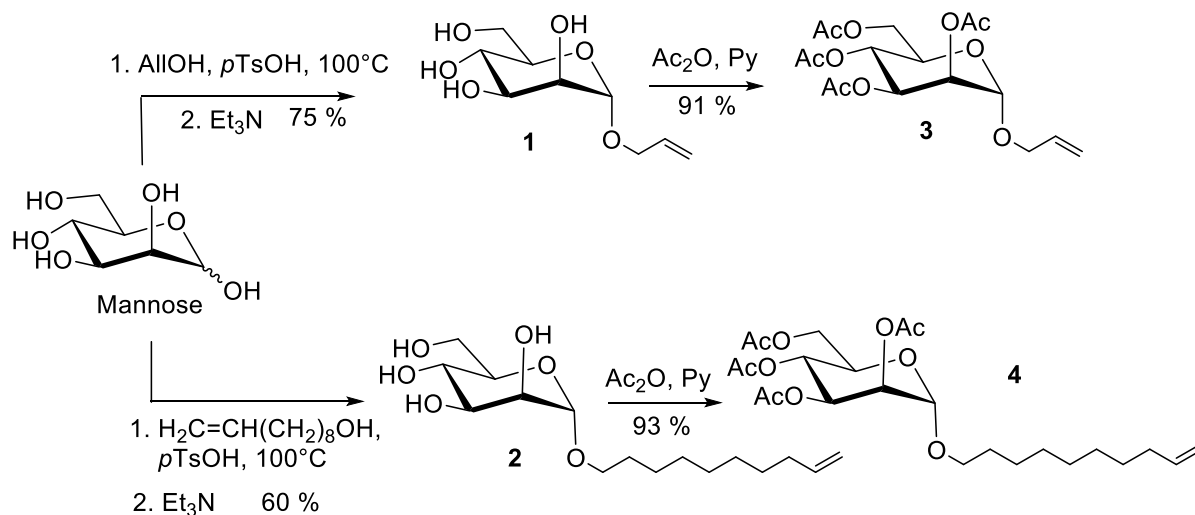
### 3.4 SYNTHESIS OF ALLYL AND DEC-9-ENYL $\alpha$ -D-MANNOPYRANOSIDES.

**3.4.1 Framework of the study.** This section reports the chemo- and stereoselective synthesis of allyl and dec-9-enyl  $\alpha$ -D-mannopyranosides from unprotected sugars, furnishing  $\alpha$ -D-glycosides functionalised with a reactive moiety (i.e., alkenyl groups) exploitable for the synthesis of glycoconjugates towards the study of various biological phenomena of carbohydrates (e.g., the decoration of biomaterials for regenerative medicine applications).<sup>332</sup> Mannose was chosen to be the glycosidic core of the synthesised alkenyl- $\alpha$ -D-glycosides, since this monosaccharide is copiously present within the brain substantially expressed high mannose glycans<sup>333</sup> and constitutes the 30% of the total O-linked carbohydrates in the mammals, being involved in muscle and brain development,<sup>334</sup> with defects related to neuromuscular and brain pathologies.<sup>335</sup> Therefore, the possibility to readily glycoconjugate  $\alpha$ -D-mannose-based glycosides could be of interest for the study of neurochemical systems. Furthermore, the surface modification of (macro)molecules with low-molecular-weight sugar moieties is still underexploited, although even simple sugary structures can elicit enormous cellular responses, as previously described in the introduction.<sup>273</sup> Nevertheless, the proposed glycosidic structures do not have to be relegated to neurochemistry applications only, but could be tested on disparate kind of cells,<sup>336</sup> since their presence within the human body is not a nervous system privilege. Alkenyl- $\alpha$ -D-mannopyranoside syntheses have been achieved via chemoselective Fischer-type glycosylation on unprotected sugars, performed by directly dissolving the carbohydrate starting material (i.e., glycosyl donor) into the chosen alcohol (i.e., glycosyl acceptor), in the presence of an acid catalyst, by adapting a patented procedure.<sup>337</sup> The main issue regarding glycosylation is stereoselective control and since the aim of the project was to produce  $\alpha$ -D-mannopyranosides, retaining the natural N- and O-mannosyl stereochemistry,<sup>338,31</sup> the generation of  $\alpha$ -(1,2-cis)-glycosides was desirable. Many procedures have been proposed to achieve the stereoselective synthesis of  $\alpha/\beta$  glycosides, but the majority of them heavily rely upon protective groups, neighbouring group participation and reaction intermediates.<sup>339,340</sup> The proposed reaction is carried out on unprotected sugars, being a quicker single step synthesis, and the modulation of stereoselectivity has been conducted via thermodynamic adaptations.<sup>341</sup>  $\alpha$ -(1,2-cis)-glycosides are glycosylation thermodynamically controlled products, while  $\beta$ -(1,2-trans)-glycosides are kinetically controlled ones. Therefore, high temperatures and long reaction times have been adopted to enhance  $\alpha$ -(1,2-cis)-product formation. Alkenyl- $\alpha$ -D-mannopyranosides are ready-to-react starting material for the synthesis of glycoconjugates, that can be efficiently performed via click chemistry approaches. The term click chemistry<sup>342,343</sup> is used for chemical transformations featured by high efficiency and selectivity (regio- and chemo-), and carried out usually in nontoxic solvents (i.e., water). Major advantages are wide applicability, high yields, few

by-products, mild reaction conditions (quite often insensitive to aerobic conditions), readily available starting materials and reagents. As a consequence, this methodology has found applications in many fields including polymer and material science, medicinal chemistry, molecular biology, and biotechnology. A range of click reactions are used in these applications, such as the copper(I)-catalyzed azide–alkyne cycloaddition (CuAAC),<sup>344</sup> the hetero-Diels–Alder reaction,<sup>345</sup> nucleophilic ring-opening of strained heterocyclic electrophiles,<sup>342</sup> or carbonyl transformation into oxime ethers and hydrazones.<sup>346</sup> Another click process that has gained renewed attention in recent times is the addition of thiols to alkenes,<sup>347</sup> called thiol–ene coupling (TEC). The reaction between an alkene and a thiol group can be induced thermally or photochemically through an anti-Markovnikov radical mechanism, which does not involve toxic transition metal catalysts. The TEC reaction can be successfully applied also to the synthesis of glycoconjugates and, as introduced before, alkenyl- $\alpha$ -D-mannopyranosides represent an ideal substrate towards this purpose.

**3.4.2  $\alpha$ -D-Mannopyranosides synthesis.** The synthesis of the alkenyl- $\alpha$ -D-mannopyranosides was performed by employing a Fischer-type glycosylation reaction on unprotected D-mannose, catalysed by *p*-toluenesulfonic acid,<sup>337</sup> towards the synthesis of allyl and decenyl  $\alpha$ -glycosides. The glycosylation reaction was performed with different amounts of the starting material (0.1 g and 1 g, 0.553 mmol and 5.53 mmol respectively) and either allyl alcohol or decenyl alcohol as acceptor. Although some protocols have already been published for the synthesis of allyl and decenyl mannopyranosides,<sup>339</sup> they usually start from protected sugars and involve intermediates, thus resulting in multi-step processes. Experimentally, the proposed one-step syntheses (**Fig. 3.4.1**) on unprotected monosaccharides displayed high stereoselectivity towards formation of  $\alpha$ -glycosides, while scaling up the reaction led to a decrease in the reaction yield (product 1). Compounds 1 and 2 (**Fig. 3.4.1**) were characterized as the corresponding acetates 3 and 4 with NMR and MS analyses (experimental details in section 4.4., NMR spectra in section 6.6).

**3.4.3 Conclusions and future perspectives.** In this project the stereoselective synthesis of alkenyl- $\alpha$ -D-mannopyranosides has been achieved through a simple, one-step, Fischer-type glycosylation reaction, furnishing  $\alpha$ -D-glycosides suitable for bioconjugation with other (macro)molecules and containing a neurologically interesting monosaccharide core to be tested in future experiments. The synthesis was proposed to and accepted by a chemical scientific journal in 2019.<sup>348</sup>



**Fig. 3.4.1.** Glycosylation reaction on  $\alpha$ -D-mannose with allyl (AlOH) and decenyl alcohols. AlOH = allyl alcohol;  $p$ TsOH = para-toluensulfonic acid;  $\text{Et}_3\text{N}$  = triethylamine;  $\text{Ac}_2\text{O}$  = acetic anhydride; Py = pyridine. For a complete description of the syntheses, please refer to the experimental section. For experimental details, please refer to section 4.4. For NMR spectra of the synthesized products, please refer to section 6.6.

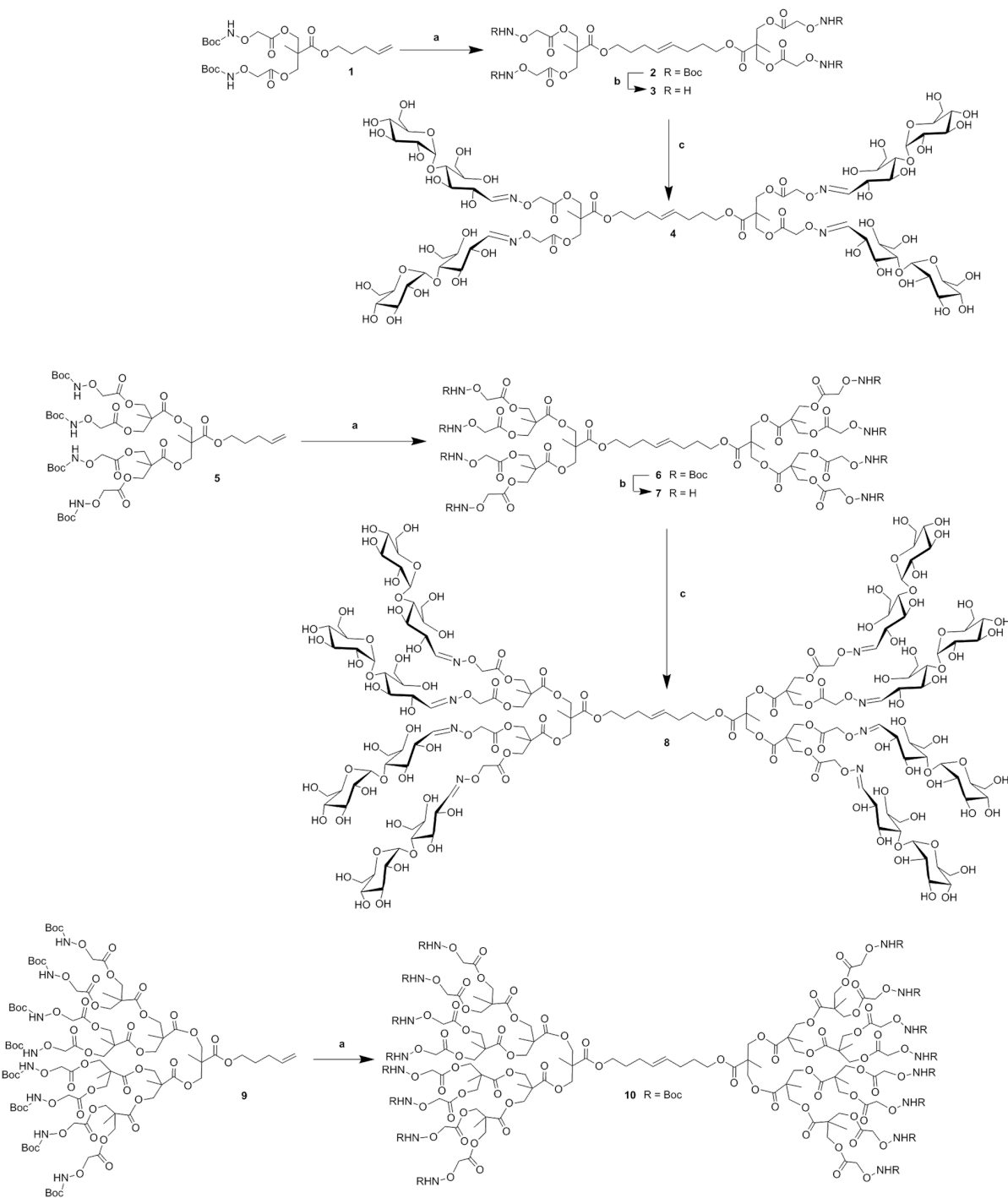
### 3.5 (GLYCO)DENDRIMERS CONVERGENT SYNTHESIS BY OLEFIN METATHESIS.

**3.5.1 Framework of the study.** This section reports the synthesis of novel hyperbranched monodisperse linear dendrimers, which extremities have been decorated with maltose moieties. As amply referenced within this thesis introduction (i.e., section 1.4.2), glycodendrimers are exploitable in a wide array of biomedical studies,<sup>280,281,349,350</sup> and maltose-decorated dendrimers in particular are widely researched towards neuromedical applications. In fact, the exposed -glucoside epitope, a fundamental signalling moiety in a variety of biochemical interactions,<sup>351,352</sup> is capable of eliciting neurochemically interesting responses when coupled with various scaffolds to create glycotools such as glycodendrimers, glyconanoparticles<sup>353</sup> and biomaterials.<sup>273</sup> In this project, the synthesis of a novel hyperbranched monodisperse linear dendrimer, based on 2,2-bis-(hydroxymethyl)-propionic acid (bis-MPA), by convergent metathesis-mediated coupling between the alkene-terminated focal point of bis-MPA dendrons has been achieved. Metathesis has been used in olefin cross-metathesis on polyolefin dendrimer surfaces,<sup>354,355</sup> for the internal incorporation of guest molecules into a dendrimer,<sup>356</sup> for post-synthetic modification of glycodendrons at focal points,<sup>357</sup> for the synthesis of cored dendrimers,<sup>358,359</sup> for dendritic linear hybrids through ring-opening metathesis polymerization,<sup>360</sup> and for cross-linking of hyperbranched dendrimeric structures.<sup>361</sup> This project delivers the first example of the use of metathesis for focal point coupling in dendrimer structures synthesis, along with glycodendrimer architectures that could be of interest in nervous system studies and, more generally, may provide good benefit to biomedical and tissue engineering applications, where high density of ligand exposure and spatial topographical presentation are crucial to bring about desired biological effects.<sup>362-364</sup>

**3.5.2 (Glyco)dendrimers synthesis.** The synthesis of symmetrical dendrimers was achieved starting from a bivalent (1), tetravalent (5) (both previously synthesized in the author's laboratory)<sup>332,365</sup> and octavalent (9) dendron monomers with a core double bond (**Fig. 3.5.1**), doubling the branching degree of each structure by a single-step metathesis reaction. Using Hoveyda-Grubbs second generation catalyst and octafluorotoluene as solvent (i.e., permitting a faster and more efficient reaction by boosting the activity of the catalyst),<sup>366</sup> dendrimers 2 and 6 were synthesized from dendrons 1 and 5 via a metathesis reaction. Deprotected dendrimers 3 and 7 were obtained from 2 and 6 by reacting them with trifluoroacetic acid for the removal of *t*-butoxycarbonyl (Boc) protecting groups. Glycodendrimers 4 and 8, exposing multiple sugar moieties at their ends, and thus potentially capable of eliciting a biological response in a biomedical context, were obtained by reacting the aminoxy-branched dendrimers with maltose, in the

presence of aniline as catalyst, in acetate buffer at pH 4.5. The addition of aniline for the aminoxy–carbonyl coupling allows the equilibrium to shift from the stable carbohydrate cyclic hemiacetal form towards a more reactive open-chain intermediate,<sup>367</sup> enhancing the reaction with the aminoxy groups. Following the same procedure described before, the synthesis of the hexadeca-valent dendrimer 10 was achieved from dendron 9, as a further demonstration of the efficacy of the metathesis reaction. NMR spectroscopy was employed towards the structural identification of the compounds and, where spectra showed a high degree of overlapping signals, as the complexity of the dendrimeric structure increased, only most significant peaks were identified. For instance, regarding glycodendrimers 4 and 8, the interpretation of the NMR spectra was complicated by the highly crowded pattern of signals belonging to the sugars, to the bis-MPA skeleton, to possible E/Z isomerism of oxime bonds, and to the amphipathic nature of these molecules. In fact, glycosylated dendrimers may tend to aggregate into micellar structures, as the glycosylation reaction proceeds in water, eventually masking the hydrophobic backbone. However, considering the tetravalent glycodendrimer 4, the oxime and double-bond signal, with relative integrals of ~4:2, are clearly showed within the <sup>1</sup>H NMR spectrum, as expected from the presence of four sugar moieties. As far as the octavalent glycodendrimer 8 is concerned, the ratio between the oxime and the double-bond signals in the <sup>1</sup>H NMR spectrum, ~7:2, suggested a partial glycosylation. The hexadeca dendrimer 10 NMR spectra were much more complicated than the others, due to the high complexity of its structure, but its <sup>1</sup>H NMR spectrum displayed the expected double bond signals. MS analyses confirmed all the (glyco)dendrimers masses, with the exception of glycodendrimer 8, which spectrum showed the presence of partially degraded products deriving from the loss of one, two, or three terminal aminoxyacetic groups.

**3.5.3 Conclusions and future perspectives.** The synthesis of the dendrimers was achieved by convergent metathesis-mediated coupling between the alkene-terminated focal point of 2,2-bis-(hydroxymethyl)-propionic acid (bis-MPA) dendrons, and a glycoconjugation reaction with maltose was explored toward glycodendrimers synthesis. The synthesised structures have the advantage to retain the internal double bond, which could be reduced to the corresponding saturated structure, thus allowing an increase in conformational flexibility, broadening the possibilities of fruitful interactions with biological targets. Another advantage of the proposed synthesis is that the length of the hydrocarbon chain can be varied at will (e.g., alkene-terminated linear polymers can be used as the dendron core), allowing an additional degree of structural variation. To the best of the author's knowledge, this work has been the first example of the use of metathesis for focal point coupling in glycodendrimers synthesis, and was thus published in 2017 as an original research paper.<sup>368</sup>



**Fig. 3.5.1.** (Glyco)dendrimers synthesis. Reaction conditions: (a) Hoveyda–Grubbs second generation, octafluorotoluene; (b) TFA 30%, dry DCM; (c) maltose, aniline, acetate buffer pH 4.5. For a detailed description of the syntheses, please refer to the experimental section.



## 4. EXPERIMENTAL SECTION.

### 4.1 A PRECISE AND VERSATILE PLATFORM FOR RAPID GLYCOSYLATION ANALYSIS OF BRAIN TISSUE.

**4.1.1 Chemicals.** All solutions were prepared using ultrapure water (resistivity of 18.2 MΩ·cm at 25 °C) and analytical/LC-MS grade solvents: methanol (MeOH) and ethanol (EtOH) were purchased from Honeywell, US; chloroform (CHCl<sub>3</sub>) and dimethyl sulfoxide (DMSO) from Sigma-Aldrich, US; acetonitrile (ACN), from ITW, US; Other chemicals such as Sodium Dodecyl Sulfate (SDS), Igepal-CA630, 2-Methylpyridine borane complex (PB), 2-Aminobenzamide (2-AB), Sodium Azide (NaN<sub>3</sub>) and Complete™ Mini EDTA-free Protease Inhibitor Cocktail were purchased from Sigma-Aldrich, US. 2-mercaptoethanol (βME) was purchased from Acros Organics, US; and acetic acid (AcOH) from Honeywell, US. Recombinant PNGase F (10.000 U/mL) from *Elizabethkingia miricola* was obtained from Promega, US. Phosphate Buffer Saline (PBS) 10X was prepared with NaCl (1.37 M), KCl (30 mM), Na<sub>2</sub>HPO<sub>4</sub> (80 mM), KH<sub>2</sub>PO<sub>4</sub> (20 mM). Radioimmunoprecipitation assay (RIPA) buffer was prepared with Tris-HCl pH 7.6 (25 mM), NaCl (150 mM), Igepal-CA630 (1% v/v), Sodium Deoxycholate (1% w/v) and SDS (0.1% w/v). Deglycosylation buffer was prepared with NaHCO<sub>3</sub> (20 mM, pH 8.6), SDS (0.35% w/v) and βME (0.60% v/v). *N*-glycan labelling solution was prepared with 2-AB (140 mM) and PB (420 mM) dissolved in acetic acid (AcOH)/DMSO (30%/70% v/v).

**4.1.2 Sample preparation.** Rat brain samples were obtained from the Laboratory Animal Unit at the Institute for Medical Research and Occupational Health (IMROH), Zagreb, in full compliance with animal ethics guidelines for the use of laboratory animals in scientific research (Approval No. 100-21/19-1). Since brain *N*-glycosylation patterns vary between brain regions,<sup>311</sup> in order to meaningfully compare HSD and LSD results for method validation, mouse brain samples were mildly blended with a FastPrep™-24 Instrument used with Lysing Matrix D 1.4 ceramic spheres (MP Biomedicals, US), employing 2 spheres for each 30 mg of tissue and operating for 5 seconds at the lowest possible speed (4 M/S). This procedure produced a brain pseudo-homogenate (*p*Homo), immediately employed for both HSD and LSD workflows to make the method comparison reliable, although this is not a requirement for either method and both methods can be easily performed even on intact brain pieces. Every HSD-LSD comparison was performed on the same *p*Homo, unless otherwise stated.

**4.1.3 LSD workflow.** Two slightly different versions of the LSD method were evaluated; LSD<sup>μL</sup> and LSD<sup>mg</sup>, which differ only in the tissue lysis step. The LSD<sup>μL</sup> version is the most efficient

version of the method and represents the final workflow to be employed (refer to supplementary materials for full protocol of the LSD<sup>μL</sup> version of the method). The LSD<sup>mg</sup> version was developed specifically for the sake of methodological validation (see below, i.e., robustness). In the LSD<sup>μL</sup> workflow, brain tissue pHomo (i.e., 100 mg) was incubated with cold RIPA buffer (recommended ratio: 10 μL for each 1 mg of tissue) containing protease inhibitors (on ice, 10 min), and then thoroughly and easily disrupted by gently passing it through a syringe, firstly using a 20G needle and then, if necessary, a thinner one. The brain lysate was then centrifuged at 12,000 RCF for 20 min and the supernatant was collected. This supernatant is stable when stored at -20°C and is the starting material for *N*-glycomics and *N*-glycoproteomics analyses. Within the LSD<sup>μL</sup> workflow version, an aliquot of the supernatant was taken from the tissue lysate to undergo glycomic analysis. Considering the LSD<sup>mg</sup> workflow version, the only difference is that no aliquot is taken from a bigger lysate, but a smaller lysate is produced directly on the tissue amount to be employed in the workflow (i.e., 1, 2, 5 10 mg, see below), and the lysate is used all at once. After the tissue lysis step, the LSD<sup>μL</sup> and LSD<sup>mg</sup> workflow are equivalent. Briefly, brain tissue pHomo was incubated with cold RIPA buffer (recommended ratio: 10 μL for each 1 mg of tissue) containing protease inhibitors (on ice, 10 min), and then thoroughly and physically homogenized through a syringe, firstly using a 20G needle and then, if necessary, a thinner one. The brain lysate was then centrifuged at 12,000 RCF for 20 min and the supernatant collected. This supernatant is stable when stored at -20°C and is the starting material for (glyco)proteomic analysis. For glycomic analysis, an aliquot of the supernatant was taken and the brain proteome was extracted with CHCl<sub>3</sub>/MeOH/H<sub>2</sub>O (1:4:4), the protein pellet was dried, resuspended in the deglycosylation buffer and denatured (60°C, 10 min). SDS was neutralized by the addition of Igepal-CA630 (10% v/v) and then PNGase F (5 U) was added and samples were sealed and incubated for *N*-glycan enzymatic release (37°C, 24 h). After that, PNGase F was added again (5 U) and samples were incubated a second time (37°C, 24 h). Released *N*-glycans were then purified with a second round of extraction using CHCl<sub>3</sub>/MeOH/H<sub>2</sub>O (1:4:4). The aqueous phase, containing the free *N*-glycans, was dried in a Savant SC210A SpeedVac vacuum concentrator (Thermo Scientific, US). Purified *N*-glycans were resuspended in ultrapure water and the *N*-glycan labelling solution was added for 2-AB conjugation via reductive amination (2 h, 65°C). Negative controls (C) underwent the same procedure, employing a labelling solution without 2-AB. Labelled *N*-glycans were then purified under vacuum, using AcroPrep™ GHP membrane 96-well filter plates (1 mL capacity, 0.2 μm membranes. Pall, US). Briefly, GHP filter plates were prepared by subsequent washings with EtOH (70% v/v in water), H<sub>2</sub>O and ACN (96% v/v in water). Labelled *N*-glycans (75 μL) were diluted in ACN (100%, 700 μL), loaded into the filter plate and washed four times with ACN (96%

v/v in water). A fourth identical wash, followed by centrifugation on an Eppendorf 5804 centrifuge equipped with an A-2-DWP rotor for plates (5 min, 164 RCF), prepared the cleaned *N*-glycans for elution: incubation with ultrapure water (90  $\mu$ L, 15 min under agitation) followed by centrifugation (5 min, 164 RCF) was performed twice, yielding the purified brain *N*-glycome (180  $\mu$ L) into a 0.2 mL skirted 96-well robotic plate (Thermo Scientific, US).

**4.1.4 HSD workflow.** HSD was performed as previously reported.<sup>196</sup> Briefly, brain tissue *p*Homo was fully homogenized with a FastPrep<sup>TM</sup>-24 Instrument (5 beads for 25 mg of brain tissue, 40 seconds at highest speed, 6 M/S), the proteome was extracted with CHCl<sub>3</sub>/MeOH/H<sub>2</sub>O (3:2:1) and deglycosylated with PNGase F (5 U, 37°C, 24 h, performed twice). *N*-glycans were purified using Amicon<sup>TM</sup> Ultra Centrifugal Filters, dried overnight in a vacuum concentrator, labelled via reductive amination (2-AB, PB, AcOH/DMSO 30%/70% v/v, 65°C, 2 h), and purified again through a GHP membrane 96-well filter plates (180  $\mu$ L final volume).

**4.1.5 HILIC-UPLC-FLR profiling and data analysis.** Labelled *N*-glycans were separated on a Waters Acquity UPLC H-class system (Waters, Milford, MA) consisting of a quaternary solvent manager, sample manager and a fluorescence (FLR) detector set with excitation and emission wavelengths of 250 and 428 nm, respectively. The instrument was under the control of Empower<sup>TM</sup> 3 software, build 3471 (Waters). *N*-glycan separation was achieved through an Acquity UPLC Glycan BEH Amide column (130 Å, 1.7  $\mu$ m, 2.1 mm  $\times$  150 mm), using ammonium formate (100mM, pH 4.4) as solvent A and ACN (100% v/v, LC-MS grade) as solvent B. Purified *N*-glycans (18  $\mu$ L) were diluted with ACN (100% v/v, 42  $\mu$ L), and separated using a linear gradient (0.561 mL/min, 27 $\rightarrow$ 29.5% v/v solvent A in the first 15 min and 29.5 $\rightarrow$ 38.7% v/v solvent A for the next 80 min). Samples were maintained at 5°C before injection, and the column temperature was 25°C. System calibration and chromatographic run quality control were carried out using water (blank), an external standard of 2-AB labelled hydrolysed glucose oligomers, and positive control samples (<sup>+</sup>C), created by mixing different 2-AB labelled brain *N*-glycomes previously obtained from various brain regions and routinely employed as representative of a consistent and typical brain profile. Due to the complexity of the chromatograms, data processing was performed manually, to reproduce the same integration pattern on all samples. All chromatograms were integrated in the same manner, subdividing them into 50 fractions (54 fractions for <sup>+</sup>C), and the proportion of *N*-glycans inside each fraction was expressed as a percentage of the total integrated area. For each sample, the intensity of the highest peak (maxEU) of each chromatogram was normalized by dividing it by the <sup>+</sup>C maxEU belonging to the same chromatographic run to give

$m_{\max EU}$  (normalized maximum intensity), whose average value across replicates was also considered when comparing sensitivity across methods.

**4.1.6 *N*-glycan enrichment by Porous Graphitized Carbon-SPE.** *N*-glycans obtained by both LSD and HSD were further purified and concentrated prior to MS analysis through porous graphitized carbon solid phase extraction (PGC-SPE). The stationary phase (300 mg) from one S\* PURE Extract-clean™ SPE Carbo column (S\*Pure Pte Ltd, Singapore) was removed and used to make a slurry phase with a final concentration of approximately 50 mg/mL by adding MeOH. 50  $\mu$ L of the slurry phase were loaded into empty ZipTips<sub>C18</sub> (Millipore, Ireland) to form small PGC columns in the pipette tips. The PGC columns were put into 2 mL tubes and centrifuged (2,000 RCF, 30 sec; applies to all centrifugations within this section) to pack the stationary phase. The PGC columns were then washed (60  $\mu$ L of ACN, twice) and equilibrated (60  $\mu$ L of water, twice) by centrifugation, discarding the flow-through. Labelled *N*-glycans obtained after the GHP filter plate purification, were loaded on the PGC columns in three rounds (60+60+40  $\mu$ L), with centrifugation performed after each load, discarding the flow-through. The PGC columns underwent a final wash (60  $\mu$ L of water) and the flow-through was again discarded after centrifugation. Elution of bound *N*-glycans was achieved using 40  $\mu$ L of elution buffer (75% ACN v/v and 25% ammonium formate 100 mM pH 4.4 v/v). An additional 10  $\mu$ L of ACN were added to the samples before LC-MS analysis.

**4.1.7 HILIC-UPLC-ESI-QqTOF MS profiling and data analysis.** PGC-cleaned samples derived from the effective range of brain tissue amounts (10, 5, 2, 1 mg) belonging to both methods were analysed by HILIC-UPLC (as described before), additionally hyphenated to a Bruker Compact QqTOF mass spectrometer, under the control of the HyStar software (Bruker, Bremen, Germany), version 3.2. An Ion Booster ion source (Bruker), was used to couple the UPLC with the mass spectrometer. The capillary voltage was set to 2250 V, with nebulizing gas at a pressure of 5.5 Bar. Drying gas was applied to the source at a flow rate of 4 L/min and temperature of 300°C. Nitrogen was used as the source gas, while Argon was used as the collision gas. Spectra were recorded within a mass range from 50 m/z to 4,000 m/z at a rate of 0.5 Spec/sec, in positive ion mode. Quadrupole ion energy and collision energy were set at 5 eV for MS analysis, transfer time was 120  $\mu$ s. Fragmentation spectra were recorded using the auto MS/MS mode, selecting the two precursor ions with the highest intensities to undergo CID fragmentation, with collision energy values chosen depending on the mass and charge state of the precursors, from 19 to 40 eV. All recorded spectra were analysed using Data Analysis software version 4.4 (Bruker). Spectra were background-subtracted to remove solvent-related signals, scans within each fraction

were averaged and signals were deconvoluted (2% abundance cut-off until fraction 37; lowered to 0.5% from fraction 38 onwards). Monoisotopic masses generated after deconvolution (abundance threshold > 2%; lowered to 0.5% for fraction 38 and 39 only) were searched against GlycoMod<sup>369</sup> (10 ppm error threshold; raised if no biologically plausible *N*-glycan monosaccharide composition was identified) to obtain a list of possible monosaccharide compositions. Where such information was available, GlycoMod hits were additionally filtered by their retention time using a  $\pm 1$  (or 2, depending on the fraction) Glucose unit (GU) threshold to exclude *N*-glycans that would not be expected to elute at the given retention time (e.g. glycan fragments). *N*-glycans for each chromatographic fraction were annotated according to GU values, measured *m/z* values, knowledge of *N*-glycan biosynthetic pathways and available fragmentation data. Structures were drawn using GlycoWorkbench.<sup>370</sup> For calculation of derived traits, fractions were allocated to groups according to the dominant *N*-glycan structure.

**4.1.8 Statistics.** Differences in precision between different analyses were tested by calculating the coefficient of variation (CV) of each fraction area for all replicates, then comparing the average chromatogram CV (*a*CV, the mean of all the CVs for all fractions across replicates) between different chromatographic runs outside replicates. To assess differences in sensitivity, signal intensity was evaluated by calculating the CV of the *m*maxEU values of replicates to give (*i*CV, the CV of intensity). The linearity of the method calibration curves was assessed considering the  $R^2$  value and the testing of replicates' homoscedasticity by performing Bartlett's test. Statistical significance was evaluated using Welch's ANOVA followed by Games-Howell post-hoc test for multiple comparisons, and results are shown as *p*-values (false discovery rate adjustment). The Wilcoxon-Mann-Whitney two sample rank sum test (two-sided) was used for binary comparisons of independent measurements, and results are shown as follows: *m*[*q*] = median [*quartiles*, 1<sup>st</sup> and 3<sup>rd</sup>] for both method's set of data; *U* = Mann-Whitney test statistics; *p* = *p*-value; *CI* [*x*, *y*] = confidence interval [*values*]; *DL* = difference in location (the median of the differences between a sample belonging to HSD and a sample belonging to LSD). The Wilcoxon signed-rank test (two-sided) was used for binary comparisons of dependent measurements. All the statistical analyses were performed using the program R, version 3.4.3.

## 4.2 THE "REVERSE GLYCOPROTEOMICS" PROJECT.

**4.2.1 Chemicals.** Chemicals used within this project are the same enlisted in the previous section, unless otherwise stated. Alkylation buffer (2X) was prepared using 0.69M Tris-HCl (pH 8.8), 20% glycerol, 8% (w/v) SDS, 0.2% (w/v) bromophenol blue, and 5mM DTT (freshly added). Acrylamide/Bis-acrylamide 37.5:1 and tetramethylethylenediamine (TEMED) were purchased from Bio-Rad, US; Ammonium persulfate (AMPS) was purchased from Sigma, Germany; PageRuler™ Plus Prestained Protein Ladder (MWM), 10 to 250 KDa, and GelCode™ Blue Stain Reagent, were purchased from Thermo Scientific, US. 30% acrylamide/bis solution, 19:1 was purchased from BioRad, US; GelCode blue stain reagent was purchased from Thermo scientific, US. Sequencing grade modified Trypsin were obtained from Promega, US. Denaturation buffer for SDS-PAGE analysis was prepared with Tris-HCl, pH 8.8 (0.69M), glycerol (20% v/v), SDS (8% w/v), and Bromophenol blue (0.2% w/v). SDS-PAGE running buffer was prepared with Tris base (250 mM), glycine (1.92 M), SDS (1%) and ultrapure water to one litre, then diluted 10 times to usage concentration.

**4.2.2 Sample preparation for SDS-PAGE fractionation.** The brain lysate used for method development was produced as described for the LSD method (i.e., sections 4.1.1 and 4.1.3). 20 µL of brain lysate (5 µL per gel lane) were denatured in 20 µL of alkylation buffer, and incubated for 60 min, 65°C. Negative control was prepared the same way using 20 µL of RIPA buffer (i.e., section 4.1.1) instead of brain lysate; while positive control was prepared adding 10 µL of alkylation buffer to 10 µL of human IgG pool (hIgG purified from blood, using standard and reproducible procedures developed at Genos Ltd). After denaturation and reduction, the brain lysate was alkylated using 20 mM iodoacetamide (60 min, RT, in the dark).

**4.2.3 SDS-PAGE recipes and run specifications.** Stacking gel (4%) was prepared using 400 µL 30% Acrylamide/Bis-acrylamide 37.5:1 (4%); 750 µL of 1M Tris-HCl, pH 6.8 (250 mM); 60 µL of 10% (w/v) SDS (0.2%); 15 µL of 10% (w/v) AMPS (0.5%); 6 µL of TEMED (0.2%); and 1769 µL of ultrapure water. Resolving gel was prepared using 2130 µL 30% Acrylamide/Bis-acrylamide 37.5:1 (8%); 5624 µL of 1M Tris-HCl, pH 8.8 (700 mM); 160 µL of 10% (w/v) SDS (0.2%); 80 µL of 10% (w/v) AMPS (0.1%); 6 µL of TEMED, 0.075%. Tris-Glycine-SDS running buffer was prepared with 250 mM Tris base; 1.92M glycine; 10% (w/v) SDS and diluted ten times to usage conditions. 10 µL of alkylated brain lysate, 20 µL of alkylated hIgG, 20 µL of negative control, and 5 µL of MWM were loaded onto the gel and run at 150V for about 90 min, in order to preserve



the 17 KDa band of the MWM. After the run the gel was rinsed three times in water, stained for 60 min with GelCode Blue, and then left at RT overnight in water for unbound dye removal.

**4.2.4 SDS-PAGE bands excision and destaining.** The gel was divided into 18 fractions according to the displayed protein bands (Fig. 3.2.2). Bands were excised from the gel using a clean scalpel, cut into gel pieces ( $\sim 1 \text{ mm}^3$ ), and then frozen for at least 120 min. Destaining was carried out by washing the gel pieces with 200  $\mu\text{L}$  of ACN for 5 min, then changing the ACN, vortexing, and washing them again for 15 min. The same steps were repeated using 20mM  $\text{NaHCO}_3$  (pH 8.6) instead of ACN. The whole cycle (two ACN, and two  $\text{NaHCO}_3$  washes) was repeated 5/6 times until gel pieces were completely destained. Gel pieces were then quickly dried in a vacuum centrifuge (about 15 min).

**4.2.5 In-gel deglycosylation (IGD).** 25  $\mu\text{L}$  of a 0.01% PNGase F solution (100U/mL in 20mM  $\text{NaHCO}_3$ , pH 8.6) were added to dried gel pieces. After the gel pieces absorbed the solution and swelled (about 15 min), another 25  $\mu\text{L}$  of the same PNGase F solution were added, and the samples were incubated at 37°C for 60 min. Gel pieces were then covered with 20mM  $\text{NaHCO}_3$ , pH 8.6, tubes were sealed with parafilm, and incubated at 37°C overnight. After the overnight incubation, the samples were vortexed, and centrifuged at 1100 RCF, and the supernatant was collected into clean tubes. 200  $\mu\text{L}$  of ultrapure water were then added to the gel pieces, they were sonicated for 30 min, and the supernatant was collected with the previous one (repeated three times). The previous step was repeated once with 200  $\mu\text{L}$  of 50% ACN. Three final washes (200  $\mu\text{L}$  100% ACN, 200  $\mu\text{L}$  ultrapure water, and 200  $\mu\text{L}$  100% ACN), were then conducted, the supernatant was added to the pool, and the pool was dried overnight under vacuum.

**4.2.6 N-glycans labelling, purification, concentration, and UPLC analysis.** A two-step labelling reaction was employed, using ProA instead of 2-AB to boost the method sensitivity. Firstly, N-glycans were resuspended in 20  $\mu\text{L}$  of 1% formic acid, incubated at RT for 40 min, dried under vacuum, and resuspended into 50  $\mu\text{L}$  of ultrapure water. To each sample were then added 25  $\mu\text{L}$  of a 30% HAC in DMSO solution, and 4.32 mg of ProA (0.018 mmol), then samples were incubated for 60 min at 65°C. After the first incubation, 25  $\mu\text{L}$  of a 30% HAC in DMSO solution with 4.48 mg of PB (0.042 mmol) were added to each sample, and these were incubated for 90 min at 65°C. Labelled N-glycans were purified through GHP procedure, concentrated with PGC-SPE, and run using HILIC-UPLC as described above (i.e., section 4.1.3, 4.1.5, and 4.1.6).

**4.2.7 In-gel trypsinisation after/without deglycosylation (IGTaD/IGT).** IGD-treated (analysis of deglycosylated peptides, IGTaD) or untreated (analysis of N-glycopeptides, IGT) gel



pieces were dried for 20 min in a vacuum centrifuge before undergoing IGTaD/IGT. Proteins trapped in the gel bands were digested with Trypsin to generate (glyco)peptides for subsequent mass spectrometry-based proteomics analyses. Sequencing grade modified trypsin (Promega, US) was prepared according to manufacturer specifications in order to obtain a 0.1  $\mu\text{g}/\mu\text{L}$  solution, by dissolving 100  $\mu\text{g}$  of the lyophilised enzyme in 1000  $\mu\text{L}$  of the given buffer. 15  $\mu\text{L}$  of the 0.1  $\mu\text{g}/\mu\text{L}$  Trypsin solution were then added to 60  $\mu\text{L}$  of 20 mM  $\text{NaHCO}_3$ , pH 8.6, in order to have a trypsin solution with a final concentration of usage of 20  $\text{ng}/\mu\text{L}$ . 75  $\mu\text{L}$  of this solution were added to the gel pieces, and samples were left for 15 min at RT to absorb the solution and swell. Gel pieces were then incubated at 4°C for 20 min, and then covered with 20 mM  $\text{NaHCO}_3$ , pH 8.6 (approximately 25  $\mu\text{L}$ ), before undergoing a second incubation at 4°C for 40 min. Then, tubes were sealed with parafilm and incubated overnight at 37°C for (deglycosylated) protein digestion. (Glyco)peptides were then recovered from the gel as in the following. Firstly, 10  $\mu\text{L}$  of 1 % formic acid were added to each sample to reduce the pH and inactivate Trypsin. Then, samples were vortexed and centrifuged for 5 min at 1100 RCF. The supernatant was removed and retained in a clean tube. 200  $\mu\text{L}$  of 20 mM  $\text{NaHCO}_3$ , pH 8.6 were added to gel pieces, samples were vortexed, and incubated for 60 min at RT in agitation. The supernatant was removed and retained in a clean tube. 200  $\mu\text{L}$  of 50% ACN were added to gel pieces, samples were vortexed, and incubated for 30 min at RT in agitation. The supernatant was removed and added to the supernatant pool. This step was repeated other three times, with 200  $\mu\text{L}$  of 70% ACN, then 200  $\mu\text{L}$  of 20 mM  $\text{NaHCO}_3$ , pH 8.6, and finally with 200  $\mu\text{L}$  of 90% ACN. Each time the supernatant was removed and added to the supernatant pool. The supernatant pool containing the extracted (glyco)peptides was then dried completely in a vacuum centrifuge.

**4.2.8 Deglycosylated peptides purification and enrichment with RP-SPE.** Deglycosylated peptide samples were purified and concentrated for MS analyses using reverse-phase solid phase extraction. 20 mL of 80% ACN were added to 1 g of C18 stationary phase (Chromabond sorbent C18 ec octadecyl modified silica phase; Macherey-Nagel, Germany), the mixture was maintained in agitation with a magnetic stirring bar while pipetting it into a 96 wells polypropylene plate (200  $\mu\text{L}$  per well, 0.7 mL capacity, polyethylene frits; Orochem Technologies, US), mounted on a vacuum manifold for deglycosylated peptides purification. The C18 stationary phase was activated with ACN (80% v/v in water; three times) and conditioned with TFA (0.1% v/v in water; three times). Dried deglycosylated peptides were resuspended in a solution of 0.1% v/v TFA in water (500  $\mu\text{L}$ ), loaded in the plate wells, and incubated for 10 min at RT before vacuuming to waste. The C18 stationary phase was then washed three times (0.1% v/v TFA in water, 200  $\mu\text{L}$ ), and the plate was centrifuged briefly to completely remove the solution from the wells and let them dry

out completely before deglycosylated peptides elution (80% v/v ACN, 200  $\mu$ L, 10 min incubation before elution) into a 0.2 mL skirted 96-well robotic plate (Thermo Scientific, US) by centrifugation on an Eppendorf 5804 centrifuge equipped with an A-2-DWP rotor for plates (from 50 to 100 RCF in 4 min and then one minute at 130 RCF). Samples were then dried under vacuum before subsequent analyses (approximately two hours).

**4.2.9 Deglycosylated peptides RP-nanoUPLC-ESI-QqTOF MS profiling.** Deglycosylated peptides were separated on a Waters nanoAcquity UPLC system (Waters, Milford, MA) consisting of a binary solvent manager, an auxiliary solvent manager, and a sample manager. Deglycosylated peptides separation was achieved through an Ascentis® Express C18 1.7 Micron capillary HPLC column (90  $\text{\AA}$ , 2.7  $\mu$ m, 15 cm  $\times$  100  $\mu$ m, Sigma-Aldrich, US), using TFA (0.1% v/v in ultrapure water) as solvent A and ACN (80% v/v, 0.1% TFA v/v, in ultrapure water) as solvent B. Sheath liquid was employed to counterbalance TFA ion suppression (50% v/v isopropanol, 20% v/v propionic acid in ultrapure water, 2  $\mu$ L/min). A  $\mu$ -Precolumn (100  $\text{\AA}$ , 300  $\mu$ m i.d. X 5 mm, C18 PepMap 100, 5  $\mu$ m; Thermo Scientific, US) was used before the analytical separation. Dried deglycosylated peptides were resuspended in ultrapure water (10  $\mu$ L, 7  $\mu$ L injected), further purified and concentrated on the precolumn (15  $\mu$ L /min, 99% v/v solvent A, 1% solvent B, 3 min) and separated using a linear gradient (0 $\rightarrow$ 50% v/v solvent B in 60 min, followed by 100% v/v solvent B for 10 min). Samples were maintained at 10°C before injection and the column temperature was 30°C. The LC part was hyphenated to a Bruker Compact QqTOF mass spectrometer, under the control of the HyStar software (Bruker, Bremen, Germany), version 3.2. An ESI ion source (Bruker), was used to couple the UPLC with the mass spectrometer. The capillary voltage was set to 4500 V, with nebulizing gas at a pressure of 0.4 Bar. Drying gas was applied to the source at a flow rate of 4 L/min and temperature of 180°C. Nitrogen was used as the source gas, while Argon was used as the collision gas. Spectra were recorded within a mass range from 50 m/z to 3000 m/z at a rate of 2.0 Spec/sec, in positive ion mode. Quadrupole ion energy and collision energy were set at 4 eV for MS analysis, transfer time was 150  $\mu$ s. Fragmentation spectra were recorded using the auto MS/MS mode, selecting the three precursor ions with the highest intensities to undergo CID fragmentation, with collision energy values chosen depending on the mass and charge state of the precursors, from 35 to 65 eV. All recorded spectra were analysed using Data Analysis software version 4.4 (Bruker) and MaxQuant 1.6.6.<sup>371</sup> For (glyco)peptides identification, raw files were uploaded directly in MaxQuant, Trypsin was chosen as protease, Asn $\rightarrow$ Asp was set as variable modification, along with oxidation and protein N-term acetylation, while carbamidomethylation of cysteines was chosen as a fixed modification.

The *Rattus norvegicus* proteome (Uniprot Proteomes entry UP000002494) was used for *in silico* digestion.

#### 4.2.10 Glycopeptides purification and enrichment with cotton-HILIC chromatography.

Each fraction of dried glycopeptides (i.e., section 4.2.7) and (glyco)peptides extraction from gel pieces) was resuspended in 60  $\mu\text{L}$  of LC-MS grade ACN (80% v/v) and TFA (1% v/v). The HILIC stationary phase was prepared by packing a 20  $\mu\text{L}$  pipette tip with 100% natural, not chemically modified cotton (cotton amount enough to fill from the pipette tip end up to 4-5 mm). Cotton HILIC column conditioning was performed with ultrapure water (20  $\mu\text{L}$ , three times), followed by column equilibration with ACN containing TFA (80% v/v ACN, 1% v/v TFA, 20  $\mu\text{L}$ ). Binding of tryptic glycopeptides was achieved by pipetting the sample up and down the column within the pipette tip (20  $\mu\text{L}$ , 20 times). The column was then washed by pipetting ACN containing TFA (80% v/v ACN, 1% v/v TFA, 20  $\mu\text{L}$ ). Glycopeptides were eluted directly in 40  $\mu\text{L}$  of ultrapure water, by pipetting up and down five times. The steps from cotton HILIC conditioning to glycopeptides elution were repeated two additional times, and the elution were collected into the same tube to enhance *N*-glycopeptide recovery.

### 4.3 CHEMOSELECTIVE MODIFICATION OF HUMAN NEUROSERPIN.

**4.3.1 Chemicals.** All chemicals were purchased from Sigma, US, unless otherwise stated; Chymotrypsin sequencing grade was purchased by Promega, US; C18 Millipore® Ziptips were purchased from Millipore-Sigma, US. All other reagents and standards were purchased from Thermo scientific, US.

**4.3.2 Dimethyl labelling of hNS.** hNS in its monomeric (mhNS) and polymeric forms (phNS) has been produced by collaborators as previously described.<sup>328,331</sup> mhNS and phNS underwent the same labelling reaction, purification steps and downstream applications, therefore the acronym hNS will be used in the following to refer to both forms. 100 µL of hNS (0.7 µg/µL, potassium phosphate buffer 20 mM, pH 8) were reacted with freshly prepared HCOH (20 µL, 4% v/v in ultrapure water) and NaBH<sub>3</sub>CN (20 µL, 85 mM in ultrapure water); reagents were added and quickly mixed by pipetting and the reaction mixture was left to react for 100 seconds at RT. The reaction was quenched with the addition of NH<sub>4</sub>OH (20 µL, 7% v/v in ultrapure water), and the pH was adjusted (i.e., pH 10 to pH 8) prior to biochemical analyses.

**4.3.3 nanoESI-QqTOF-MS, Far-UV CD, SEC and FLR analyses of intact mhNS.** mhNS was analysed in its native form, prior and after dimethyl labelling with nanoESI-QqTOF-MS, circular dichroism, size-exclusion chromatography and Trp/Tyr fluorescence, in collaboration with the Stefano Ricagno's group (University of Milano), and the Rita Grandori's group (University of Milano-Bicocca), as previously described.<sup>328,329</sup>

**4.3.4 In-solution enzymatic digestion of hNS.** hNS was digested using chymotrypsin at RT, for 18 hours, at pH 8, following manufacturer's indications (diluted to usage concentration of 1 µg/µL, and used 5 µL per sample, protease:protein = 1:100). The reaction was stopped by enzyme inactivation with formic acid (FA, 1% v/v, 10 µL). No reduction nor alkylation step was performed before endopeptidase digestion, since hNS does not have any cysteine. Chymotrypsin was preferred over trypsin since lysine dimethylation could interfere with the enzyme cleavage mechanism (i.e., at lysine C-T), thus increasing the chances of miscleavages, and because its employment furnished better peptide chromatograms (i.e., separation, intensity), something evaluated during analytical optimisation experiments (data not shown).

**4.3.5 Peptides purification and enrichment with RP-SPE.** hNS peptides were purified and enriched using C18 Millipore® Ziptips (Merck Millipore, US). Briefly, Ziptips (10 µL) were conditioned four times with ACN (100% v/v in ultrapure water, 10 µL) and equilibrated four

times with FA (1% v/v in ultrapure water, 10  $\mu$ L). Acidified samples were then passed through the pipette-tips stationary phase by pipetting up and down twelve times directly into the sample tube. Pipette-tips stationary phase was then washed twelve times with FA (1% v/v in ultrapure water, 10  $\mu$ L), and peptides were finally eluted in ACN and FA (50% v/v and 0.5% v/v, respectively, 20  $\mu$ L) by pipetting up and down five times. Peptide eluates were dried under vacuum (approximately two hours).

**4.3.6 Orbitrap Fusion HR-MS analysis of hNS peptides.** hNS peptides were separated on an EASY-nLC™ 1000 system (Thermo scientific, US), consisting of a binary nano-flow gradient pump, and a cooled autosampler. hNS peptides separation was achieved through an EASY-Spray™ PepMap RSLC C18 column (100  $\text{\AA}$ , 2  $\mu$ m, 15 cm  $\times$  150  $\mu$ m, Thermo scientific, US), using FA (0.1% v/v in ultrapure water) as solvent A and ACN (80% v/v, 0.1% FA v/v, in ultrapure water) as solvent B. Dried hNS peptides were resuspended in FA (0.1% v/v in ultrapure water, 5  $\mu$ L, 2  $\mu$ L injected), and separated using a 60 min gradient (5 $\rightarrow$ 40% v/v solvent B in 40 min, 40 $\rightarrow$ 75% v/v solvent B in the next 15 min, followed by 100% v/v solvent B for 5 min; 200 nL/min). A mixture of BSA tryptic peptides (Thermo scientific, US) was used as positive control to ensure the MS run reliability and consistency. Samples were maintained at 10°C before injection and the column temperature was 40°C. The UPLC part was hyphenated to an Orbitrap Fusion™ mass spectrometer (Thermo scientific, US), equipped with a nanoESI ion source (Thermo scientific, US), under the control of the XCalibur software. The capillary voltage was set to 2000 V and the transfer tube T° to 275 °C. Spectra were acquired in data dependent mode, with a cycle time of 3 sec comprising a master scan in the Orbitrap (OTMS), monoisotopic precursor selection, application of intensity (5.0e3) and charge state (2 to 7) thresholds, dynamic exclusion (10 sec, exclusion after 3 times, 10 ppm mass tolerance), and fragmentation analysis in the ion trap (ITMS<sup>2</sup>). The master scan (MS) analysis was performed in positive ion mode in the Orbitrap by scanning from m/z 375 to 1500, with a resolution of 60000 (at m/z 200), a targeted automatic gain control (AGC) value of 4.0e5 and a maximum injection time of 50 ms. Selected ions were isolated in the quadrupole with an isolation window of 1.6 m/z, and then fragmented and measured in the ion trap (ddMS<sup>2</sup> IT HCD), with a resolution of 30000 (at m/z 200), a normalized collision energy of 30%, a targeted AGC value of 1.0e4, and a maximum fill time of 35 ms. Chromatograms were analysed using the software Freestyle version 1.4, and spectra were analysed using Proteome discoverer, version 2.2 (Thermo scientific, US). For peptides identification, chymotrypsin (FLMWY) was chosen as the protease, and dimethylation (+ 28.031300 u), N-acetylation (+ 42.010565 u), and oxidation (+ 15.995) were set as dynamic modifications. The homo sapiens NS sequence (Uniprot KB entry Q99574) was used for *in silico* digestion.

**4.3.7 Statistics.** The Wilcoxon-Mann-Whitney two sample rank sum test (two-sided) was used for binary comparisons of independent measurements, and results are shown as follows:  $m[q]$  = median [quartiles, 1<sup>st</sup> and 3<sup>rd</sup>] for both method's set of data;  $U$  = Mann-Whitney test statistics;  $p$  = p-value;  $CI [x, y]$  = confidence interval [values];  $DL$  = difference in location (the median of the differences between a sample belonging to HSD and a sample belonging to LSD). All the statistical analyses were performed using the program R, version 3.4.3.

#### 4.4 SYNTHESIS OF ALLYL AND DEC-9-ENYL $\alpha$ -D-MANNOPYRANOSIDES.

**4.4.1 General Methods.** Reactions were performed with commercially available reagents and solvents, without further purification. Reactions were monitored by thin-layer chromatography (TLC) on silica gel 60F<sub>254</sub> coated glass plates (Merck), and visualized was effected by charring with 10:45:45 (volumes) H<sub>2</sub>SO<sub>4</sub>-EtOH-H<sub>2</sub>O or with (NH<sub>4</sub>)<sub>6</sub>Mo<sub>7</sub>O<sub>24</sub> (21 g) and Ce(SO<sub>4</sub>)<sub>2</sub> (1 g), in a solution of concentrated H<sub>2</sub>SO<sub>4</sub> (31 mL) in water (500 mL). All reactions were terminated when differences in their course could no longer be seen (TLC). Flash column chromatography was performed on silica gel 230–400 mesh (Merck). NMR spectra were recorded at 400 MHz (<sup>1</sup>H) and 100.6 MHz (<sup>13</sup>C) with a Varian Mercury or with a Bruker Advance Neo instrument. Chemical shifts are reported in ppm referenced to residual solvent signal as an internal standard; *J* values are given in Hertz. For all the compounds, assignments of <sup>1</sup>H and <sup>13</sup>C NMR spectra were based on 2D proton–proton shift-correlation and 2D carbon-proton heteronuclear correlation spectra. Mass spectra were recorded on a QTRAP instrument (AB Sciex) equipped with an electrospray ion source. The samples were directly injected by a steel capillary, employing a spray voltage of 5.5 kV and a declustering potential of 5 V.

**4.4.2 Allyl  $\alpha$ -D-mannopyranoside synthesis (1).** D-Mannose 0.1 g or 1 g of (Sigma-Aldrich, 0.56 and 5.56 mmol) was suspended in 5.5 and 6.5 mL of allyl alcohol, respectively, and *p*TsOH monohydrate (42 mg, 0.22 mmol and 422 mg, 2.22 mmol, 0.4 equiv, respectively) was added. The suspension was stirred at 100 °C (oil bath) overnight. The clear solution was cooled to rt, triethylamine (50 or 500  $\mu$ L, 0.33 or 3.3 mmol, 1.5 equiv.) was added and the solvent was evaporated under reduced pressure. The crude product was chromatographed (9:1 EtOAc–EtOH), affording the desired mannopyranoside 1 (94 mg, 0.43 mmol, 75% and 511 mg, 2.32 mmol, 40% yield,  $\alpha$  with trace amount of  $\beta$  visible in the acetylated product 3, *R<sub>f</sub>* = 0.5 (5:1 EtOAc–EtOH) as a light-yellow oil.  $[\alpha]_{20}^D + 70.0$  (*c* 1.2, CH<sub>3</sub>OH); lit.<sup>372</sup>  $[\alpha]_{20}^D + 73.6$  (*c* 1.0, CH<sub>3</sub>OH); <sup>1</sup>H NMR (400 MHz, MeOD):  $\delta$  6.00–5.88 (m, 1 H, CH<sub>2</sub>=CH-CH<sub>2</sub>), 5.29 (dd, 1 H, *J* = 17.2, 1.7 Hz, CH<sub>2</sub>=CH-CH<sub>2</sub>), 5.17 (dd, 1 H, *J* = 10.5, 1.7 Hz, CH<sub>2</sub>=CH-CH<sub>2</sub>), 4.79 (d, 1 H, *J* = 1.6 Hz H-1), 4.22 (dd, 1 H, *J* = 13.0, 5.5 Hz, -O-CH<sub>2</sub>-CH=CH<sub>2</sub>), 4.00 (dd, 1 H, *J* = 13.0, 5.5 Hz, -O-CH<sub>2</sub>-CH=CH<sub>2</sub>), 3.86–3.78 (m, 2 H, H-2, H-6a), 3.74–3.67 (m, 2 H, H-3, H-6b), 3.60 (t, 1 H, *J* = 9.5 Hz, H-4), 3.53 (ddd, 1 H, *J* = 9.5, 5.7, 2.3 Hz, H-5). <sup>13</sup>C NMR (101 MHz, MeOD):  $\delta$  135.50 (CH<sub>2</sub>=CH-CH<sub>2</sub>), 117.25 (CH<sub>2</sub>=CH-CH<sub>2</sub>), 100.75 (C-1), 74.74 (C-5), 72.65 (C-3), 72.20 (C-2), 68.84 (O-CH<sub>2</sub>-



CH=CH<sub>2</sub>), 68.67 (C-4), 62.95 (C-6). ESI-MS:  $m/z$  [M+H]<sup>+</sup> calcd for C<sub>9</sub>H<sub>16</sub>O<sub>6</sub>, 220.0947; found, 220.1002.

**4.4.3 Dec-9-enyl  $\alpha$ -D-mannopyranoside synthesis (2).** D-Mannose (500 mg, 2.78 mmol) was suspended in 5 mL of 9-decen-1-ol, pTsOH (211 mg, 1.108 mmol, 0.4 equiv) was added, and the suspension was stirred at 100 °C overnight. The suspension (the starting material did not dissolve completely) was cooled to rt and triethylamine (230  $\mu$ L, 1.662 mmol, 1.5 equiv) was added. After concentration, the crude product was chromatographed (9.9:0.1 $\rightarrow$ 9.5:0.5 EtOAc–EtOH), affording the desired, amorphous mannopyranoside **2** (435 mg, 1.67 mmol, 60%, mainly  $\alpha$  but with trace amount of  $\beta$ ,  $R_f$  = 0.5 (5:1 EtOAc–EtOH). Crystallization from MeOH, EtOH and CHCl<sub>3</sub> was unsuccessful.  $[\alpha]_{20}^D$  + 42.9 ( $c$  1.1, CH<sub>3</sub>OH); lit.  $[\alpha]_{20}^D$  + 56 ( $c$  0.5, CH<sub>3</sub>OH)<sup>373</sup>,  $[\alpha]_{20}^D$  + 50 ( $c$  0.9, CH<sub>3</sub>OH).<sup>339</sup> <sup>1</sup>H NMR (400 MHz, MeOD):  $\delta$  5.81 (ddt, 1 H,  $J$  = 17.0, 10.2, 6.7 Hz, CH<sub>2</sub>=CH-CH<sub>2</sub>), 4.98 (dd, 1 H,  $J$  = 17.1, 1.5 Hz, CH<sub>2</sub>=CH-CH<sub>2</sub>), 4.91 (dd, 1 H,  $J$  = 10.2, 2.2 Hz, CH<sub>2</sub>=CH-CH<sub>2</sub>), 4.73 (d, 1 H,  $J$  = 0.9 Hz, H-1), 3.82 (dd, 1 H,  $J$  = 11.8, 2.2 Hz, H-6a), 3.78 (dd, 1 H,  $J$  = 3.0, 1.6 Hz, H-2), 3.77 – 3.66 (m, 3 H, -O-CH<sub>2</sub>-, H-3, H-6b), 3.61 (t, 1 H,  $J$  = 9.5 Hz, H-4), 3.55 – 3.49 (m, 1 H, H-5), 3.41 (dt, 1 H,  $J$  = 9.6, 6.3 Hz, -O-CH<sub>2</sub>-), 2.05 (q, 2 H,  $J$  = 6.9 Hz, CH<sub>2</sub>=CH-CH<sub>2</sub>-), 1.64 – 1.53 (m, 2 H, O-CH<sub>2</sub>-CH<sub>2</sub>-), 1.45 – 1.28 (m, 10 H, -(CH<sub>2</sub>)<sub>5</sub>-); <sup>13</sup>C NMR (101 MHz, MeOD):  $\delta$  140.12 (CH<sub>2</sub>=CH-CH<sub>2</sub>), 114.71 (CH<sub>2</sub>=CH-CH<sub>2</sub>), 101.53 (C-1), 74.55 (C-5), 72.67 (C-3), 72.28 (C-2), 68.61 (C-4), 68.56 (-O-CH<sub>2</sub>-(CH<sub>2</sub>)<sub>7</sub>), 62.91 (C-6), 34.87 (CH<sub>2</sub>=CH-CH<sub>2</sub>-(CH<sub>2</sub>)<sub>7</sub>-O), 30.60 (O-CH<sub>2</sub>-CH<sub>2</sub>-(CH<sub>2</sub>)<sub>6</sub>), 30.54, 30.51, 30.17, 30.10, 27.33 (O-CH<sub>2</sub>-CH<sub>2</sub>-(CH<sub>2</sub>)<sub>5</sub>-CH<sub>2</sub>-CH=CH<sub>2</sub>). ESI-MS:  $m/z$  [M+H]<sup>+</sup> calcd for C<sub>16</sub>H<sub>30</sub>O<sub>6</sub>: 318.2042; observed 318.1263; monoisotopic  $m/z$  = 341.0400 (Na<sup>+</sup> adduct), 357.0900 (K<sup>+</sup> adduct). Anal. calcd for C<sub>16</sub>H<sub>30</sub>O<sub>6</sub>: C, 60.35; H, 9.50; found C, 60.42; H, 9.49.

**4.4.4 Allyl 2,3,4,6-tetra-*O*-acetyl- $\alpha$ -D-mannopyranoside synthesis (3).** Compound **1** 120 mg (0.55 mmol) was dissolved in a mixture of pyridine (4 mL) and Ac<sub>2</sub>O (2 mL) and the solution was stirred at rt overnight. MeOH (1 mL) was added, and the solvent was evaporated under vacuum. The crude product was suspended in AcOEt (15 mL) and the solution was washed successively with 5% HCl (2 x 15 mL) and H<sub>2</sub>O (15 mL). The organic phase was dried and the solvent was removed under reduced pressure affording the desired mannopyranoside **3** (192 mg, 0.50 mmol, 91% yield), as a light-yellow oil.  $[\alpha]_{20}^D$  + 48.3 ( $c$  1.0, CHCl<sub>3</sub>); lit.  $[\alpha]_{20}^D$  + 46.9 ( $c$  1.0, CHCl<sub>3</sub>).<sup>374</sup> <sup>1</sup>H NMR (400 MHz, CDCl<sub>3</sub>):  $\delta$  5.96-5.84 (m, 1 H, CH=CH<sub>2</sub>), 5.36 (dd, 1 H,  $J$  = 10.0, 3.4 Hz, H-3), 5.33 – 5.20 (m, 4 H, H-2, H-4, CH=CH<sub>2</sub>), 4.86 (d, 1 H,  $J$  = 1.8 Hz, H-1), 4.28 (dd, 1 H,  $J$  = 12.2, 5.3 Hz, CH<sub>2</sub>CH=CH<sub>2</sub>), 4.18 (dd, 1 H,  $J$  = 12.8, 5.3 Hz, H-6a), 4.10 (dd, 1 H,  $J$  = 12.2, 2.2 Hz, CH<sub>2</sub>CH=CH<sub>2</sub>), 4.06 – 3.97 (m, 2 H, H-5, H-6b), 2.14 (s, 3 H, CH<sub>3</sub>CO), 2.10 (s, 3 H,

CH<sub>3</sub>CO), 2.03 (s, 3 H, CH<sub>3</sub>CO), 1.98 (s, 3 H, CH<sub>3</sub>CO). <sup>13</sup>C NMR (101 MHz, CDCl<sub>3</sub>): δ 170.78, 170.19, 170.02, 169.88 (4 C=O), 133.04 (CH=CH<sub>2</sub>), 118.58 (CH=CH<sub>2</sub>), 96.72 (C-1), 69.76, 69.21, 68.67, 66.33 (C-2, C-3, C-4, C-5), 68.79 (CH<sub>2</sub>CH=CH<sub>2</sub>), 62.60 (C-6), 21.00, 20.85, 20.81, 20.81 (4 CH<sub>3</sub>CO)ESI-MS:  $m/z$  [M+H]<sup>+</sup> calcd for C<sub>17</sub>H<sub>24</sub>O<sub>10</sub> 388.1369, observed monoisotopic  $m/z$  = 411.1272 (Na<sup>+</sup> adduct). All characterization data are in accordance with the literature data.<sup>375,376</sup>

**4.4.5 Dec-9-enyl 2,3,4,6-tetra-O-acetyl- $\alpha$ -D-mannopyranoside synthesis (4).** A solution of compound **2** (100 mg (0.31 mmol) in 2:1 pyridine–Ac<sub>2</sub>O (6 mL) was stirred at rt overnight. The full conversion was confirmed by TLC. MeOH (1 mL) was added, and the solvent was evaporated under vacuum. The crude product was chromatographed (7.3:2.7 petroleum ether–EtOAc), affording the desired mannopyranoside **4** (140 mg, 0.29 mmol, 93% yield) as a light-yellow oil.  $[\alpha]_{20}^D + 40.1$  ( $c$  1.1, CHCl<sub>3</sub>); lit.  $[\alpha]_{20}^D + 38.4$  ( $c$  0.9, CHCl<sub>3</sub>).<sup>339</sup> <sup>1</sup>H NMR (400 MHz, CDCl<sub>3</sub>): δ 5.80 (ddt, 1 H,  $J = 16.9, 10.2, 6.7$  Hz, CH=CH<sub>2</sub>), 5.34 (dd, 1 H,  $J = 10.0, 3.4$  Hz, H-3), 5.26 (t, 1 H,  $J = 10.0$  Hz, H-4), 5.22 (dd, 1 H,  $J = 3.2, 1.6$  Hz, H-2), 4.98 (dd, 1 H,  $J = 17.1, 1.5$  Hz, CH=CH<sub>2</sub>), 4.92 (d, 1 H,  $J = 10.2$  Hz, CH=CH<sub>2</sub>), 4.79 (bs, 1 H, H-1), 4.27 (dd, 1 H,  $J = 12.2, 5.3$  Hz, H-6a), 4.09 (dd, 1 H,  $J = 12.2, 2.2$  Hz, H-6b), 3.97 (ddd, 1 H,  $J = 9.5, 5.2, 2.2$  Hz, H-5), 3.66 (dt, 1 H,  $J = 9.4, 6.8$  Hz, OCH<sub>2</sub>), 3.43 (dt, 1 H,  $J = 9.5, 6.6$  Hz, OCH<sub>2</sub>), 2.14 (s, 3 H, CH<sub>3</sub>CO), 2.09 (s, 3 H, CH<sub>3</sub>CO), 2.04 – 2.00 (m, 1 H, –CH<sub>2</sub>–CH=CH<sub>2</sub>) 2.03 (s, 3 H, CH<sub>3</sub>CO), 1.98 (s, 3 H, CH<sub>3</sub>CO), 1.59–1.56 (m, 2 H, OCH<sub>2</sub>CH<sub>2</sub>), 1.41 – 1.23 (m, 11 H, –(CH<sub>2</sub>)<sub>5</sub>–CH<sub>2</sub>–CH=CH<sub>2</sub>). <sup>13</sup>C NMR (101 MHz, CDCl<sub>3</sub>): δ 170.79, 170.24, 170.03, 169.89 (4 C=O), 139.28 (CH=CH<sub>2</sub>), 114.27 (CH=CH<sub>2</sub>), 97.69 (C-1), 69.87, 69.28, 68.50 (C-2, C-3, C-4), 68.68 (OCH<sub>2</sub>), 66.41 (C-5), 62.66 (C-6), 33.88 (CH<sub>2</sub>=CH–CH<sub>2</sub>–(CH<sub>2</sub>)<sub>7</sub>–O), 29.47, 29.41, 29.37, 29.16, 29.00, 26.17 (6 CH<sub>2</sub>), 21.03, 20.86, 20.82, 20.82 (4 CH<sub>3</sub>CO). ESI-MS:  $m/z$  [M+H]<sup>+</sup> calcd for C<sub>24</sub>H<sub>38</sub>O<sub>10</sub> 486.2465, observed monoisotopic  $m/z$  = 509.2368 (Na<sup>+</sup> adduct), 525.2108 (K<sup>+</sup> adduct). Anal. calcd for C<sub>24</sub>H<sub>38</sub>O<sub>10</sub> C, 59.24; H, 7.87; found C, 59.48; H, 7.85.

## 4.5 (GLYCO)DENDRIMERS CONVERGENT SYNTHESIS BY OLEFIN METATHESIS.

**4.5.1 General Methods.** All reagents were purchased from Sigma-Aldrich and used without any further purification. Reactions were monitored by thin-layer chromatography (TLC) on silica gel 60F<sub>254</sub> coated glass plates (Merck). The spots were visualized by charring with a concentrated H<sub>2</sub>SO<sub>4</sub>/EtOH/H<sub>2</sub>O solution (10/45/45 v/v/v) or with a solution of (NH<sub>4</sub>)<sub>6</sub>Mo<sub>7</sub>O<sub>24</sub> (21 g), Ce(SO<sub>4</sub>)<sub>2</sub> (1 g), concentrated H<sub>2</sub>SO<sub>4</sub> (31 mL) in water (500 mL) and then by heating to 110 °C for 5 min. Flash column chromatography was performed on silica gel 230 – 400 mesh (Merck). Routine <sup>1</sup>H and <sup>13</sup>C NMR spectra were recorded on a Varian Mercury instrument at 400 MHz (<sup>1</sup>H NMR) or 100.57 MHz (<sup>13</sup>C NMR). Chemical shifts are reported in parts per million downfield from TMS as an internal standard; *J* values are given in Hertz. Mass spectra were recorded on a QSTAR Elite instrument (AB Sciex) equipped with a nano-electrospray ion source. The samples were directly injected at RT by borosilicate capillaries (Thermo Scientific) employing a spray voltage of 1.1 kV and a declustering potential of 80 V.

**4.5.2 Dendrimer precursors synthesis (1, 5, 9).** To obtain several progressive family of dendrons, sequential condensation reactions were performed following modified literature procedures starting from 2,2,5-trimethyl-1,3-dioxane-5- carboxylic acid as a building block through sequential condensation steps (DCC, PPT 0.04 equiv., dry DCM 0.1 mol/L, RT)<sup>377</sup> and deprotection. Products were purified by flash chromatography column and obtained in 20%–40% yields using a mixture of petroleum ether and EtOAc as eluent.

**4.5.3 Boc-protected tetravalent dendrimer synthesis (2).** 425 mg of compound 1 (0.775 mmol), 22 mg of Hoveyda–Grubbs second generation catalyst (4% mol in respect to 1), were dissolved in anhydrous octafluorotoluene (0.1 mol/L). The solution was stirred at RT, in the dark, and under argon atmosphere. After 48 h, the solvent was evaporated under vacuum, and then, the crude product was purified by flash chromatography (petroleum ether/EtOAc, 6/4), affording compound 2 (152 mg, 37% yield). <sup>1</sup>H NMR (400 MHz, CDCl<sub>3</sub>) δ: 7.92 (bs, 4H, NH–O), 5.40 (bs, 2H, CH=CH), 4.43 (s, 8H, NH–O–CH<sub>2</sub>), 4.34 (ABq, *J* = 11.1 Hz, 8H, CO–CH<sub>2</sub>), 4.13 (t, *J* = 6.4 Hz, 4H, CO–CH<sub>2</sub>–CH<sub>2</sub>), 2.07–1.97 (bs, 4H, CH<sub>2</sub>–CH=), 1.74–1.64 (m, 4H, CH<sub>2</sub>–CH<sub>2</sub>–CH), 1.47 (s, 36H, CH<sub>3</sub>(Boc)), 1.27 (s, 6H, CH<sub>3</sub>). <sup>13</sup>C NMR (101 MHz, CDCl<sub>3</sub>) δ: 172.34 (2s, 2COO), 169.15 (4s, 4COO), 156.22 (4s, 4CONH), 129.52 (2d, 2CH=CH), 82.23 (4s, 4C(Boc)), 72.34 (4t, 4NH–O–CH<sub>2</sub>), 65.42 (4t, 4COOCH<sub>2</sub>C), 64.92 (2t, 2COOCH<sub>2</sub>CH<sub>2</sub>), 46.30 (2t, 2C(CH<sub>2</sub>OCO)<sub>2</sub>), 28.65 (2t, 2CH<sub>2</sub>–CH=), 28.33 (2t, 2CH<sub>2</sub>–CH<sub>2</sub>–CH=), 28.14 (12q, 12CH<sub>3</sub>(Boc)), 17.93 (2q,

2CH<sub>3</sub>). NanoESI-MS: C<sub>46</sub>H<sub>76</sub>O<sub>24</sub>N<sub>4</sub> calcd mass 1068.48, observed  $m/z = 1069.10$  (H<sup>+</sup> adduct) and  $m/z = 1091.10$  (Na<sup>+</sup> adduct), experimental mass 1068.00.

**4.5.4 Deprotected tetravalent dendrimer synthesis (3).** A solution of 2 (108 mg, 0.101 mmol) in anhydrous dichloromethane (DCM, 0.1 mol/L) was cooled to 0 °C; then, trifluoroacetic acid (TFA) was added dropwise and stirred for 2 h. The reaction was quenched with saturated aq. Na<sub>2</sub>CO<sub>3</sub> to neutrality, extracted twice with DCM, and the organic layers were collected and dried over anhydrous Na<sub>2</sub>SO<sub>4</sub>. The solvent was evaporated affording product 3 quantitatively (66 mg). The product was used for the subsequent reaction without any further purification. <sup>1</sup>H NMR (400 MHz, CDCl<sub>3</sub>) δ: 5.81 (bs, 8H, NH<sub>2</sub>-O), 5.39 (bs, 2H, CH=CH), 4.33 (ABq, *J* = 11.1 Hz, 8H, CO-CH<sub>2</sub>), 4.22 (s, 8H, NH-O-CH<sub>2</sub>), 4.11 (t, *J* = 6.5 Hz, 4H, CO-CH<sub>2</sub>-CH<sub>2</sub>), 2.11–1.98 (bs, 4H, CH<sub>2</sub>-C =), 1.75–1.58 (m, 4H, CH<sub>2</sub>-CH<sub>2</sub>-CH), 1.24 (s, 6H, CH<sub>3</sub>). <sup>13</sup>C NMR (101 MHz, CDCl<sub>3</sub>) δ: 172.46 (2s, 2COO), 170.30 (4s, 4COO), 129.79 (2d, 2CH=CH), 72.27 (4t, 4NH-O-CH<sub>2</sub>), 65.45 (4t, 4COOCH<sub>2</sub>C), 64.77 (2t, 2COOCH<sub>2</sub>CH<sub>2</sub>), 46.31 (2s, 2C(CH<sub>2</sub>OCO)<sub>2</sub>), 28.65 (2t, 2CH<sub>2</sub>-CH=), 28.17 (2t, 2CH<sub>2</sub>-CH<sub>2</sub>-CH=), 17.88 (2q, 2CH<sub>3</sub>). NanoESI-MS: C<sub>26</sub>H<sub>44</sub>O<sub>16</sub>N<sub>4</sub> calcd mass 668.27, observed  $m/z = 669.00$  (H<sup>+</sup> adduct), experimental mass 668.00.

**4.5.5 Tetravalent glycosylated dendrimer synthesis (4).** To obtain multifunctional glycosylated dendrimer 4, 25 mg of compound 3 (0.037 mmol) were dissolved in 2.5 mL acetate buffer (pH 4.5), and then, maltose (101 mg, 0.296 mmol) and aniline (41 mg, 0.444 mmol) were added. After 72 h, the product was recovered by washing with a small amount of DCM. The aqueous phase was concentrated to dryness and the crude product purified by flash chromatography (gradient eluent from 100% EtOH to EtOH/H<sub>2</sub>O 9/1), affording compound 4 (22 mg, 30% yield). <sup>1</sup>H NMR (400 MHz, D<sub>2</sub>O) δ: 7.48 (d, *J* = 6.0 Hz, 3H, CH=N), 7.42 (d, *J* = 6.3 Hz, 1H, CH=N), 5.31 (bs, 2H, CH=CH), 2.11–1.98 (bs, 4H, CH<sub>2</sub>-CH). NanoESI-MS: C<sub>74</sub>H<sub>124</sub>O<sub>56</sub>N<sub>4</sub> calcd mass 1964.70, observed  $m/z = 1005.35$  (2Na<sup>+</sup> adduct), experimental mass 1964.70

**4.5.6 Boc-protected octavalent dendrimer synthesis (6).** A solution of compound 5 (834 mg, 0.740 mmol) and 18 mg Hoveyda-Grubbs second generation catalyst (4% in mol in respect to 5) was prepared in anhydrous octafluorotoluene (0.2 mol/L) and reacted as described for compound 2. After 24 h, the solvent was evaporated by rotary evaporator, and the crude product was purified by flash chromatography (petroleum ether/EtOAc 5/5), affording pure product 6 (143 mg, 30% yield calculated on reacted 5) and 350 mg of unreacted 5. <sup>1</sup>H NMR (400 MHz,

CDCl<sub>3</sub>)  $\delta$ : 8.02 (bs, 8H, NH–O), 5.42 (bs, 2H, CH=CH), 4.44 (s, 16H, NH–O–CH<sub>2</sub>), 4.35–4.23 (ABq,  $J$  = 11.2 Hz, 24H, CO–CH<sub>2</sub>), 4.10 (t,  $J$  = 6.4 Hz, 4H, CO–CH<sub>2</sub>–CH<sub>2</sub>), 2.11–2.00 (bs, 4H, CH<sub>2</sub>–CH=), 1.69 (bs, 4H, CH<sub>2</sub>–CH<sub>2</sub>–CH), 1.47 (s, 72H, CH<sub>3</sub>(Boc)), 1.24 (s, 18H, CH<sub>3</sub>). <sup>13</sup>C NMR (101 MHz, CDCl<sub>3</sub>)  $\delta$ : 171.67 (2s, 2COO), 169.16 (4s, 4COO), 161.63 (8s, 8COO), 156.31 (8s, 8CONH), 129.78 (2d, 2CH=CH), 82.17 (8s, 8C(Boc)), 72.34 (8t, 8NH–O–CH<sub>2</sub>), 65.60, (4t, 4COOCH<sub>2</sub>C), 65.25 (8t, 8CO–CH<sub>2</sub>), 65.06 (2t, 2COOCH<sub>2</sub>CH<sub>2</sub>), 46.51 (2s, 2C(CH<sub>2</sub>OCO)<sub>2</sub>), 46.43 (4s, 4C(CH<sub>2</sub>OCO)<sub>2</sub>), 28.67 (2t, 2CH<sub>2</sub>–CH), 28.15 (24q, 24CH<sub>3</sub>(Boc)), 27.92 (2t, 2CH<sub>2</sub>–CH<sub>2</sub>–CH), 17.84 (6q, 6CH<sub>3</sub>). NanoESI–MS: C<sub>94</sub>H<sub>152</sub>O<sub>52</sub>N<sub>8</sub> calcd mass 2224.95, observed  $m/z$  = 2247.30 (Na<sup>+</sup> adduct), experimental mass 2224.27.

**4.5.7 Deprotected octavalent dendrimer synthesis (7).** A solution of 6 (210 mg, 0.094 mmol) in dry DCM (0.1 mol/L) was cooled to 0 °C and then TFA was added dropwise and stirred for 2 h at 0 °C. The reaction was quenched with saturated aq. Na<sub>2</sub>CO<sub>3</sub> to neutrality, the crude product was extracted twice with DCM, and the organic layers were dried over anhydrous Na<sub>2</sub>SO<sub>4</sub>. The solvent was evaporated to give compound 7 (114 mg, 85% yield) that was used for the subsequent reaction without any further purification. <sup>1</sup>H NMR (400 MHz, CDCl<sub>3</sub>)  $\delta$ : 6.22–5.50 (bs, 16H, NH<sub>2</sub>–O), 5.42 (bs, 2H, CH=CH), 4.35–4.23 (bs, 32H, NH–O–CH<sub>2</sub>, CO–CH<sub>2</sub>), 4.17 (8H, CO–CH<sub>2</sub>), 4.11 (t,  $J$  = 6.5 Hz, 4H, CO–CH<sub>2</sub>–CH<sub>2</sub>), 2.14–1.98 (bs, 4H, CH<sub>2</sub>–CH), 1.75–1.64 (bs, 4H, CH<sub>2</sub>–CH<sub>2</sub>–CH), 1.25 (s, 18H, CH<sub>3</sub>). <sup>13</sup>C NMR (101 MHz, CDCl<sub>3</sub>)  $\delta$ : 172.10 (2s, 2COO), 171.84 (4s, 4COO), 170.31 (8s, 8COO), 129.78 (2d, 2CH=CH), 72.25 (8t, 8CO–CH<sub>2</sub>), 65.65 (4t, 4CO–CH<sub>2</sub>), 65.34 (8t, 8NH–O–CH<sub>2</sub>), 64.97 (2t, 2 COCH<sub>2</sub>CH<sub>2</sub>), 46.54, 46.46 (6s, 6C(CH<sub>3</sub>)<sub>3</sub>), 28.51 (2t, 2t, 2CH<sub>2</sub>–CH=), 28.22 (2t, 2CH<sub>2</sub>–CH<sub>2</sub>–CH=), 17.79 (6q, 6CH<sub>3</sub>). NanoESI–MS: C<sub>54</sub>H<sub>88</sub>O<sub>36</sub>N<sub>8</sub> calcd mass 1424.53, observed  $m/z$  = 713.50 (2H<sup>+</sup> adduct), experimental mass 1425.00.

**4.5.8 Octavalent glycosylated dendrimer synthesis (8).** First, 81 mg of compound 7 (0.057 mmol) were dissolved in 2.5 mL acetate buffer (pH = 4.5); subsequently, 312 mg of maltose and 126 mg aniline (0.912 mmol and 1.36 mmol, respectively) were added and the mixture was allowed to stir. After 72 h, the reaction was stopped and washed twice with DCM. Finally, crude product was purified through flash chromatography (EtOH + 0.2% AcOH), affording compound 8 (13 mg, 6% yield). <sup>1</sup>H NMR (400 MHz, D<sub>2</sub>O)  $\delta$ : 7.47 (d,  $J$  = 6.1 Hz, 5H, CH=N), 7.41 (d,  $J$  = 6.6 Hz, 1H, CH=N), 5.31 (bs, 2H, CH=CH), 2.11–1.98 (bs, 4H, CH<sub>2</sub>–CH). NanoESI–MS: C<sub>150</sub>H<sub>248</sub>O<sub>116</sub>N<sub>8</sub> calcd mass 4017.37, observed  $m/z$  = 1832.50 (adduct, minus one aminoxyacetic moiety,

$C_{14}H_{24}O_{12}N$ ),  $m/z = 1634.00$  ( $2Na^+$  adduct, minus two aminoxyacetic moieties) and  $m/z = 1435.50$  ( $2Na^+$  adduct, minus three aminoxyacetic moieties), experimental mass 4017.13.

**4.5.9 Boc-protected hexadeca dendrimer synthesis (10).** Compound 9 (110 mg, 0.048 mmol) and 2 mg (7% mol in respect to 9) Hoveyda–Grubbs second generation dissolved in anhydrous octafluorotoluene (0.2 mol/L) were reacted as described for compound 2. After 72 h, the solvent was evaporated under vacuum, and then, the crude product was purified by flash chromatography (petroleum ether/EtOAc 4/6) to afford pure 10 (34 mg, 31% yield).  $^1H$  NMR (400 MHz,  $CDCl_3$ )  $\delta$ : 8.10 (s, 16H, NH–O), 5.44 (bs, 1H, CH=CH), 5.12 (bs, 1H, CH=CH), 4.45 (s, 32H, NH–O–CH<sub>2</sub>), 4.31–4.20 (ABq,  $J = 11.6$  Hz, 56H, CO–CH<sub>2</sub>), 4.11 (t,  $J = 6.6$  Hz, 4H, CO–CH<sub>2</sub>–CH<sub>2</sub>), 2.02 (bs, 4H, CH<sub>2</sub>–CH), 1.66 (bs, 4H, CH<sub>2</sub>–CH<sub>2</sub>–CH), 1.47 (s, 144H, CH<sub>3</sub>(Boc)), 1.26 (bs, 42H, CH<sub>3</sub>).  $^{13}C$  NMR (101 MHz,  $CDCl_3$ )  $\delta$ : 173.54 (2s, 2COO), 171.69 (4s, 4COO), 171.43 (8s, 8COO), 169.22 (16s, 16COO), 156.40, (16s, 16CONH), 82.11 (16s, 16C(Boc)), 72.34 (16t, 16NH–O–CH<sub>2</sub>), 65.84, (16t, 16CO–CH<sub>2</sub>), 65.26 (12t, 12CO–CH<sub>2</sub>), 65.06 (2t, 2COOCH<sub>2</sub>CH<sub>2</sub>) 46.64, 46.43(14s, 14C(CH<sub>2</sub>OCO)<sub>2</sub>), 34.01 (2CH<sub>2</sub>–CH), 31.83 (2t, 2CH<sub>2</sub>–CH<sub>2</sub>–CH), 28.16 (48q, 48CH<sub>3</sub>(Boc)), 17.79 (14q, 14CH<sub>3</sub>). NanoESI–MS:  $C_{190}H_{304}O_{108}N_{16}$  calcd mass 4537.88, observed  $m/z = 2291.90$  ( $2Na^+$  adduct), experimental mass 4537.80.

## 5. CONCLUDING REMARKS.

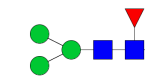
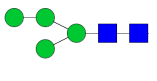
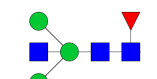
The research reported in this thesis stemmed from a main theme, which is neuroglycobiology, and evolved towards several related topics. A novel, reliable, versatile, and efficient method for the analysis of *N*-glycans from brain tissue is reported (Section 3.1). This project will deliver to the glycoanalyst community a thoroughly tested, efficiently performing and versatile tool to investigate *N*-glycan patterns on brain and other solid tissues, in a research field in which methodological innovation and validation are essential premises towards solid biological studies (Sections 3.1.1 and 1.3.7). The newly developed method, along with its thorough methodological validation and accurate comparison to similar workflows published in the literature (Tab. 3.1.1), is the topic of an original research paper currently under submission to a high impact scientific journal.<sup>378</sup> Stemming from the analysis of brain *N*-glycans, the reverse glycoproteomics project (Section 3.2) is an ongoing work in which *N*-glycoproteins carrying neurologically interesting *N*-glycans are investigated. Brain evolutionary and biomedically suitable biomarkers are necessary to deepen the scientific community knowledge about human's most complex organ and, since *N*-glycans are fairly present in mammalian brains (Section 1.2), the investigation of glycobiomarkers represents a promising area of biomedical research. In this context this thesis reports encouraging methodological advancements, delivering an optimised method for the analysis of brain *N*-glycans and *N*-glycoproteins from the same sample, capable of identifying proteins, *N*-glycoproteins and *N*-glycosylation sites from solid tissues and, although basically still at the level of methodological development, already being capable to provide some putative candidates for the *N*-glycoprotein targets (Section 3.2.5). Moving from the big picture (omics) towards more specific targets, human Neuroserpin, a brain *N*-glycoprotein involved in neurodegeneration, has been efficiently investigated towards the elucidation of the molecular determinants of its polymerisation behaviour (Section 3.3). A suitable chemical tool for the project has been developed, analytically tested, and shown to be able to provide the type of information for which it was created, in an efficient and precise way (Fig. 3.3.6), therefore being applicable to answer interesting biological questions. The work has amassed a solid pool of chemical, analytical and biological data and is currently under refinement towards the preparation of a scientific publication. Finally, the syntheses of glycotools (i.e., sections 3.4 and 3.5) towards neurochemistry studies, has afforded six novel chemical structures, published within two original research papers, valuable in a wide array of medicinal neurochemistry applications. The whole body of products delivered within this thesis will benefit the glycochemistry community, especially in the field of neurochemistry, by adding new pieces of knowledge about CNS components, and by delivering novel methods and molecules to carry on

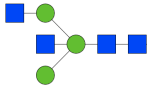
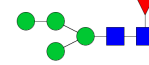
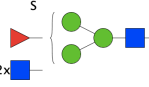
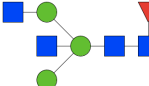
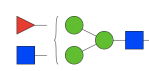

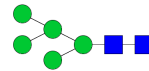
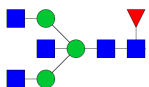


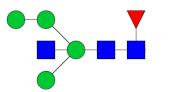


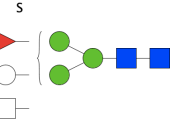
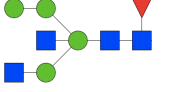
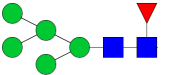
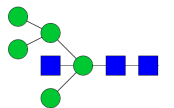
the investigation of glycans-related effects in neurological and neuromedical context. By the point of view of the author, the skills acquired during the PhD, spanning from chemical synthesis, protein biochemistry and bioanalytical techniques, have provided substantial professional development and precious skills specialisation in the field of *N*-glycomics and (*N*-glyco)proteomics, and will certainly be of great benefit in future working opportunities and career developments.

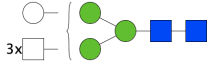
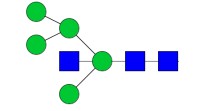
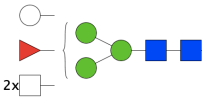
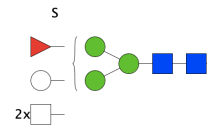
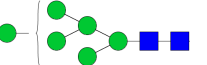
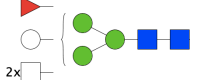
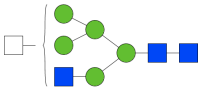
## 6. APPENDIX.

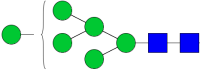
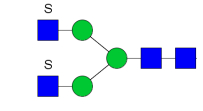
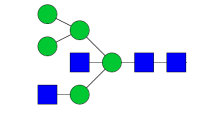
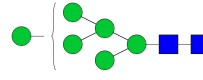
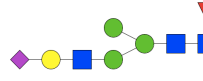
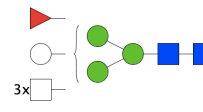

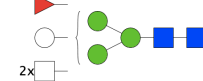
**6.1 MS analysis of samples prepared by LSD and HSD (Table A-1).** Structures are listed in order of decreasing abundance. CF = Chromatographic Fraction; GS = Glycan Structure (Green = good confidence; Yellow = reasonable; Red = low confidence); MMM = Measured Monoisotopic Mass,  $[M+2AB+H]^+$  (Red= LSD only; White = both methods); MUM = Measured Unlabeled Monoisotopic Glycan Mass; TUM = Theoretical Unlabeled Monoisotopic Glycan Mass; TLM = Theoretical Labeled Monoisotopic Mass  $[M+2AB+H]^+$ ; RMA = Relative Mass Accuracy ( $(|MMM-TLM|/TLM)*10\%$ ); MC = Monosaccharide Composition; MS<sup>2</sup> = Fragmentation data (Y = Informative or partially informative fragments; N = No fragments); DFI = Diagnostic Fragments Identified (Red = fragmentation spectra found only in the LSD sample; Blue = fragmentation spectra found only in the HSD sample; White = fragmentation spectra found in both LSD and HSD samples; H = Hexose, N = N-Acetylhexosamine, F = Deoxyhexose (Fucose), S = N-Acetylneuraminic Acid (Sialic acid), Su = Sulphate, P = Phosphate; Int = Intact, precursor ion chosen for fragmentation and relative charge state, if not singly charged. In the case of singly charged ions, the intact signal equals the MMM value. All the listed fragments are mono-protonated, singly charged fragments); CF = Core Fucose, AF = Antennary Fucose, Bis = Bisecting, Hyb/HM = Hybrid/High Mannose, 2AB = 2-Aminobenzamide); PGS = Proposed Glycan Structure (N-glycan structures are depicted without 2-AB).

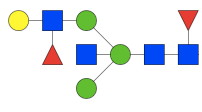
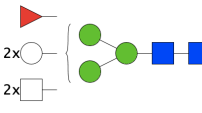
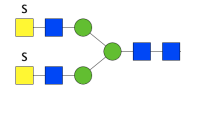
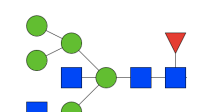
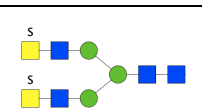
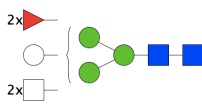
CF	GS	MMM (u)	TUM (u)	MFM (u)	TLM (u)	RMA (ppm)	MC	MS <sup>2</sup>	DFI	PGS
1		1177.4552	1056.3857	1056.3786	1177.4622	6.0	H3N2F1	Y	1177 (Int); 1031 (-F); 1015 (-H); 869 (-F -H); 853 (-2H); 707 (-F -2H); 545 (2N2AB); 528 (2HN); 488 (NF2AB, CF); 366 (HN); 342 (N2AB); 325 (2H)	
2		1193.4505	1072.3806	1072.3739	1193.4571	5.6	H4N2	Y	1193 (Int); 1031 (-H); 869 (-2H); 852 (-N2AB); 707 (-3H); 545 (-4H); 528 (2HN); 366 (HN); 342 (N2AB); 325 (2H)	
3	A	1380.5321	1259.4651	1259.4555	1380.5416	6.9	H3N3F1	Y	1380 (Int); 1234 (-F); 1218 (-H); 1177 (-N, CF); 1072 (-F -H); 1031 (-FN); 1015 (-H -N); 910 (H3N2AB, Bis); 853 (-2H -N); 569 (2NH/Bis?); 488 (NF2AB, CF); 366 (HN); 342 (N2AB); 325 (2H)	

	B	1437.5527	1316.4866	1316.4761	1437.5631	7.3	H3N4	Y	1437 (Int); 1234 (-N); 1096 (-N2AB); 1072 (-H - N); 1031 (-2N); 910 (H3N2AB, Bis); 893 (3H2N); 869 (-2N -H); 707 (-2N -2H); 569 (2NH/Bis?); 545 (2N2AB); 528 (2HN); 366 (HN); 342 (N2AB); 325 (2H)	
4	A	1339.5072	1218.4385	1218.4306	1339.5150	5.8	H4N2F1	Y	1339 (Int); 1193 (-F); 1177 (-H, CF); 1031 (-F -H); 1031 (-HF); 1015 (-2H); 869 (-2H -F); 707 (-3H -F); 488 (NF2AB, CF); 545 (2N2AB); 528 (2HN); 366 (HN); 342 (N2AB); 325 (2H)	
	B	1663.5633	1542.5013	1542.4867	1663.5778	8.7	H3N4F1Su1	N		
5	A	1583.6068	1462.5445	1462.53023	1583.6210	9.0	H3N4F1	Y	1583 (Int); 1437 (-F); 1380 (-N); 1234 (-N -F); 1218 (-N -H); 1177 (-2N, CF); 1056 (-N -2H, Bis + CF); 1072 (-N -H -F); 1015 (-2N -H); 910 (H3N2AB, Bis); 853 (-2N -2H); 707 (-2N -2H -F); 691 (-2N -3H, CF); 569 (2NH/Bis?); 488 (NF2AB, CF); 545 (2N2AB); 528 (2HN); 366 (HN); 342 (N2AB); 325 (2H)	
	B	1380.5311	1259.4651	1259.45453	1380.5416	7.6	H3N3F1	N		
6		1583.608	1462.5445	1462.53143	1583.6210	8.2	H3N4F1	N		
7		1355.5002	1234.4334	1234.42363	1355.5099	7.2	H5N2	Y	1355 (Int); 1193 (-H); 1014 (-N2AB); 869 (-3H); 707 (-4H); 545 (2N2AB); 528 (2HN); 487 (3H, Hyb/HM); 366 (HN); 342 (N2AB); 325 (2H)	
8	A	1786.683	1665.6239	1665.60643	1786.7004	9.8	H3N5F1	Y	1786 (Int); 1640 (-F); 1583 (-N); 1437 (-F -N); 1380 (-2N); 1234 (-F -2N); 1218 (-2H); 1177 (-3N, CF); 1056 (-2N -2H, Bis + CF); 1031 (-3N -F); 1015 (-3N -H); 910 (H3N2AB, Bis); 853 (-3N -2H); 707 (-3N -2H -F); 691 (2NF2AB, CF); 488 (NF2AB, CF); 569 (2NH/Bis?); 545 (2N2AB); 366 (HN); 342 (N2AB); 325 (2H)	

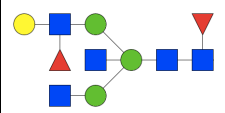
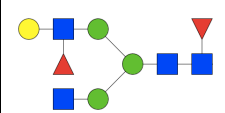
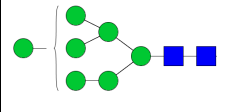
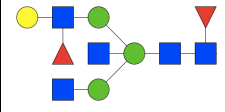
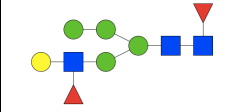
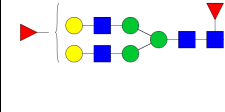
9	B	1542.5827	1421.5179	1421.50613	1542.5944	7.6	H4N3F1	Y	1542 (Int); 1396 (-F); 1380 (-H); 1177 (-H -N, CF); 1031 (-HNF) 910 (H3N2AB, Bis); 707 (-3HNF); 691 (2NF2AB, CF); 488 (NF2AB, CF); 569 (2NH/Bis?); 545 (2N2AB); 528 (2HN); 366 (HN); 342 (N2AB); 325 (2H)	
	C	1583.6048	1462.5445	1462.52823	1583.6210	10.2	H3N4F1	N		
		1786.6936	1665.6239	1665.61703	1786.7004	3.8	H3N5F1	N		
		1825.6286	1704.5541	1704.55203	1825.6306	1.1	H4N4F1Su1	N		
11	A	1745.6601	1624.5973	1624.58353	1745.6738	7.9	H4N4F1	Y	1745 (Int); 1599 (-F); 1583 (-H); 1437 (-H -F); 1380 (-H -N); 1234 (-H -N -F); 1218 (-2H -N); 1177 (-2NH, CF); 1072 (-2H -N -F); 910 (-3H -N -F, Bis); 691 (2NF2AB, CF); 488 (NF2AB, CF); 569 (2NH/Bis?); 545 (2N2AB); 528 (2HN); 366 (HN); 342 (N2AB); 325 (2H)	
	B	1501.559	1380.4913	1380.48243	1501.5678	5.9	H5N2F1	Y	1501 (Int); 1355 (-F); 1339 (-H); 1117 (-2H); 1193 (-H -F); 1031 (-2H -F); 1014 (-2N2AB); 707 (2NH); 488 (NF2AB, CF); 545 (2N2AB); 528 (2HN); 366 (HN); 342 (N2AB); 325 (2H)	
	C	1558.5847	1437.5128	1437.50813	1558.5893	3.0	H5N3	Y	1558 (Int); 1396 (-H); 1234 (-2H); 1217 (-N2AB); 1072 (-3H); 1031 (-2HN); 1014 (-2N2AB); 852 (-H, -2N2AB); 910 (H3N2AB, Bis); 707 (-4HN); 569 (2NH/Bis?); 545 (2N2AB); 528 (2HN); 366 (HN); 342 (N2AB)	

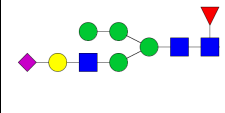
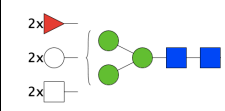
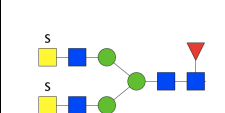

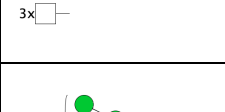

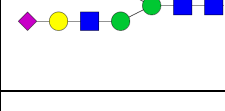
12	D	1802.6876	1681.6188	1681.61103	1802.6953	4.3	H4N5	N		
	A	1558.5801	1437.5128	1437.50353	1558.5893	5.9	H5N3	Y	1558 (Int); 1396 (-H); 1234 (-2H); 1217 (-N2AB); 1072 (-3H); 1031 (-2HN); 1014 (-2N2AB); 852 (-H, -2N2AB); 910 (H3N2AB, Bis); 707 (-4HN); 569 (2NH/Bis?); 545 (2N2AB); 528 (2HN); 366 (HN); 342 (N2AB); 325 (2H)	
	B	1745.6623	1624.5973	1624.58573	1745.6738	6.6	H4N4F1	N		
13	C	1825.6271	1704.5541	1704.55053	1825.6306	1.9	H4N4F1Su1	N		
	A	1517.5512	1396.4862	1396.47463	1517.5627	7.6	H6N2	Y	1517 (Int); 1355 (-H); 1176 (-N2AB); 1193 (-2H); 1031(-3H); 869 (-4H); 545 (2N2AB); 811 (5H, Hyb/HM); 545 (2N2AB); 528 (2HN); 487 (3H, Hyb/HM); 366 (HN); 342 (N2AB); 325 (2H)	
	B	1745.6639	1624.5973	1624.58733	1745.6738	5.7	H4N4F1	N		
	C	1761.6573	1640.5922	1640.58073	1761.6687	6.5	H5N4	Y	1761 (Int); 1599 (-H); 1558 (-N); 1437 (-2H); 1420 (-N2AB); 1396 (-H -N); 1217 (-2N2AB); 1072 (-3H -N); 707 (-4H -2N); 569 (2NH/Bis?); 545 (2N2AB); 528 (2HN); 487 (3H, Hyb/HM); 342 (N2AB); 366 (NH); 325 (2H)	

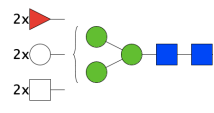
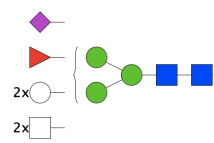
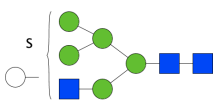
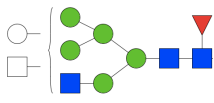
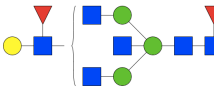
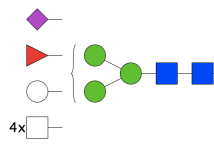
14	A	1517.551	1396.4862	1396.47443	1517.5627	7.7	H6N2	Y	1517 (Int); 1355 (-H); 1176 (-N2AB); 1193 (-2H); 1031 (-3H); 869 (-4H); 545 (2N2AB); 811 (5H, Hyb/HM); 545 (2N2AB); 528 (2HN); 487 (3H, Hyb/HM); 366 (HN); 342 (N2AB); 325 (2H)	
	B	1597.4912	1476.4002	1476.41463	1597.4767	9.1	H3N4Su2	Y	1597 (Int); 1152 (-NSuH); 366 (HN)	
15	A	1761.6548	1640.5922	1640.57823	1761.6687	7.9	H5N4	Y	1761 (Int); 1599 (-H); 1558 (-N); 1437 (-2H); 1420 (-N2AB); 1396 (-H -N); 1275 (-3H); 1217 (-2N2AB); 1072 (-3H -N); 910 (H3N2AB, Bis); 707 (-4H -2N); 569 (2NH/Bis?); 545 (2N2AB); 528 (2HN); 487 (3H, Hyb/HM); 342 (N2AB); 366 (NH); 325 (2H)	
	B	1517.5514	1396.4862	1396.47483	1517.5627	7.5	H6N2	N		
16	A	1833.677	1712.6133	1712.6004	1833.6898	7.0	H4N3F1S1	Y	1833 (Int); 1687 (-F); 1671 (-H); 1542 (-S); 1525 (-FS); 1380 (-SH); 1346 (-NF2AB); 1234 (-SHF); 1177 (-SHN, CF); 1031 (-SHNF); 657 (SHN); 488 (NF2AB, CF); 454 (SH); 366 (HN); 342 (N2AB); 325 (2H)	
	B	1948.7375	1827.6767	1827.6609	1948.7532	8.1	H4N5F1	N		
	C	1761.6727	1640.5922	1640.5961	1761.6687	2.3	H5N4	N		
	D	1745.675	1624.5973	1624.5984	1745.6738	0.7	H4N4F1	N		

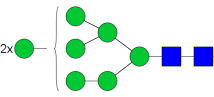
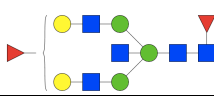
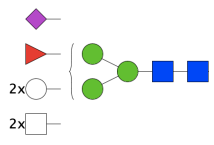
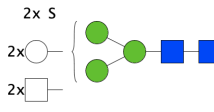
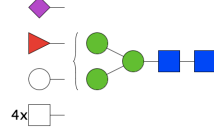
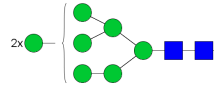
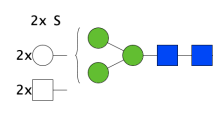
17	A	1891.7153	1770.6552	1770.6387	1891.7317	8.7	H4N4F2	Y	1891 (Int); 1745 (-F); 1729 (-H); 1599 (-2F); 1583 (-H -F); 1437 (-H -2F); 1404 (-N2AB); 1380 (-H -N -F); 1234 (-H -N - 2F); 1201 (-2N2AB); 1177 (-2NHF, CF); 1072 (-2H -N -2F); 1056 (-HNF, Bis + CF); 910 (H3N2AB, Bis); 707 (-4H -N - 2F); 691 (2NF2AB, CF); 569 (2NH/Bis?); 545 (2N2AB); 528 (2HN); 512 (HNF, AF); 488 (NF2AB, CF); 342 (N2AB); 366 (NH); 325 (2H)	
	B	1907.7127	1786.6501	1786.6361	1907.7266	7.3	H5N4F1	N		
	C	2003.617	1882.5590	1882.5404	2003.6355	9.2	H3N6Su2	N		
18	A	1907.7116	1786.6501	1786.6350	1907.7266	7.9	H5N4F1	Y	1907 (Int); 1761 (-F); 1745 (-H); 1704 (-N); 1599 (-H -F); 1583 (-2H); 1501 (-2N); 1437 (-2H -F); 1420 (-N2AB); 1339 (-2NH); 1234 (-2H -F -N); 1217 (-2N2AB); 1177 (-2H2N, CF); 1031 (-2N2HF); 1015 (-2N3H); 910 (3NH2AB, Bis); 852 (-H -2N - N2AB -F); 691 (2NF2AB, CF); 569 (2NH/Bis?); 545 (2N2AB); 528 (2HN); 488 (NF2AB, CF); 342 (N2AB); 366 (NH); 325 (2H)	
	B	2003.6247	1882.5590	1882.5481	2003.6355	5.4	H3N6Su2	N		
	C	1891.7162	1770.6552	1770.6396	1891.7317	8.2	H4N4F2	N		

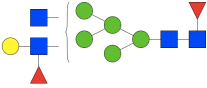
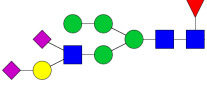
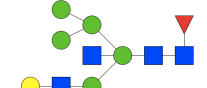
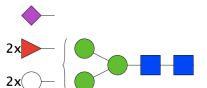
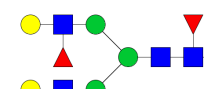
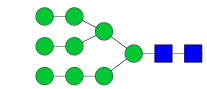


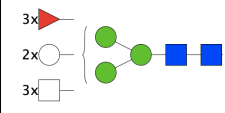
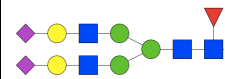
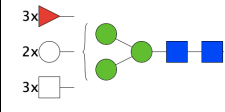
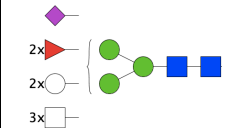
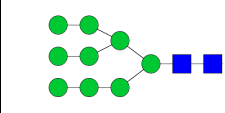
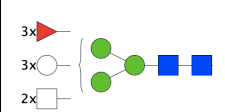
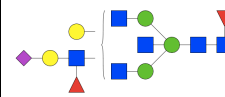
19	A	2094.8139	1973.7346	1973.73733	2094.8111	1.3	H4N5F2	Y	2094 (Int); 1948 (-F); 1932 (-H); 1891 (-N); 1802 (-2F); 1786 (-H -F); 1607 (-N2AB); 1583 (-H -F -N); 1437 (-H -2F -N); 1404 (-2N2AB); 1380 (-H -F -2N); 1218 (-2H -F -2N); 1177 (-3NHF, CF); 1056 (3H -F -2N, Bis + CF); 910 (H3N2AB, Bis); 853 (-3H -2F -3N); 691 (2NF2AB, CF); 569 (2NH/Bis?); 545 (2N2AB); 528 (2HN); 512 (HNF, AF); 488 (NF2AB, CF); 366 (NH); 342 (N2AB)	
	B	1891.7159	1770.6552	1770.63933	1891.7317	8.4	H4N4F2	Y	1891 (Int); 1745 (-F); 1729 (-H); 1599 (-2F); 1583 (-H -F); 1437 (-H -2F); 1404 (-N2AB); 1380 (-H -N - F); 1234 (-H -N - 2F); 1218 (-2HNF); 1201 (-2N2AB); 1177 (-2NHF, CF); 1072 (-H -N -2F); 707 (-4H -N - 2F); 569 (2NH/Bis?); 545 (2N2AB); 528 (2HN); 512 (HNF, AF); 488 (NF2AB, CF); 342 (N2AB)	
20	A	1679.6038	1558.5390	1558.52723	1679.6155	7.0	H7N2	Y	1679 (Int); 1517 (-H); 1355 (-2H); 1338 (-N2AB); 1193 (-3H); 1176 (-H, -N2AB); 811 (5H, Hyb/HM); 649 (4H, Hyb/HM); 545 (2N2AB); 528 (2HN); 487 (3H, Hyb/HM); 366 (NH); 342 (N2AB); 325 (2H)	
	B	2094.8131	1973.7346	1973.73653	2094.8111	0.9	H4N5F2	Y	2094 (Int); 1948 (-F); 1932 (-H); 1891(-N); 1802 (-2F); 1729 (-HN); 1607 (-N2AB); 1583 (-H -F -N); 1437 (-H -2F -N); 1404 (-2N2AB); 1380 (-H -F -2N); 1218 (-2H -F -2N); 1056 (-3H -F -2N, Bis + CF); 910 (H3N2AB, Bis); 691 (2NF2AB, CF); 569 (2NH/Bis?); 545 (2N2AB); 528 (2HN); 512 (HNF, AF); 488 (NF2AB, CF); 366 (NH); 342 (N2AB); 325 (2H)	
	C	1850.6895	1729.6286	1729.61293	1850.7051	8.4	H5N3F2	Y	1850 (Int); 1177 (3H2NF2AB, CF); 545 (2N2AB); 528 (2HN); 512 (HNF, AF); 488 (NF2AB, CF); 342 (N2AB)	
21	A	2053.7686	1932.7080	1932.6920	2053.7845	7.8	H5N4F2	Y	2053 (Int); 1907 (-F); 1891 (-H); 1762 (-2F); 1745 (-HF); 1729 (-2H); 1688 (-HN); 1566 (-N2AB); 1526 (-2HN); 1380 (-2H -N -F); 1234 (-2H -N -2F); 1363 (-2N2AB); 1177 (-2H -2N -F, CF); 853 (-3H -2N -F); 836 (3HNF); 691 (2NF2AB, CF); 674 (2HNF); 569 (2NH/Bis?); 545 (2N2AB); 528 (2HN); 512 (HNF, AF); 488 (NF2AB, CF); 366 (NH); 342 (N2AB)	

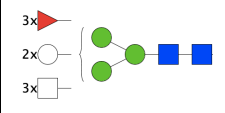
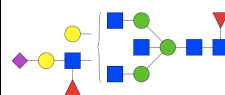
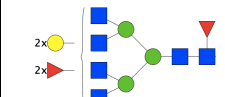
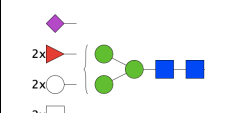
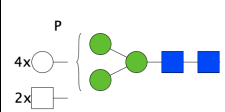
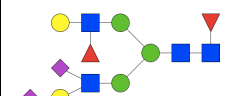
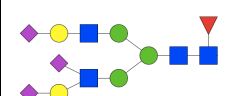
	B	1995.7349	1874.6661	1874.65833	1995.7426	3.9	H5N3F1S1	Y	1995 (Int); 1849 (-F); 1704 (-S); 1558 (-SF); 1542 (-SH); 1339 (-SHN); 1177 (-2HNS, CF); 657 (SHN); 545 (2N2AB); 528 (2HN); 488 (NF2AB, CF); 454 (HS); 366 (NH); 342 (N2AB); 325 (2H)	
	C	2094.8087	1973.7346	1973.73213	2094.8111	1.2	H4N5F2	N		
	D	2149.6845	2028.6169	2028.60793	2149.6934	4.2	H3N6F1Su2	N		
	E	2239.8511	2118.7721	2118.77453	2239.8486	1.1	H4N5F1S1	N		
	A	1597.5227	1476.4525	1476.44613	1597.5290	4.0	H6N2P1	Y	1597 (Int); 1435 (-H (P)); 1273 (-2H (P)); 1256 (-N2AB (P)); 1111 (-3H (P)); 567 (3H (P)); 545 (2N2AB); 528 (2HN); 405 (2H (P)); 366 (NH); 342 (N2AB); 325 (2H)	
22	B	1995.7349	1874.6661	1874.65832	1995.7426	3.9	H5N3F1S1	Y	1995 (Int); 1849 (-F); 1704 (-S); 1558 (-SF); 1542 (-SH); 1339 (-SHN); 1177 (-2HNS, CF); 657 (SHN); 545 (2N2AB); 528 (2HN); 488 (NF2AB, CF); 454 (HS); 366 (NH); 342 (N2AB); 325 (2H)	
	C	2239.8434	2118.7721	2118.76683	2239.8486	2.3	H4N5F1S1	Y	2239 (Int); 1948 (-S); 1786 (-SH); 1752 (-NF2AB); 1583 (-SHN); 1549 (-N2F2AB); 1380 (-SH2N); 1234 (-SHF2N); 910 (H3N2AB, Bis); 657 (SHN); 569 (2NH/Bis?); 545 (2N2AB); 528 (2HN); 488 (NF2AB, CF); 454 (SH); 366 (NH); 342 (N2AB)	

D	2053.7739	1932.7080	1932.69733	2053.7845	5.2	H5N4F2	N			
	E	2198.8124	2077.7455	2077.73583	2198.8220	4.4	H5N4F1S1	N		
	F	1800.5961	1679.5224	1679.51953	1800.5989	1.6	H6N3Su1	N		
23	2069.7724	1948.7029	1948.69583	2069.7794	3.4	H6N4F1	Y	<p>2069 (Int); 1379 (-2N2AB); 1217 (-H -2N2AB); 1014 (-H -N -2N2AB); 852 (-2H -N -2N2AB); 691 (2NF2AB, CF); 545 (2N2AB); 528 (2HN); 488 (NF2AB, CF); 366 (NH)</p>		
A	2297.8949	2176.8140	2176.81833	2297.8905	1.9	H4N6F2	Y	<p>1149.4514 (Int, 2+); 1056 (-3H -F -2N, Bis + CF); 910 (H3N2AB, Bis); 691 (2NF2AB, CF); 569 (2NH/Bis?); 545 (2N2AB); 528 (2HN); 512 (HNF, AF); 488 (NF2AB, CF); 366 (NH)</p>		
24	B	2442.9253	2321.8515	2321.84873	2442.9280	1.1	H4N6F1S1	N		

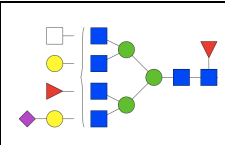
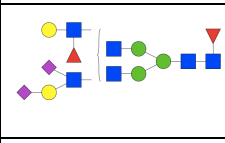
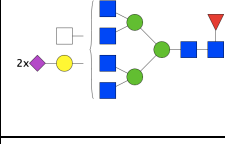
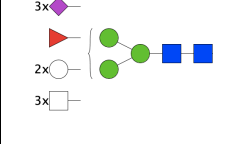
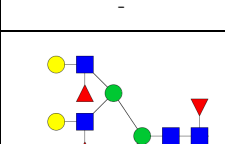
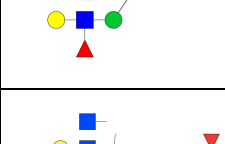
25	A	1841.6559	1720.5918	1720.57933	1841.6683	6.7	H8N2	Y	1841 (Int); 1679 (-H); 1517 (-2H); 1500 (-N2AB); 811 (5H, Hyb/HM); 649 (4H, Hyb/HM); 545 (2N2AB); 528 (2HN); 487 (3H, Hyb/HM), 366 (NH); 342 (N2AB); 325 (2H)	
	B	2256.8664	2135.7874	2135.78983	2256.8639	1.1	H5N5F2	Y	2256 (Int); 2110 (-F); 1769 (-NF2AB); 1745 (-HNF); 1583 (-2HNF); 1566 (-2NF2AB); 1380 (-2H2N2F); 691 (2NF2AB, CF); 569 (2NH/Bis?); 545 (2N2AB); 528 (2HN); 512 (HNF, AF); 488 (NF2AB, CF); 366 (NH); 342 (N2AB)	
	C	2198.8192	2077.7455	2077.74263	2198.8220	1.3	H5N4F1S1	N		
	D	1921.5991	1800.5058	1800.52253	1921.5823	8.7	H5N4Su2	N		
	E	2442.9277	2321.8515	2321.85113	2442.9280	0.1	H4N6F1S1	N		
26	A	1841.6555	1720.5918	1720.57893	1841.6683	7.0	H8N2	Y	1841 (Int); 1679 (-H); 1517 (-2H); 1500 (-N2AB); 1355 (-3H); 1193 (-4H); 1031 (-5H); 973 (6H, Hyb/HM); 869 (-6H); 811 (5H, Hyb/HM); 707 (-7H); 649 (4H, Hyb/HM); 545 (2N2AB); 528 (2HN); 487 (3H, Hyb/HM), 366 (NH); 342 (N2AB); 325 (2H)	
	B	1921.5991	1800.5058	1800.52253	1921.5823	8.7	H5N4Su2	N		

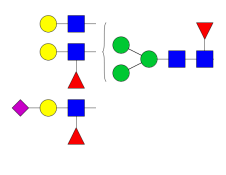
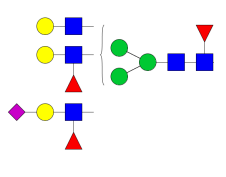
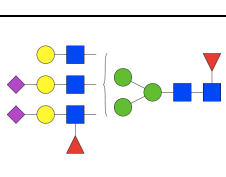
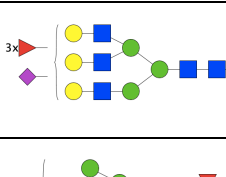
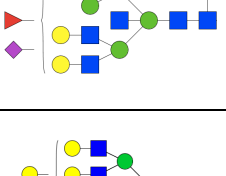
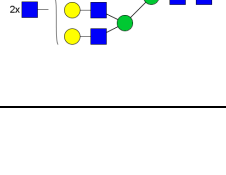
27	A	2215.83	2094.7608	2094.7534	2215.8373	3.3	H6N4F2	Y	2215 (Int); 2053 (-H); 1704 (-HNF); 1542 (-2HNF); 691 (2NF2AB, CF); 569 (2NH/Bis?); 545 (2N2AB); 528 (2HN); 512 (HNF, AF); 488 (NF2AB, CF); 366 (NH); 342 (N2AB)	
	B	2286.8465	2165.7615	2165.7699	2286.8381	3.7	H5N3F1S2	Y	2286.8097 (Int); 1177 (3H2NF2AB, CF); 948 (Di-Sialyl Lewis C); 657 (SHN); 545 (2N2AB); 528 (2HN); 495 (SN); 488 (NF2AB, CF)	
28	A	2215.8305	2094.7608	2094.7539	2215.8373	3.1	H6N4F2	Y	2215 (Int); 2053 (-H); 1704 (-HNF); 1542 (-2HNF); 910 (3NH2AB, Bis); 691 (2NF2AB, CF); 569 (2NH/Bis?); 545 (2N2AB); 528 (2HN); 512 (HNF, AF); 488 (NF2AB, CF); 366 (NH); 342 (N2AB)	
	B	2344.872	2223.8034	2223.7954	2344.8799	3.4	H5N4F2S1	N		
	C	2199.8453	2078.7659	2078.7687	2199.8424	1.3	H5N4F3	Y	2199 (Int); 2053 (-F); 1712 (-N2AB); 1688 (-H -N -F); 1526 (-2H -N -F); 1177 (-2H -2N -2F, CF); 674 (2HNF); 545 (2N2AB); 528 (2HN); 512 (HNF, AF); 488 (NF2AB, CF); 366 (HN); 342 (N2AB)	
29	A	2003.7058	1882.6446	1882.6292	2003.7211	7.6	H9N2	Y	2003 (Int); 1841 (-H); 1679 (-2H); 1662 (-N2AB); 1517 (-3H); 1355 (-4H); 1193 (-5H); 1031 (-5H); 973 (6H, Hyb/HM); 869 (-6H); 811 (5H, Hyb/HM); 649 (4H, Hyb/HM); 487 (3H, Hyb/HM); 545 (2N2AB); 528 (2HN); 366 (HN); 342 (N2AB); 325 (2H).	

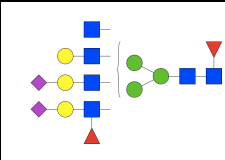
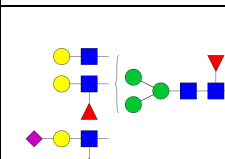
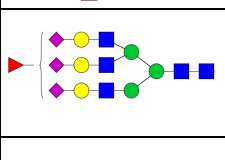
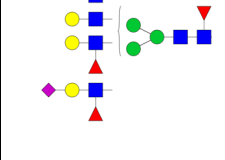
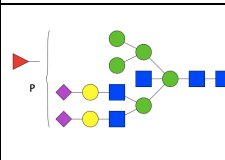
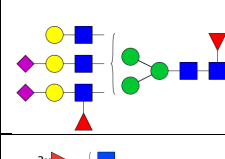
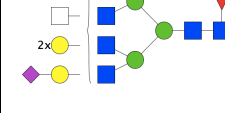
	B	2402.9225	2281.8453	2281.8459	2402.9218	0.3	H5N5F3	N		
	A	2489.9197	2368.8409	2368.8431	2489.9174	0.9	H5N4F1S2	Y	1245.4656 (Int, 2+); 1177 (-2S2H2N, CF); 657 (SHN); 569 (2NH/Bis?); 545 (2N2AB); 528 (2HN); 488 (NF2AB, CF); 454 (SH); 366 (NH)	
	B	2402.9407	2281.8453	2281.8641	2402.9218	7.9	H5N5F3	N		
30	C	2547.9635	2426.8828	2426.88693	2547.9593	1.6	H5N5F2S1	N		
	D	2003.7022	1882.6446	1882.6256	2003.7211	9.4	H9N2	N		
	E	2361.89	2240.8187	2240.8134	2361.8952	2.2	H6N4F3	N		
31	A	2751.0454	2629.9622	2629.96883	2751.0387	2.4	H5N6F2S1	Y	1376.0269 (Int, 2+); 1056 (-S -4H -F -4N , Bis + CF); 803 (SHNF); 691 (2NF2AB, CF); 657 (SHN); 569 (2NH/Bis?); 545 (2N2AB); 528 (2HN); 512 (HNF, AF); 488 (NF2AB, CF); 454 (SH); 366 (NH)	

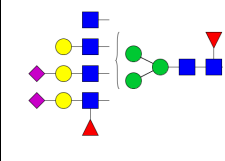
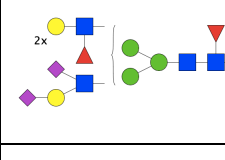
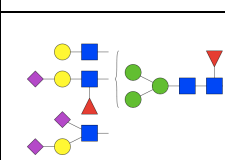
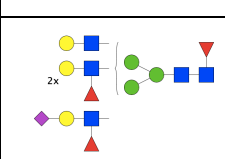
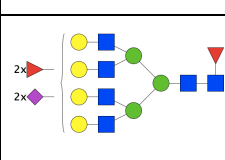
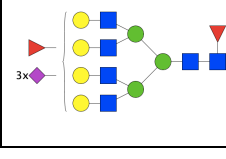
	B	2402.9152	2281.8453	2281.8386	2402.9218	2.8	H5N5F3	N		
32	A	2751.0597	2629.9622	2629.9831	2751.0387	7.6	H5N6F2S1	Y	1376.0226 (Int, 2+); 1056 (-S -4H -F -4N , Bis + CF); 803 (SHNF); 691 (2NF2AB, CF); 657 (SHN); 569 (2NH/Bis?); 545 (2N2AB); 528 (2HN); 512 (HNF, AF); 488 (NF2AB, CF); 454 (SH); 366 (NH)	
	B	2606.0072	2484.9247	2484.9306	2606.0012	2.3	H5N6F3	Y	1303.5068 (Int, 2+); 691 (2NF2AB, CF); 569 (2NH/Bis?); 545 (2N2AB); 528 (2HN); 512 (HNF, AF); 488 (NF2AB, CF); 366 (NH)	
	C	2344.8836	2223.8034	2223.8070	2344.8799	1.6	H5N4F2S1	N		
33		2165.7558	2044.6641	2044.6792	2165.7406	7.0	H7N4P1	N		
34		2635.9883	2514.8988	2514.9117	2635.9753	4.9	H5N4F2S2	Y	1318.4985 (Int, 2+); 948 (Di-Sialyl Lewis C); 657 (SHN); 545 (2N2AB); 528 (2HN); 512 (HNF, AF); 495 (SN); 488 (NF2AB, CF); 454 (SH); 366 (NH)	
35	A	2781.0361	2659.9363	2659.9595	2781.0128	8.4	H5N4F1S3	Y	1391.0172 (Int, 2+); 1177 (-3S-2H-2N, CF); 948 (Di-Sialyl Lewis C); 657 (SHN); 545 (2N2AB); 528 (2HN); 495 (SN); 488 (NF2AB, CF); 454 (SH); 366 (NH)	

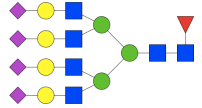
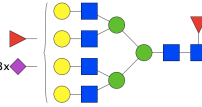
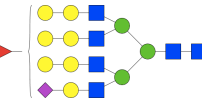


	B	2954.1348	2833.0416	2833.0582	2954.1181	5.6	H5N7F2S1	Y	1477.5587 (Int, 2+); 691 (2NF2AB, CF); 657 (SHN); 569 (2NH/Bis?); 545 (2N2AB); 512 (HNF, AF); 488 (NF2AB, CF); 366 (NH)	
36		3042.1615	2921.0576	2921.08493	3042.1341	9.0	H5N6F2S2	Y	1521.5854 (Int, 2+); 948 (Di-Sialyl Lewis C); 691 (2NF2AB, CF); 657 (SHN); 545 (2N2AB); 528 (2HN); 512 (HNF, AF); 495 (SN); 488 (NF2AB, CF); 454 (SH); 366 (NH)	
37		3099.1646	2978.0791	2978.08803	3099.1556	2.9	H5N7F1S2	Y	1550.0871 (Int, 2+); 691 (2NF2AB, CF); 657 (SHN); 454 (SH); 366 (HN)	
38		2984.0954	2863.0157	2863.01883	2984.0922	1.1	H5N5F1S3	N		
39		-	-	-	-	-	-	-	-	-
40	Λ	2711.0469	2589.9560	2589.97033	2711.0325	5.3	H6N5F4	Y	1356.0256 (Int, 2+); 691 (2NF2AB, CF); 545 (2N2AB); 528 (2HN); 512 (HNF, AF); 488 (NF2AB, CF); 366 (NH)	
	B	3059.151	2938.0729	2938.07443	3059.1494	0.5	H6N6F3S1	Y	1530.0842 (Int, 2+); 803 (SHNF); 691 (2NF2AB, CF); 657 (SHN); 569 (2NH/Bis?); 545 (2N2AB); 528 (2HN); 512 (HNF, AF); 488 (NF2AB, CF); 454 (SH); 366 (NH)	

	C	2856.0722	2734.9935	2734.99563	2856.0700	0.8	H6N5F3S1	Y	1428.5416 (Int, 2+); 803 (SHNF); 657 (SHN); 528 (2HN); 512 (HNF, AF); 488 (NF2AB, CF); 366 (NH)	
41		2856.0767	2734.9935	2735.00013	2856.0700	2.3	H6N5F3S1	Y	1428.5438 (Int, 2+); 803 (SHNF); 691 (2NF2AB, CF); 657 (SHN); 545 (2N2AB); 528 (2HN); 512 (HNF, AF); 488 (NF2AB, CF); 454 (SH); 366 (NH)	
	A	3001.1207	2880.0310	2880.04413	3001.1075	4.4	H6N5F2S2	Y	1501.0598 (Int, 2+); 803 (SHNF); 691 (2NF2AB, CF); 657 (SHN); 545 (2N2AB); 528 (2HN); 512 (HNF, AF); 488 (NF2AB, CF); 454 (SH); 366 (NH)	
	B	2856.0731	2734.9935	2734.99653	2856.0700	1.1	H6N5F3S1	N		
42	C	2952.0876	2830.9547	2831.01103	2952.0645	19.1	H7N5F2S1P1	Y	1476.5499 (Int, 2+); 910 (H3N2AB, Bis); 657 (SHN); 528 (2HN); 512 (HNF, AF); 488 (NF2AB, CF); 366 (NH)	
	D	3060.1448	2939.0682	2939.06823	3060.1447	0.0	H8N8	N		

43	E	3204.1862	3083.1104	3083.10963	3204.1869	0.2	H6N6F2S2	Y	1602.5936 (Int, 2+); 803 (SHNF); 657 (SHN); 545 (2N2AB); 512 (HNF, AF); 488 (NF2AB, CF); 366 (NH)	
	A	2856.073	2734.9935	2734.99643	2856.0700	1.0	H6N5F3S1	Y	1428.5212 (Int, 2+); 803 (SHNF); 657 (SHN); 545 (2N2AB); 528 (2HN); 512 (HNF, AF); 488 (NF2AB, CF); 366 (NH)	
	B	3146.1361	3025.0685	3025.05953	3146.1450	2.8	H6N5F1S3	Y	1573.5708 (Int, 2+); 657 (SHN); 528 (2HN); 512 (HNF, AF); 454 (SH); 366 (NH)	
	C	3059.1513	2938.0729	2938.07473	3059.1494	0.6	H6N6F3S1	Y	1530.0888 (Int, 2+); 803 (SHNF); 691 (2NF2AB, CF); 657 (SHN); 545 (2N2AB); 512 (HNF, AF); 488 (NF2AB, CF); 366 (NH)	
44	D	3097.1227	2975.9922	2976.04613	3097.1020	17.4	H7N5F1S2P1	N		
	A	3001.1261	2880.0310	2880.04953	3001.1075	6.2	H6N5F2S2	Y	1501.0799 (Int, 2+); 803 (SHNF); 657 (SHN); 528 (2HN); 512 (HNF, AF); 488 (NF2AB, CF); 366 (NH)	
	B	3262.2224	3141.1523	3141.14583	3262.2288	2.0	H6N7F3S1	Y	1631.6172 (Int, 2+); 691 (2NF2AB, CF); 657 (SHN); 512 (HNF, AF); 488 (NF2AB, CF); 366 (NH)	

	C	3204.1857	3083.1104	3083.10913	3204.1869	0.4	H6N6F2S2	Y	1602.5952 (Int, 2+); 803 (SHNF); 657 (SHN); 528 (2HN); 512 (HNF, AF); 488 (NF2AB, CF); 454 (SH); 366 (NH)	
	D	3147.1426	3026.0889	3026.06603	3147.1654	7.3	H6N5F3S2	Y	1574.0702 (Int, 2+); 948 (Di-Sialyl Lewis C); 657 (SHN); 528 (2HN); 512 (HNF, AF); 495 (SN); 488 (NF2AB, CF); 366 (NH)	
45		-	-	-	-	-	-	-	-	-
46		3292.1921	3171.1264	3171.11553	3292.2029	3.3	H6N5F2S3	Y	1646.6024 (Int, 2+); 948 (Di-Sialyl Lewis C); 803 (SHNF); 657 (SHN); 528 (2HN); 512 (HNF, AF); 495 (SN); 488 (NF2AB, CF); 454 (SH); 366 (NH)	
47		3367.2671	3246.1836	3246.19053	3367.2601	2.1	H7N6F4S1	Y	1684.1317 (Int, 2+); 803 (SHNF); 657 (SHN); 512 (HNF, AF); 488 (NF2AB, CF); 366 (NH)	
48	A	3512.291	3391.2211	3391.21443	3512.2976	1.9	H7N6F3S2	Y	1756.6328 (Int, 2+); 803 (SHNF); 657 (SHN); 512 (HNF, AF); 488 (NF2AB, CF); 454 (SH); 366 (NH)	
	B	3657.3498	3536.2586	3536.27323	3657.3351	4.0	H7N6F2S3	Y	1829.1770 (Int, 2+); 803 (SHNF); 657 (SHN); 512 (HNF, AF); 488 (NF2AB, CF); 454 (SH); 366 (NH)	

	C	3802.3761	3681.2961	3681.29953	3802.3726	0.9	H7N6F1S4	Y	1901.6887 (Int, 2+); 657 (SHN); 488 (NF2AB, CF); 366 (NH)	
49		3657.3559	3536.2586	3536.27933	3657.3351	5.7	H7N6F2S3	Y	1829.1786 (Int, 2+); 803 (SHNF); 657 (SHN); 512 (HNF, AF); 488 (NF2AB, CF); 366 (NH)	
50		3415.2528	3294.1683	3294.17623	3415.2448	2.3	H10N6F1S1	Y	1708.1232 (Int, 2+); 657 (SHN); 512 (HNF, AF); 366 (HN)	

**6.2 Calculation of derived traits.** The chromatographic fractions assigned to each group are listed below for each method.

Paucimannose

LSD: 1,2,3,4.

HSD: 1,2,3,4.

Oligomannose

LSD: 7,13,14,20,22,25,26,29.

HSD: 7,13,14,15,20,25,26,29,30.

Hybrid

LSD: 11,12,15,18,23,27,28,33.

HSD: 11,18,22,27,28,33.

Complex

LSD: 5,6,8,9,10,16,17,19,21,24,30,31,32,34,35,36,37,38,40,41,42,43,44,46,47,48,49,50.

HSD: 5,6,8,9,10,17,19,21,24,31,32,34,35,36,37,40,41,42,43,44,46,47,48,49.

Sialylated

LSD: 16,30,31,32,34,35,36,37,38,41,42,43,44,46,47,48,49,50.

HSD: 22,31,32,34,35,36,37,41,42,43,44,46,47,48,49.

Bisecting GlcNAc

LSD: 3,5,8,11,12,15,17,18,19,24,28,31,32.

HSD: 3,5,8,11,17,18,19,24,31,32.

Not determined

LSD: 39,45.

HSD: 12,16,23,38,39,45,50.

**6.3 Glycoproteins identified by downstream proteomics applications (Table A-2).** Identified glycoproteins demonstrate the IGTaD suitability towards the intended purpose, along with LSD lysate compatibility with glycoproteomics analyses. IgP = identified glycoprotein; UPI = Uniprot KB identifier; pC = peptide count (unique deglycosylated peptides); SC = sequence coverage (unique deglycosylated peptides); NDS = experimentally highlighted Asn→Asp site position; UP? = was the *N*-glycosylation at given site reported in Uniprot KB before this analysis?; MW (kDa) = Uniprot KB sequence-based theoretical MW (*N*-glycosylation not considered); IPe = identified deglycosylated peptides (NDS site is highlighted in green); IPe m/z = identified deglycosylated peptides mass to charge ratio; IPe Ch. = identified deglycosylated peptides charge; IPe RT = identified deglycosylated peptides retention time; IPe ME = identified deglycosylated peptide mass error (ppm); F = SDS-PAGE fraction in which the glycoprotein has been identified; \*protein homodimerization reported (Uniprot KB); \*\*protein homotrimerization reported (Uniprot KB).

**Table A-2. Examples of glycoproteins, glycopeptides and glycosylation sites identified by downstream proteomics applications using the LSD lysate.**

IgP	UPI	pC	SC (%)	NDS	UP?	MW (kDa)	IPe	IPe m/z	IPe Ch.	IPe RT (min)	IPe ME (ppm)	F
Neural cell adhesion molecule 1	F1LNY3	2	3	N444	N	92.721	ALASEWKPEIR DGQLLPSS <span style="background-color: #90EE90;">N</span> YSNIK	768.8806 650.3564	2+ 2+	36.30 37.20	1.5 6.0	1
Contactin-1	Q63198	3	4.5	N494	Y	113,495	<span style="background-color: #90EE90;">A</span> STGTLVITNPTR TDGAAPNVAPSDVGGGGGTNRVQ VTSQEYSAR	723.3833 935.4379 634.3174	2+ 2+ 2+	32.40 25.30 23.50	4.1 6.4 0.8	2
Myelin-associated glycoprotein	PO7722	3	8.1	N99	Y	64.291*	<span style="background-color: #90EE90;">N</span> CTLLSTLSPELGGK NLYGTQSLELPFQGAHR SNPEPSVAFELPSR	852.4478 965.9921 765.3833	2+ 2+ 2+	50.67 45.76 40.49	3.0 0.7 0.9	3
Excitatory amino acid transporter 2	P31596	2	4.4	N205	Y	62.106**	SELDTIDSQHR VLVAPPSEEA <span style="background-color: #90EE90;">N</span> ITK	650.810 728.8801	2+ 2+	26.01 29.27	0.2 0.6	4, 5, 6
Dihydropyrimidinase-related protein 2	P47942	14	37.4	N356	N	62.28	DIGAIAQVHAENGDIIEEQQR DNFTLIPEGT <span style="background-color: #90EE90;">N</span> GTEER FQMPDQGMTSADDFQGTK GLYDGPVCEVSVTPK GSPLVVISQGK GTVVYGEPIASLGTDGSHYWSK ISVGSADLVIWDPDSVK IVLEDGTLHVTEGSGR	1189.090 897.4130 1091.956 810.9005 1084.636 1213.087 958.4860 841.9390	2+ 2+ 2+ 2+ 1+ 2+ 2+ 2+	40.11 39.64 39.15 38.34 34.72 45.45 50.39 36.42	1.2 6 2.8 1.3 3.6 1.6 1.4 3.5	7



							MDENQFVAVTSTNAAK MVIPGGIDVHTR QIGENLIVPGGVK SAAEVIAQAR SITIANQTNCPYVTK VFNLVPR	871.4067 655.8479 1323.763 1015.553 911.9720 908.4988	2+ 2+ 1+ 1+ 2+ 1+	31.66 33.09 39.82 27.41 38.06 38.06	4.0 3.2 0.1 1.5 2 1.2	
BTB domain-containing 18	D3Z9A5	1	2.2	N201	N	79.27	SNLPNAD█LSDTLLK	865.4463	2+	39.56	5.0	9
Sodium/potassium- transporting ATPase subunit beta-2	P13638	1	4.5	N238	Y	33.40	FHV█YTQPLVAVK	758.9115	2+	41.66	1.9	11
Thy-1 membrane glycoprotein	P01830	1	6.2	N93	Y	18.17	VLTLA█FTTK	1108.624	1+	45.30	1.2	17

**6.4 Chymotryptic peptides identified from mhNS MS analysis (Table A-3).** Peptides derived from a single technical replicate are shown as an example. PSMs = Peptide Spectrum Match (i.e., the number of times the same peptide is fragmented by the instrument); MC = n° of miscleavages; TMM = theoretical monoisotopic mass ; DC = instrumental degree of confidence; z = peptide charge (i.e., by search engine: Sequest HT); m/Z = peptide mass to charge ratio (i.e., by search engine: Sequest HT);  $\Delta m$  [ppm] = relative mass accuracy; RT = retention time.

Sequence	Modifications	PSMs	MC	TMM [Da]	DC	z	m/z [Da]	$\Delta m$ [ppm]	RT [min]
LPRFTVEQEIDLKDV L	1xDimethyl [K13]	166	3	1943.0848	High	3	648.36688	0.66	28.4305
VMKIANS LF	1xDimethyl [K3]	78	1	1050.60161	High	2	525.80536	1.75	22.6053
SFTKDDSEVQIPMMY	1xOxidation [M]; 1xDimethyl [K4]	30	1	1963.86636	High	2	982.42934	-7.61	26.7029
SNMVTAKESQY	1xDimethyl [K7]	20	0	1285.60928	High	2	643.30813	-0.24	10.075
SFTKDDSEVQIPMMY	1xOxidation [M]	20	1	1935.83506	High	2	968.42103	-0.14	23.6571
SFTKDDSEVQIPMMY		19	1	1919.84014	High	2	960.42318	-0.55	26.9237
VMKIANS LF	1xOxidation [M2]; 1xDimethyl [K3]	13	1	1066.59653	High	2	533.80167	-0.44	18.4356
SNMVTAKESQY	1xOxidation [M3]; 1xDimethyl [K7]	13	0	1301.60419	High	2	651.30593	0.3	9.2212
KEFSNMVTAKESQY	2xDimethyl [K1; K10]	11	1	1717.84655	High	3	573.28652	-0.9	12.9677
SFTKDDSEVQIPMMY	1xDimethyl [K4]	11	1	1947.87144	High	2	974.4389	-0.48	27.1886
SFLKEFSNMVTAKESQY	2xDimethyl [K4; K13]	11	3	2065.03105	High	3	689.01564	0.63	25.9931
ATLEPLVKAQLVEEW	1xDimethyl [K8]	11	3	1753.97346	High	2	877.49213	2	28.9536
AMGM MELGAQGSTQKEIRHSMGY	1xOxidation [M]; 1xDimethyl [K15]	10	1	2557.16659	High	3	853.0576	-3.27	17.4213
SIALAMGM MELGAQGSTQKEIRHSMGY	1xOxidation [M]; 1xDimethyl [K19]	9	2	2941.40386	High	3	981.1411	1.66	23.7185
IKDANLTGLSDNKEIF	2xDimethyl [K2; K13]	8	2	1833.99565	High	3	612.00304	-0.59	20.3779
KALGITEIF	1xDimethyl [K1]	7	1	1019.61356	High	2	510.31075	0.65	23.1757
AMGM MELGAQGSTQKEIRHSMGY	1xDimethyl [K15]	7	1	2541.17168	High	3	847.72944	0.82	19.3144
KEFSNMVTAKESQY	1xDimethyl [K]	6	1	1689.81525	High	3	563.94311	-0.27	12.9614
SFLKEFSNMVTAKESQY	1xDimethyl [K]	6	3	2036.99975	High	3	679.67135	-0.13	25.312
VENN'TNNLVKDLVSPRDFDAATY	1xDimethyl [K10]	5	3	2623.29983	High	3	875.10445	-0.39	26.7095

GAQGSTQKEIRHSMGY	1xDimethyl [K8]	5	0	1777.86499	High	3	593.29317	-0.03	8.0897
SFLKEFSNMVTAKESQY	1xOxidation [M9]; 2xDimethyl [K4; K13]	5	3	2081.02597	High	3	694.34736	0.75	21.4204
VENN'TNNLVKDLVSPRDFDAATY		5	3	2595.26853	High	3	865.76173	0.8	26.7102
KALGITEIFIKDANL	2xDimethyl [K1; K11]	4	2	1702.01493	High	3	568.01017	0.6	26.1871
LPRFTVEQEIDLKDV L		4	3	1915.0535	High	3	639.02245	-0.37	28.5716
GITEIFIKDANLTGLSDNKEIF	2xDimethyl [K8; K19]	4	3	2494.34393	High	3	832.11981	0.38	32.2307
SFTKDDSEVQIPMMY	2xOxidation [M14; M15]	4	1	1951.82997	High	2	976.41719	-1.47	20.4761
VQNGFHVNEEFLQMMKKY	2xDimethyl [K16; K17]	4	3	2298.14096	High	3	766.71851	0.01	24.4313
VQNGFHVNEEFLQMMKKY	1xDimethyl [K]	4	3	2270.10966	High	4	568.28245	-0.74	24.4135
SNMVTAKESQY	1xOxidation [M3]	4	0	1273.57289	High	2	637.2898	-0.45	6.763
TGLSDNKEIFL	1xDimethyl [K7]	4	2	1264.67834	High	2	632.84178	-1.63	21.7385
ANSVKKQKVEVY	3xDimethyl [K5; K6; K8]	4	0	1476.87844	High	3	492.9645	0.35	4.6091
INKWVENN'TNNLVKDL	1xDimethyl [K3]	3	2	1942.03925	High	3	648.01757	-0.57	21.0558
KNGEEFSFLKEF	2xDimethyl [K1; K10]	3	3	1530.78387	High	3	510.93286	0.1	23.44
AMGM MELGAQGSTQKEIRHSMGYDSLKNGEEF	2xDimethyl [K15; K27]	3	3	3588.65897	High	3	1196.88832	-2.39	21.5258
KEFSNMVTAKESQY	1xOxidation [M6]; 2xDimethyl [K1; K10]	3	1	1733.84146	High	3	578.61831	-0.63	12.651
SFTKDDSEVQIPMMY	2xOxidation [M14; M15]; 1xDimethyl [K4]	3	1	1979.86127	High	2	990.43346	-0.82	21.0876
KALGITEIFIKDANLTGL	2xDimethyl [K1; K11]	3	3	1973.16814	High	2	987.08899	1.3	29.9527
ANSVKKQKVEVY	2xDimethyl [K6; K]	3	0	1448.84714	High	3	483.62072	0.32	4.3506
TVEQEIDLKDV L	1xDimethyl [K9]	3	1	1429.77845	High	2	715.39308	0.3	26.2337
DSLKNGEEF	1xDimethyl [K4]	3	1	1066.50513	High	2	533.75606	-0.27	11.9202
TGLSDNKEIF	1xDimethyl [K7]	3	1	1151.59428	High	2	576.30078	0.01	16.8332
GITEIFIKDANLTGL	1xDimethyl [K8]	3	2	1632.9207	High	2	816.96391	-0.09	32.343
SIALAMGM MELGAQGSTQKEIRHSMGYDSL	1xDimethyl [K19]	3	3	3240.55199	High	3	1080.85213	-3.13	27.7368
VENN'TNNLVKDL		2	1	1372.70668	High	2	686.85679	-0.28	16.7979
VKDLVSPRDFDAATY	1xDimethyl [K2]	2	2	1724.88538	High	2	862.94509	-1.43	19.3183
VMKIANS L	1xDimethyl [K3]	2	0	903.5332	High	2	452.26977	-1.05	13.3399
SDNKEIF	1xDimethyl [K4]	2	0	880.44107	High	2	440.72382	-0.82	10.6082

LSKAIHKSF	1xDimethyl [K]	2	1	1058.63569	High	2	529.82118	-0.57	4.3065
VMKIANSLF		2	1	1022.57031	High	2	511.78873	-0.13	21.0221
INKWVENNTNNLVKDLVSPRDF	2xDimethyl [K3; K14]	2	3	2671.42022	High	4	668.61024	-0.41	25.6979
INKWVENNTNNLVKDL	2xDimethyl [K3; K14]	2	2	1970.07055	High	3	657.36134	-0.55	20.9495
VKAQLVEEW	1xDimethyl [K2]	2	1	1129.62519	High	2	565.31689	1.16	18.9029
SIALAMGMELGAQGSTQKEIRHSMGY	1xDimethyl [K19]	2	2	2925.40895	High	3	975.80711	-0.74	26.3888
INKWVENNTNNL	1xDimethyl [K3]	2	1	1486.76487	High	2	743.88586	-0.28	15.241
AMGMELGAQGSTQKEIRHSMGY		2	1	2513.14038	High	3	838.38408	-1.07	19.2082
HVNEEFLOMMKKY	1xOxidation [M]; 2xDimethyl [K11; K12]	2	2	1768.87607	High	3	590.29732	0.75	15.658
DSLKNGEEFSF	1xDimethyl [K4]	2	2	1300.60557	High	2	650.80676	0.51	21.3866
GITEIFIKDANL	1xDimethyl [K8]	2	1	1361.76749	High	2	681.38737	-0.02	28.0991
DSLKNGEEFSFL	1xDimethyl [K4]	2	3	1413.68964	High	2	707.34805	-0.57	27.0482
IKDANLTGLSDNKEIF	1xDimethyl [K]	2	2	1805.96435	High	3	602.66039	1.26	19.8593
ATLEPLVKAQLVEEW		2	3	1725.94216	High	2	863.4761	1.6	28.7665
AMGMELGAQGSTQKEIRHSMGYDSLKNGEEF	2xOxidation [M]; 1xDimethyl [K15]	2	3	3592.6175	High	5	719.32967	0.48	20.933
GAQGSTQKEIRHSMGY	1xOxidation [M14]; 1xDimethyl [K8]	2	0	1793.85991	High	3	598.62479	-0.04	5.0191
AMGMELGAQGSTQKEIRHSMGYDSLKNGEEF	1xOxidation [M21]; 1xDimethyl [K]	2	3	3576.62258	High	4	894.9187	8.5	21.617
AMGMELGAQGSTQKEIRHSMGYDSL	1xDimethyl [K15]	2	2	2856.31472	High	3	952.77716	0.78	21.3827
GAQGSTQKEIRHSMGYDSL	1xDimethyl [K8]	2	1	2093.00803	High	3	698.34076	-0.14	11.643
SRQEVPLATLEPLVKAQL	1xDimethyl [K15]	1	3	2020.1801	High	3	674.0653	0.62	26.1733
TGLSDNKEIFL		1	2	1236.64704	High	2	618.82622	-1.52	21.2462
EPLVKAQLVEEW	1xDimethyl [K5]	1	2	1468.80461	High	2	734.90538	-0.76	24.5872
TKDDESEVQIPMMY	1xDimethyl [K2]	1	0	1713.771	High	2	857.39073	1.85	25.0701
DSLKNGEEF		1	1	1038.47383	High	2	519.7387	-3.57	11.2304
TGLSDNKEIF		1	1	1123.56298	High	2	562.28457	-0.99	16.3794
VENNTNNLVKDL	1xDimethyl [K10]	1	1	1400.73798	High	2	700.87208	-0.78	16.9464
VENNTNNLVKDLVSPRDF	1xDimethyl [K10]	1	2	2102.08766	High	3	701.36765	0.36	23.9706
ATLEPLVKAQL	1xDimethyl [K8]	1	2	1210.74055	High	2	605.87375	-0.26	20.728

ANSVKKQKVEVYLPRF	3xDimethyl [K5; K6; K8]	1	2	1990.18479	High	4	498.30145	-0.42	14.0871
VKAQLVEEW		1	1	1101.59389	High	2	551.30087	0.53	17.7042
ANSVKKQKVEVYLPRF	2xDimethyl [K5; K6]	1	2	1962.15349	High	4	491.29502	2.42	13.8206
VKDLVSPRDFDAATY		1	2	1696.85408	High	3	566.28935	-0.35	19.1329
ANSVKKQKVEVY	1xDimethyl [K8]	1	0	1420.81584	High	3	474.27675	-0.09	4.0673
VKDLVSPRDFDAATYL		1	3	1809.93814	High	3	603.98377	-0.77	24.4094
VKDLVSPRDFDAATYL	1xDimethyl [K2]	1	3	1837.96944	High	3	613.32863	1.02	24.5532
AMGMELGAQGSTQKEIRHSMGYDSLKNGEEF	1xOxidation [M21]; 2xDimethyl [K15; K27]	1	3	3604.65388	High	4	901.91935	0.47	19.2141
VMKIANSLF	1xOxidation [M2]	1	1	1038.56523	High	2	519.78607	-0.35	17.1395
VMKIANSLFVQNGF	1xDimethyl [K3]	1	2	1595.86141	High	2	798.43534	1.25	26.4694
VEEWANSVKKQKVEVY	3xDimethyl [K9; K10; K12]	1	1	2020.11135	High	3	674.04216	0.29	14.1329
FKGNWKSQF	1xDimethyl [K6]	1	2	1169.6102	High	2	585.30872	-0.03	11.8579
SIALAMGMELGAQGSTQKEIRHSMGYDSL	1xOxidation [M25]; 1xDimethyl [K19]	1	3	3256.5469	High	3	1086.19146	3.97	25.575
SNMVTAKESQY		1	0	1257.57798	High	2	629.29262	-0.01	9.2071
LKEFSNMVTAKESQY	2xDimethyl [K2; K11]	1	2	1830.93061	High	3	610.97954	-3.57	16.2384
LKEFSNMVTAKESQY	1xOxidation [M7]; 2xDimethyl [K2; K11]	1	2	1846.92553	High	3	616.31327	-0.14	12.8478
IKDANLTGLSDNKEIF		1	2	1777.93305	High	3	593.31583	-0.07	19.783
IKDANLTGL	1xDimethyl [K2]	1	1	972.57242	High	2	486.79107	2.52	14.2739
IKDANLTGL		1	1	944.54112	High	2	472.77428	0.17	13.9066
KSQFRPENTRTF	1xDimethyl [K1]	1	1	1538.8074	High	4	385.45681	-1.3	7.3745
KNGEEFSFLKEF	1xDimethyl [K10]	1	3	1502.75257	High	3	501.58922	0.35	23.3798
KNGEEFSFL	1xDimethyl [K1]	1	2	1098.5466	High	2	549.77716	0.4	21.3852
LSKAIHKSF		1	1	1030.60439	High	2	515.80587	0.07	3.9129
KGWKSQF	2xDimethyl [K1; K5]	1	1	1050.57309	High	2	525.79005	-0.26	7.8577
LSKAIHKSFL	1xDimethyl [K7]	1	2	1171.71976	High	2	586.36338	-0.23	7.7498
QMMKKYF	2xDimethyl [K4; K5]	1	1	1031.54166	High	2	516.27482	0.69	10.3576
GAQGSTQKEIRHSMGY		1	0	1749.83369	High	3	583.94927	-0.25	8.1196
KGWKSQF	1xDimethyl [K5]	1	1	1022.54179	High	2	511.77596	2.8	6.8723

SDNKEIFL	1xDimethyl [K4]	1	1	993.52514	High	2	497.26651	0.6	16.9644
SFLKEFSNMVTAKESQY		1	3	2008.96845	High	3	670.32837	1.04	25.4568
KEFSNMVTAKESQY	1xOxidation [M6]; 1xDimethyl [K10]	1	1	1705.81016	High	3	569.27427	-1.11	9.6175
KEFSNMVTAKESQY		1	1	1661.78395	High	2	831.39724	1.96	12.5163
KALGITEIFIKDANL	1xDimethyl [K1]	1	2	1673.98363	High	3	558.66738	2.36	26.0199
HVNEEFQMMKKYF	2xDimethyl [K11; K12]	1	3	1899.94957	High	3	633.9875	-0.86	26.9208
HVNEEFQMMKKY	2xDimethyl [K11; K12]	1	2	1752.88116	High	3	584.96602	1.35	19.2091
GITEIFIKDANL		1	1	1333.73619	High	2	667.37257	1.25	27.8135
GAQGSTQKEIRHSMGYDSL	1xOxidation [M14]; 1xDimethyl [K8]	1	1	2109.00294	High	3	703.67295	0.64	8.5457
SFTKDESEVQIPMMYQQGEF	1xDimethyl [K4]	1	2	2537.12107	High	2	1269.06206	-1.66	29.6484
SIALAMGMELGAQGSTQKEIRHSMGY		1	2	2897.37765	High	4	725.10012	0.35	26.3012
GAQGSTQKEIRHSMGY	1xOxidation [M14]	1	0	1765.82861	High	3	589.28102	-0.05	5.0368
SDNKEIFL		1	1	965.49384	High	2	483.24999	-1.18	16.4196
IKDANLTGLSDNKEIFL	1xDimethyl [K2]	1	3	1919.04842	High	3	640.35553	1.88	22.9346

**6.5 Chymotryptic peptides identified from phNS MS analysis (Table A-4).** Peptides derived from a single technical replicate are shown as an example. PSMs = Peptide Spectrum Match (i.e., the number of times the same peptide is fragmented by the instrument); MC = n° of miscleavages; TMM = theoretical monoisotopic mass ; DC = instrumental degree of confidence; z = peptide charge (i.e., by search engine: Sequest HT); m/Z = peptide mass to charge ratio (i.e., by search engine: Sequest HT);  $\Delta m$  [ppm] = relative mass accuracy; RT = retention time.

**Table A-4. Chymotryptic peptides identified from phNS MS analysis**

Sequence	Modifications	PSMs	MC	TMM [Da]	DC	z	m/z [Da]	$\Delta m$ [ppm]	RT [min]
NAAVNHVDFSQNVAVANY		110	1	1932.91986	High	2	966.96387	0.31	20.9308
FNAAVNHVDFSQNVAVANY		96	2	2079.98828	High	2	1040.49735	-0.41	23.9626
LPRFTVEQEIDLKDV L	1xDimethyl [K13]	55	3	1943.0848	High	3	648.3664	-0.08	28.873
SFTKDDESEVQIPMMY	1xDimethyl [K4]	35	1	1947.87144	High	2	974.43884	-0.53	27.4263
SFTKDDESEVQIPMMY	1xOxidation [M]; 1xDimethyl [K4]	29	1	1963.86636	High	2	982.43625	-0.58	26.7801
RPENRTRTF		24	0	1020.52212	High	2	510.76418	-1.02	3.9208
MGRVMHPETMNTSGHDFEEL		22	1	2317.99985	High	3	773.33763	-0.65	15.8744
MGRVMHPETMNTSGHDFEEL	1xOxidation [M]	22	1	2333.99476	High	3	778.66969	-0.1	13.9963
QVLEIPYEGDEISMML	1xOxidation [M]	21	2	1882.88128	High	2	941.94489	0.65	36.2813
NRLRATGEDENILFSPL		21	3	1945.01376	High	3	649.00958	0.22	23.9447
VMKIANSLF	1xDimethyl [K3]	20	1	1050.60161	High	2	525.80359	-1.62	22.4128
SIALAMGM MEL	1xOxidation [M]	14	1	1182.55671	High	2	591.78207	0.12	30.2939
SIALAMGM MEL		12	1	1166.5618	High	2	583.78435	-0.33	35.5168
MRGSHHHHHHTDPTGATFPEEAIADLSVNMY		12	2	3495.57056	High	5	699.92105	1.6	20.4941
FMGRVMHPETMNTSGHDFEEL		10	2	2465.06826	High	3	822.36061	-0.4	19.6702
EIPYEGDEISMML	1xOxidation [M]	10	1	1542.67022	High	2	771.83701	-2.25	34.1803
QVLEIPYEGDEISMML		9	2	1866.88636	High	2	933.94614	-0.72	38.441
VMKIANSLF	1xOxidation [M2]; 1xDimethyl [K3]	9	1	1066.59653	High	2	533.80244	1.01	19.2008
RATGEDENILFSPL		9	2	1561.78566	High	2	781.39681	0.43	25.6972
YYGEFSDGSNEAGGIY		8	3	1728.70239	High	2	864.85555	0.84	25.5093



EIPYEGDEISMML		8	1	1526.67531	High	2	763.84225	1.25	34.799
SIALAMGMELGAQGSTQKEIRHSMGY	1xDimethyl [K19]	7	2	2925.40895	High	3	975.80774	-0.1	26.55
SNMVTAKESQY	1xDimethyl [K7]	7	0	1285.60928	High	2	643.30795	-0.51	9.7232
SNMVTAKESQY	1xOxidation [M3]; 1xDimethyl [K7]	7	0	1301.60419	High	2	651.30473	-1.55	9.0256
SFLKEFSNMVTAKESQY	2xDimethyl [K4; K13]	7	3	2065.03105	High	3	689.01574	0.78	26.0168
SFLKEFSNMVTAKESQY	1xDimethyl [K]	6	3	2036.99975	High	2	1019.00305	-0.46	26.0986
FMGRVMHPETMNTSGHDFEEL	1xOxidation [M]	6	2	2481.06318	High	3	827.69112	-1.76	17.005
VQNGFHVNEEFLQMMKKY	1xDimethyl [K]	5	3	2270.10966	High	3	757.37856	5.05	24.6487
ATLEPLVKAQLVEEW	1xDimethyl [K8]	5	3	1753.97346	High	2	877.49062	0.29	29.2083
SIALAMGMELGAQGSTQKEIRHSMGY	1xOxidation [M]; 1xDimethyl [K19]	5	2	2941.40386	High	3	981.14094	1.5	23.8298
AMGMELGAQGSTQKEIRHSMGY	1xDimethyl [K15]	5	1	2541.17168	High	3	847.72813	-0.73	19.3432
IKDANLTGLSDNKEIF	2xDimethyl [K2; K13]	5	2	1833.99565	High	3	612.00358	0.29	20.3513
KEFSNMVTAKESQY	2xDimethyl [K1; K10]	5	1	1717.84655	High	3	573.28702	-0.03	12.8566
KEFSNMVTAKESQY	1xDimethyl [K]	5	1	1689.81525	High	3	563.94338	0.2	12.2604
VENN'TNNLVKDLVSPRDFDAATY	1xDimethyl [K10]	4	3	2623.29983	High	3	875.10482	0.03	26.7511
VQNGFHVNEEFLQMMKKY	2xDimethyl [K16; K17]	4	3	2298.14096	High	3	766.71853	0.03	24.7514
YGEFSDGSNEAGGIY		4	2	1565.63906	High	2	783.32343	0.34	23.5698
KALGTEIFIKDANLTGL	2xDimethyl [K1; K11]	4	3	1973.16814	High	3	658.39446	0.34	30.3155
VKDLVSPRDFDAATY	1xDimethyl [K2]	3	2	1724.88538	High	2	862.94854	2.56	19.5002
IKDANLTGLSDNKEIF	1xDimethyl [K]	3	2	1805.96435	High	3	602.65982	0.31	19.9482
GAQGSTQKEIRHSMGYDSL	1xDimethyl [K8]	3	1	2093.00803	High	3	698.34084	-0.02	10.335
INKWVENN'TNNLVKDL	2xDimethyl [K3; K14]	3	2	1970.07055	High	3	657.36089	-1.23	21.2046
SQNVAVANY		3	0	965.46869	High	2	483.23869	1.47	12.6657
TGLSDNKEIF	1xDimethyl [K7]	3	1	1151.59428	High	2	576.30142	1.12	16.5191
QVLEIPYEGDEISMMLVL		3	3	2079.03884	High	2	1040.02852	5.26	43.8593
VLSRQEVPLATL		3	2	1325.77873	High	2	663.39217	-1.26	20.3353
VMKIANSL	1xDimethyl [K3]	3	0	903.5332	High	2	452.26996	-0.62	12.7292
YPQVIVDHPFFF		3	3	1508.75726	High	2	754.88245	0.24	31.7865

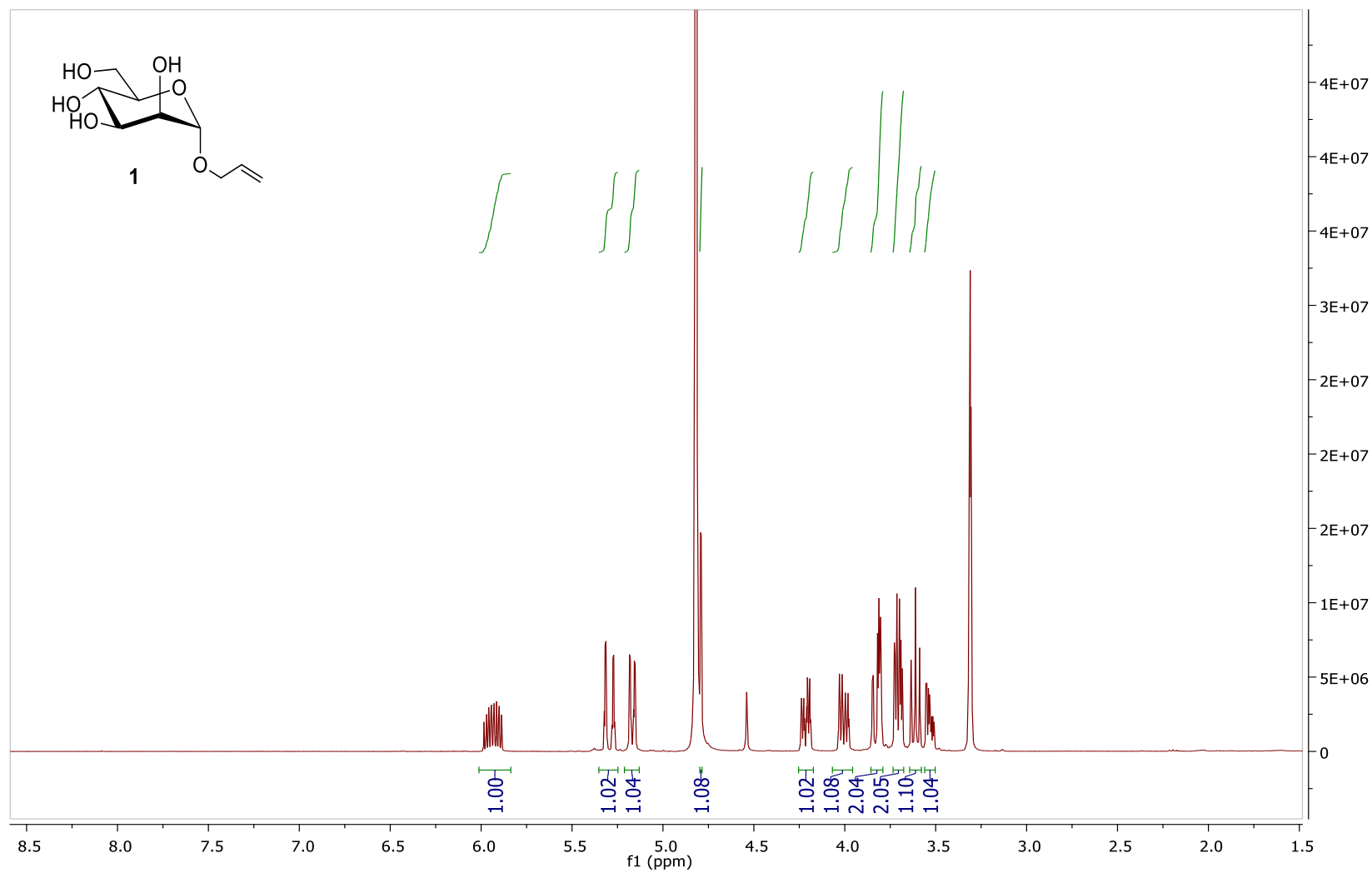
ANSVKKQKVEVY	2xDimethyl [K6; K]	3	0	1448.84714	High	3	483.61942	-2.37	4.0147
SFTKDDESEVQIPMMY	2xOxidation [M14; M15]; 1xDimethyl [K4]	3	1	1979.86127	High	2	990.4308	-3.51	21.2855
SFTKDDESEVQIPMMYQQGEF	1xDimethyl [K4]	3	2	2537.12107	High	2	1269.06148	-2.12	29.8364
VMKIANSFLVQNGF	1xDimethyl [K3]	3	2	1595.86141	High	2	798.43489	0.69	26.5509
KALGITEIFIKDANL	2xDimethyl [K1; K11]	3	2	1702.01493	High	3	568.00964	-0.33	26.5262
GITEIFIKDANLTGLSDNKEIF	2xDimethyl [K8; K19]	3	3	2494.34393	High	3	832.11968	0.23	32.2597
SFTKDDESEVQIPMMY		3	1	1919.84014	High	2	960.42411	0.42	27.1188
HVNEEFLQMMKKYF	2xDimethyl [K11; K12]	3	3	1899.94957	High	3	633.98688	-1.83	27.1563
TKDDESEVQIPMMY	1xDimethyl [K2]	2	0	1713.771	High	2	857.38935	0.25	25.2674
YPQVVDHPFF		2	2	1361.68885	High	2	681.34643	-2.4	27.3293
YPQVVDHPF		2	1	1214.62044	High	2	607.81391	0.09	22.0932
QVLEIPYEGDEISMMLVL	1xOxidation [M]	2	3	2095.03376	High	2	1048.01244	-7.71	43.851
RATGEDENILF		2	1	1264.61681	High	2	632.81237	0.53	18.6616
AMGMELGAQGSTQKEIRHSMGYDSLKNGEEF	2xDimethyl [K15; K27]	2	3	3588.65897	High	4	897.9202	0	21.8984
SRQEVPLATLEPL		2	2	1452.80567	High	2	726.90642	-0.07	23.572
FNAAVNHVDF		2	1	1133.53743	High	2	567.27231	-0.08	17.4791
YGEFSDGSNEAGGIYQVL		2	3	1905.85011	High	2	953.42894	0.26	31.852
SPLSIAMGMELGAQGSTQKEIRHSMGY	1xDimethyl [K22]	2	3	3222.57781	High	4	806.3987	-1.5	33.9943
SFTKDDESEVQIPMMYQQGEFY	1xDimethyl [K4]	2	3	2700.1844	High	3	900.73321	0.25	31.2109
SPLSIAMGMEL		2	2	1463.73066	High	2	732.36952	0.75	44.2072
ANSVKKQKVEVY	3xDimethyl [K5; K6; K8]	2	0	1476.87844	High	3	492.96377	-1.13	4.5415
RATGEDENILFSPSIAL		2	3	1946.02293	High	2	973.51137	-3.84	35.0277
SFLKEFSNMVTAKESQY	1xOxidation [M9]; 2xDimethyl [K4; K13]	2	3	2081.02597	High	3	694.34924	3.46	22.1599
SIALAMGMELGAQGSTQKEIRHSMGYDSL	1xDimethyl [K19]	2	3	3240.55199	High	3	1080.85221	-3.06	27.9936
HVNEEFLQMMKKY	2xDimethyl [K11; K12]	2	2	1752.88116	High	3	584.96514	-0.17	19.2875
LALINAVY		2	2	876.51893	High	2	438.76303	-0.17	27.2719
VLSRQEVPLATLEPL		2	3	1664.95815	High	2	832.98236	-0.43	26.0495
VKAQLVEEW	1xDimethyl [K2]	2	1	1129.62519	High	2	565.31672	0.86	17.8007

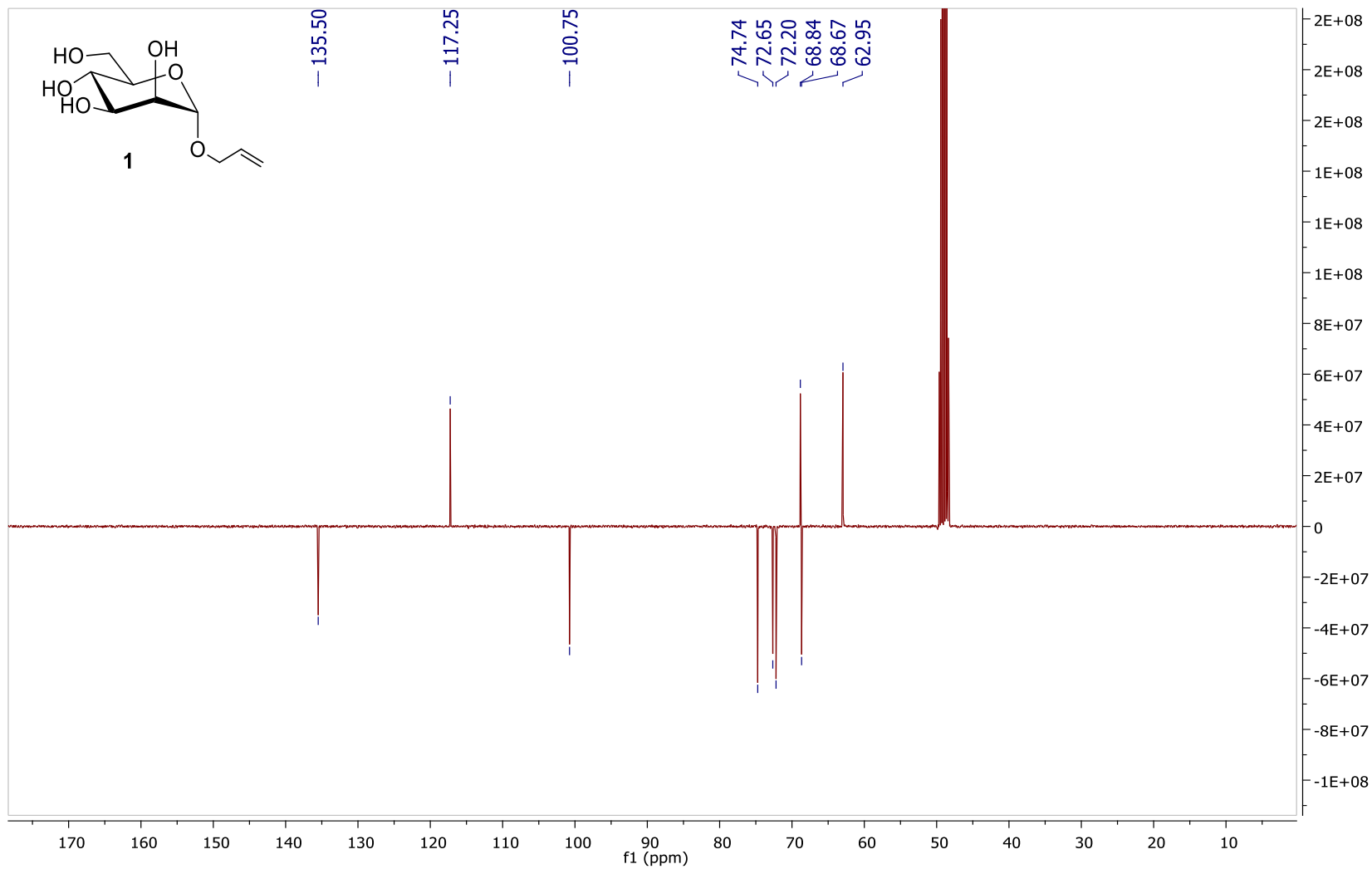
TVEQEIDLKDV L	1xDimethyl [K9]	2	1	1429.77845	High	2	715.39133	-2.14	26.1533
AMGMMELGAQGSTQKEIRHSMGYDSL	1xDimethyl [K15]	2	2	2856.31472	High	4	714.8341	-0.06	21.6315
KEFSNMVTAKESQY	1xOxidation [M6]; 2xDimethyl [K1; K10]	2	1	1733.84146	High	3	578.6185	-0.3	9.7148
KALGITEIF	1xDimethyl [K1]	2	1	1019.61356	High	2	510.31022	-0.39	23.6567
VMKIANSLF		2	1	1022.57031	High	2	511.78843	-0.72	21.3501
KNGEEFSLKEF	2xDimethyl [K1; K10]	2	3	1530.78387	High	3	510.93298	0.34	23.703
MGRVMHPETMNTSGHDFEEL	2xOxidation [M5; M]	2	1	2349.98968	High	3	784.00217	0.97	11.4645
GITEIFIKDANLTGL	1xDimethyl [K8]	2	2	1632.9207	High	2	816.96361	-0.46	32.5032
MRGSHHHHHHTDPTGATFPEEAIADLSVNMY	1xOxidation [M]	2	2	3511.56548	High	4	878.6469	0.09	18.6465
MRGSHHHHHHTDPTGATFPEEAIADLSVNMY	1xAcetyl [N-Term]	2	2	3537.58113	High	4	885.15454	4.3	21.8568
NAAVNHVDF		2	0	986.46902	High	2	493.73834	0.38	10.8305
DSLKNGEEF	1xDimethyl [K4]	2	1	1066.50513	High	2	533.75635	0.27	11.2784
DSLKNGEEFSFL	1xDimethyl [K4]	2	3	1413.68964	High	2	707.34771	-1.06	27.0166
VQNGFHVNEEF		1	1	1319.60149	High	2	660.30416	-0.34	17.2924
VQNGFHVNEEFL		1	2	1432.68555	High	2	716.8463	-0.16	22.1757
TVEQEIDLKDV LKAL	2xDimethyl [K9; K13]	1	2	1770.02589	High	3	590.68016	0.02	30.4364
VSPRDFDAATYL		1	2	1354.66376	High	2	677.83519	-0.48	24.4354
VENNTNNLVKDLVSPRDFDAATY		1	3	2595.26853	High	3	865.76063	-0.46	26.9173
VENNTNNLVKDLVSPRDF	1xDimethyl [K10]	1	2	2102.08766	High	3	701.36961	3.14	24.2446
SRQEVPLATL		1	1	1113.62625	High	2	557.31731	0.99	16.1947
VENNTNNLVKDL	1xDimethyl [K10]	1	1	1400.73798	High	2	700.87528	3.78	16.7122
SRQEVPLATLEPLVKAQL	1xDimethyl [K15]	1	3	2020.1801	High	3	674.0651	0.31	26.3764
TGLSDNKEIFL	1xDimethyl [K7]	1	2	1264.67834	High	2	632.84252	-0.46	21.7908
VKAQLVEEW		1	1	1101.59389	High	2	551.30075	0.31	17.4682
VEEWANSVKKQKVEVY	3xDimethyl [K9; K10; K12]	1	1	2020.11135	High	3	674.04264	1	13.5202
ATLEPLVKAQL	1xDimethyl [K8]	1	2	1210.74055	High	2	605.87381	-0.17	20.8844
SIALAMGMMELGAQGSTQKEIRHSMGY		1	2	2897.37765	High	4	725.10362	5.17	26.4028
IKDANLTGL		1	1	944.54112	High	2	472.77375	-0.95	13.4423

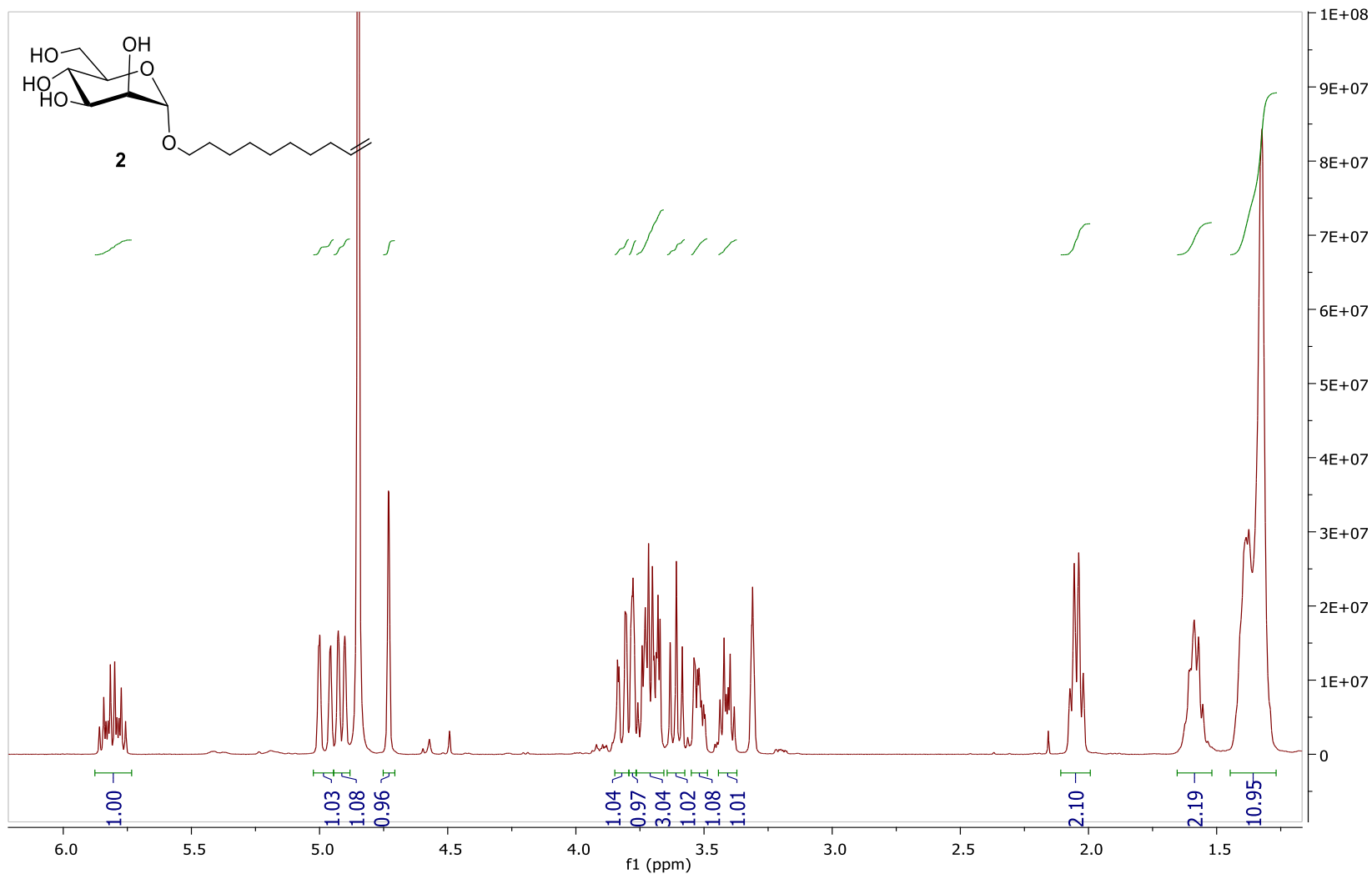
LEVNEEGSEAAAVSGMIAISRMVLYPQVIVDHPF		1	3	3742.88189	High	3	1248.30155	2.19	40.5359
LEVNEEGSEAAAVSGMIAISRMVLY	1xOxidation [M16]	1	2	2726.33754	High	3	909.45605	5.89	39.2933
KSQFRPENTRTF	1xDimethyl [K1]	1	1	1538.8074	High	4	385.45723	-0.21	7.8083
KGNWKSQF	2xDimethyl [K1; K5]	1	1	1050.57309	High	2	525.7897	-0.92	8.0038
KGNWKSQF	1xDimethyl [K5]	1	1	1022.54179	High	2	511.77473	0.39	7.5858
KALGITEIFIKDANLTGL	1xDimethyl [K1]	1	3	1945.13684	High	3	649.05281	3.62	30.0857
IKDANLTGL	1xDimethyl [K2]	1	1	972.57242	High	2	486.79001	0.33	13.8428
KALGITEIFIKDANL	1xDimethyl [K1]	1	2	1673.98363	High	3	558.66644	0.68	26.2198
GEFSDGSNEAGGIYQVL		1	2	1742.78678	High	2	871.89723	0.23	29.7402
GAQGSTQKEIRHSMGYDSL		1	1	2064.97673	High	3	688.99799	1.31	10.4255
GAQGSTQKEIRHSMGY	1xDimethyl [K8]	1	0	1777.86499	High	3	593.29151	-2.82	8.4848
GAQGSTQKEIRHSMGY		1	0	1749.83369	High	3	583.94976	0.6	8.5274
FVQNGFHVNEEFL		1	3	1579.75397	High	2	790.3804	-0.28	24.9927
FVQNGFHVNEEF		1	2	1466.6699	High	2	733.83598	-3.55	21.1218
FSPLSIAMGMMEL		1	3	1610.79907	High	2	805.90427	1.36	46.7347
GTTEIFIKDANL	1xDimethyl [K8]	1	1	1361.76749	High	2	681.38685	-0.79	28.1473
SNMVTAKESQY		1	0	1257.57798	High	2	629.29187	-1.21	9.4418
LKEFSNMVTAKESQY	2xDimethyl [K2; K11]	1	2	1830.93061	High	3	610.9815	-0.37	15.8708
INKWVENNTNNLVKDL	1xDimethyl [K3]	1	2	1942.03925	High	3	648.01883	1.38	21.271
ANSVKKQKVEVY	1xDimethyl [K6]	1	0	1420.81584	High	3	474.27685	0.1	3.8914
SFLKEFSNMVTAKESQY		1	3	2008.96845	High	3	670.32653	-1.7	25.5773
SDNKEIFL	1xDimethyl [K4]	1	1	993.52514	High	2	497.26612	-0.17	16.7044
SDNKEIF	1xDimethyl [K4]	1	0	880.44107	High	2	440.7242	0.05	10.3146
SDGSNEAGGIYQVLEIPYEGDEISMML		1	3	2917.31178	High	2	1459.15736	-1.49	45.0553
SDGSNEAGGIYQVL		1	1	1409.65431	High	2	705.33023	-0.8	26.2318
ATLEPLVKAQLVEEW		1	3	1725.94216	High	2	863.4722	-2.92	28.8349
INKWVENNTNNL	1xDimethyl [K3]	1	1	1486.76487	High	2	743.89006	5.36	14.612
RATGEDENIL		1	0	1117.54839	High	2	559.27797	0.24	10.5459

DSLKNGEEF		1	1	1038.47383	High	2	519.74064	0.16	10.72
NRLRATGEDENILF		1	2	1647.84491	High	3	549.95299	-0.29	17.6164
NRLRATGEDENIL		1	1	1500.77649	High	3	500.93113	1.56	10.963
DSLKNGEEFSF	1xDimethyl [K4]	1	2	1300.60557	High	2	650.80675	0.5	21.4568
LSKAIHKSFLVNEEGSEAAAVSGMIAISRMAVL	2xDimethyl [K3; K7]	1	3	3614.92845	High	5	723.79231	1.1	31.0114
EPLVKAQLVEEW	1xDimethyl [K5]	1	2	1468.80461	High	2	734.90579	-0.21	24.7456
LPRFTVEQEIDLKDV		1	3	1915.0535	High	3	639.02341	1.14	28.4669
QVLEIPYEGDEISMML	2xOxidation [M14; M15]	1	2	1898.87619	High	2	949.94357	1.94	31.9868
ALINAVYFKGNW	1xDimethyl [K9]	1	3	1423.77325	High	2	712.39025	-0.02	27.1726

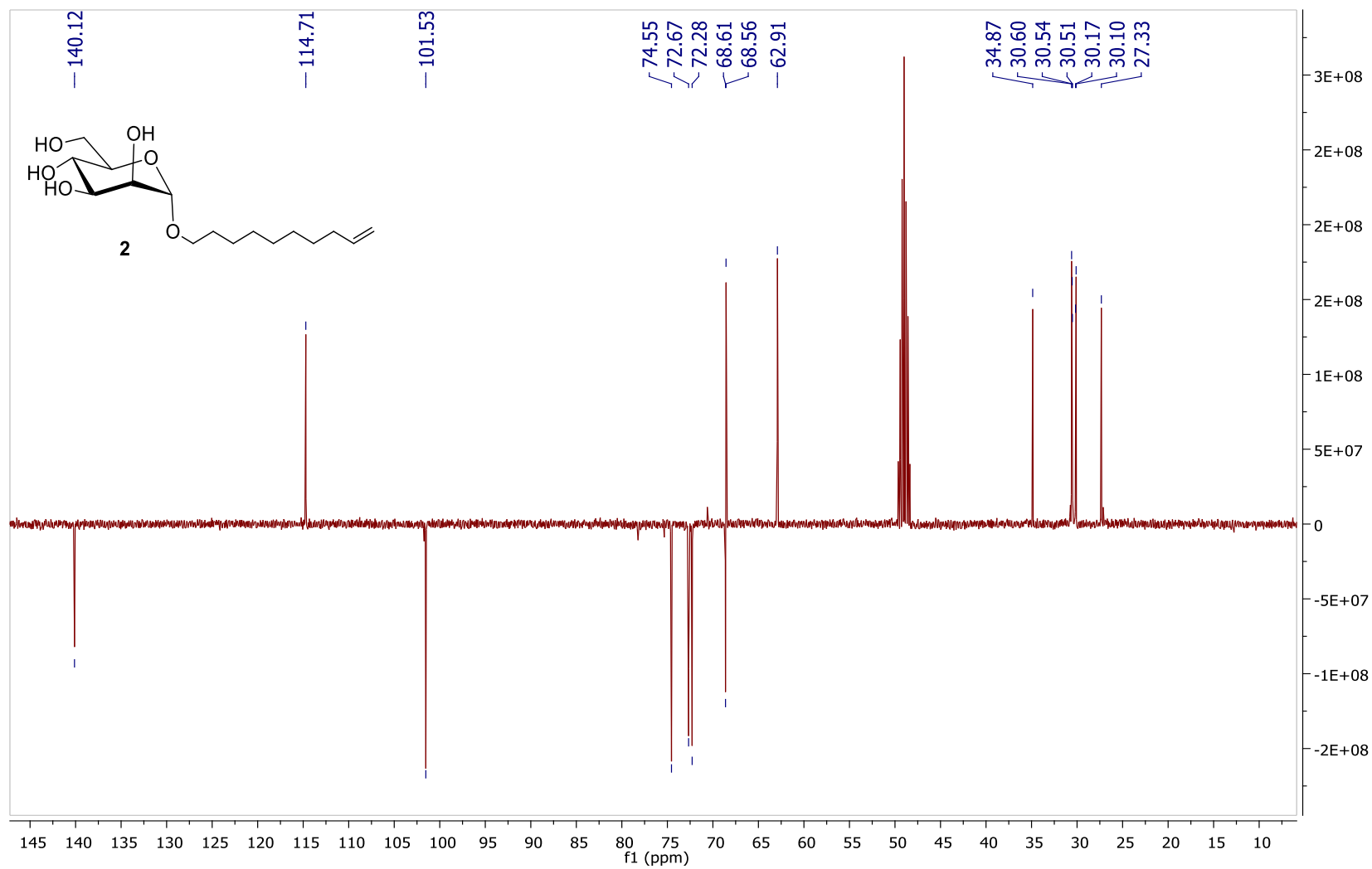
**6.6 Alkenyl- $\alpha$ -D-mannopyranosides NMR spectra.** NMR spectra of compounds 1-4 are reported below as  $^1\text{H}$  (first) and  $^{13}\text{C}$  NMR (second) spectra.

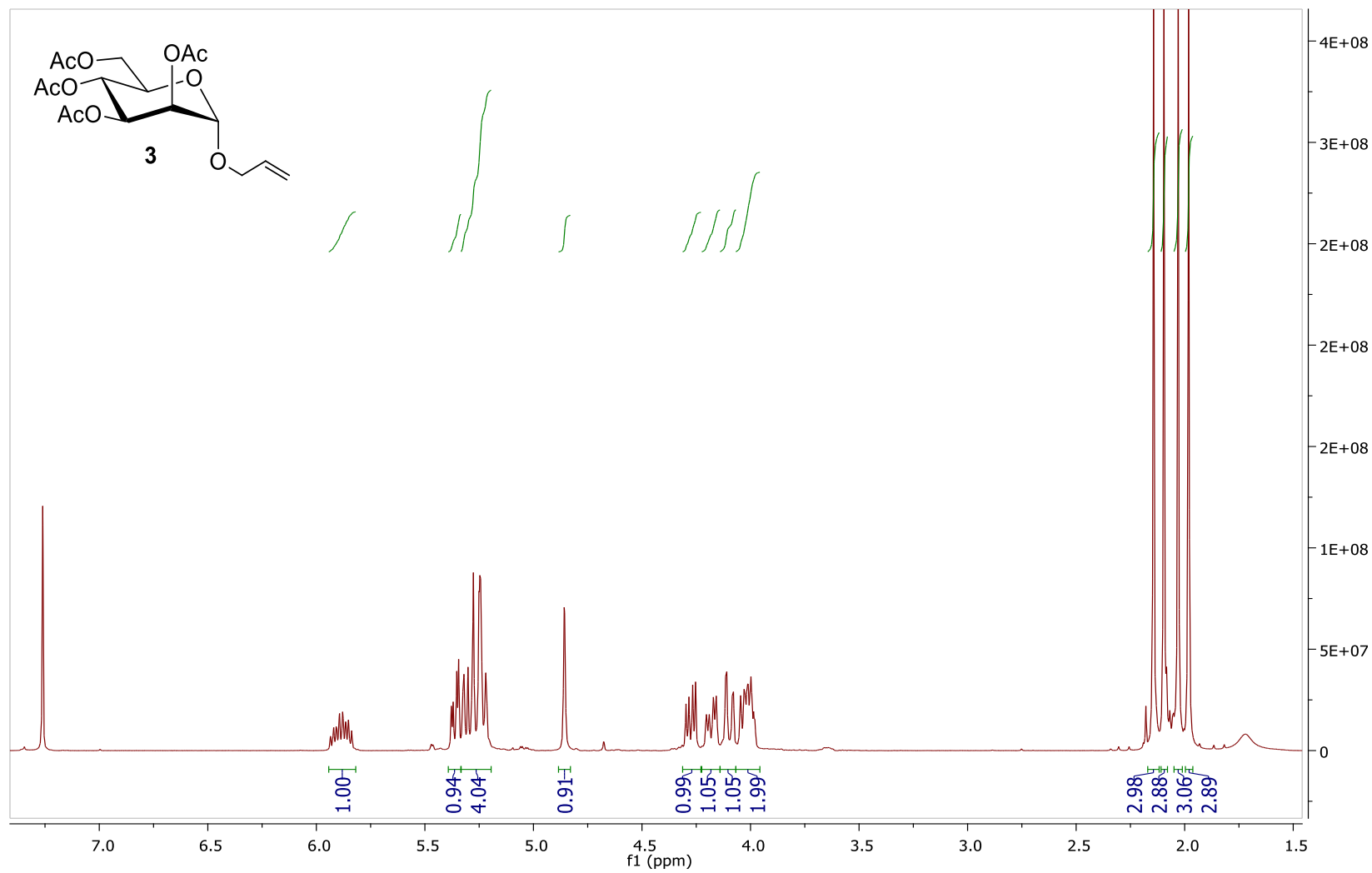


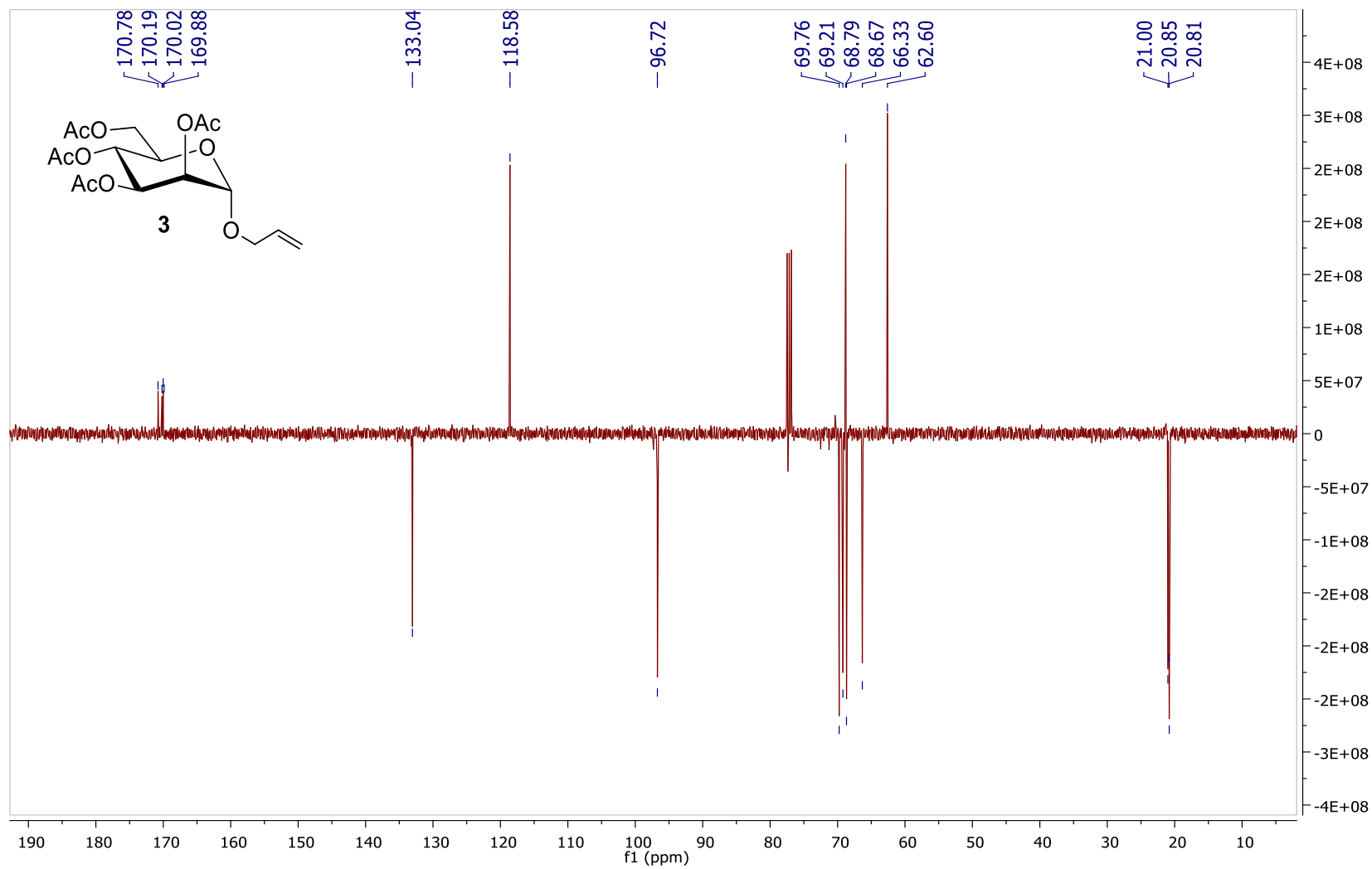


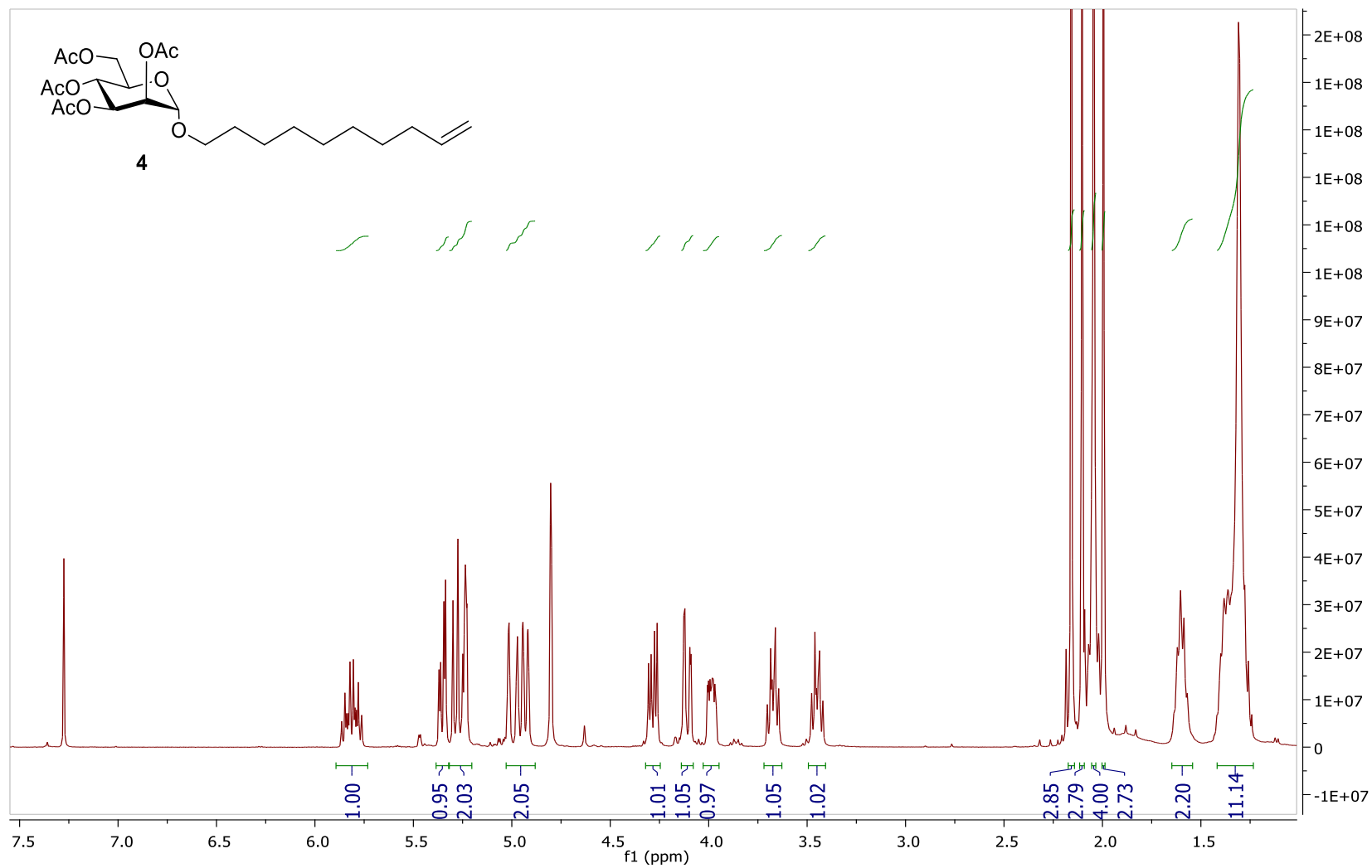


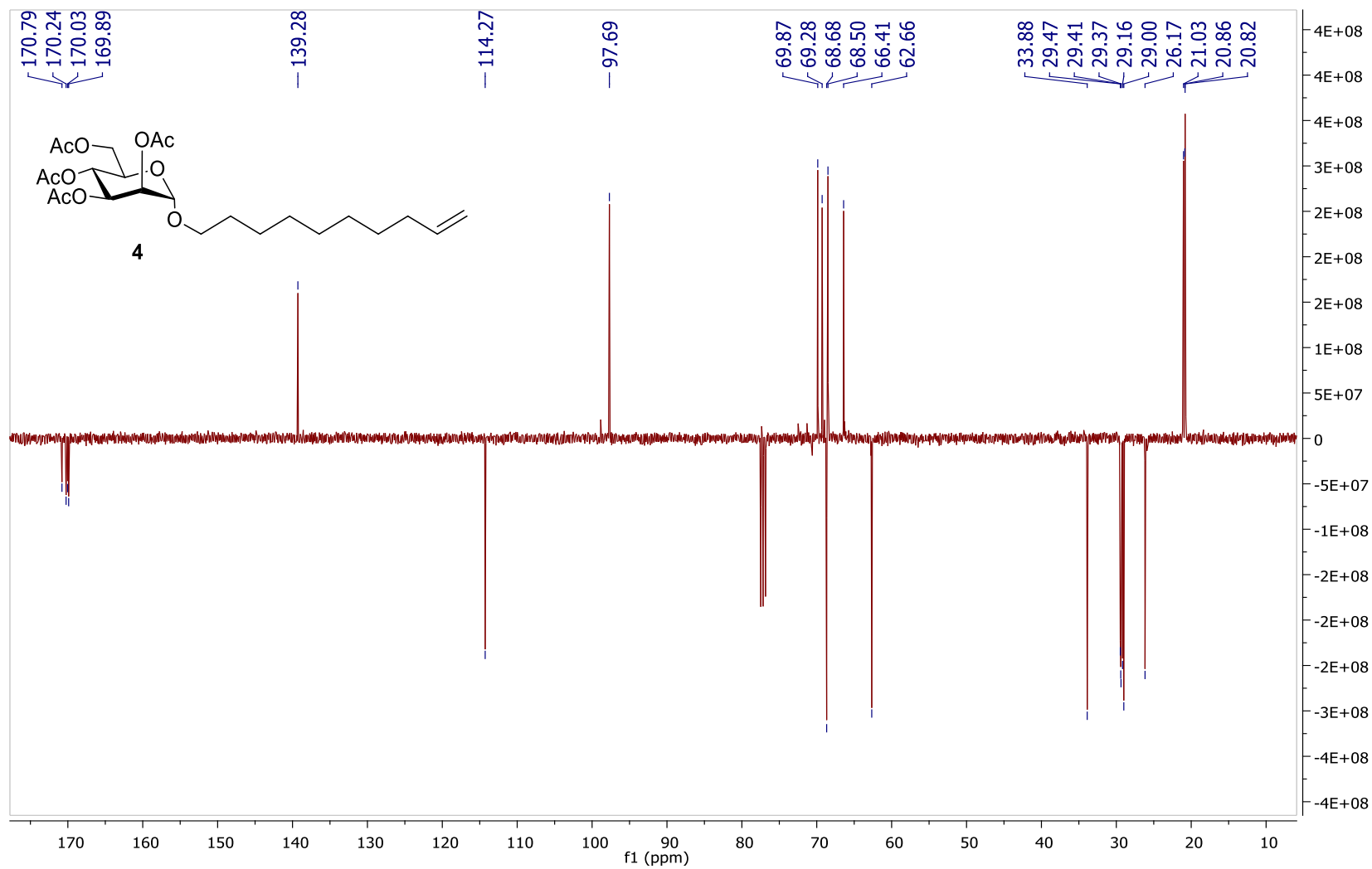












## 7. BIBLIOGRAPHY.

- (1) Varki, A.; Cummings, R. D.; Esko, J. D.; Stanley, P.; Hart, G. W.; Aebi, M.; Darvill, A. G.; Kinoshita, T.; Packer, N. H.; Prestegard, J. H.; et al. *Essentials of Glycobiology*; Cold Spring Harbor Laboratory Press, 2017.
- (2) Eichler, J.; Koomey, M. Sweet New Roles for Protein Glycosylation in Prokaryotes. *Trends Microbiol.* **2017**, *25* (8), 662–672.
- (3) Hudak, J. E.; Bertozzi, C. R. Glycotherapy: New Advances Inspire a Reemergence of Glycans in Medicine. *Chemistry and Biology*. 2014, pp 16–37.
- (4) Becker, B.; Cooper, M. A. Aminoglycoside Antibiotics in the 21st Century. *ACS Chem. Biol.* **2013**, *8* (1), 105–115.
- (5) von Itzstein, M.; Wu, W.-Y.; Kok, G. B.; Pegg, M. S.; Dyason, J. C.; Jin, B.; Van Phan, T.; Smythe, M. L.; White, H. F.; Oliver, S. W.; et al. Rational Design of Potent Sialidase-Based Inhibitors of Influenza Virus Replication. *Nature* **1993**, *363* (6428), 418–423.
- (6) Miglitol: MedlinePlus Drug Information  
<https://medlineplus.gov/druginfo/meds/a601079.html> (accessed Sep 26, 2019).
- (7) Abian, O.; Alfonso, P.; Velazquez-Campoy, A.; Giraldo, P.; Pocovi, M.; Sancho, J. Therapeutic Strategies for Gaucher Disease: Miglustat (NB-DNJ) as a Pharmacological Chaperone for Glucocerebrosidase and the Different Thermostability of Velaglucerase Alfa and Imiglucerase. *Mol. Pharm.* **2011**, *8* (6), 2390–2397.
- (8) Ada, G.; Isaacs, D. Carbohydrate—Protein Conjugate Vaccines. *Clin. Microbiol. Infect.* **2003**, *9* (2), 79–85.
- (9) Verez-Bencomo, V.; Fernández-Santana, V.; Hardy, E.; Toledo, M. E.; Rodríguez, M. C.; Heynngnezz, L.; Rodríguez, A.; Baly, A.; Herrera, L.; Izquierdo, M.; et al. A Synthetic Conjugate Polysaccharide Vaccine Against Haemophilus Influenzae Type B. *Science (80- )*. **2004**, *305* (5683), 522–525.
- (10) Aussedat, B.; Vohra, Y.; Park, P. K.; Fernández-Tejada, A.; Alam, S. M.; Dennison, S. M.; Jaeger, F. H.; Anasti, K.; Stewart, S.; Blinn, J. H.; et al. Chemical Synthesis of Highly Congested Gp120 V1V2 N-Glycopeptide Antigens for Potential HIV-1-Directed Vaccines.

- J. Am. Chem. Soc.* **2013**, *135* (35), 13113–13120.
- (11) Dimitrov, D. S. Therapeutic Proteins. In *Methods in molecular biology* (Clifton, N.J.); 2012; Vol. 899, pp 1–26.
  - (12) Seeberger, P. H.; Cummings, R. D. Glycans in Biotechnology and the Pharmaceutical Industry. In *Essentials of Glycobiology*; Cold Spring Harbor Laboratory Press, 2017.
  - (13) Apweiler, R.; Hermjakob, H.; Sharon, N. On the Frequency of Protein Glycosylation, as Deduced from Analysis of the SWISS-PROT Database. *Biochim. Biophys. Acta* **1999**, *1473* (1), 4–8.
  - (14) Sethuraman, N.; Stadheim, T. A. Challenges in Therapeutic Glycoprotein Production. *Curr. Opin. Biotechnol.* **2006**, *17* (4), 341–346.
  - (15) Arnold, J. N.; Wormald, M. R.; Sim, R. B.; Rudd, P. M.; Dwek, R. A. The Impact of Glycosylation on the Biological Function and Structure of Human Immunoglobulins. *Annu. Rev. Immunol.* **2007**, *25* (1), 21–50.
  - (16) Hossler, P.; Khattak, S. F.; Li, Z. J. Optimal and Consistent Protein Glycosylation in Mammalian Cell Culture. *Glycobiology* **2009**, *19* (9), 936–949.
  - (17) Gupta, S. K.; Shukla, P. Glycosylation Control Technologies for Recombinant Therapeutic Proteins. *Appl. Microbiol. Biotechnol.* **2018**, *102* (24), 10457–10468.
  - (18) Mastrangeli, R.; Palinsky, W.; Bierau, H. Glycoengineered Antibodies: Towards the next-Generation of Immunotherapeutics. *Glycobiology* **2019**, *29* (3), 199–210.
  - (19) Shepard, H. M.; Phillips, G. L.; D Thanos, C.; Feldmann, M. Developments in Therapy with Monoclonal Antibodies and Related Proteins. *Clin. Med. (Northfield. Il)*. **2017**, *17* (3), 220–232.
  - (20) Matucci, A.; Cammelli, D.; Cantini, F.; Goletti, D.; Marino, V.; Milano, G. M.; Scarpa, R.; Tocci, G.; Maggi, E.; Vultaggio, A. Influence of Anti-TNF Immunogenicity on Safety in Rheumatic Disease: A Narrative Review. *Expert Opin. Drug Saf.* **2016**, *15* (sup1), 3–10.
  - (21) Davis, C.; Naci, H.; Gurpinar, E.; Poplavska, E.; Pinto, A.; Aggarwal, A. Availability of Evidence of Benefits on Overall Survival and Quality of Life of Cancer Drugs Approved

- by European Medicines Agency: Retrospective Cohort Study of Drug Approvals 2009-13. *BMJ* **2017**, *359*, j4530.
- (22) Kim, C.; Prasad, V. Strength of Validation for Surrogate End Points Used in the US Food and Drug Administration's Approval of Oncology Drugs. *Mayo Clin. Proc.* **2016**, *91* (6), 713–725.
- (23) Moremen, K. W.; Tiemeyer, M.; Nairn, A. V. Vertebrate Protein Glycosylation: Diversity, Synthesis and Function. *Nat. Rev. Mol. Cell Biol.* **2012**, *13* (7), 448–462.
- (24) Patnaik, S. K.; Stanley, P. Lectin-Resistant CHO Glycosylation Mutants. In *Methods in enzymology*; 2006; Vol. 416, pp 159–182.
- (25) Metzler, M.; Gertz, A.; Sarkar, M.; Schachter, H.; Schrader, J. W.; Marth, J. D. Complex Asparagine-Linked Oligosaccharides Are Required for Morphogenic Events during Post-Implantation Development. *EMBO J.* **1994**, *13* (9), 2056–2065.
- (26) Ioffe, E.; Stanley, P. Mice Lacking N-Acetylglucosaminyltransferase I Activity Die at Mid-Gestation, Revealing an Essential Role for Complex or Hybrid N-Linked Carbohydrates. *Proc. Natl. Acad. Sci. U. S. A.* **1994**, *91* (2), 728–732.
- (27) Freeze, H. H.; Schachter, H.; Kinoshita, T. Genetic Disorders of Glycosylation. In *Essentials of Glycobiology*; Cold Spring Harbor (NY): Cold Spring Harbor Laboratory Press, 2017.
- (28) Freeze, H. H.; Hart, G. W.; Schnaar, R. L. Glycosylation Precursors. In *Essentials of Glycobiology*; Cold Spring Harbor Laboratory Press, 2017.
- (29) Cummings, R. D. The Repertoire of Glycan Determinants in the Human Glycome. *Mol. Biosyst.* **2009**, *5* (10), 1087.
- (30) Aoki, K. F.; Yamaguchi, A.; Okuno, Y.; Akutsu, T.; Ueda, N.; Kanehisa, M.; Mamitsuka, H. Efficient Tree-Matching Methods for Accurate Carbohydrate Database Queries. *Genome Inform.* **2003**, *14*, 134–143.
- (31) Stanley, P.; Taniguchi, N.; Aebi, M. N-Glycans. In *Essentials of Glycobiology*; Varki A, Cummings RD, Esko JD, et al., Ed.; Cold Spring Harbor Laboratory Press, 2017.
- (32) Schachter, H. The “yellow Brick Road” to Branched Complex N-Glycans. *Glycobiology* **1991**,



- 1 (5), 453–461.
- (33) Zacchi, L. F.; Schulz, B. L. N-Glycoprotein Macroheterogeneity: Biological Implications and Proteomic Characterization. *Glycoconj. J.* **2016**, *33* (3), 359–376.
- (34) Stanley, P.; Cummings, R. D. Structures Common to Different Glycans. In *Essentials of Glycobiology*; Cold Spring Harbor (NY): Cold Spring Harbor Laboratory Press, 2017.
- (35) Dennis, J. W.; Nabi, I. R.; Demetriou, M. Metabolism, Cell Surface Organization, and Disease. *Cell* **2009**, *139* (7), 1229–1241.
- (36) German, J. B.; Freeman, S. L.; Lebrilla, C. B.; Mills, D. A. Human Milk Oligosaccharides: Evolution, Structures and Bioselectivity as Substrates for Intestinal Bacteria. In *Personalized Nutrition for the Diverse Needs of Infants and Children*; KARGER: Basel, 2008; Vol. 62, pp 205–222.
- (37) Kronewitter, S. R.; An, H. J.; de Leoz, M. L.; Lebrilla, C. B.; Miyamoto, S.; Leiserowitz, G. S. The Development of Retrosynthetic Glycan Libraries to Profile and Classify the Human Serum N-Linked Glycome. *Proteomics* **2009**, *9* (11), 2986–2994.
- (38) Hong, Q.; Ruhaak, L. R.; Stroble, C.; Parker, E.; Huang, J.; Maverakis, E.; Lebrilla, C. B. A Method for Comprehensive Glycosite-Mapping and Direct Quantitation of Serum Glycoproteins. *J. Proteome Res.* **2015**, *14* (12), 5179–5192.
- (39) Chen, Y.-J.; Wing, D. R.; Guile, G. R.; Dwek, R. A.; Harvey, D. J.; Zamze, S. Neutral N-Glycans in Adult Rat Brain Tissue. Complete Characterisation Reveals Fucosylated Hybrid and Complex Structures. *Eur. J. Biochem.* **1998**, *251* (3), 691–703.
- (40) Wu, S.; Grimm, R.; German, J. B.; Lebrilla, C. B. Annotation and Structural Analysis of Sialylated Human Milk Oligosaccharides. *J. Proteome Res.* **2011**, *10* (2), 856–868.
- (41) Wu, S.; Tao, N.; German, J. B.; Grimm, R.; Lebrilla, C. B. Development of an Annotated Library of Neutral Human Milk Oligosaccharides. *J. Proteome Res.* **2010**, *9* (8), 4138–4151.
- (42) Dennis, J. W.; Lau, K. S.; Demetriou, M.; Nabi, I. R. Adaptive Regulation at the Cell Surface by N-Glycosylation. *Traffic* **2009**, *10* (11), 1569–1578.
- (43) Varki, A. Biological Roles of Oligosaccharides: All of the Theories Are Correct. *Glycobiology*

- 1993, 3 (2), 97–130.
- (44) Haltiwanger, R. S.; Lowe, J. B. Role of Glycosylation in Development. *Annu. Rev. Biochem.* **2004**, 73 (1), 491–537.
- (45) Šebestík, J.; Reiniš, M.; Ježek, J. Sugar Code (Glycocode). In *Biomedical Applications of Peptide-, Glyco- and Glycopeptide Dendrimers, and Analogous Dendrimeric Structures*; Springer, Vienna, 2012; pp 23–27.
- (46) Gabius, H.; Roth, J. An Introduction to the Sugar Code. *Histochem. Cell Biol.* **2017**, 147, 111–117.
- (47) Gabius, H.-J. The Sugar Code: Why Glycans Are so Important. *BioSystems* **2017**.
- (48) Scott, H.; Panin, V. M. N-Glycosylation in Regulation of the Nervous System. In *Glycobiology of the nervous system*; Springer, New York, NY, 2015; pp 367–394.
- (49) Higuero, A. M.; Díez-Revuelta, N.; Abad-Rodríguez, J. The Sugar Code in Neuronal Physiology. *Histochem. Cell Biol.* **2017**, 147, 257–267.
- (50) Freeze, H. H.; Eklund, E. A.; Ng, B. G.; Patterson, M. C. Neurological Aspects of Human Glycosylation Disorders. *Annu. Rev. Neurosci.* **2015**, 38, 105–125.
- (51) Abou-Abbass, H.; Abou-El-Hassan, H.; Bahmad, H.; Zibara, K.; Zebian, A.; Youssef, R.; Ismail, J.; Zhu, R.; Zhou, S.; Dong, X.; et al. Glycosylation and Other PTMs Alterations in Neurodegenerative Diseases: Current Status and Future Role in Neurotrauma. *Electrophoresis* **2016**, 37 (11), 1549–1561.
- (52) Frenkel-Pinter, M.; Shmueli, M. D.; Raz, C.; Yanku, M.; Zilberzwige, S.; Gazit, E.; Segal, D. Interplay between Protein Glycosylation Pathways in Alzheimer's Disease. *Sci. Adv.* **2017**, 3 (9), e1601576.
- (53) Zhou, T.-T.; Zhang, Z.-W.; Liu, J.; Zhang, J.-P.; Jiao, B.-H. Glycosylation of the Sodium Channel B4 Subunit Is Developmentally Regulated and Involves in Neuritic Degeneration. *Int. J. Biol. Sci.* **2012**, 8 (5), 630–639.
- (54) Yi, C.-W.; Wang, L.-Q.; Huang, J.-J.; Pan, K.; Chen, J.; Liang, Y. Glycosylation Significantly Inhibits the Aggregation of Human Prion Protein and Decreases Its Cytotoxicity. *Sci. Rep.*

- 2018, 8 (1), 13486.
- (55) Freeze, H. H.; Eklund, E. A.; Ng, B. G.; Patterson, M. C. Neurology of Inherited Glycosylation Disorders. *Lancet Neurol.* **2012**, 11 (5), 453–466.
- (56) Lowe, J. B.; Marth, J. D. A Genetic Approach to Mammalian Glycan Function. *Annu. Rev. Biochem.* **2003**, 72 (1), 643–691.
- (57) Ye, Z.; Marth, J. D. N-Glycan Branching Requirement in Neuronal and Postnatal Viability. *Glycobiology* **2004**, 14 (6), 547–558.
- (58) Davies, L. R. L.; Varki, A. Why Is N-Glycolylneuraminic Acid Rare in the Vertebrate Brain? *Top Curr Chem.* **2015**, 366, 31–54.
- (59) Naito-Matsui, Y.; Davies, L. R. L.; Takematsu, H.; Chou, H.-H.; Tangvoranuntakul, P.; Carlin, A. F.; Verhagen, A.; Heyser, C. J.; Yoo, S.-W.; Choudhury, B.; et al. Physiological Exploration of the Long Term Evolutionary Selection against Expression of N-Glycolylneuraminic Acid in the Brain. *J. Biol. Chem.* **2017**, 292 (7), 2557–2570.
- (60) Varki, A.; Schnaar, R. L.; Schauer, R. Sialic Acids and Other Nonulosonic Acids. In *Essentials of Glycobiology*; Cold Spring Harbor (NY): Cold Spring Harbor Laboratory Press, 2017.
- (61) Sato, C.; Kitajima, K. Disialic, Oligosialic and Polysialic Acids: Distribution, Functions and Related Disease. *J. Biochem.* **2013**, 154 (2), 115–136.
- (62) Colley, K. J. Structural Basis for the Polysialylation of the Neural Cell Adhesion Molecule. In *Advances in experimental medicine and biology*; 2010; Vol. 663, pp 111–126.
- (63) Mühlenhoff, M.; Oltmann-Norden, I.; Weinhold, B.; Hildebrandt, H.; Gerardy-Schahn, R. Brain Development Needs Sugar: The Role of Polysialic Acid in Controlling NCAM Functions. *Biol. Chem.* **2009**, 390 (7), 567–574.
- (64) Rutishauser, U. Polysialic Acid in the Plasticity of the Developing and Adult Vertebrate Nervous System. *Nat. Rev. Neurosci.* **2008**, 9 (1), 26–35.
- (65) Angata, K.; Huckaby, V.; Ranscht, B.; Terskikh, A.; Marth, J. D.; Fukuda, M. Polysialic Acid-Directed Migration and Differentiation of Neural Precursors Are Essential for Mouse

- Brain Development. *Mol. Cell. Biol.* **2007**, 27 (19), 6659–6668.
- (66) Weinhold, B.; Seidenfaden, R.; Röckle, I.; Mühlenhoff, M.; Schertzinger, F.; Conzelmann, S.; Marth, J. D.; Gerardy-Schahn, R.; Hildebrandt, H. Genetic Ablation of Polysialic Acid Causes Severe Neurodevelopmental Defects Rescued by Deletion of the Neural Cell Adhesion Molecule. *J. Biol. Chem.* **2005**, 280 (52), 42971–42977.
- (67) Sato, C.; Kitajima, K. Sialic Acids in Neurology. In *Advances in carbohydrate chemistry and biochemistry*; 2019; Vol. 76, pp 1–64.
- (68) Henion, T. R.; Schwarting, G. A. N-Linked Polylactosamine Glycan Synthesis Is Regulated by Co-Expression of B3GnT2 and GCNT2. *J. Cell. Physiol.* **2014**, 229 (4), 471–478.
- (69) Henion, T. R.; Faden, A. A.; Knott, T. K.; Schwarting, G. A. B3GnT2 Maintains Adenylyl Cyclase-3 Signaling and Axon Guidance Molecule Expression in the Olfactory Epithelium. *J. Neurosci.* **2011**, 31 (17), 6576–6586.
- (70) Henion, T. R.; Madany, P. A.; Faden, A. A.; Schwarting, G. A. B3GnT2 Null Mice Exhibit Defective Accessory Olfactory Bulb Innervation. *Mol. Cell. Neurosci.* **2013**, 52, 73–86.
- (71) Abo, T.; Balch, C. M. A Differentiation Antigen of Human NK and K Cells Identified by a Monoclonal Antibody (HNK-1). *J. Immunol.* **1981**, 127 (3), 1024–1029.
- (72) Kleene, R.; Schachner, M. Glycans and Neural Cell Interactions. *Nat. Rev. Neurosci.* **2004**, 5 (3), 195–208.
- (73) Yanagisawa, M.; Taga, T.; Nakamura, K.; Ariga, T.; Yu, R. K. Characterization of Glycoconjugate Antigens in Mouse Embryonic Neural Precursor Cells. *J. Neurochem.* **2005**, 95 (5), 1311–1320.
- (74) Morise, J.; Takematsu, H.; Oka, S. The Role of Human Natural Killer-1 (HNK-1) Carbohydrate in Neuronal Plasticity and Disease. *Biochim. Biophys. Acta. Gen. Subj.* **2017**, 1861 (10), 2455–2461.
- (75) Yamamoto, S.; Oka, S.; Inoue, M.; Shimuta, M.; Manabe, T.; Takahashi, H.; Miyamoto, M.; Asano, M.; Sakagami, J.; Sudo, K.; et al. Mice Deficient in Nervous System-Specific Carbohydrate Epitope HNK-1 Exhibit Impaired Synaptic Plasticity and Spatial Learning. *J. Biol. Chem.* **2002**, 277 (30), 27227–27231.

- (76) Rollenhagen, A.; Czaniera, R.; Albert, M.; Wintergerst, E. S.; Schachner, M. Immunocytological Localization of the HNK-1 Carbohydrate in Murine Cerebellum, Hippocampus and Spinal Cord Using Monoclonal Antibodies with Different Epitope Specificities. *J. Neurocytol.* **2001**, *30* (4), 337–351.
- (77) Morita, I.; Kakuda, S.; Takeuchi, Y.; Itoh, S.; Kawasaki, N.; Kizuka, Y.; Kawasaki, T.; Oka, S. HNK-1 Glyco-Epitope Regulates the Stability of the Glutamate Receptor Subunit GluR2 on the Neuronal Cell Surface. *J. Biol. Chem.* **2009**, *284* (44), 30209–30217.
- (78) Nakamura, A.; Morise, J.; Yabuno-Nakagawa, K.; Hashimoto, Y.; Takematsu, H.; Oka, S. Site-Specific HNK-1 Epitope on Alternatively Spliced Fibronectin Type-III Repeats in Tenascin-C Promotes Neurite Outgrowth of Hippocampal Neurons through Contactin-1. *PLoS One* **2019**, *14* (1), e0210193.
- (79) Senn, C.; Kutsche, M.; Saghatelian, A.; Bösl, M. R.; Löhler, J.; Bartsch, U.; Morellini, F.; Schachner, M. Mice Deficient for the HNK-1 Sulfotransferase Show Alterations in Synaptic Efficacy and Spatial Learning and Memory. *Mol. Cell. Neurosci.* **2002**, *20* (4), 712–729.
- (80) Gurevicius, K.; Gureviciene, I.; Sivukhina, E.; Irintchev, A.; Schachner, M.; Tanila, H. Increased Hippocampal and Cortical Beta Oscillations in Mice Deficient for the HNK-1 Sulfotransferase. *Mol. Cell. Neurosci.* **2007**, *34* (2), 189–198.
- (81) Yoshihara, T.; Sugihara, K.; Kizuka, Y.; Oka, S.; Asano, M. Learning/Memory Impairment and Reduced Expression of the HNK-1 Carbohydrate in B4-Galactosyltransferase-II-Deficient Mice. *J. Biol. Chem.* **2009**, *284* (18), 12550–12561.
- (82) Traynelis, S. F.; Wollmuth, L. P.; McBain, C. J.; Menniti, F. S.; Vance, K. M.; Ogden, K. K.; Hansen, K. B.; Yuan, H.; Myers, S. J.; Dingledine, R. Glutamate Receptor Ion Channels: Structure, Regulation, and Function. *Pharmacol. Rev.* **2010**, *62* (3), 405–496.
- (83) Sumikawa, K.; Parker, I.; Miledi, R. Effect of Tunicamycin on the Expression of Functional Brain Neurotransmitter Receptors and Voltage-Operated Channels in *Xenopus* Oocytes. *Brain Res.* **1988**, *464* (3), 191–199.
- (84) Everts, I.; Villmann, C.; Hollmann, M. N-Glycosylation Is Not a Prerequisite for Glutamate Receptor Function but Is Essential for Lectin Modulation. *Mol. Pharmacol.* **1997**, *52* (5), 861–873.

- (85) Gill, M. B.; Vivithanaporn, P.; Swanson, G. T. Glutamate Binding and Conformational Flexibility of Ligand-Binding Domains Are Critical Early Determinants of Efficient Kainate Receptor Biogenesis. *J. Biol. Chem.* **2009**, *284* (21), 14503–14512.
- (86) Nanao, M. H.; Green, T.; Stern-Bach, Y.; Heinemann, S. F.; Choe, S. Structure of the Kainate Receptor Subunit GluR6 Agonist-Binding Domain Complexed with Domoic Acid. *Proc. Natl. Acad. Sci.* **2005**, *102* (5), 1708–1713.
- (87) Everts, I.; Petroski, R.; Kizelsztejn, P.; Teichberg, V. I.; Heinemann, S. F.; Hollmann, M. Lectin-Induced Inhibition of Desensitization of the Kainate Receptor GluR6 Depends on the Activation State and Can Be Mediated by a Single Native or Ectopic N-Linked Carbohydrate Side Chain. *J. Neurosci.* **1999**, *19* (3), 916–927.
- (88) Chen, L. In Pursuit of the High-Resolution Structure of Nicotinic Acetylcholine Receptors. *J. Physiol.* **2010**, *588* (Pt 4), 557–564.
- (89) Miwa, J. M.; Freedman, R.; Lester, H. A. Neural Systems Governed by Nicotinic Acetylcholine Receptors: Emerging Hypotheses. *Neuron* **2011**, *70* (1), 20–33.
- (90) Gehle, V. M.; Walcott, E. C.; Nishizaki, T.; Sumikawa, K. N-Glycosylation at the Conserved Sites Ensures the Expression of Properly Folded Functional ACh Receptors. *Brain Res. Mol. Brain Res.* **1997**, *45* (2), 219–229.
- (91) Chen, D.; Dang, H.; Patrick, J. W. Contributions of N-Linked Glycosylation to the Expression of a Functional Alpha7-Nicotinic Receptor in *Xenopus* Oocytes. *J. Neurochem.* **1998**, *70* (1), 349–357.
- (92) Nishizaki, T. N-Glycosylation Sites on the Nicotinic ACh Receptor Subunits Regulate Receptor Channel Desensitization and Conductance. *Brain Res. Mol. Brain Res.* **2003**, *114* (2), 172–176.
- (93) daCosta, C. J. B.; Kaiser, D. E. E.; Baenziger, J. E. Role of Glycosylation and Membrane Environment in Nicotinic Acetylcholine Receptor Stability. *Biophys. J.* **2005**, *88* (3), 1755–1764.
- (94) Dellisanti, C. D.; Yao, Y.; Stroud, J. C.; Wang, Z.-Z.; Chen, L. Crystal Structure of the Extracellular Domain of NACHR A1 Bound to  $\alpha$ -Bungarotoxin at 1.94 Å Resolution. *Nat.*

- Neurosci.* **2007**, *10* (8), 953–962.
- (95) Janz, R.; Goda, Y.; Geppert, M.; Missler, M.; Südhof, T. C. SV2A and SV2B Function as Redundant Ca<sup>2+</sup> Regulators in Neurotransmitter Release. *Neuron* **1999**, *24* (4), 1003–1016.
- (96) Chang, W.-P.; Südhof, T. C. SV2 Renders Primed Synaptic Vesicles Competent for Ca<sup>2+</sup> - Induced Exocytosis. *J. Neurosci.* **2009**, *29* (4), 883–897.
- (97) Kwon, S. E.; Chapman, E. R. Glycosylation Is Dispensable for Sorting of Synaptotagmin 1 but Is Critical for Targeting of SV2 and Synaptophysin to Recycling Synaptic Vesicles. *J. Biol. Chem.* **2012**, *287* (42), 35658–35668.
- (98) Caterina, M. J.; Schumacher, M. A.; Tominaga, M.; Rosen, T. A.; Levine, J. D.; Julius, D. The Capsaicin Receptor: A Heat-Activated Ion Channel in the Pain Pathway. *Nature* **1997**, *389* (6653), 816–824.
- (99) Veldhuis, N. A.; Lew, M. J.; Abogadie, F. C.; Poole, D. P.; Jennings, E. A.; Ivanusic, J. J.; Eilers, H.; Bunnett, N. W.; McIntyre, P. N-Glycosylation Determines Ionic Permeability and Desensitization of the TRPV1 Capsaicin Receptor. *J. Biol. Chem.* **2012**, *287* (26), 21765–21772.
- (100) Pertusa, M.; Madrid, R.; Morenilla-Palao, C.; Belmonte, C.; Viana, F. N-Glycosylation of TRPM8 Ion Channels Modulates Temperature Sensitivity of Cold Thermoreceptor Neurons. *J. Biol. Chem.* **2012**, *287* (22), 18218–18229.
- (101) Lazniewska, J.; Weiss, N. Glycosylation of Voltage-Gated Calcium Channels in Health and Disease. *Biochim. Biophys. Acta - Biomembr.* **2017**, *1859* (5), 662–668.
- (102) Weiss, N.; Black, S. A. G.; Bladen, C.; Chen, L.; Zamponi, G. W. Surface Expression and Function of Cav3.2 T-Type Calcium Channels Are Controlled by Asparagine-Linked Glycosylation. *Pflugers Arch.* **2013**, *465* (8), 1159–1170.
- (103) Montpetit, M. L.; Stocker, P. J.; Schwetz, T. A.; Harper, J. M.; Norring, S. A.; Schaffer, L.; North, S. J.; Jang-Lee, J.; Gilmartin, T.; Head, S. R.; et al. Regulated and Aberrant Glycosylation Modulate Cardiac Electrical Signaling. *Proc. Natl. Acad. Sci.* **2009**, *106* (38), 16517–16522.
- (104) Ednie, A. R.; Parrish, A. R.; Sonner, M. J.; Bennett, E. S. Reduced Hybrid/Complex N-



- Glycosylation Disrupts Cardiac Electrical Signaling and Calcium Handling in a Model of Dilated Cardiomyopathy. *J. Mol. Cell. Cardiol.* **2019**, *132*, 13–23.
- (105) Vicente, P. C.; Kim, J. Y.; Ha, J.-J.; Song, M.-Y.; Lee, H.-K.; Kim, D.-H.; Choi, J.-S.; Park, K.-S. Identification and Characterization of Site-Specific N-Glycosylation in the Potassium Channel Kv3.1b. *J. Cell. Physiol.* **2018**, *233* (1), 549–558.
- (106) Ednie, A. R.; Bennett, E. S. Modulation of Voltage-Gated Ion Channels by Sialylation. In *Comprehensive Physiology*; John Wiley & Sons, Inc.: Hoboken, NJ, USA, 2012; Vol. 2, pp 1269–1301.
- (107) Roberts, R. H.; Barchi, R. L. The Voltage-Sensitive Sodium Channel from Rabbit Skeletal Muscle. Chemical Characterization of Subunits. *J. Biol. Chem.* **1987**, *262* (5), 2298–2303.
- (108) Isaev, D.; Zhao, Q.; Kleen, J. K.; Lenck-Santini, P. P.; Adstamongkonkul, D.; Isaeva, E.; Holmes, G. L. Neuroaminidase Reduces Interictal Spikes in a Rat Temporal Lobe Epilepsy Model. *Epilepsia* **2011**, *52* (3), e12–e15.
- (109) Isaeva, E.; Lushnikova, I.; Savrasova, A.; Skibo, G.; Holmes, G. L.; Isaev, D. Blockade of Endogenous Neuraminidase Leads to an Increase of Neuronal Excitability and Activity-Dependent Synaptogenesis in the Rat Hippocampus. *Eur. J. Neurosci.* **2010**, *32* (11), 1889–1896.
- (110) Murray, H. C.; Low, V. F.; Swanson, M. E. V; Dieriks, B. V; Turner, C.; Faull, R. L. M.; Curtis, M. A. Distribution of PSA-NCAM in Normal, Alzheimer’s and Parkinson’s Disease Human Brain. *Neuroscience* **2016**, *330*, 359–375.
- (111) Schedin-Weiss, S.; Winblad, B.; Tjernberg, L. O. The Role of Protein Glycosylation in Alzheimer Disease. *FEBS J.* **2014**, *281* (1), 46–62.
- (112) Sato, Y.; Naito, Y.; Grundke-Iqbal, I.; Iqbal, K.; Endo, T. Analysis of N-Glycans of Pathological Tau: Possible Occurrence of Aberrant Processing of Tau in Alzheimer’s Disease. *FEBS Lett.* **2001**, *496* (2–3), 152–160.
- (113) Gizaw, S. T.; Koda, T.; Amano, M.; Kamimura, K.; Ohashi, T.; Hinou, H.; Nishimura, S.-I. A Comprehensive Glycome Profiling of Huntington’s Disease Transgenic Mice. *Biochim. Biophys. Acta* **2015**, *1850* (9), 1704–1718.



- (114) Edri-Brami, M.; Rosental, B.; Hayoun, D.; Welt, M.; Rosen, H.; Wirguin, I.; Nefussy, B.; Drory, V. E.; Porgador, A.; Lichtenstein, R. G. Glycans in Sera of Amyotrophic Lateral Sclerosis Patients and Their Role in Killing Neuronal Cells. *PLoS One* **2012**, *7* (5), e35772.
- (115) Charles, P.; Reynolds, R.; Seilhean, D.; Rougon, G.; Aigrot, M. S.; Niezgoda, A.; Zalc, B.; Lubetzki, C. Re-Expression of PSA-NCAM by Demyelinated Axons: An Inhibitor of Remyelination in Multiple Sclerosis? *Brain* **2002**, *125* (9), 1972–1979.
- (116) Stanta, J. L.; Saldova, R.; Struwe, W. B.; Byrne, J. C.; Leweke, F. M.; Rothermund, M.; Rahmoune, H.; Levin, Y.; Guest, P. C.; Bahn, S.; et al. Identification of N-Glycosylation Changes in the CSF and Serum in Patients with Schizophrenia. *J. Proteome Res.* **2010**, *9* (9), 4476–4489.
- (117) Barbeau, D.; Liang, J. J.; Robitalille, Y.; Quirion, R.; Srivastava, L. K. Decreased Expression of the Embryonic Form of the Neural Cell Adhesion Molecule in Schizophrenic Brains. *Proc. Natl. Acad. Sci. U. S. A.* **1995**, *92* (7), 2785–2789.
- (118) Bauer, D.; Haroutunian, V.; Meador-Woodruff, J. H.; McCullumsmith, R. E. Abnormal Glycosylation of EAAT1 and EAAT2 in Prefrontal Cortex of Elderly Patients with Schizophrenia. *Schizophr. Res.* **2010**, *117* (1), 92–98.
- (119) Tucholski, J.; Simmons, M. S.; Pinner, A. L.; Haroutunian, V.; McCullumsmith, R. E.; Meador-Woodruff, J. H. Abnormal N-Linked Glycosylation of Cortical AMPA Receptor Subunits in Schizophrenia. *Schizophr. Res.* **2013**, *146* (1–3), 177–183.
- (120) Tucholski, J.; Simmons, M. S.; Pinner, A. L.; McMillan, L. D.; Haroutunian, V.; Meador-Woodruff, J. H. N-Linked Glycosylation of Cortical N-Methyl-D-Aspartate and Kainate Receptor Subunits in Schizophrenia. *Neuroreport* **2013**, *24* (12), 688–691.
- (121) Toghi Eshghi, S.; Yang, S.; Wang, X.; Shah, P.; Li, X.; Zhang, H. Imaging of N-Linked Glycans from Formalin-Fixed Paraffin-Embedded Tissue Sections Using MALDI Mass Spectrometry. *ACS Chem. Biol.* **2014**, *9* (9), 2149–2156.
- (122) VanderMeulen, D. L.; Prasad, V. V. T. S.; Moskal, J. R. The Identification of Glioblastoma-Associated, Fucose-Containing Glycoproteins Induced by Retinoic Acid. In *Molecular and Chemical Neuropathology*; Humana Press, 1994; Vol. 21, pp 311–327.

- (123) Amoureux, M.-C.; Coulibaly, B.; Chinot, O.; Loundou, A.; Metellus, P.; Rougon, G.; Figarella-Branger, D. Polysialic Acid Neural Cell Adhesion Molecule (PSA-NCAM) Is an Adverse Prognosis Factor in Glioblastoma, and Regulates Olig2 Expression in Glioma Cell Lines. *BMC Cancer* **2010**, *10* (1), 91.
- (124) Rebbaa, A.; Chou, P. M.; Vucic, I.; Mirkin, B. L.; Tomita, T.; Bremer, E. G. Expression of Bisecting GlcNAc in Pediatric Brain Tumors and Its Association with Tumor Cell Response to Vinblastine. *Clin. Cancer Res.* **1999**, *5* (11), 3661–3668.
- (125) Gudelj, I.; Lauc, G.; Pezer, M. Immunoglobulin G Glycosylation in Aging and Diseases. *Cell. Immunol.* **2018**, *333*, 65–79.
- (126) Plomp, R.; Bondt, A.; De Haan, N.; Rombouts, Y.; Wuhrer, M. Recent Advances in Clinical Glycoproteomics of Immunoglobulins (Igs). *Mol. Cell. Proteomics* **2016**, *15* (7), 2217–2228.
- (127) Clerc, F.; Reiding, K. R.; Jansen, B. C.; Kammeijer, G. S. M.; Bondt, A.; Wuhrer, M. Human Plasma Protein N-Glycosylation. *Glycoconj J* **2016**, *33* (3), 309–343.
- (128) Young Choi, N.; Hwang, H.; Sun Ji, E.; Wook Park, G.; Yeon Lee, J.; Kyoung Lee, H.; Young Kim, J.; Shin Yoo, J. Direct Analysis of Site-Specific N-Glycopeptides of Serological Proteins in Dried Blood Spot Samples. *Anal. Bioanal. Chem.* **2017**, *409* (21), 4971–4981.
- (129) Wing, D. R.; Rademacher, T. W.; Field, M. C.; Dwek, R. A.; Schmitz, B.; Thor, G.; Schachner, M. Use of Large-Scale Hydrazinolysis in the Preparation of N-Linked Oligosaccharide Libraries: Application to Brain Tissue. *Glycoconj. J.* **1992**, *9* (6), 293–301.
- (130) Krusius, T.; Finne, J. Structural Features of Tissue Glycoproteins. Fractionation and Methylation Analysis of Glycopeptides Derived from Rat Brain, Kidney and Liver. *Eur. J. Biochem.* **1977**, *78* (2), 369–379.
- (131) Smalheiser, N. R.; Kim, E. Purification of Cranin, a Laminin Binding Membrane Protein. *J. Biol. Chem.* **1995**, *270* (25), 15425–15433.
- (132) Rose, S. P. Glycoproteins and Memory Formation. *Behav. Brain Res.* **1995**, *66* (1–2), 73–78.
- (133) Rose, S. P.; Jork, R. Long-Term Memory Formation in Chicks Is Blocked by 2-Deoxygalactose, a Fucose Analog. *Behav. Neural Biol.* **1987**, *48* (2), 246–258.

- (134) Bullock, S.; Rose, S. P.; Zamani, R. Characterisation and Regional Localisation of Pre- and Postsynaptic Glycoproteins of the Chick Forebrain Showing Changed Fucose Incorporation Following Passive Avoidance Training. *J. Neurochem.* **1992**, *58* (6), 2145–2154.
- (135) Zamze, S.; Harvey, D. J.; Chen, Y.-J.; Guile, G. R.; Dwek, R. A.; Wing, D. R. Sialylated N-Glycans in Adult Rat Brain Tissue. A Widespread Distribution of Disialylated Antennae in Complex and Hybrid Structures. *Eur. J. Biochem.* **1998**, *258* (1), 243–270.
- (136) Osterwalder, T.; Contartese, J.; Stoeckli, E. T.; Kuhn, T. B.; Sonderegger, P. Neuroserpin, an Axonally Secreted Serine Protease Inhibitor. *EMBO J.* **1996**, *15* (12), 2944–2953.
- (137) Olson, S. T.; Gettins, P. G. W. Regulation of Proteases by Protein Inhibitors of the Serpin Superfamily. In *Progress in molecular biology and translational science*, 2011; Vol. 99, pp 185–240.
- (138) Huntington, J. A.; Read, R. J.; Carrell, R. W. Structure of a Serpin–Protease Complex Shows Inhibition by Deformation. *Nature* **2000**, *407* (6806), 923–926.
- (139) Makarova, A.; Mikhailenko, I.; Bugge, T. H.; List, K.; Lawrence, D. A.; Strickland, D. K. The Low Density Lipoprotein Receptor-Related Protein Modulates Protease Activity in the Brain by Mediating the Cellular Internalization of Both Neuroserpin and Neuroserpin-Tissue-Type Plasminogen Activator Complexes. *J. Biol. Chem.* **2003**, *278* (50), 50250–50258.
- (140) Krueger, S. R.; Ghisu, G. P.; Cinelli, P.; Gschwend, T. P.; Osterwalder, T.; Wolfer, D. P.; Sonderegger, P. Expression of Neuroserpin, an Inhibitor of Tissue Plasminogen Activator, in the Developing and Adult Nervous System of the Mouse. *J. Neurosci.* **1997**, *17* (23), 8984–8996.
- (141) Teesalu, T.; Kulla, A.; Simisker, A.; Sirén, V.; Lawrence, D.; Asser, T.; Vaheri, A. Tissue Plasminogen Activator and Neuroserpin Are Widely Expressed in the Human Central Nervous System. *Thromb. Haemost.* **2004**, *92* (08), 358–368.
- (142) Cinelli, P.; Madani, R.; Tsuzuki, N.; Vallet, P.; Arras, M.; Zhao, C. N.; Osterwalder, T.; Rüllicke, T.; Sonderegger, P. Neuroserpin, a Neuroprotective Factor in Focal Ischemic Stroke. *Mol. Cell. Neurosci.* **2001**, *18* (5), 443–457.
- (143) Osterwalder, T.; Cinelli, P.; Baici, A.; Pennella, A.; Krueger, S. R.; Schrimpf, S. P.; Meins, M.; Sonderegger, P. The Axonally Secreted Serine Proteinase Inhibitor, Neuroserpin,

- Inhibits Plasminogen Activators and Plasmin but Not Thrombin. *J. Biol. Chem.* **1998**, *273* (4), 2312–2321.
- (144) Hastings, G. A.; Coleman, T. A.; Haudenschild, C. C.; Stefansson, S.; Smith, E. P.; Barthlow, R.; Cherry, S.; Sandkvist, M.; Lawrence, D. A. Neuroserpin, a Brain-Associated Inhibitor of Tissue Plasminogen Activator Is Localized Primarily in Neurons. Implications for the Regulation of Motor Learning and Neuronal Survival. *J. Biol. Chem.* **1997**, *272* (52), 33062–33067.
- (145) Lee, T. W.; Tsang, V. W. K.; Loef, E. J.; Birch, N. P. Physiological and Pathological Functions of Neuroserpin: Regulation of Cellular Responses through Multiple Mechanisms. *Semin. Cell Dev. Biol.* **2017**, *62*, 152–159.
- (146) Davies, M. J.; Miranda, E.; Roussel, B. D.; Kaufman, R. J.; Marciniak, S. J.; Lomas, D. A. Neuroserpin Polymers Activate NF-KappaB by a Calcium Signaling Pathway That Is Independent of the Unfolded Protein Response. *J. Biol. Chem.* **2009**, *284* (27), 18202–18209.
- (147) Gooptu, B.; Lomas, D. A. Conformational Pathology of the Serpins: Themes, Variations, and Therapeutic Strategies. *Annu. Rev. Biochem.* **2009**, *78* (1), 147–176.
- (148) Roussel, B. D.; Irving, J. A.; Ekeowa, U. I.; Belorgey, D.; Haq, I.; Ordóñez, A.; Kruppa, A. J.; Duvoix, A.; Rashid, S. T.; Crowther, D. C.; et al. Unravelling the Twists and Turns of the Serpinopathies. *FEBS J.* **2011**, *278* (20), 3859–3867.
- (149) Belorgey, D.; Sharp, L. K.; Crowther, D. C.; Onda, M.; Johansson, J.; Lomas, D. A. Neuroserpin Portland (Ser52Arg) Is Trapped as an Inactive Intermediate That Rapidly Forms Polymers: Implications for the Epilepsy Seen in the Dementia FENIB. *Eur. J. Biochem.* **2004**, *271* (16), 3360–3367.
- (150) Davis, R. L.; Shrimpton, A. E.; Holohan, P. D.; Bradshaw, C.; Feiglin, D.; Collins, G. H.; Sonderegger, P.; Kinter, J.; Becker, L. M.; Lacbawan, F.; et al. Familial Dementia Caused by Polymerization of Mutant Neuroserpin. *Nature* **1999**, *401* (6751), 376–379.
- (151) Schipanski, A.; Oberhauser, F.; Neumann, M.; Lange, S.; Szalay, B.; Krasemann, S.; van Leeuwen, F. W.; Galliciotti, G.; Glatzel, M. The Lectin OS-9 Delivers Mutant Neuroserpin to Endoplasmic Reticulum Associated Degradation in Familial Encephalopathy with Neuroserpin Inclusion Bodies. *Neurobiol. Aging* **2014**, *35* (10), 2394–2403.

- (152) Moriconi, C.; Ordoñez, A.; Lupo, G.; Gooptu, B.; Irving, J. A.; Noto, R.; Martorana, V.; Manno, M.; Timpano, V.; Guadagno, N. A.; et al. Interactions between N-Linked Glycosylation and Polymerisation of Neuroserpin within the Endoplasmic Reticulum. *FEBS J.* **2015**.
- (153) Bager, R.; Johansen, J. S.; Jensen, J. K.; Stensballe, A.; Jendroszek, A.; Buxbom, L.; Sørensen, H. P.; Andreasen, P. A. Protein Conformational Change Delayed by Steric Hindrance from an N-Linked Glycan. *J. Mol. Biol.* **2013**, *425* (16), 2867–2877.
- (154) James, P. Protein Identification in the Post-Genome Era: The Rapid Rise of Proteomics. *Q. Rev. Biophys.* **1997**, *30* (4), 279–331.
- (155) Cummings, R. D.; Darvill, A. G.; Etzler, M. E.; Hahn, M. G. Glycan-Recognizing Probes as Tools. In *Essentials of Glycobiology*; Cold Spring Harbor Laboratory Press, 2015.
- (156) Yoshihara, Y. Visualizing Selective Neural Pathways with WGA Transgene: Combination of Neuroanatomy with Gene Technology. *Neurosci. Res.* **2002**, *44* (2), 133–140.
- (157) Levy, S. L.; White, J. J.; Lackey, E. P.; Schwartz, L.; Sillitoe, R. V. WGA-Alexa Conjugates for Axonal Tracing. In *Current Protocols in Neuroscience*; John Wiley & Sons, Inc.: Hoboken, NJ, USA, 2017; Vol. 79, pp 1.28.1-1.28.24.
- (158) Tabuchi, K.; Sawamoto, K.; Suzuki, E.; Ozaki, K.; Sone, M.; Hama, C.; Tanifuji-Morimoto, T.; Yuasa, Y.; Yoshihara, Y.; Nose, A.; et al. GAL4/UAS-WGA System as a Powerful Tool for Tracing *Drosophila* Transsynaptic Neural Pathways. *J. Neurosci. Res.* **2000**, *59* (1), 94–99.
- (159) Libbrecht, S.; Van den Haute, C.; Malinouskaya, L.; Gijsbers, R.; Baekelandt, V. Evaluation of WGA-Cre-Dependent Topological Transgene Expression in the Rodent Brain. *Brain Struct. Funct.* **2017**, *222* (2), 717–733.
- (160) Jacobsen, J. H. W.; Parker, L. M.; Everest-Dass, A. V.; Schartner, E. P.; Tsiminis, G.; Staikopoulos, V.; Hutchinson, M. R.; Mustafa, S. Novel Imaging Tools for Investigating the Role of Immune Signalling in the Brain. *Brain. Behav. Immun.* **2016**, *58*, 40–47.
- (161) Sterner, E.; Flanagan, N.; Gildersleeve, J. C. Perspectives on Anti-Glycan Antibodies Gleaned from Development of a Community Resource Database. *ACS Chem. Biol.* **2016**, *11* (7), 1773–1783.

- (162) Fewou, S. N.; Ramakrishnan, H.; Büssow, H.; Gieselmann, V.; Eckhardt, M. Down-Regulation of Polysialic Acid Is Required for Efficient Myelin Formation. *J. Biol. Chem.* **2007**, *282* (22), 16700–16711.
- (163) Cheng, B.; Xie, R.; Dong, L.; Chen, X. Metabolic Remodeling of Cell-Surface Sialic Acids: Principles, Applications, and Recent Advances. *ChemBiochem* **2016**, *17* (1), 11–27.
- (164) Xie, R.; Dong, L.; Du, Y.; Zhu, Y.; Hua, R.; Zhang, C.; Chen, X. In Vivo Metabolic Labeling of Sialoglycans in the Mouse Brain by Using a Liposome-Assisted Bioorthogonal Reporter Strategy. *Proc. Natl. Acad. Sci. U. S. A.* **2016**, *113* (19), 5173–5178.
- (165) Gagiannis, D.; Gossrau, R.; Reutter, W.; Zimmermann-Kordmann, M.; Horstkorte, R. Engineering the Sialic Acid in Organs of Mice Using N-Propanoylmannosamine. *Biochim. Biophys. Acta* **2007**, *1770* (2), 297–306.
- (166) Shajahan, A.; Parashar, S.; Goswami, S.; Ahmed, S. M.; Nagarajan, P.; Sampathkumar, S.-G. Carbohydrate-Neuroactive Hybrid Strategy for Metabolic Glycan Engineering of the Central Nervous System in Vivo. *J. Am. Chem. Soc.* **2017**, *139* (2), 693–700.
- (167) Song, X.; Ju, H.; Lasanajak, Y.; Kudelka, M. R.; Smith, D. F.; Cummings, R. D. Oxidative Release of Natural Glycans for Functional Glycomics. *Nat. Methods* **2016**, *13* (6), 528–534.
- (168) Sandoval, W. N.; Arellano, F.; Arnott, D.; Raab, H.; Vandlen, R.; Lill, J. R. Rapid Removal of N-Linked Oligosaccharides Using Microwave Assisted Enzyme Catalyzed Deglycosylation. *Int. J. Mass Spectrom.* **2007**, *259* (1–3), 117–123.
- (169) Ren, X.; Bai, H.; Pan, Y.; Tong, W.; Qin, P.; Yan, H.; Deng, S.; Zhong, R.; Qin, W.; Qian, X. A Graphene Oxide-Based Immobilized PNGase F Reagent for Highly Efficient N-Glycan Release and MALDI-TOF MS Profiling. *Anal. Methods* **2014**, *6* (8), 2518.
- (170) Tretter, V.; Altmann, F.; März, L. Peptide-N4-(N-Acetyl-Beta-Glucosaminyl)Asparagine Amidase F Cannot Release Glycans with Fucose Attached Alpha 1-3 to the Asparagine-Linked N-Acetylglucosamine Residue. *Eur. J. Biochem.* **1991**, *199* (3), 647–652.
- (171) Wang, T.; Cai, Z. P.; Gu, X. Q.; Ma, H. Y.; Du, Y. M.; Huang, K.; Voglmeir, J.; Liu, L. Discovery and Characterization of a Novel Extremely Acidic Bacterial N-Glycanase with Combined Advantages of PNGase F and A. *Biosci. Rep.* **2014**, *34* (6), e00149.

- (172) Maley, F.; Trimble, R. B.; Tarentino, A. L.; Plummer, T. H. Characterization of Glycoproteins and Their Associated Oligosaccharides through the Use of Endoglycosidases. *Anal. Biochem.* **1989**, *180* (2), 195–204.
- (173) Hirabayashi, J. Lectin-Based Structural Glycomics: Glycoproteomics and Glycan Profiling. *Glycoconj. J.* **2004**, *21* (1/2), 35–40.
- (174) Selman, M. H. J.; Hemayatkar, M.; Deelder, A. M.; Wührer, M. Cotton HILIC SPE Microtips for Microscale Purification and Enrichment of Glycans and Glycopeptides. *Anal. Chem.* **2011**, *83* (7), 2492–2499.
- (175) Kim, Y.-G.; Jeong, H.-J.; Jang, K.-S.; Yang, Y.-H.; Song, Y.-S.; Chung, J.; Kim, B.-G. Rapid and High-Throughput Analysis of N-Glycans from Ovarian Cancer Serum Using a 96-Well Plate Platform. *Anal. Biochem.* **2009**, *391* (2), 151–153.
- (176) Jiang, K.; Zhu, H.; Xiao, C.; Liu, D.; Edmunds, G.; Wen, L.; Ma, C.; Li, J.; Wang, P. G. Solid-Phase Reductive Amination for Glycomic Analysis. *Anal. Chim. Acta* **2017**, *962*, 32–40.
- (177) Walker, S. H.; Lilley, L. M.; Enamorado, M. F.; Comins, D. L.; Muddiman, D. C. Hydrophobic Derivatization of N-Linked Glycans for Increased Ion Abundance in Electrospray Ionization Mass Spectrometry. *J. Am. Soc. Mass Spectrom.* **2011**, *22* (8), 1309–1317.
- (178) Wang, X.; Chen, X.; Chen, L.; Wang, B.; Peng, C.; He, C.; Tang, M.; Zhang, F.; Hu, J.; Li, R.; et al. Optimizing High-Performance Liquid Chromatography Method for Quantification of Glucosamine Using 6-Aminoquinolyl-N-Hydroxysuccinimidyl Carbamate Derivatization in Rat Plasma: Application to a Pharmacokinetic Study. *Biomed. Chromatogr.* **2008**, *22* (11), 1265–1271.
- (179) Capon, B.; Connett, B. E. The Mechanism of the Hydrolysis of N-Aryl-D-Glucosylamines. *J. Chem. Soc. Perkin 1* **1965**, 4497–4502.
- (180) Na, Y.; Shen, H.; Byers, L. D. N-Phenylglucosylamine Hydrolysis: A Mechanistic Probe of  $\beta$ -Glucosidase. *Bioorg. Chem.* **2011**, *39* (3), 111–113.
- (181) Pabst, M.; Kolarich, D.; Pörtl, G.; Dalik, T.; Lubec, G.; Hofinger, A.; Altmann, F.



- Comparison of Fluorescent Labels for Oligosaccharides and Introduction of a New Postlabeling Purification Method. *Anal. Biochem.* **2009**, *384* (2), 263–273.
- (182) Anumula, K. R. Advances in Fluorescence Derivatization Methods for High-Performance Liquid Chromatographic Analysis of Glycoprotein Carbohydrates. *Anal. Biochem.* **2006**, *350* (1), 1–23.
- (183) Keser, T.; Pavić, T.; Lauc, G.; Gornik, O. Comparison of 2-Aminobenzamide, Procainamide and RapiFluor-MS as Derivatizing Agents for High-Throughput HILIC-UPLC-FLR-MS N-Glycan Analysis. *Front. Chem.* **2018**, *6*, 324.
- (184) Honda, S.; Akao, E.; Suzuki, S.; Okuda, M.; Kakehi, K.; Nakamura, J. High-Performance Liquid Chromatography of Reducing Carbohydrates as Strongly Ultraviolet-Absorbing and Electrochemically Sensitive 1-Phenyl-3-Methyl-5-Pyrazolone Derivatives. *Anal. Biochem.* **1989**, *180* (2), 351–357.
- (185) Kakehi, K.; Suzuki, S.; Honda, S.; Lee, Y. C. Precolumn Labeling of Reducing Carbohydrates with 1-(p-Methoxy)Phenyl-3-Methyl-5-Pyrazolone: Analysis of Neutral and Sialic Acid-Containing Oligosaccharides Found in Glycoproteins. *Anal. Biochem.* **1991**, *199* (2), 256–268.
- (186) Gil, G.-C.; Kim, Y.-G.; Kim, B.-G. A Relative and Absolute Quantification of Neutral N-Linked Oligosaccharides Using Modification with Carboxymethyl Trimethylammonium Hydrazide and Matrix-Assisted Laser Desorption/Ionization Time-of-Flight Mass Spectrometry. *Anal. Biochem.* **2008**, *379* (1), 45–59.
- (187) Jang, K.-S.; Kim, Y.-G.; Gil, G.-C.; Park, S.-H.; Kim, B.-G. Mass Spectrometric Quantification of Neutral and Sialylated N-Glycans from a Recombinant Therapeutic Glycoprotein Produced in the Two Chinese Hamster Ovary Cell Lines. *Anal. Biochem.* **2009**, *386* (2), 228–236.
- (188) Ruhaak, L. R.; Zauner, G.; Huhn, C.; Bruggink, C.; Deelder, A. M.; Wuhrer, M. Glycan Labeling Strategies and Their Use in Identification and Quantification. *Anal. Bioanal. Chem.* **2010**, *397* (8), 3457–3481.
- (189) Reiding, K. R.; Blank, D.; Kuijper, D. M.; Deelder, A. M.; Wuhrer, M. High-Throughput Profiling of Protein N-Glycosylation by MALDI-TOF-MS Employing Linkage-Specific



- Sialic Acid Esterification. *Anal. Chem.* **2014**, *86* (12), 5784–5793.
- (190) Ciucanu, I.; Kerek, F. A Simple and Rapid Method for the Permethylation of Carbohydrates. *Carbohydr. Res.* **1984**, *131* (2), 209–217.
- (191) Ciucanu, I.; Costello, C. E. Elimination of Oxidative Degradation during the Per-O-Methylation of Carbohydrates. *J. Am. Chem. Soc.* **2003**, *125* (52), 16213–16219.
- (192) Kang, P.; Mechref, Y.; Klouckova, I.; Novotny, M. V. Solid-Phase Permethylation of Glycans for Mass Spectrometric Analysis. *Rapid Commun. Mass Spectrom.* **2005**, *19* (23), 3421–3428.
- (193) Shubhakar, A.; Kozak, R. P.; Reiding, K. R.; Royle, L.; Spencer, D. I. R.; Fernandes, D. L.; Wuhler, M. Automated High-Throughput Permethylation for Glycosylation Analysis of Biologics Using MALDI-TOF-MS. *Anal. Chem.* **2016**, *88* (17), 8562–8569.
- (194) Zhou, S.; Wooding, K. M.; Mechref, Y. Analysis of Permethylated Glycan by Liquid Chromatography (LC) and Mass Spectrometry (MS). In *Methods in molecular biology (Clifton, N.J.)*; 2017; Vol. 1503, pp 83–96.
- (195) Jiang, K.; Zhu, H.; Li, L.; Guo, Y.; Gashash, E.; Ma, C.; Sun, X.; Li, J.; Zhang, L.; Wang, P. G. Sialic Acid Linkage-Specific Permethylation for Improved Profiling of Protein Glycosylation by MALDI-TOF MS. *Anal. Chim. Acta* **2017**, *981*, 53–61.
- (196) Klarić, T.; Gudelj, I. HILIC-UPLC Analysis of Brain Tissue N-Glycans. In *High-Throughput Glycomics and Glycoproteomics*; G., L., M., W., Eds.; Humana Press, New York, NY, 2017; pp 207–216.
- (197) Abrahams, J. L.; Campbell, M. P.; Packer, N. H. Building a PGC-LC-MS N-Glycan Retention Library and Elution Mapping Resource. *Glycoconj. J.* **2018**, *35* (1), 15–29.
- (198) Lu, G.; Carihfield, C. L.; Gattu, S.; Veltri, L. M.; Holland, L. A. Capillary Electrophoresis Separations of Glycans. *Chem. Rev.* **2018**, *118* (17), 7867–7885.
- (199) Chen, Z.; Glover, M. S.; Li, L. Recent Advances in Ion Mobility–Mass Spectrometry for Improved Structural Characterization of Glycans and Glycoconjugates. *Curr. Opin. Chem. Biol.* **2018**, *42*, 1–8.

- (200) Smith, J.; Mittermayr, S.; Váradi, C.; Bones, J. Quantitative Glycomics Using Liquid Phase Separations Coupled to Mass Spectrometry. *Analyst* **2017**, *142* (5), 700–720.
- (201) Swartz, M. E. UPLC<sup>TM</sup>: An Introduction and Review. *J. Liq. Chromatogr. Relat. Technol.* **2005**, *28* (7–8), 1253–1263.
- (202) Fanali, S. An Overview to Nano-Scale Analytical Techniques: Nano-Liquid Chromatography and Capillary Electrochromatography. *Electrophoresis* **2017**, *38* (15), 1822–1829.
- (203) Varki, A. Glycan-Based Interactions Involving Vertebrate Sialic-Acid-Recognizing Proteins. *Nature* **2007**, *446* (7139), 1023–1029.
- (204) Chovanec, M.; Plzák, J.; Betka, J.; Brabec, J.; Kodet, R.; Smetana, K. Comparative Analysis of Alpha2,3/2,6-Linked N-Acetylneuraminic Acid and Cytokeratin Expression in Head and Neck Squamous Cell Carcinoma. *Oncol. Rep.* **2004**, *12* (2), 297–301.
- (205) Zhou, S.; Hu, Y.; Mechref, Y. High-Temperature LC-MS/MS of Permethylated Glycans Derived from Glycoproteins. *Electrophoresis* **2016**, *37* (11), 1506–1513.
- (206) Aizpurua-Olaizola, O.; Sastre Toraño, J.; Falcon-Perez, J. M.; Williams, C.; Reichardt, N.; Boons, G.-J. Mass Spectrometry for Glycan Biomarker Discovery. *TrAC Trends Anal. Chem.* **2018**, *100*, 7–14.
- (207) Alpert, A. J. Hydrophilic-Interaction Chromatography for the Separation of Peptides, Nucleic Acids and Other Polar Compounds. *J. Chromatogr.* **1990**, *499*, 177–196.
- (208) Hemström, P.; Irgum, K. Hydrophilic Interaction Chromatography. *J. Sep. Sci.* **2006**, *29* (12), 1784–1821.
- (209) Wuhrer, M.; de Boer, A. R.; Deelder, A. M. Structural Glycomics Using Hydrophilic Interaction Chromatography (HILIC) with Mass Spectrometry. *Mass Spectrom. Rev.* **2009**, *28* (2), 192–206.
- (210) Takegawa, Y.; Deguchi, K.; Ito, H.; Keira, T.; Nakagawa, H.; Nishimura, S.-I. Simple Separation of Isomeric Sialylated N-Glycopeptides by a Zwitterionic Type of Hydrophilic Interaction Chromatography. *J. Sep. Sci.* **2006**, *29* (16), 2533–2540.

- (211) Zauner, G.; Koeleman, C. A. M.; Deelder, A. M.; Wührer, M. Protein Glycosylation Analysis by HILIC-LC-MS of Proteinase K-Generated N- and O-Glycopeptides. *J. Sep. Sci.* **2010**, *33* (6–7), 903–910.
- (212) Mariño, K.; Bones, J.; Kattla, J. J.; Rudd, P. M. A Systematic Approach to Protein Glycosylation Analysis: A Path through the Maze. *Nat. Chem. Biol.* **2010**, *6* (10), 713–723.
- (213) Pabst, M.; Altmann, F. Glycan Analysis by Modern Instrumental Methods. *Proteomics* **2011**, *11* (4), 631–643.
- (214) Gbormittah, F. O.; Hincapie, M.; Hancock, W. S. Development of an Improved Fractionation of the Human Plasma Proteome by a Combination of Abundant Proteins Depletion and Multi-Lectin Affinity Chromatography. *Bioanalysis* **2014**, *6* (19), 2537–2548.
- (215) Parker, B. L.; Thaysen-Andersen, M.; Solis, N.; Scott, N. E.; Larsen, M. R.; Graham, M. E.; Packer, N. H.; Cordwell, S. J. Site-Specific Glycan-Peptide Analysis for Determination of N-Glycoproteome Heterogeneity. *J. Proteome Res.* **2013**, *12* (12), 5791–5800.
- (216) Handa-Narumi, M.; Yoshimura, T.; Konishi, H.; Fukata, Y.; Manabe, Y.; Tanaka, K.; Bao, G.-M.; Kiyama, H.; Fukase, K.; Ikenaka, K. Branched Sialylated N-Glycans Are Accumulated in Brain Synaptosomes and Interact with Siglec-H. *CELL Struct. Funct.* **2018**, *43*, 141–152.
- (217) Badr, H. A.; AlSadek, D. M.; Darwish, A. A.; ElSayed, A. I.; Bekmanov, B. O.; Khussainova, E. M.; Zhang, X.; Cho, W. C.; Djansugurova, L. B.; Li, C.-Z. Lectin Approaches for Glycoproteomics in FDA-Approved Cancer Biomarkers. *Expert Rev. Proteomics* **2014**, *11* (2), 227–236.
- (218) Ruiz-May, E.; Hucko, S.; Howe, K. J.; Zhang, S.; Sherwood, R. W.; Thannhauser, T. W.; Rose, J. K. C. A Comparative Study of Lectin Affinity Based Plant N-Glycoproteome Profiling Using Tomato Fruit as a Model. *Mol. Cell. Proteomics* **2014**, *13* (2), 566–579.
- (219) Alpert, A. J. Electrostatic Repulsion Hydrophilic Interaction Chromatography for Isocratic Separation of Charged Solutes and Selective Isolation of Phosphopeptides. *Anal. Chem.* **2008**, *80* (1), 62–76.
- (220) Zacharias, L. G.; Hartmann, A. K.; Song, E.; Zhao, J.; Zhu, R.; Mirzaei, P.; Mechref, Y.

- HILIC and ERLIC Enrichment of Glycopeptides Derived from Breast and Brain Cancer Cells. *J. Proteome Res.* **2016**, *15* (10), 3624–3634.
- (221) Häggglund, P.; Bunkenborg, J.; Elortza, F.; Jensen, O. N.; Roepstorff, P. A New Strategy for Identification of N-Glycosylated Proteins and Unambiguous Assignment of Their Glycosylation Sites Using HILIC Enrichment and Partial Deglycosylation. *J. Proteome Res.* **2004**, *3* (3), 556–566.
- (222) Mysling, S.; Palmisano, G.; Højrup, P.; Thaysen-Andersen, M. Utilizing Ion-Pairing Hydrophilic Interaction Chromatography Solid Phase Extraction for Efficient Glycopeptide Enrichment in Glycoproteomics. *Anal. Chem.* **2010**, *82* (13), 5598–5609.
- (223) Huang, G.; Sun, Z.; Qin, H.; Zhao, L.; Xiong, Z.; Peng, X.; Ou, J.; Zou, H. Preparation of Hydrazine Functionalized Polymer Brushes Hybrid Magnetic Nanoparticles for Highly Specific Enrichment of Glycopeptides. *Analyst* **2014**, *139* (9), 2199.
- (224) Xie, Y.; Liu, Q.; Li, Y.; Deng, C. Core-Shell Structured Magnetic Metal-Organic Framework Composites for Highly Selective Detection of N-Glycopeptides Based on Boronic Acid Affinity Chromatography. *J. Chromatogr. A* **2018**, *1540*, 87–93.
- (225) Yu, A.; Zhao, J.; Peng, W.; Banazadeh, A.; Williamson, S. D.; Goli, M.; Huang, Y.; Mechref, Y. Advances in Mass Spectrometry-based Glycoproteomics. *Electrophoresis* **2018**, *39* (24), 3104–3122.
- (226) Hua, S.; Nwosu, C. C.; Strum, J. S.; Seipert, R. R.; An, H. J.; Zivkovic, A. M.; German, J. B.; Lebrilla, C. B. Site-Specific Protein Glycosylation Analysis with Glycan Isomer Differentiation. *Anal. Bioanal. Chem.* **2012**, *403* (5), 1291–1302.
- (227) Cao, X.; Song, D.; Yang, M.; Yang, N.; Ye, Q.; Tao, D.; Liu, B.; Wu, R.; Yue, X. Comparative Analysis of Whey N-Glycoproteins in Human Colostrum and Mature Milk Using Quantitative Glycoproteomics. *J. Agric. Food Chem.* **2017**, *65* (47), 10360–10367.
- (228) Thaysen-Andersen, M.; Packer, N. H.; Schulz, B. L. Maturing Glycoproteomics Technologies Provide Unique Structural Insights into the N-Glycoproteome and Its Regulation in Health and Disease. *Mol. Cell. Proteomics* **2016**, *15* (6), 1773–1790.
- (229) Pan, S. Quantitative Glycoproteomics for N-Glycoproteome Profiling. In *Methods in*

*molecular biology* (Clifton, N.J.); 2014; Vol. 1156, pp 379–388.

- (230) Giménez, E.; Ramos-Hernan, R.; Benavente, F.; Barbosa, J.; Sanz-Nebot, V. Analysis of Recombinant Human Erythropoietin Glycopeptides by Capillary Electrophoresis Electrospray–Time of Flight–Mass Spectrometry. *Anal. Chim. Acta* **2012**, *709*, 81–90.
- (231) Creese, A. J.; Cooper, H. J. Separation and Identification of Isomeric Glycopeptides by High Field Asymmetric Waveform Ion Mobility Spectrometry. *Anal. Chem.* **2012**, *84* (5), 2597–2601.
- (232) Tarasova, I. A.; Masselon, C. D.; Gorshkov, A. V.; Gorshkov, M. V. Predictive Chromatography of Peptides and Proteins as a Complementary Tool for Proteomics. *Analyst* **2016**, *141* (16), 4816–4832.
- (233) Kozlik, P.; Goldman, R.; Sanda, M. Study of Structure-Dependent Chromatographic Behavior of Glycopeptides Using Reversed Phase NanoLC. *Electrophoresis* **2017**, *38* (17), 2193–2199.
- (234) Ozohanics, O.; Turiák, L.; Puerta, A.; Vékey, K.; Drahos, L. High-Performance Liquid Chromatography Coupled to Mass Spectrometry Methodology for Analyzing Site-Specific N-Glycosylation Patterns. *J. Chromatogr. A* **2012**, *1259*, 200–212.
- (235) Zhao, Y.; Szeto, S. S. W.; Kong, R. P. W.; Law, C. H.; Li, G.; Quan, Q.; Zhang, Z.; Wang, Y.; Chu, I. K. Online Two-Dimensional Porous Graphitic Carbon/Reversed Phase Liquid Chromatography Platform Applied to Shotgun Proteomics and Glycoproteomics. *Anal. Chem.* **2014**, *86* (24), 12172–12179.
- (236) Wohlgemuth, J.; Karas, M.; Jiang, W.; Hendriks, R.; Andrecht, S. Enhanced Glyco-Profiling by Specific Glycopeptide Enrichment and Complementary Monolithic Nano-LC (ZIC-HILIC/RP18e)/ESI-MS Analysis. *J. Sep. Sci.* **2010**, *33* (6–7), 880–890.
- (237) Stavenhagen, K.; Plomp, R.; Wuhrer, M. Site-Specific Protein N- and O-Glycosylation Analysis by a C18-Porous Graphitized Carbon–Liquid Chromatography–Electrospray Ionization Mass Spectrometry Approach Using Pronase Treated Glycopeptides. *Anal. Chem.* **2015**, *87* (23), 11691–11699.
- (238) Xu, G.; Davis, J. C.; Goonatilake, E.; Smilowitz, J. T.; German, J. B.; Lebrilla, C. B.

- Absolute Quantitation of Human Milk Oligosaccharides Reveals Phenotypic Variations during Lactation. *J. Nutr.* **2017**, *147* (1), 117–124.
- (239) Zhang, H.; Wang, Z.; Stupak, J.; Ghribi, O.; Geiger, J. D.; Liu, Q. Y.; Li, J. Targeted Glycomics by Selected Reaction Monitoring for Highly Sensitive Glycan Compositional Analysis. *Proteomics* **2012**, *12* (15–16), 2510–2522.
- (240) Ruhaak, L. R.; Xu, G.; Li, Q.; Goonatileke, E.; Lebrilla, C. B. Mass Spectrometry Approaches to Glycomic and Glycoproteomic Analyses. *Chem. Rev.* **2018**, *118* (17), 7886–7930.
- (241) Harvey, D. J.; Struwe, W. B. Structural Studies of Fucosylated N-Glycans by Ion Mobility Mass Spectrometry and Collision-Induced Fragmentation of Negative Ions. *J. Am. Soc. Mass Spectrom.* **2018**, *29* (6), 1179–1193.
- (242) Ito, H.; Takegawa, Y.; Deguchi, K.; Nagai, S.; Nakagawa, H.; Shinohara, Y.; Nishimura, S.-I. Direct Structural Assignment of Neutral and Sialylated N-Glycans of Glycopeptides Using Collision-Induced Dissociation MS<sup>n</sup> Spectral Matching. *Rapid Commun. Mass Spectrom.* **2006**, *20* (23), 3557–3565.
- (243) An, H. J.; Lebrilla, C. B. Structure Elucidation of Native N- and O-Linked Glycans by Tandem Mass Spectrometry (Tutorial). *Mass Spectrom. Rev.* **2011**, *30* (4), 560–578.
- (244) Mechref, Y. Use of CID/ETD Mass Spectrometry to Analyze Glycopeptides. In *Current Protocols in Protein Science*; John Wiley & Sons, Inc.: Hoboken, NJ, USA, 2012; Vol. Chapter 12, pp 12.11.1-12.11.11.
- (245) Frese, C. K.; Altelaar, A. F. M.; van den Toorn, H.; Nolting, D.; Griep-Raming, J.; Heck, A. J. R.; Mohammed, S. Toward Full Peptide Sequence Coverage by Dual Fragmentation Combining Electron-Transfer and Higher-Energy Collision Dissociation Tandem Mass Spectrometry. *Anal. Chem.* **2012**, *84* (22), 9668–9673.
- (246) Ko, B. J.; Brodbelt, J. S. Comparison of Glycopeptide Fragmentation by Collision Induced Dissociation and Ultraviolet Photodissociation. *Int. J. Mass Spectrom.* **2015**, *377*, 385–392.
- (247) Riley, N. M.; Hebert, A. S.; Westphall, M. S.; Coon, J. J. Capturing Site-Specific Heterogeneity with Large-Scale N-Glycoproteome Analysis. *Nat. Commun.* **2019**, *10* (1),

1311.

- (248) Domon, B.; Costello, C. E. A Systematic Nomenclature for Carbohydrate Fragmentations in FAB-MS/MS Spectra of Glycoconjugates. *Glycoconj. J.* **1988**, *5* (4), 397–409.
- (249) Wuhrer, M.; Deelder, A. M.; van der Burgt, Y. E. M. Mass Spectrometric Glycan Rearrangements. *Mass Spectrom. Rev.* **2011**, *30* (4), 664–680.
- (250) Prien, J. M.; Ashline, D. J.; Lapadula, A. J.; Zhang, H.; Reinhold, V. N. The High Mannose Glycans from Bovine Ribonuclease B Isomer Characterization by Ion Trap MS. *J. Am. Soc. Mass Spectrom.* **2009**, *20* (4), 539–556.
- (251) Park, Y.; Lebrilla, C. B. Application of Fourier Transform Ion Cyclotron Resonance Mass Spectrometry to Oligosaccharides. *Mass Spectrom. Rev.* **2005**, *24* (2), 232–264.
- (252) An, H. J.; Lebrilla, C. B. A Glycomics Approach to the Discovery of Potential Cancer Biomarkers. *Methods Mol. Biol.* **2010**, *600*, 199–213.
- (253) Wang, X.; Emmett, M. R.; Marshall, A. G. Liquid Chromatography Electrospray Ionization Fourier Transform Ion Cyclotron Resonance Mass Spectrometric Characterization of N-Linked Glycans and Glycopeptides. *Anal. Chem.* **2010**, *82* (15), 6542–6548.
- (254) Totten, S. M.; Feasley, C. L.; Bermudez, A.; Pitteri, S. J. Parallel Comparison of N-Linked Glycopeptide Enrichment Techniques Reveals Extensive Glycoproteomic Analysis of Plasma Enabled by SAX-ERLIC. *J. Proteome Res.* **2017**, *16* (3), 1249–1260.
- (255) Hong, Q.; Lebrilla, C. B.; Miyamoto, S.; Ruhaak, L. R. Absolute Quantitation of Immunoglobulin G and Its Glycoforms Using Multiple Reaction Monitoring. *Anal. Chem.* **2013**, *85* (18), 8585–8593.
- (256) Ruhaak, L. R.; Taylor, S. L.; Miyamoto, S.; Kelly, K.; Leiserowitz, G. S.; Gandara, D.; Lebrilla, C. B.; Kim, K. Chip-Based NLC-TOF-MS Is a Highly Stable Technology for Large Scale High-Throughput Analyses. *Anal. Bioanal. Chem.* **2013**, *405* (14), 4953.
- (257) Harvey, D. J. Matrix-Assisted Laser Desorption/Ionization Mass Spectrometry of Carbohydrates. *Mass Spectrom. Rev.* **1999**, *18* (6), 349–450.
- (258) Kolarich, D.; Windwarder, M.; Alagesan, K.; Altmann, F. Isomer-Specific Analysis of



- Released N-Glycans by LC-ESI MS/MS with Porous Graphitized Carbon. In *Methods in molecular biology* (Clifton, N.J.); 2015; Vol. 1321, pp 427–435.
- (259) Jürgen H. Gross. *Mass Spectrometry, a Textbook*, 3rd ed.; Springer International Publishing, 2017.
- (260) Ishii, A.; Ikeda, T.; Hitoshi, S.; Fujimoto, I.; Torii, T.; Sakuma, K.; Nakakita, S.-I.; Hase, S.; Ikenaka, K. Developmental Changes in the Expression of Glycogenes and the Content of N-Glycans in the Mouse Cerebral Cortex. *Glycobiology* **2007**, *17* (3), 261–276.
- (261) Ishii, A.; Ikenaka, K.; Pfeiffer, S. E. The N-Glycan Profile of Mouse Myelin, a Specialized Central Nervous System Membrane. *J. Neurochem.* **2007**, *103* (s1), 25–31.
- (262) Yoshimura, T.; Yamada, G.; Narumi, M.; Koike, T.; Ishii, A.; Sela, I.; Mitrani-Rosenbaum, S.; Ikenaka, K. Detection of N-Glycans on Small Amounts of Glycoproteins in Tissue Samples and Sodium Dodecyl Sulfate-Polyacrylamide Gels. *Anal. Biochem.* **2012**, *423* (2), 253–260.
- (263) Hu, Y.; Zhou, S.; Khalil, S. I.; Renteria, C. L.; Mechref, Y. Glycomic Profiling of Tissue Sections by LC-MS. *Anal. Chem.* **2013**, *85* (8), 4074–4079.
- (264) Torii, T.; Yoshimura, T.; Narumi, M.; Hitoshi, S.; Takaki, Y.; Tsuji, S.; Ikenaka, K. Determination of Major Sialylated N-Glycans and Identification of Branched Sialylated N-Glycans That Dynamically Change Their Content during Development in the Mouse Cerebral Cortex. *Glycoconj J* **2014**, *31* (9), 671–683.
- (265) Ji, I. J.; Hua, S.; Shin, D. H.; Seo, N.; Hwang, J. Y.; Jang, I.-S.; Kang, M.-G.; Choi, J.-S.; An, H. J. Spatially-Resolved Exploration of the Mouse Brain Glycome by Tissue Glyco-Capture (TGC) and Nano-LC/MS. *Anal. Chem.* **2015**, *87* (5), 2869–2877.
- (266) Gizaw, S. T.; Ohashi, T.; Tanaka, M.; Hinou, H.; Nishimura, S.-I. Glycoblotting Method Allows for Rapid and Efficient Glycome Profiling of Human Alzheimer's Disease Brain, Serum and Cerebrospinal Fluid towards Potential Biomarker Discovery. *Biochim. Biophys. Acta* **2016**, *1860* (8), 1716–1727.
- (267) Hsiao, C.-T.; Wang, P.-W.; Chang, H.-C.; Chen, Y.-Y.; Wang, S.-H.; Chern, Y.; Khoo, K.-H. Advancing a High Throughput Glycotope-Centric Glycomics Workflow Based on



- NanoLC-MS 2-Product Dependent-MS 3 Analysis of Permethylated Glycans. *Mol. Cell. Proteomics* **2017**, *16* (12), 2268–2280.
- (268) Shiro, A.; Ohno, K.; Kozo, N. On the Hydrazinolysis of Proteins and Peptides: A Method for the Characterization of Carboxyl-Terminal Amino Acids in Proteins. *Bull. Chem. Soc. Jpn.* **1952**, *25* (3), 214–218.
- (269) Shen, Y.; You, Y.; Xiao, K.; Chen, Y.; Tian, Z. Large-Scale Identification and Fragmentation Pathways Analysis of N-Glycans from Mouse Brain. *J. Am. Soc. Mass Spectrom.* **2019**, *30* (7), 1254–1261.
- (270) Mao, A. S.; Mooney, D. J. Regenerative Medicine: Current Therapies and Future Directions. *Proc. Natl. Acad. Sci.* **2015**, *112* (47), 14452–14459.
- (271) Russo, L.; Cipolla, L. Glycomics: New Challenges and Opportunities in Regenerative Medicine. *Chem. Eur.J* **2016**, *22*, 13380–13388.
- (272) Russo, L.; Sgambato, A.; Guizzardi, R.; Vesentini, S.; Cipolla, L.; Nicotra, F. Glyco-Functionalised Biomaterials in Neuroregeneration. In *Drug and Gene Delivery to the Central Nervous System for Neuroprotection*; Springer, Cham, 2017; pp 179–198.
- (273) Russo, L.; Sgambato, A.; Lecchi, M.; Pastori, V.; Raspanti, M.; Natalello, A.; Doglia, S. M.; Nicotra, F.; Cipolla, L. Neoglycosylated Collagen Matrices Drive Neuronal Cells to Differentiate. *ACS Chem. Neurosci.* **2014**, *5*, 261–265.
- (274) Masand, S. N.; Perron, I. J.; Schachner, M.; Shreiber, D. I. Neural Cell Type-Specific Responses to Glycomimetic Functionalized Collagen. *Biomaterials* **2012**, *33* (3), 790–797.
- (275) Kalovidouris, S. A.; Gama, C. I.; Lee, L. W.; Hsieh-Wilson, L. C. A Role for Fucose  $\alpha(1-2)$  Galactose Carbohydrates in Neuronal Growth. *J. Am. Chem. Soc.* **2005**, *127* (5), 1340–1341.
- (276) Zhang, S.; Wang, X.-J.; Li, W.-S.; Xu, X.-L.; Hu, J.-B.; Kang, X.-Q.; Qi, J.; Ying, X.-Y.; You, J.; Du, Y.-Z. Polycaprolactone/Polysialic Acid Hybrid, Multifunctional Nanofiber Scaffolds for Treatment of Spinal Cord Injury. *Acta Biomater.* **2018**, *77*, 15–27.
- (277) Fradet, A.; Chen, J.; Hellwich, K.-H.; Horie, K.; Kahovec, J.; Mormann, W.; Stepto, R. F. T.; Vohlídal, J.; Wilks, E. S. Nomenclature and Terminology for Dendrimers with Regular Dendrons and for Hyperbranched Polymers (IUPAC Recommendations 2017). *Pure Appl.*

*Chem.* **2019**, *91* (3), 523–561.

- (278) Grayson, S. M.; Fréchet, J. M. Convergent Dendrons and Dendrimers: From Synthesis to Applications. *Chem. Rev.* **2001**, *101* (12), 3819–3868.
- (279) Newkome, G. R.; Shreiner, C. D. Poly(Amidoamine), Polypropylenimine, and Related Dendrimers and Dendrons Possessing Different 1 / 2 Branching Motifs: An Overview of the Divergent Procedures. *Polym. with aligned carbon Nanotub. Act. Compos. Mater.* **2007**, *49*, 1–173.
- (280) Wu, L.; Ficker, M.; Christensen, J. B.; Trohopoulos, P. N.; Moghimi, S. M. Dendrimers in Medicine: Therapeutic Concepts and Pharmaceutical Challenges. *Bioconjug. Chem.* **2015**, *26* (7), 1198–1211.
- (281) Abbasi, E.; Aval, S.; Akbarzadeh, A.; Milani, M.; Nasrabadi, H.; Joo, S.; Hanifehpour, Y.; Nejati-Koshki, K.; Pashaei-Asl, R. Dendrimers: Synthesis, Applications, and Properties. *Nanoscale Res. Lett.* **2014**, *9* (1), 247.
- (282) Andreozzi, E.; Antonelli, A.; Cangiotti, M.; Canonico, B.; Sfara, C.; Pianetti, A.; Bruscolini, F.; Sahre, K.; Appelhans, D.; Papa, S.; et al. Interactions of Nitroxide-Conjugated and Non-Conjugated Glycodendrimers with Normal and Cancer Cells and Biocompatibility Studies. *Bioconjug. Chem.* **2017**, *28*, 524–538.
- (283) Röglin, L.; Lempens, E. H. M.; Meijer, E. W. A Synthetic “Tour de Force”: Well-Defined Multivalent and Multimodal Dendritic Structures for Biomedical Applications. *Angew. Chemie Int. Ed.* **2011**, *50* (1), 102–112.
- (284) Balzani, V.; Ceroni, P.; Maestri, M.; Vicinelli, V. Light-Harvesting Dendrimers. *Curr. Opin. Chem. Biol.* **2003**, *7* (6), 657–665.
- (285) Selin, M.; Peltonen, L.; Hirvonen, J.; Bimbo, L. M. Dendrimers and Their Supramolecular Nanostructures for Biomedical Applications. *Journal of Drug Delivery Science and Technology*. 2016.
- (286) Zeng, Y.; Li, Y.-Y.; Chen, J.; Yang, G.; Li, Y. Dendrimers: A Mimic Natural Light-Harvesting System. *Chem. Asian J.* **2010**, *5* (5), 992–1005.
- (287) Roy, R.; Zanini, D.; Meunier, S. J.; Romanowska, A. Solid-Phase Synthesis of Dendritic

- Sialoside Inhibitors of Influenza A Virus Haemagglutinin. *J. Chem. Soc. Chem. Commun.* **1993**, 0 (24), 1869.
- (288) Janaszewska, A.; Mączyńska, K.; Matuszko, G.; Appelhans, D.; Voit, B.; Klajnert, B.; Bryszewska, M. Cytotoxicity of PAMAM, PPI and Maltose Modified PPI dendrimers in Chinese Hamster Ovary (CHO) and Human Ovarian Carcinoma (SKOV3) Cells. *New J. Chem.* **2012**, 36 (2), 428–437.
- (289) Janaszewska, A.; Ziemba, B.; Ciepluch, K.; Appelhans, D.; Voit, B.; Klajnert, B.; Bryszewska, M. The Biodistribution of Maltotriose Modified Poly(Propylene Imine) (PPI) Dendrimers Conjugated with Fluorescein—Proofs of Crossing Blood–Brain–Barrier. *New J. Chem.* **2012**, 36 (2), 350–353.
- (290) Ciolkowski, M.; Palecz, B.; Appelhans, D.; Voit, B.; Klajnert, B.; Bryszewska, M. The Influence of Maltose Modified Poly(Propylene Imine) Dendrimers on Hen Egg White Lysozyme Structure and Thermal Stability. *Colloids Surfaces B Biointerfaces* **2012**, 95, 103–108.
- (291) Appelhans, D.; Klajnert-Maculewicz, B.; Janaszewska, A.; Lazniewska, J.; Voit, B. Dendritic Glycopolymers Based on Dendritic Polyamine Scaffolds: View on Their Synthetic Approaches, Characteristics and Potential for Biomedical Applications. *Chem. Soc. Rev.* **2015**, 44 (12), 3968–3996.
- (292) Vacchini, M.; Edwards, R.; Guizzardi, R.; Palmioli, A.; Ciaramelli, C.; Paiotta, A.; Airoidi, C.; La Ferla, B.; Cipolla, L. Glycan Carriers As Glycotools For Medicinal Chemistry Applications. *Curr. Med. Chem.* **2019**, 26 (1).
- (293) Westergard, L.; Christensen, H. M.; Harris, D. A. The Cellular Prion Protein (Pr<sup>PC</sup>): Its Physiological Function and Role in Disease. *Biochim Biophys Acta* **2007**, 1772 (6), 629–644.
- (294) Lazzari, C.; Peggion, C.; Stella, R.; Massimino, M. L.; Lim, D.; Bertoli, A.; Sorgato, M. C. Cellular Prion Protein Is Implicated in the Regulation of Local Ca<sup>2+</sup> Movements in Cerebellar Granule Neurons. *J. Neurochem.* **2011**, 116 (5), 881–890.
- (295) Aguzzi, A.; Lakkaraju, A. K. K.; Frontzek, K. Toward Therapy of Human Prion Diseases. *Annu. Rev. Pharmacol. Toxicol.* **2018**, 58 (1), 331–351.
- (296) McCarthy, J. M.; Appelhans, D.; Tatzelt, J.; Rogers, M. S. Nanomedicine for Prion Disease

- Treatment. *Prion* **2013**, 7 (3), 198–202.
- (297) Taneja, V.; Verma, M.; Vats, A. Toxic Species in Amyloid Disorders: Oligomers or Mature Fibrils. *Ann. Indian Acad. Neurol.* **2015**, 18 (2), 138.
- (298) He, Y.; Zheng, M.-M.; Ma, Y.; Han, X.-J.; Ma, X.-Q.; Qu, C.-Q.; Du, Y.-F. Soluble Oligomers and Fibrillar Species of Amyloid  $\beta$ -Peptide Differentially Affect Cognitive Functions and Hippocampal Inflammatory Response. *Biochem. Biophys. Res. Commun.* **2012**, 429 (3–4), 125–130.
- (299) Zhang, Y.; Lu, L.; Jia, J.; Jia, L.; Geula, C.; Pei, J.; Xu, Z.; Qin, W.; Liu, R.; Li, D.; et al. A Lifespan Observation of a Novel Mouse Model: In Vivo Evidence Supports A $\beta$  Oligomer Hypothesis. *PLoS One* **2014**, 9 (1), e85885.
- (300) Janaszewska, A.; Klajnert-Maculewicz, B.; Marcinkowska, M.; Duchnowicz, P.; Appelhans, D.; Grasso, G.; Deriu, M. A.; Danani, A.; Cangiotti, M.; Francesca Ottaviani, M. Multivalent Interacting Glycodendrimer to Prevent Amyloid-Peptide Fibril Formation Induced by Cu(II): A Multidisciplinary Approach. *Nano Res.* **2018**, 11 (3), 1204–1226.
- (301) Kozłowski, H.; Luczkowski, M.; Remelli, M.; Valensin, D. Copper, Zinc and Iron in Neurodegenerative Diseases (Alzheimer's, Parkinson's and Prion Diseases). *Coord. Chem. Rev.* **2012**, 256, 2129–2141.
- (302) Klementieva, O.; Aso, E.; Filippini, D.; Benseny-Cases, N.; Carmona, M.; Juvés, S.; Appelhans, D.; Cladera, J.; Ferrer, I. Effect of Poly(Propylene Imine) Glycodendrimers on  $\beta$ -Amyloid Aggregation in Vitro and in APP/PS1 Transgenic Mice, as a Model of Brain Amyloid Deposition and Alzheimer's Disease. *Biomacromolecules* **2013**, 14 (10), 3570–3580.
- (303) Klementieva, O.; Benseny-Cases, N.; Gella, A.; Appelhans, D.; Voit, B.; Cladera, J. Dense Shell Glycodendrimers as Potential Nontoxic Anti-Amyloidogenic Agents in Alzheimer's Disease. Amyloid–Dendrimer Aggregates Morphology and Cell Toxicity. *Biomacromolecules* **2011**, 12 (11), 3903–3909.
- (304) Ziemba, B.; Janaszewska, A.; Ciepluch, K.; Krotewicz, M.; Fogel, W. A.; Appelhans, D.; Voit, B.; Bryszewska, M.; Klajnert, B. In Vivo Toxicity of Poly(Propyleneimine) Dendrimers. *J. Biomed. Mater. Res. Part A* **2011**, 99A (2), 261–268.

- (305) Klajnert, B.; Appelhans, D.; Komber, H.; Morgner, N.; Schwarz, S.; Richter, S.; Brutschy, B.; Ionov, M.; Tonkikh, A. K.; Bryszewska, M.; et al. The Influence of Densely Organized Maltose Shells on the Biological Properties of Poly(Propylene Imine) Dendrimers: New Effects Dependent on Hydrogen Bonding. *Chemistry (Easton)*. **2008**, *14* (23), 7030–7041.
- (306) McCarthy, J. M.; Rasines Moreno, B.; Filippini, D.; Komber, H.; Maly, M.; Cernescu, M.; Brutschy, B.; Appelhans, D.; Rogers, M. S. Influence of Surface Groups on Poly(Propylene Imine) Dendrimers Antiprion Activity. *Biomacromolecules* **2013**, *14* (1), 27–37.
- (307) Baker, M. 1,500 Scientists Lift the Lid on Reproducibility. *Nature* **2016**, *533* (7604), 452–454.
- (308) Fachi, M. M.; Leonart, L. P.; Cerqueira, L. B.; Pontes, F. L. D.; de Campos, M. L.; Pontarolo, R. A Systematic and Critical Review on Bioanalytical Method Validation Using the Example of Simultaneous Quantitation of Antidiabetic Agents in Blood. *J. Chromatogr. B* **2017**, *1055–1056*, 61–71.
- (309) Kadian, N.; Raju, K. S. R.; Rashid, M.; Malik, M. Y.; Taneja, I.; Wahajuddin, M. Comparative Assessment of Bioanalytical Method Validation Guidelines for Pharmaceutical Industry. *J. Pharm. Biomed. Anal.* **2016**, *126*, 83–97.
- (310) USFDA. *Bioanalytical Method Validation. Guidance for Industry*; 2018.
- (311) Yamakawa, N.; Vanbeselaere, J.; Chang, L.-Y.; Yu, S.-Y.; Ducrocq, L.; Harduin-Lepers, A.; Kurata, J.; Aoki-Kinoshita, K. F.; Sato, C.; Khoo, K.-H.; et al. Systems Glycomics of Adult Zebrafish Identifies Organ-Specific Sialylation and Glycosylation Patterns. *Nat. Commun.* **2018**, *9* (1), 4647.
- (312) *International Conference On Harmonisation of Technical Requirements For Registration Of Pharmaceuticals For Human Use (ICH). Validation of Analytical Procedures: Text and Methodology Q2(R1)*; 2005.
- (313) Jaworska, K.; Ratajczak, J.; Huang, L.; Whalen, K.; Yang, M.; Stevens, B. K.; Kinsey, G. R. Both PD-1 Ligands Protect the Kidney from Ischemia Reperfusion Injury. *J Immunol.* **2015**, *194* (1), 325–333.
- (314) Reineke, D. C.; Müller-Schweinitzer, E.; Winkler, B.; Kunz, D.; Konerding, M. A.;

- Grussenmeyer, T.; Carrel, T. P.; Eckstein, F. S.; Grapow, M. T. R. Rapamycin Impairs Endothelial Cell Function in Human Internal Thoracic Arteries. *Eur. J. Med. Research* **2015**, *20* (59).
- (315) Kin, K.; Maziarz, J.; Günter, P. W. Immunohistological Study of the Endometrial Stromal Fibroblasts in the Opossum, *Monodelphis Domestica*: Evidence for Homology with Eutherian Stromal Fibroblasts. *Biol. Reprod.* **2014**, *90* (5), 1–12.
- (316) Chung, S.-H.; Bae, C.-W. Association of Surfactant Protein with Expression of Hoxa5 and Hoxb5 in Rabbit Fetal Lung. *Int. J. Med. Sci* **2017**, *14* (12), 1189–1196.
- (317) Kirby, E. D.; Kuwahara, A. A.; Messer, R. L.; Wyss-Coray, T. Adult Hippocampal Neural Stem and Progenitor Cells Regulate the Neurogenic Niche by Secreting VEGF. *PNAS* **2015**, *112* (13), 4128–4133.
- (318) Deng, J.; Zhang, J.; Feng, C.; Xiong, L.; Zuo, Z. Critical Role of Matrix Metalloprotease-9 in Chronic High Fat Diet-Induced Cerebral Vascular Remodelling and Increase of Ischaemic Brain Injury in Mice. *Cardiovasc. Res.* **2014**, *103*, 473–484.
- (319) National Research Council (US) Committee on Assessing the Importance and Impact of Glycomics and Glycosciences. *Transforming Glycoscience: A Roadmap for the Future*, 2012.
- (320) Huang, Y.; Orlando, R. Kinetics of N-Glycan Release from Human Immunoglobulin G (IgG) by PNGase F: All Glycans Are Not Created Equal. *J. Biomol. Tech.* **2017**, *28* (4), 150.
- (321) Takehara, S.; Onda, M.; Zhang, J.; Nishiyama, M.; Yang, X.; Mikami, B.; Lomas, D. A. The 2.1-Å Crystal Structure of Native Neuroserpin Reveals Unique Structural Elements That Contribute to Conformational Instability. *J. Mol. Biol.* **2009**, *388*, 11–20.
- (322) Noto, R.; Randazzo, L.; Raccosta, S.; Caccia, S.; Moriconi, C.; Miranda, E.; Martorana, V.; Manno, M. The Stability and Activity of Human Neuroserpin Are Modulated by a Salt Bridge That Stabilises the Reactive Centre Loop. *Nat. Publ. Gr.* **2015**.
- (323) Farhan Ali, M.; Kaushik, A.; Kapil, C.; Gupta, D.; Aman Jairajpuri, M. A Hydrophobic Patch Surrounding Trp154 in Human Neuroserpin Controls the Helix F Dynamics with Implications in Inhibition and Aggregation. *Nat. Publ. Gr.* **2017**.
- (324) Santangelo, M. G.; Noto, R.; Levantino, M.; Cupane, A.; Ricagno, S.; Pezzullo, M.;

- Bolognesi, M.; Mangione, M. R.; Martorana, V.; Manno, M. On the Molecular Structure of Human Neuroserpin Polymers. *Proteins Struct. Funct. Bioinforma.* **2012**.
- (325) Yamasaki, M.; Li, W.; Johnson, D. J. D.; Huntington, J. A. Crystal Structure of a Stable Dimer Reveals the Molecular Basis of Serpin Polymerization. *Nature* **2008**.
- (326) Lee, T. W.; Tsang, V. W. K.; Loef, E. J.; Birch, N. P. Physiological and Pathological Functions of Neuroserpin: Regulation of Cellular Responses through Multiple Mechanisms. *Semin. Cell Dev. Biol.* **2017**, *62*, 152–159.
- (327) Jhan, S.-Y.; Huang, L.-J.; Wang, T.-F.; Chou, H.-H.; Chen, S.-H. Dimethyl Labeling Coupled with Mass Spectrometry for Topographical Characterization of Primary Amines on Monoclonal Antibodies. *Anal. Chem.* **2017**, *89* (7), 4255–4263.
- (328) Saga, G.; Sessa, F.; Barbiroli, A.; Santambrogio, C.; Russo, R.; Sala, M.; Raccosta, S.; Martorana, V.; Caccia, S.; Noto, R.; et al. Embelin Binds to Human Neuroserpin and Impairs Its Polymerisation. *Nat. Publ. Gr.* **2015**.
- (329) Noto, R.; Santangelo, M. G.; Levantino, M.; Cupane, A.; Mangione, M. R.; Parisi, D.; Ricagno, S.; Bolognesi, M.; Manno, M.; Martorana, V. Functional and Dysfunctional Conformers of Human Neuroserpin Characterized by Optical Spectroscopies and Molecular Dynamics. *Biochim. Biophys. Acta - Proteins Proteomics* **2015**, *1854* (2), 110–117.
- (330) Ricagno, S.; Pezzullo, M.; Barbiroli, A.; Manno, M.; Levantino, M.; Santangelo, M. G.; Bonomi, F.; Bolognesi, M. Two Latent and Two Hyperstable Polymeric Forms of Human Neuroserpin. *Biophys. J.* **2010**, *99* (10), 3402–3411.
- (331) Ricagno, S.; Caccia, S.; Sorrentino, G.; Antonini, G.; Bolognesi, M. Human Neuroserpin: Structure and Time-Dependent Inhibition. *J. Mol. Biol.* **2009**, *388* (1), 109–121.
- (332) Bini, D.; Russo, L.; Battocchio, C.; Natalello, A.; Polzonetti, G.; Doglia, S. M.; Nicotra, F.; Cipolla, L. Dendron Synthesis and Carbohydrate Immobilization on a Biomaterial Surface by a Double-Click Reaction. *Org. Lett.* **2014**.
- (333) Iqbal, S.; Ghanimi Fard, M.; Everest-Dass, A.; Packer, N. H.; Parker, L. M. Understanding Cellular Glycan Surfaces in the Central Nervous System. *Biochem. Soc. Trans.* **2019**, *47* (1), 89–100.



- (334) Endo, T. Structure, Function and Pathology of O-Mannosyl Glycans. *Glycoconj. J.* **2004**, *21* (1/2), 3–7.
- (335) Lommel, M.; Winterhalter, P. R.; Willer, T.; Dahlhoff, M.; Schneider, M. R.; Bartels, M. F.; Renner-Muller, I.; Ruppert, T.; Wolf, E.; Strahl, S. Protein O-Mannosylation Is Crucial for E-Cadherin-Mediated Cell Adhesion. *Proc. Natl. Acad. Sci.* **2013**, *110* (52), 21024–21029.
- (336) Schneider, A.; Bolcato-Bellemin, A.-L.; Francius, G.; Jedrzejwska, J.; Schaaf, P.; Voegel, J.-C.; Frisch, B.; Picart, C. Glycated Polyelectrolyte Multilayer Films: Differential Adhesion of Primary versus Tumor Cells. *Biomacromolecules* **2006**, *7*, 2882–2889.
- (337) Seeberger, P. H.; Stallforth, P.; De Libero, G.; Cavallari, M. Carbohydrate-Glycolipid Conjugate Vaccines. US 20150238597 A1, 2013.
- (338) Lommel, M.; Strahl, S. Protein O-Mannosylation: Conserved from Bacteria to Humans. *Glycobiology* **2009**, *19* (8), 816–828.
- (339) Baldoni, L.; Marino, C. Synthetic Tools for the Characterization of Galactofuranosyl Transferases: Glycosylations via Acylated Glycosyl Iodides. *Carbohydr. Res.* **2013**, *374*, 75–81.
- (340) Mydock, L. K.; Demchenko, A. V. Mechanism of Chemical O-Glycosylation: From Early Studies to Recent Discoveries. **2009**.
- (341) Nigudkar, S. S.; Demchenko, A. V. Stereocontrolled 1,2-Cis Glycosylation as the Driving Force of Progress in Synthetic Carbohydrate Chemistry. *Chem. Sci.* **2015**, *6*, 2687–2704.
- (342) Kolb, H. C.; Finn, M. G.; Sharpless, K. B. Click Chemistry: Diverse Chemical Function from a Few Good Reactions. *Angew. Chem. Int. Ed. Engl.* **2001**, *40* (11), 2004–2021.
- (343) Kolb, H. C.; Sharpless, K. B. The Growing Impact of Click Chemistry on Drug Discovery. *Drug Discov. Today* **2003**, *8* (24), 1128–1137.
- (344) Liang, L.; Astruc, D. The Copper(I)-Catalyzed Alkyne-Azide Cycloaddition (CuAAC) “Click” Reaction and Its Applications. An Overview. *Coord. Chem. Rev.* **2011**, *255* (23–24), 2933–2945.
- (345) Corey, E. J. Catalytic Enantioselective Diels-Alder Reactions: Methods, Mechanistic



- Fundamentals, Pathways, and Applications. *Angew. Chemie Int. Ed.* **2002**, *41* (10), 1650–1667.
- (346) Rostovtsev, V. V.; Green, L. G.; Fokin, V. V.; Sharpless, K. B. A Stepwise Huisgen Cycloaddition Process: Copper(I)-Catalyzed Regioselective “Ligation” of Azides and Terminal Alkynes. *Angew. Chemie Int. Ed.* **2002**, *41* (14), 2596–2599.
- (347) Dondoni, A. The Emergence of Thiol-Ene Coupling as a Click Process for Materials and Bioorganic Chemistry. *Angew. Chemie - Int. Ed.* **2008**, *47*, 8995–8997.
- (348) Vacchini, M.; Guizzardi, R.; Cipolla, L.; La Ferla, B.; Lahmann, M. Synthesis of Allyl and Dec-9-Enyl  $\alpha$ -D-Mannopyranosides from D-Mannose. *Carbohydr. Chem. Proven Synth. Methods Vol 5*. **2019**, *Accepted*.
- (349) Mintzer, M. A.; Grinstaff, M. W. Biomedical Applications of Dendrimers: A Tutorial. *Chem. Soc. Rev.* **2011**, *40* (1), 173–190.
- (350) Röglin, L.; Lempens, E. H. M.; Meijer, E. W. A Synthetic “Tour de Force”: Well-Defined Multivalent and Multimodal Dendritic Structures for Biomedical Applications. *Angew. Chemie - Int. Ed.* **2011**, *50*, 102–112.
- (351) Ghazarian, H.; Idoni, B.; Oppenheimer, S. B. A Glycobiology Review: Carbohydrates, Lectins and Implications in Cancer Therapeutics. *Acta Histochem.* **2011**, *113* (3), 236–247.
- (352) Ribeiro, J. P.; Diercks, T.; Jiménez-Barbero, J.; André, S.; Gabius, H.-J.; Cañada, F. J. Fluorinated Carbohydrates as Lectin Ligands: (19)F-Based Direct STD Monitoring for Detection of Anomeric Selectivity. *Biomolecules* **2015**, *5* (4), 3177–3192.
- (353) Gromnicova, R.; Yilmaz, C. U.; Orhan, N.; Kaya, M.; Davies, H.; Williams, P.; Romero, I. A.; Sharrack, B.; Male, D. Localization and Mobility of Glucose-Coated Gold Nanoparticles within the Brain. *Nanomedicine (Lond)*. **2016**, *11* (6), 617–625.
- (354) Astruc, D.; Diallo, A. K.; Gatard, S.; Liang, L.; Ornelas, C.; Martinez, V.; Méry, D.; Ruiz, J. Olefin Metathesis in Nano-Sized Systems. *Beilstein J. Org. Chem.* **2011**, *7* (1), 94–103.
- (355) Kreye, O.; Kugele, D.; Faust, L.; Meier, M. A. R. Divergent Dendrimer Synthesis via the Passerini Three-Component Reaction and Olefin Cross-Metathesis. *Macromol. Rapid Commun.* **2014**, *35* (3), 317–322.

- (356) Catherine, O. L.; Fréchet, J. M. J. Incorporation of Functional Guest Molecules into an Internally Functionalizable Dendrimer through Olefin Metathesis. *Macromolecules* **2005**, *38* (15), 6276–6284.
- (357) Lindhorst, T. K.; Elsner, K. Postsynthetic Functionalization of Glycodendrons at the Focal Point. *Beilstein J. Org. Chem.* **2014**, *10* (1), 1482–1487.
- (358) Wendland, M. S.; Zimmerman, S. C. Synthesis of Cored Dendrimers. *J. Am. Chem. Soc.* **1999**, *121* (6), 1389–1390.
- (359) Schultz, L. G.; Zhao, Y.; Zimmerman, S. C. Synthesis of Cored Dendrimers with Internal Cross-Links. *Angew. Chemie Int. Ed.* **2001**, *40* (10), 1962–1966.
- (360) Kim, J.; Yun, M. H.; Lee, J.; Kim, J. Y.; Wudl, F.; Yang, C. A Synthetic Approach to a Fullerene-Rich Dendron and Its Linear Polymer via Ring-Opening Metathesis Polymerization. *Chem. Commun.* **2011**, *47* (11), 3078.
- (361) Zill, A. T.; Licha, K.; Haag, R.; Zimmerman, S. C. Synthesis and Properties of Fluorescent Dyes Conjugated to Hyperbranched Polyglycerols. *New J. Chem.* **2012**, *36* (2), 419–427.
- (362) Vida, Y.; Collado, D.; Najera, F.; Claros, S.; Becerra, J.; Andrades, J. A.; Perez-Inestrosa, E. Dendrimer Surface Orientation of the RGD Peptide Affects Mesenchymal Stem Cell Adhesion. *RSC Adv.* **2016**, *6* (55), 49839–49844.
- (363) Chabre, Y. M.; Roy, R. Multivalent Glycoconjugate Syntheses and Applications Using Aromatic Scaffolds. *Chem. Soc. Rev.* **2013**, *42* (11), 4657–4708.
- (364) Bini, D.; Marchetti, R.; Russo, L.; Molinaro, A.; Silipo, A.; Cipolla, L. Multivalent Ligand Mimetics of LecA from *P. Aeruginosa*: Synthesis and NMR Studies. *Carbohydr. Res.* **2016**, *429*, 23–28.
- (365) Bini, D.; Nicotra, F.; Cipolla, L. Bifunctional Dendrons for Multiple Carbohydrate Presentation via Carbonyl Chemistry. *Beilstein J. Org. Chem.* **2014**, *10*, 1686–1691.
- (366) Samojłowicz, C.; Bieniek, M.; Pazio, A.; Makal, A.; Woźniak, K.; Poater, A.; Cavallo, L.; Wójcik, J.; Zdanowski, K.; Grela, K. The Doping Effect of Fluorinated Aromatic Solvents on the Rate of Ruthenium-Catalysed Olefin Metathesis. *Chemistry* **2011**, *17* (46), 12981–12993.

- (367) Thygesen, M. B.; Munch, H.; Sauer, J.; Cló, E.; Jørgensen, M. R.; Hindsgaul, O.; Jensen, K. J. Nucleophilic Catalysis of Carbohydrate Oxime Formation by Anilines. *J. Org. Chem.* **2010**, *75* (5), 1752–1755.
- (368) Guizzardi, R.; Vacchini, M.; Santambrogio, C.; Cipolla, L. Convergent Dendrimer Synthesis by Olefin Metathesis and Studies toward Glycoconjugation. *Can. J. Chem.* **2017**, *95*, 1008–1012.
- (369) Cooper, C. A.; Gasteiger, E.; Packer, N. H. GlycoMod - A Software Tool for Determining Glycosylation Compositions from Mass Spectrometric Data. *Proteomics* **2001**, *1* (2), 340–349.
- (370) Ceroni, A.; Maass, K.; Geyer, H.; Geyer, R.; Dell, A.; Haslam, S. M. GlycoWorkbench: A Tool for the Computer-Assisted Annotation of Mass Spectra of Glycans. *J. Proteome Res.* **2008**, *7* (4), 1650–1659.
- (371) Cox, J.; Mann, M. MaxQuant Enables High Peptide Identification Rates, Individualized p.p.b.-Range Mass Accuracies and Proteome-Wide Protein Quantification. *Nat. Biotechnol.* **2008**, *26* (12), 1367–1372.
- (372) Poláková, M.; Roslund, M. U.; Ekholm, F. S.; Saloranta, T.; Leino, R. Synthesis of  $\beta$ -(1-2)-Linked Oligomannosides. *European J. Org. Chem.* **2009**, 870–888.
- (373) Nikolaev, A. V; Rutherford, T. J.; Ferguson, M. A. J.; Brimacombe, J. S. Parasite Glycoconjugates. Part 4. Chemical Synthesis of Disaccharide and Phosphorylated Oligosaccharide Fragments of Leishmania Donovanii Antigenic Lipophosphoglycan. *J. Chem. Soc. PERKIN TRANS* **1995**, *1*, 1977–1987.
- (374) Martín, A.; Quintanal, L. M.; Suárez, E. Hydrogen Atom Transfer Experiments Provide Chemical Evidence for the Conformational Differences between C- and O-Glycosides. *Tetrahedron Lett.* **2007**, *48*, 5507–5511.
- (375) León, E. I.; Martín, Á.; Pérez-Martín, I.; Quintanal, L. M.; Suárez, E. C-C Bond Formation by Sequential Intramolecular Hydrogen Atom Transfer/Intermolecular Radical Allylation Reaction in Carbohydrate Systems. *European J. Org. Chem.* **2012**, *2012* (20), 3818–3829.
- (376) Pagé, D.; Roy, R. Optimizing Lectin-Carbohydrate Interactions: Improved Binding of Divalent Alpha-Mannosylated Ligands towards Concanavalin A. *Glycoconj. J.* **1997**, *14* (3),

345–356.

- (377) Ihre, H.; Hult, A.; Fré, J. M. J.; Gitsov, I. Double-Stage Convergent Approach for the Synthesis of Functionalized Dendritic Aliphatic Polyesters Based on 2,2-Bis(Hydroxymethyl)Propionic Acid. *Macromolecules* **1998**, *31*, 4061–4068.
- (378) Vacchini, M.; Cipolla, L.; Gornik, O.; Lauc, G.; Klarić, T. A Precise and Versatile Platform for Rapid Glycosylation Analysis of Brain Tissue. *Anal. Methods* **2019**, Submitted.

## 8. ACKNOWLEDGMENTS.

A big thank you to the best supervisor I have ever had, Tom Klarić. You have welcomed me, taught me, tolerated me, supported me like none else has ever done before. It has been and it will be a pleasure to work together, as colleagues and friends. Eventually, I won't freak out again next time the  $n$ -round of paper corrections will fall upon me like a heavy rain of words crashed on a white email background (you were right, btw).

Many thanks to all the Genos glycoscience team, for having made the Erasmus period abroad so peaceful and fruitful. Many thanks to Olga, Marija and Anne-Marie, for the very good company and the several, fit-for-the-gods, alcoholic stuff you brought to fuel the work in general and my PhD in particular (ya know the game, girlz). A special thank to Maja and Jelena, for answering my thousandfold questions about countless, probably insignificant, and surely annoying experimental details, and for the time dedicated to my training in the lab. A big big thank to Ivana, for the patience showed in taking care of the nitty-gritty of an Erasmus student-accompanying bureaucracy. Thanks to the iridescent Thomas, his constant laughter and joyful company; to Jerko, Siniša and Genadij for MS advice and support; to Gordan for giving me the possibility to walk through such a nice experience.

Thanks to Roberto, my senior PhD student, for the support and advice provided especially in the first steps of my PhD, for the beers, sipped together during the hottest summer in Milan, and the general willingness to help. And many thanks also to all the other guys in Milan I am not listing here who helped me in many, many ways.

A great thank to my family, of course, the deepest foundations of my very being.

The biggest thank to Francesca, who has always been there and, hopefully, always will be.

## 9. PUBLICATIONS.

Vacchini, M., Cipolla, L., Gornik, O., Lauc, G., Klarić, T. *A precise and versatile platform for rapid glycosylation analysis of brain tissue*. Analytical Methods (2019, Submitted).

Guizzardi R., Vacchini M., Cipolla L. (2019) *Carbohydrates in Regenerative Medicine: From Scaffolds to Cell Fate Modulators*. In: Duscher D., Shiffman M. (eds) Regenerative Medicine and Plastic Surgery. Springer, Cham.

Vacchini, M., Guizzardi, R., Cipolla, L., La Ferla, B., Lahmann, M. *Synthesis of allyl and dec-9-enyl  $\alpha$ -D-mannopyranosides from D-mannose*. Carbohydrate Chemistry: Proven Synthetic Methods Vol 5 (2019, Accepted).

Vacchini M., Edwards R., Guizzardi R., Palmioli A., Ciaramelli C., Paiotta A., Airoidi C., La Ferla B., Cipolla L. *Glycan Carriers As Glycotools for Medicinal Chemistry Applications*. Current Medicinal Chemistry (2019) 26: 6349.

Guizzardi R., Vacchini M., Santambrogio C., Cipolla L. *Convergent dendrimer synthesis by olefin metathesis and studies toward glycoconjugation*. Can. J. Chem. 95: 1008–1012 (2017).